The Thalamic Nucleus Reuniens Facilitates Communication Between Prefrontal Cortex and Hippocampus

by

Brandon Evan Hauer

A thesis submitted in partial fulfillment of the requirements for the degree of

Doctor of Philosophy

Neuroscience

University of Alberta

Abstract

Decades of research have established that two brain regions, the medial prefrontal cortex (mPFC) and hippocampus (HPC), have dissociable but critical roles in memory. Often, these roles are co-operative and enable for the richness of episodic remembrances. It has remained relatively elusive, however, how these distant sites communicate to achieve this. To this end, I have investigated an anatomically interposed but somewhat understudied brain region: the thalamic nucleus reuniens (RE). The overall goal of this thesis was to understand how mPFC and HPC coordinate their activity, particularly during slow oscillations (SOs, ~1 Hz). SOs were of particular interest given their implication in the sleep-dependent consolidation of episodic memories, a process that involves bidirectional communication between these sites. I learned, however, that the mPFC-HPC circuitry operates in fundamentally different ways, both as a function of forebrain state, and of the activity patterns of RE neurons.

In Chapter 2, I first showed that neuronal activity in the RE is intimately coupled to the ongoing mPFC SO. As well, optogenetic activation of the RE, or of its ipsilateral afferent fibers to the HPC, reliably produced a robust excitation at the site of RE terminals in CA1, the stratum lacunosum moleculare (SLM), which also happens to be the locus of SO generation in HPC. Electrical stimulation of the mPFC produced a similar pattern of short-latency excitation in HPC. Crucially, when the RE was chemogenetically inactivated, the mPFC-evoked excitation at SLM was selectively eliminated and SO coherence between these sites dropped significantly. The RE as such plays an essential role in mediating the coupled SO dialogue between mPFC and HPC.

In Chapter 3, I explored how overall brain state affects the responses in HPC following stimulation of either RE or mPFC. Optogenetic activation of the RE, or its fibers targeting the HPC, consistently evoked a larger response at SLM during SO as compared to theta states.

Similarly, excitation of RE yielded a larger mPFC field response during SO states. While electrical stimulation of mPFC produced a similar short-latency pattern of SLM responding during SO, this response appeared surprisingly delayed during theta. Interestingly, stimulation of the mPFC also evoked excitation in the dentate gyrus (DG) which did not change across states. Chemogenetic inhibition of RE abolished the mPFC responses in SLM during SO, leaving the DG responses intact, while no differences were observed during theta. The magnitude of responding in HPC via both RE and mPFC stimulation was additionally shown to be modified by the phase of the ongoing oscillation, whether during SO or theta. The way mPFC and HPC communicate and therefore process information is variable by brain state. The interposed RE acts as a crucial hub for biasing the preferred circuitry of information transfer, and is as such posed to be a key modulator in timing-dependent mnemonic processes.

In Chapter 4, I investigated the role of neuronal activity states within the RE in mediating both mPFC-HPC SO dialogue, as well as the larger evoked responses observed during SO. Specifically, I tested the functional circuit implications of up-regulating RE activity using optogenetics. Optogenetically stimulating the RE robustly and tonically increased its multiunit activity, in a manner comparable to that observed during spontaneous theta. Interestingly, performing this manipulation decreased the amplitude of excitatory SLM responses to mPFC stimulation, specifically during SO states. Consistent with this, tonic upregulation of RE activity also decreased SO coherence between mPFC and HPC. Thus, modulating the activity dynamics of the RE to mimic those observed during theta, despite the forebrain otherwise exhibiting an SO state, was sufficient to disrupt mPFC-HPC coupling. It thus appears that during SO, the RE is primed by the mPFC-HPC circuitry to both receive and transmit SO information, whereas this is not the case during the particular activity patterns shown during theta.

Finally, in Chapter 5, I showed that brief optogenetic stimulation of the RE was sufficient to reset the ongoing HPC theta rhythm. This was true both with direct RE stimulation during theta states, as well as with stimulation of its HPC-projecting afferents. The RE therefore has the ability to fundamentally affect the internal oscillator of the HPC, the resetting of which may mechanistically underlie its capacity to synchronize mPFC and HPC at theta frequencies and augment activity-dependent mnemonic processes.

Taken all together, the results in this thesis show that the thalamic nucleus reuniens is a fundamentally important processing node for mPFC-HPC information exchange, a circuit crucially involved in episodic memory.

Preface

All ideas, data, and analyses presented here are my own, developed in collaboration with my supervisors Drs. Clayton Dickson and Silvia Pagliardini. This thesis was a part of two larger projects, which received research ethics approval from the University of Alberta Biosciences Animal Care and Use Committee (AUP00000092; project name: Cellular and Network Dynamics of Neo- and Limbic-Cortical Brain Structures) and from the University of Alberta Health Sciences Animal Care and Use Committee (AUP00000461; project name: Neural control of breathing in rodents in vivo). Beyond my two co-supervisors, I am the sole author and contributor to all data collection, analysis, and authorship of everything in this dissertation.

Chapter 2 of this thesis has been published as Hauer, B.E., Pagliardini, S., Dickson, C.T. (2019). The Reuniens Nucleus of the Thalamus has an Essential Role in Coordinating Slow Wave Activity between Neocortex and Hippocampus. *eNeuro*, 6(5). doi: 10.1523/ENEURO.0365-19.2019. All data collection and analysis, figure creations, as well as manuscript composition was conducted by me. S. Pagliardini was a supervisory author and contributed to concept formation, methodological planning, and manuscript edits. C. T. Dickson was also a supervisory author, and contributed to concept formation, methodological planning, data analysis, figure creation, and manuscript edits.

Chapter 3 of this thesis has been accepted for publication in a special topic ("Anatomical substrate of neural circuit physiology") in *Frontiers in Neuroanatomy* as Hauer, B.E., Pagliardini, S., Dickson, C.T. (2022). Prefrontal-Hippocampal Pathways Through the Nucleus Reuniens Are Functionally Biased by Brain State. *In press*. Accepted on 13 Dec., 2021, doi: 10.3389/fnana.2021.804872. The version of Chapter 3 that appears in this dissertation is not identical to what is being published, as the *in press* version has now been peer-reviewed and

edited. All data collection and analysis, figure creations, as well as manuscript composition was conducted by me. S. Pagliardini was a supervisory author and contributed to concept formation, methodological planning, and manuscript edits. C. T. Dickson was also a supervisory author, and contributed to concept formation, methodological planning, data analysis, figure creation, and manuscript edits.

"What is the nature of such relatively autonomous activities in the cerebrum? Not even a tentative answer is available. We know a good deal about the afferent pathways to the cortex, about the efferent pathways from it, and about many structures linking the two. But the links are complex, and we know practically nothing about what goes on between [them]."

Donald Olding Hebb, 1949

From *The Organization of Behavior*

Acknowledgments

The work in this thesis was supported by Natural Sciences and Engineering Research Council of Canada (NSERC) Discovery grants 2016-06576 and 2021-02926 awarded to Clayton Dickson, NSERC grant 435843 to Silvia Pagliardini, as well as NSERC Alexander Graham Bell Canada Graduate Scholarship – Masters (CGS-M) and NSERC Doctoral Postgraduate Scholarship (PGS-D) grants awarded to me.

I must first acknowledge my primary supervisor, Dr. Clayton Dickson, whose guidance, support, and utterly unwavering enthusiasm and passion for science were invaluable throughout my degree. I can scarcely recount how many times I'd gone into a meeting with Clay feeling totally defeated by data, analysis, or graduate school in general. Somehow, over the course of every single meeting, I would come to share Clay's enthusiasm for whatever nightmarish collage of figures I was showing him. "This is looking really good," seemed to conclude every last meeting. Thank you, Clay.

I would also like to extend my sincere appreciation to my co-supervisor, Dr. Silvia Pagliardini. Silvia taught me a tremendous deal when it came to collecting data and problem solving. So much so, that when I was still a training graduate student, I would imagine "what would Silvia tell me to do in this case," and most times, I'd be able to solve the problem. Even more important than that, both Silvia and Clayton always prioritized me as a human first, beyond a researcher or student. The open door policy shared by both ensured I always felt comfortable approaching them with concerns even beyond the scope of graduate school.

I would like to thank my supervisory committee members, Dr. Kyle Mathewson and Dr. Jesse Jackson. Throughout my degree, both helped me to become a better scientist by suggesting

challenging readings and asking questions about my data well beyond the scope of anything I had previously considered.

I would like to thank my fellow Brain Rhythms Lab and Pagliardini Lab members, both past and present. The fun, passion, and countless hours shared both in the lab and outside of it with members that have come and gone are memories I will cherish always. I would like to extend particular thanks to Rachel, who started at the same time as me on this incredible voyage through graduate school, and who rapidly became one of my closest friends and mind-twins throughout my degree.

Finally, thank you to all of my loved ones, family, and friends, without whose unwavering support I would be nowhere.

Table of Contents

Table of Figures

List of Abbreviations

Adeno-associated virus	AAV
Alternating current	AC
Analysis of variance	ANOVA
Anterior cingulate cortex	ACC
Antero-posterior	AP
Channelrhodopsin-2	ChR2
Cingulum bundle	CB
Clozapine *N*-oxide	CNO
Continuous wavelet transform	CWT
Cornu ammonis 1	CA1
Cornu ammonis 3	CA3
Cortex	CTX
Current source density	CSD
Dentate gyrus	DG
Designer receptor exclusively activated by designer drug	DREADD
Direct current	DC
Dorso-ventral	DV
Enhanced yellow fluorescent protein	EYFP
Entorhinal cortex	EC
Excitatory postsynaptic potential	EPSP
Fast Fourier transform	FFT
Frontal cortex	FC
γ-aminobutyric acid	GABA
Green fluorescent protein	GFP
Hippocampus	HPC
Human influenza hemagglutinin	HA
Human M4 muscarinic inhibitory DREADD	hM4Di
Human synapsin	hSyn
Infralimbic cortex	IL
Inter-stimulus interval	ISI

Interoanteromedial nucleus	IAM
Intraperitoneal	*i.p.*
Lateral entorhinal cortex	LEC
Local field potential	LFP
Long-term depression	LTD
Long-term potentiation	LTP
Medial agranular cortex	AGm
Medial entorhinal cortex	MEC
Medial prefrontal cortex	mPFC
Medio-lateral	ML
Multiunit activity	MUA
Neocortex	nCTX
N-methyl-D-aspartate	NMDA
Neuronal nuclear marker	NeuN
Non-rapid eye movement	Non-REM
Normal donkey serum	NDS
Not significant	n.s.
Nucleus reuniens	RE
Phosphate-buffered saline	PBS
Prefrontal cortex	PFC
Prelimbic cortex	PL
Rapid eye movement	REM
Rhomboid nucleus	Rh
Root mean square	RMS
Single unit	SU
Slow oscillation	SO
Slow-wave sleep	SWS
Spike-triggered average	STA
Standard deviation	SD
Standard error of the mean	SEM
Stratum lacunosum-moleculare	SLM

Stratum moleculare	SMol
Stratum oriens	SOr
Stratum pyramidale	SPyr
Stratum radiatum	SRad
Subcutaneous	*s.c.*
Third ventricle	3V

1 Introduction

Introduction

1.1 The function of the brain

How does anything happen? How do you *do* anything? The complexities and richness of experience and existence are made possible only by being able to observe, process, and respond to inputs. But what is the black box between observation and reaction? Countless years of evolution have led to the most remarkable, and remarkably complex, squishy ball of meat: The brain.

Of the near infinite amounts of information available to be experienced at any given moment, the brain faces a seemingly insurmountable task, but one that it ostensibly accomplishes with relative ease. First, the brain must receive input. Environmental energy has to be somehow converted into some type of neural energy, able to be used by the brain. This energy, the "currency" of neural computation, is electricity. The units of neural computation, neurons, are able to receive continuous, analog input and convert it into a digital signal via the firing of action potentials – threshold "all-or-none" events indicative of a stimulus sufficient to generate a response. This leads directly to the second primary function of the brain: processing information. Having received input, transmuted it into a digital, electrical code, the brain then rapidly and reliably relays these electrical potentials between inter-related neurons. The incredible processing capacity of the brain is most evident here, as both supra-threshold (e.g., action potentials) and sub-threshold (receptor- and synaptic-potential) responses repeatedly convert the signal from digital to continuous format and back again. Synaptic potentials generated from neurotransmitter release (*i.e.,* chemical signaling) modulate neuronal membrane excitability, moving the membrane potential closer to (as in excitatory post-synaptic potentials) or further from (as in inhibitory post-synaptic potentials) the threshold for action potential generation. As

such, the initial input becomes a continuously represented signal, capable of being processed across distributed networks. Perhaps obviously at this point, the capacity of a single neuron to represent information or ideas entirely independently is dubious at best. Instead, the representation of exterior (to the brain) information gets created across massive networks of interconnected neurons: a neuronal ensemble. Ensemble coding allows for further re-processing of the created digital code as it gets continuously integrated across synapses throughout the network. Ensemble coding is also the key intermediary before the final primary function of the brain: response. In reductionist terms, the brain acts as an input-output device. Input is achieved via digital representations of continuous information in the world, and processing is performed by neuronal ensembles. The end goal of that processing is to be able to respond to the initial input: to produce output; to produce a response that is adaptive for the animal within whom the brain resides. A behaviour, a thought, a recollection – any of the unbelievable complexities of life – are the output of this miraculous symphony of orchestrated processing.

It would be convenient and indeed, highly evolutionarily advantageous if the organism who expended the energy and time required to receive, process, and respond to an input could maintain some form of this processed representation for subsequent or repeated use. This is exactly the idea underlying a memory engram: a neuronal ensemble that acts as a substrate for storing and recalling memories (Josselyn and Tonegawa, 2020). The idea that augmented synaptic strength and neuronal connectivity mechanistically underlie or at least contribute to memory formation is a foundational one in neuroscience (Hebb, 1949), and one that continues to be explored today (Josselyn et al., 2015). Engrams then, as maintained representations of ensemble coding, are an emergent property of the chemical-electric neural code generated as information courses through inter-related networks of individual neurons. Representing this

information most effectively requires spatiotemporally correlated changes in the activity of neurons within the network (Azarfar et al., 2018). That is, the firing of neurons is modulated across both spatial (*i.e.,* proximal inputs can generate larger responses) and temporal (*i.e.,* firing closely in time can generate larger responses) dimensions. The mechanism by which these neuronal ensembles are formed most effectively is therefore by coincidental but precisely timed interactions between neurons: synchrony.

1.1.1 Neuronal oscillations

The complexities of interacting with an environment require the coordination of the units of neural computation, neurons. The synchronization of brain activity over both disparate and proximal regions manifests as oscillations: rhythmic fluctuations in neuronal membrane potentials in time. Oscillations are an emergent phenomenon inherent to the intrinsic properties of neurons (Buzsaki et al., 2012). These oscillations can be measured as local field potentials (LFPs) and reflect the summation of transmembrane currents occurring near the site of the recording electrode, whether those currents are driven by local or long-range inputs (Buzsaki et al., 2012). Transmembrane currents can be comprised of any excitable membrane, whether dendrites, spines, soma, axons, or axon terminals. Any change in transmembrane current implies both an intracellular and extracellular (*i.e.,* LFP) voltage deflection, both of which can be recorded. The actual characteristics of the recorded waveform depend on the relative contributions of the surrounding sources, as well as the geometry and properties of the brain tissue (Buzsaki et al., 2012). It is, of course, prudent to consider what the LFPs being recorded reflect. Volume conduction refers to a phenomenon wherein an electric field (such as the type generated by transmembrane currents) can be transmitted through a medium (such as brain

tissue). Commonly, this reflects the return currents of dipoles, rather than an accurate reflection of the activity occurring proximal to the recording site (Linden et al., 2010). Various analytical techniques will be discussed in the sections that follow, which provide an attempt to understand neuronal computation through electrical fields.

One of the advantages of recording from brain tissue is the conveniently laminar organization of many regions of interest (see sections 1.2.1 and 1.2.2 for discussions of cytoarchitecture). The horizontal arrangements of pyramidal cells in particular (the most populous neuron type), with soma lined up relatively side-by-side and long, thick apical dendrites extending in the same direction gives rise to an electrical dipole. The hallmark of a dipole is two charges of opposite polarity, with some separation between them. The electrical field this creates is ideal for electrophysiological recording, because it creates a reliable separation of the active sink (or source) from the return currents. In other words, the creation of a dipole leads to significant movement of ions in the extracellular medium, making a considerable contribution to the extracellular field. While spatial arrangement is one critical determinant of the generated (and subsequently recorded) field, the other key factor is temporal synchrony. Multiple fluctuations in transmembrane current that occur in close temporal proximity to each other summates to a larger field fluctuation. This type of synchrony is most commonly brought about through network oscillations (Buzsaki et al., 2012). One consequence of this is that LFPs of different frequencies generally have different amplitudes. A general quantitative rule is that the magnitude of the LFP power is inversely related to the temporal frequency (f), leading to a $1/f$ scaling (also known as pink noise).

Certain types of neurons have properties inherent to them that lead to network oscillations. Some neurons have ionic conductances responsible for their excitability which,

through the unending push-and-pull of inward and outward current flow, provide them with autorhythmical oscillatory properties (Llinas, 1988). These neurons in turn have chemical (more commonly) or direct electrical contacts between each other. In this type of network, these neurons may be truly autorhythmic – that is, they are pacemakers, generating and setting an inherent rhythm – or they may be resonators. Resonance means that these neurons respond optimally to inputs of a particular frequency or frequency range (Llinas, 1988). The resulting rhythmic, coordinated discharge of action potentials provides an ideal platform for efficient processing, transfer, and storage of information. Simply, oscillation-based synchrony (*i.e.*, phasic coherence between signals and regions) is the most energy efficient means of temporal coordination (Mirollo and Strogatz, 1990; Buzsaki and Draguhn, 2004).

Synchronized oscillations among groups of neurons occur at frequency ranges spanning five orders of magnitude, and are phylogenetically preserved across mammals, suggesting they have conserved functional relevance (Buzsaki and Draguhn, 2004). Indeed, synchronized oscillatory activity is a hallmark of information processing in the brain, and is correlated with a host of cognitive functions: learning, memory, consciousness, attention, perception, etc. (Plankar et al., 2013). While many of these represent conscious, waking states, the importance of these rhythmic bouts of activity during so-called "offline" states like sleep is increasingly being appreciated. For instance, sleep has an important role in facilitating hippocampal-dependent memory consolidation (discussed in section 1.2.4), but it is the coordinated slow-wave activity patterns that emerge during sleep that appear to be central to this phenomenon (Born, 2010; Diekelmann and Born, 2010). The slow oscillation (SO), a ~1 Hz rhythm apparent during both slow-wave sleep (SWS) and certain types of anesthesia (e.g., urethane), is comprised of alternating activity states (active: UP; silent: DOWN) (Steriade et al., 1993a; Amzica and

Steriade, 1995). The SO is a global brain phenomenon, capable of influencing wide swaths of forebrain at once. Moreover, the SO groups and organizes other faster, localized rhythms because of its inherent UP and DOWN state fluctuations. Specifically, the SO nests thalamocortical spindles (Steriade et al., 1993b; Molle et al., 2009; Nir et al., 2011), gamma (Timofeev and Steriade, 1997; Steriade, 2006), and the comparatively punctate sharp-wave/ ripple events of the hippocampus (Sirota et al., 2003; Battaglia et al., 2004; Molle et al., 2009) during its active ON phase. Nesting of faster rhythms into coordinated sequences of activity during the SO may allow for the types of spike timing-dependent modifications of synapses important for memory consolidation (Dan and Poo, 2004). In fact, exogenous stimulation of cortical networks at SO frequencies during sleep has been shown to potentiate memory (Marshall et al., 2006). The cortical SO is dynamically coordinated with a hippocampal SO (Isomura et al., 2006; Wolansky et al., 2006). This hippocampal SO occurs in similar situations following the cortical SO, but displays some independence in terms of how it is initiated, coordinated, and its coherence with the cortical SO. The precise timing and coordination of these rhythms provides a platform for synchronization-dependent synaptic plasticity between disparate memory-relevant sites (Wolansky et al., 2006). The specific means by which these rhythms are coordinated remains somewhat contentious, and will be explored in this thesis.

Another highly prominent oscillatory phenomenon is theta activity, a ~4-10 Hz hippocampal rhythm. Unlike the SO, theta rhythmicity is the hallmark of activated or rapid eye movement (REM) sleep / REM-like episodes. A common theory explaining the profound rhythmicity of theta and its capacity to be entrained by several different theta oscillators throughout the brain, is that individual theta cycles may package related information for more efficient spatial memory processing (Colgin, 2013). More generally, the theta oscillations can be

thought of as representing the "online" state of the hippocampus, and is thought to be vital for the temporal coding/ decoding of active neuronal ensembles and modifying synaptic weights (Buzsaki, 2002). The functional implications of many of these oscillatory events and rhythms will be discussed in more detail in the follow sections, particularly as they pertain to memory.

1.1.2 Forebrain state

The previously described rhythmic events and oscillations do not all occur contemporaneously. Instead, oscillations emerge differentially as a function of both behavioural and brain state. Theta, for instance, is modulated by the initiation and type of movement, increasing sharply in amplitude at the onset of large movements like running or jumping (Whishaw and Vanderwolf, 1973). Locomotion is one "online" behavioral state that can produce theta, but so too is theta a hallmark of REM sleep (Jouvet, 1969; Buzsaki, 2002). That theta only appears during certain stages of sleep is another important indicator that behavioral or "online" state is not the only modulator of electrographic forebrain patterns. Indeed, sleep is characterized by remarkably different activity states in the brain.

The activity of the sleeping mammalian brain (as well as other vertebrate brains) has been classically dichotomized into a slow-wave state (SWS) occurring any time it is not in a REM state (hence, non-REM), and a "paradoxical" state (REM), so named because cortical activity in this state appears remarkably similar to that during waking, but yet with a total absence of electromyographic activity in the majority of skeletal musculature (Jouvet, 1969). REM sleep is marked by theta rhythmicity, increased heart rate, reduced thermal regulation, increased brain metabolism and cerebral blood flow (Ward-Flanagan and Dickson, 2019). Further subdivisions

can be made in terms of the depth of the non-REM stages (Carskadon and Dement, 2005). More important here is that these states alternate spontaneously during a sleep epoch, typically naturally cycling through REM and non-REM with an approximately 90 minute cycle in humans and an approximately 10-12 minute cycle in rodents (Borbely, 1976; Carskadon and Dement, 2005; Clement et al., 2008). As the sleep episode continues, fewer non-REM stages occur while REM duration increases. As discussed above, the SO is a hallmark of SWS, which occurs during non-REM states. The SO has an established role in replaying previously experienced events and, consistently, with memory formation and stabilization (Born, 2010; Diekelmann and Born, 2010). More broadly, non-REM sleep (and the SO inherent within) has important implications information processing, synaptic plasticity, and cellular recovery processes (Vyazovskiy and Delogu, 2014). Brief excursions into REM sleep then potentially provide a "selection" process, where networks and ensembles that sufficiently recovered during previous non-REM episodes are excluded from recovery processes in future non-REM episodes (Vyazovskiy and Delogu, 2014). REM sleep has also been implicated in memory consolidation through the precise timing of the theta rhythm (Boyce et al., 2016).

However, investigating the exact roles and functional implications of these states, with their naturally fluctuating neuronal rhythms and extracellular *milieu,* is problematic during sleep given the ease of arousal and the lack of analgesia. To this end, various anesthetic models have been used to mimic the physiological dynamics of natural sleep. Perhaps no anesthetic is better suited to this type of study than urethane (Clement et al., 2008; Pagliardini et al., 2013b; Ward-Flanagan and Dickson, 2019; Silver et al., 2021). Urethane anesthesia produces regularly cycling alternations between non-REM-like and REM-like states (Clement et al., 2008), concomitant with the oscillatory dynamics and physiological hallmarks (heart rate, respiration, muscle tone,

etc.) of their natural sleep analogues (Pagliardini et al., 2012). These patterns are consistent across both rats and mice (Pagliardini et al., 2013a), and are stable throughout long-duration recordings (Silver et al., 2021). Urethane anesthesia as such offers a unique experimental model to assay many of the dynamics of sleep, and of particular relevance for this thesis, many of the electrographic hallmarks of non-REM-like and REM-like states (Ward-Flanagan and Dickson, 2019).

Overall, the electrophysiological features that comprise distinct brain states have considerable implications for their functional, behavioural relevance. As discussed above, brain regions separated by even considerable distances must coordinate their inputs and outputs with remarkable temporal precision for there to be any semblance of order to their dialogue. This dialogue, and the efficiency with which it must be maintained for information exchange and mnemonic processing, is a recurrent theme throughout this thesis. Two sites with established and complimentary roles in memory, the prefrontal cortex and hippocampus, share certain anatomical connections and oscillatory dynamics likely to be paramount for their operation. The architecture of these regions, and both the nature and implications of their continued dialogue will be described next.

1.2 Prefrontal cortico-hippocampal interactions

1.2.1 Prefrontal neuroanatomy

The term “prefrontal cortex” anatomically refers to different things depending on who you ask. Neuroscientists studying either human or non-human primates would understand PFC to mean granular and orbital parts of frontal cortex (Laubach et al., 2018). Anterior cingulate cortex

(ACC) would in turn correspond to agranular areas in medial frontal cortex. Conversely, for rodent researchers (and therefore for the remainder of this dissertation), PFC refers to those same medial frontal areas commonly referred to as ACC in primates (Laubach et al., 2018). Rodent medial PFC (mPFC) can be broadly subcategorized into four primary subdivisions, from dorsal to ventral: medial agranular cortex (AGm), ACC, prelimbic cortex (PL), and infralimbic cortex (IL) (Figure 1.1) (Berendse and Groenewegen, 1991; Ongur and Price, 2000; Vertes, 2004; Vogt and Paxinos, 2014).

A wide variety of functions have been attributed to mPFC, from oculomotor control, to attentional processes, visceromotor activity, decision making, goal-directed behavior, and working memory (Kolb, 1990; Petrides, 1995; Courtney et al., 1998; Miller and Cohen, 2001). Importantly, it appears these aforementioned mPFC subdivisions underlie distinct functions. For example, more dorsal regions of mPFC (AGm and ACC) have an established role in various motor behaviours, while the comparatively ventral regions (PL and IL) appear relevant for emotional, cognitive, and mnemonic processes (Vertes, 2004).

Of particular interest here are these ventral zones of mPFC, and the mnemonic functions they are associated with (see section 1.2.3). Consistently, the efferents from these zones are quite distinct. Both PL and IL commonly project to orbitomedial PFC, the olfactory forebrain, and midline thalamus. In particular, both regions strongly project to the midline thalamic nucleus reuniens (RE). Generally speaking, IL projects more to areas associated with control of visceral/ autonomic activity, akin to the orbitomedial PFC in primates, while the efferents of PL primarily target regions with a role in limbic-cognitive functions, homologous to primate dorsolateral PFC (Vertes, 2004). Neither site projects directly to the hippocampal formation (Ammon's horn,

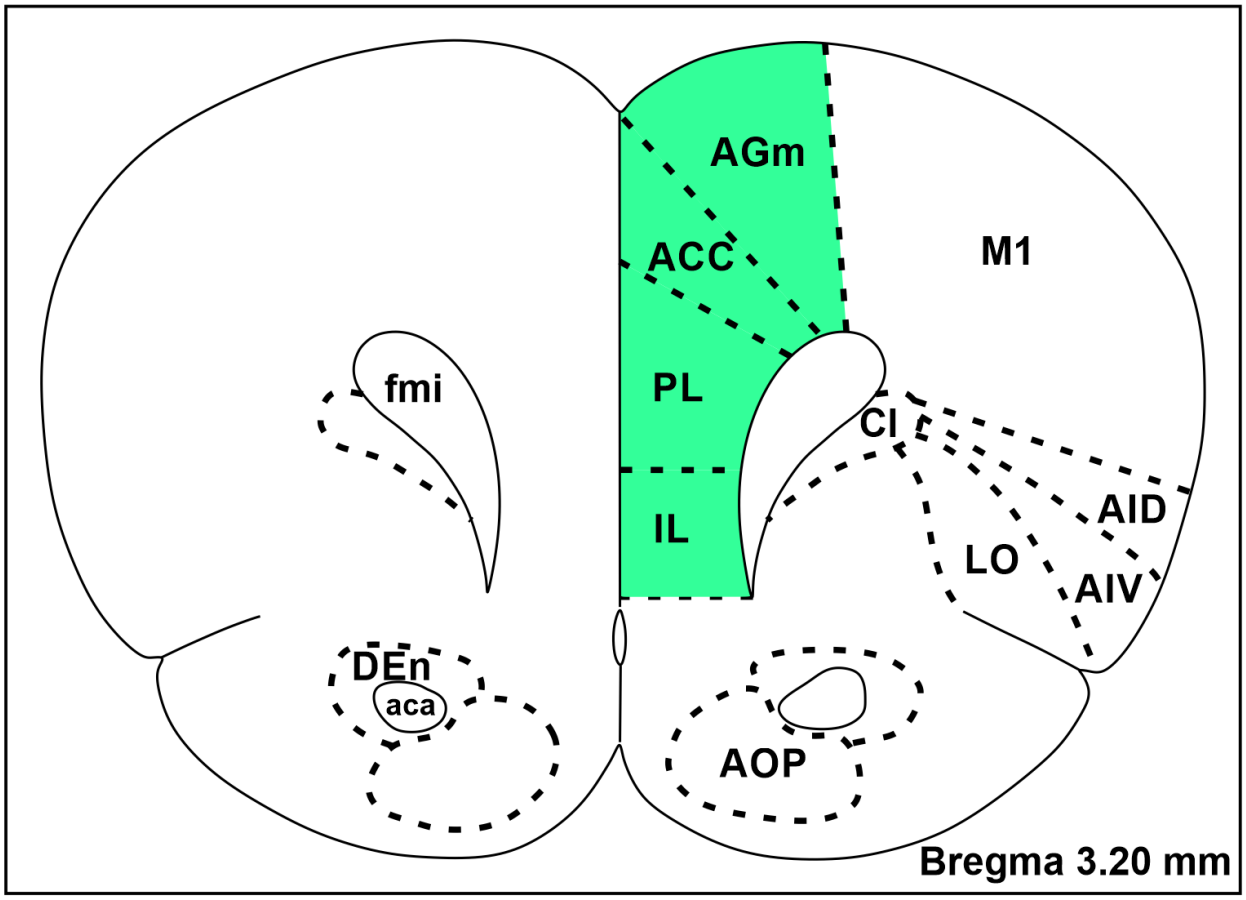

Figure 1.1 Schematic representation of rat medial prefrontal cortex.

This is a coronal schematic of the rat mPFC approximately 3.2 mm anterior to bregma, reproduced from Paxinos and Watson (1998). The four primary subdivisions of mPFC are highlighted in light green. Note that AGm is also referred to as "M2", and ACC as "Cg1", but both were changed from the original atlas for added clarity here. (AGm: medial agranular cortex; ACC: anterior cingulate cortex; PL: prelimbic cortex; IL: infralimbic cortex; M1: primary motor cortex; AID: agranular insular cortex, dorsal part; AIV: agranular insular cortex, ventral part; LO: lateral orbital cortex; Cl: claustrum; AOP: anterior olfactory area, posterior part; aca: anterior commissure, anterior part; DEn: dorsal endopiriform nucleus; fmi: forceps minor of the corpus callosum).

dentate gyrus (DG), or subiculum), but both project moderately to the entorhinal area (Vertes, 2004).

Cytoarchitecturally, mPFC follows the laminar scheme common across much of the cortex (Mountcastle, 1997; Molyneaux et al., 2007). Six morphologically distinct cell layers comprise mPFC, from the molecular layer I, to the external and internal granular (II, IV) and pyramidal (III, V) layers, and finally a multiform layer VI. The majority of neurons in the neocortex (70-85%) are pyramidal cells and, with few exceptions, are the only projection neurons of the cerebral cortex (Cajal, 1911; DeFelipe and Farinas, 1992; Wang et al., 2018). Corticothalamic neurons (that is, neurons that project subcortically to various thalamic nuclei) are primarily located in cortical layer VI, with a smaller subpopulation in layer V (Molyneaux et al., 2007).

1.2.2 Hippocampal neuroanatomy

Perhaps one of the most widely studied brain structures, the hippocampus (HPC) has both a striking appearance and remarkably organized cytoarchitectural structure. The term "hippocampus" is originally derived from the Greek word for "sea horse" (original citation Arantius (1587), as cited in Schultz and Engelhardt (2014)). Somewhat more recently, a different analogy was made to describe the HPC's appearance: that of a ram's horn. This led to the moniker "Ammon's horn," after the ram-headed ancient Egyptian god Ammon. Renowned neurophysiologist Rafael Lorente de Nó later used the Latin "Cornu Ammonis" to refer to parts of the hippocampal formation proper, which is from where the well-known CA subfields of today are derived (Lorente de Nó (1934) as cited in Schultz and Engelhardt (2014)).

Part of the allure of studying the hippocampus assuredly arises from its striking laminations. Unlike the previously described six-layered neocortex, the hippocampus is instead comprised of the far more ancient three-layered organization, and is therefore technically referred to as archicortex. These morphologically-derived layers are, simply, molecular, pyramidal, and polymorphic. However, further subdivisions can be made within the major subfields of the hippocampus proper (CA1-CA3), and within the hippocampal formation (including DG, the subicular complex, and the entorhinal cortex; Schultz and Engelhardt (2014)). In the rat, these laminae (at least within the bulk of the dorsal CA1) are organized conveniently parallel to the dorsal surface of the brain (Figure 1.2). Beginning at its most dorsal extent, the alveus is comprised of myelinated axons from pyramidal neurons in the HPC proper and subiculum which sheath the HPC itself. Just within the HPC, the axons comprising the alveus merge into the fimbria, a fringe of myelinated fibers which coalesce into the fornix for informational output (Schultz and Engelhardt, 2014). Between the alveus and the primary cell layer of the HPC (the pyramidal layer) are the basal dendrites of those pyramidal neurons as well as several interneuron types, which together make up the stratum oriens. The layer of pyramidal neurons (stratum pyramidale) extend their apical dendrites ventrally towards the hippocampal fissure, and the next layer is referred to as stratum radiatum. In CA3 only, another layer known as stratum lucidum exists, which is where mossy fibers from DG granule cells (described below) travel and form synapses with the proximal dendrites of stratum pyramidale (Schultz and Engelhardt, 2014). Conversely, the distal dendrites of these pyramidal cells terminate proximal to the hippocampal fissure, in stratum lacunosum-moleculare (SLM). Below the hippocampal fissure lies the C-shaped structure of the DG, whose principal cell layer is densely packed with granule cell soma. Their spiny dendrites extend into the dentate molecular layer, just on the other

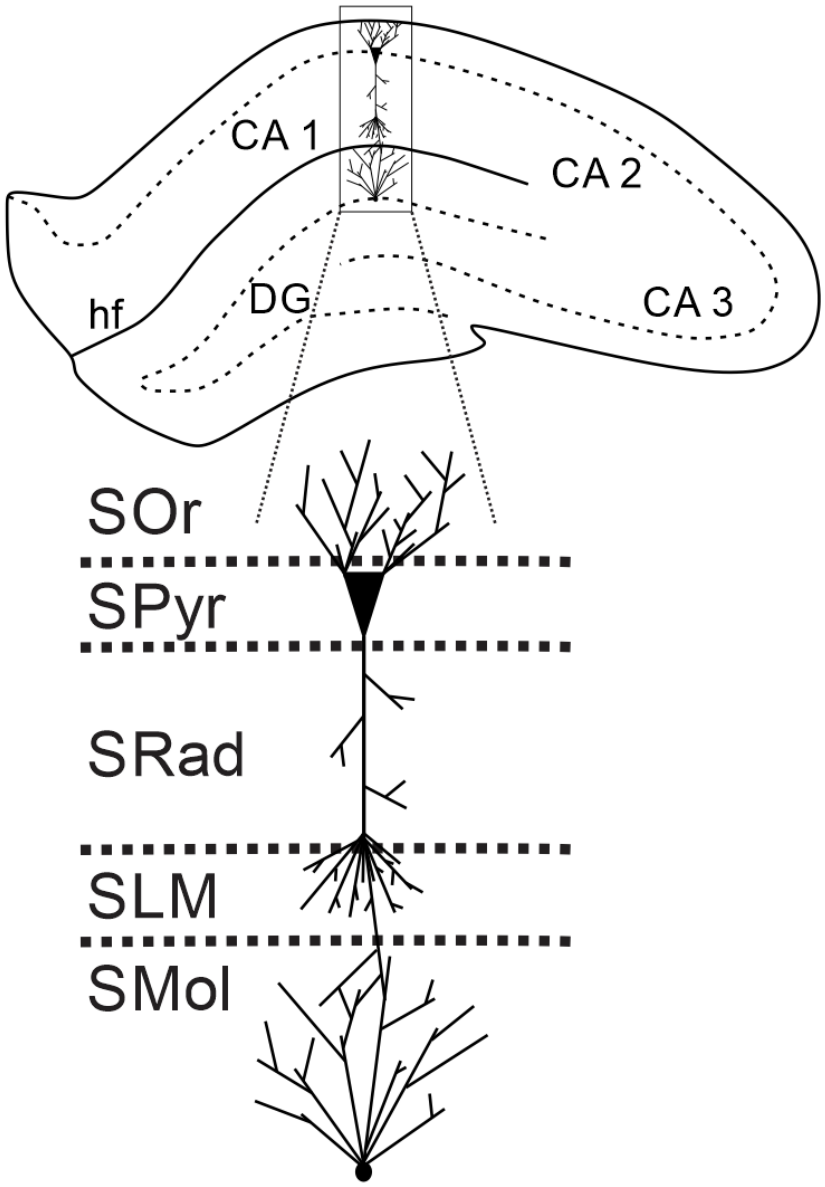

Figure 1.2 Schematic of hippocampal cell lamina.

Schematic illustration of an example coronal section of rat hippocampus. General morphology is outlined, with principal cell layers indicated by dashed lines. The inset shows a schematic cartoon of the major hippocampal cell lamina, from dorsal to ventral, relative to where they occur in a coronal hippocampal section (small rectangle). (hf: hippocampal fissure; CA: cornu ammonis; DG: dentate gyrus; SOr: stratum oriens; SPyr: stratum pyramidale; SRad: stratum radiatum; SLM: stratum lacunosum-moleculare; SMol: stratum moleculare of the dentate gyrus).

side of the hippocampal fissure as stratum moleculare (Schultz and Engelhardt, 2014). The innermost third layer of DG is known either as the polymorphic layer or hilus, whose cells exclusively project within the DG (Laurberg and Sorensen, 1981). The ease with which these numerous and varied lamina can be distinguished (particularly electrophysiologically) because of this horizontal arrangement has no doubt greatly contributed to the extensive study and subsequent understanding of the hippocampus.

The anatomical connections and circuitries inherent to the hippocampus and its various laminae constrain and define its functional operation. Principally, the hippocampus communicates with all parts of the neocortex via the entorhinal cortex (EC; Witter et al. (2017)). This arrangement suggests two main principles for the function of the hippocampus: 1) if the ultimate output targets of the hippocampus are the same as its inputs, this hippocampus should be expected to have some sort of role in processing information (whether mnemonic, limbic, sensory, or otherwise), and subsequently modifying the connections of those inputs; and 2) if all aspects of the neocortex are represented in some capacity in the hippocampus, and those same regions can be updated by the output of the hippocampal-entorhinal circuitry, hippocampal operations should likely reflect neocortical operations (Buzsaki, 1996). The expectation then is that information that reaches the hippocampus via the entorhinal cortex undergoes some kind of processing, and can subsequently modify these original inputs by supplying them with a "reafferented copy" (Buzsaki, 1996).

Briefly, it is worth discussing the organization of the entorhinal cortex in the context of this circuitry. It is, like the rest of the neocortex, 6-layered, with two acellular layers (I and IV; *lamina dessicans*). The superficial cellular layers of EC (II and III) project directly to hippocampus. Layer II projects via the perforant pathway to the dentate gyrus, and via so-called

mossy fibers to CA3. This trisynaptic circuit is completed by the Schaffer collaterals, which relay activity from CA3 to CA1 (Sloviter and Lømo, 2012). The entorhinal cortex can also directly access CA1 via the temporoammonic pathway from layer III. The processed information is then relayed back out from the pyramidal cells of CA1 primarily to the subiculum, which in turn projects to the pre- and para-subiculum (Schultz and Engelhardt, 2014). All three of the subicular cortices then project to the deep layers of EC. A hippocampally processed copy of the information is relayed back to layer Vb in particular, suggesting that layer Vb may be well-positioned as an integrator of sets of information from different sources (Witter et al., 2017).

The hippocampus also notably projects to the mPFC (Rosene and Van Hoesen, 1977; Simons and Spiers, 2003). Prelimbic and infralimbic cortices in particular are targeted by CA1 (Jay and Witter, 1991; Thierry et al., 2000; Hoover and Vertes, 2007). Indeed, it has long been established that there are both direct monosynaptic projections, as well as indirect polysynaptic projections between HPC and mPFC (Hoover and Vertes, 2007; Varela et al., 2014; Jin and Maren, 2015). Injecting retrograde tracers into various mPFC regions robustly label neurons in the subiculum and ventral hippocampus (Jay et al., 1989; Hoover and Vertes, 2007). Consistent with this, injecting an anterograde tracer into HPC showed prominent direct projections throughout the entire rostro-caudal extent of the mPFC (Jay and Witter, 1991). Importantly, these connections all arrive from ventral CA1 and ventral subiculum, without any direct mPFC-projecting neurons found in either dorsal hippocampus or DG (Jin and Maren, 2015). The hippocampus can also access the mPFC via polysynaptic routes, including through the nucleus accumbens and ventral tegmental area, the amygdala, entorhinal cortex, and the midline thalamus (Russo and Nestler, 2013; Jin and Maren, 2015; Wolff et al., 2015). These complex, multi-synaptic afferents via both cortical and subcortical regions are particularly noteworthy

given that some of them are evidently bidirectionally functional (Hoover and Vertes, 2012; Varela et al., 2014). Moreover, the mPFC does not have a direct return projection to any region of HPC, and instead must access it potentially via these multi-synaptic routes (Laroche et al., 2000), although cf. a direct route from ACC to contralateral CA3 (Rajasethupathy et al., 2015).

The physiology of this circuitry has been studied extensively. HPC afferents to mPFC synapse on excitatory glutamatergic pyramidal neurons, terminating on either principal cells or GABAergic interneurons (Carr and Sesack, 1996; Tierney et al., 2004). PFC interneurons reliably fire before PFC pyramidal neurons in response to hippocampal stimulation, suggesting that the direct activity of the hippocampus is capable of feedforward inhibition in this circuitry (Tierney et al., 2004). This inhibitory process can therefore temporally and spatially synchronize large subsets of PFC neurons with ongoing hippocampal activity.

1.2.3 Behavioral and mnemonic implications of prefronto-hippocampal interactions

A long-standing view in the literature is that the hippocampus (and indeed, the medial temporal lobe as a whole) is associated with encoding, storage, and retrieval of long-term memories, while the prefrontal cortex is more often thought to underlie cognitive control processes like selection, engagement, monitoring, and inhibition (Simons and Spiers, 2003).

The hippocampus has an established role in humans and other mammals in underlying a certain type of memory processing. Specific experiences are composed of a representation of the relations between events and the contexts they were experienced in, referred to as episodic memory (Eichenbaum, 2017). The hippocampus also engages in organizing the relations between memories that make up more general knowledge of the world, referred to as semantic

memory (Eichenbaum, 2017). In rodent work in particular, it has become resoundingly clear that the HPC is crucial in tasks requiring the animal to remember events in both the spatial and temporal contexts in which they were experienced (Eacott and Norman, 2004; Langston and Wood, 2010; Eichenbaum, 2017). Spatial memory, particularly as it pertains to updating contextual representations in the face of shifting task exigencies, will be used as an example for the type of episodic memory processing served by the HPC, and how the mPFC plays a key complimentary role.

A direct pathway from the HPC and subiculum to the mPFC has been classically understood to underlie cognitive and emotional regulation of mnemonic processes (Jin and Maren, 2015). Both HPC and mPFC are heavily implicated in working memory processes and, moreover, the communication between them has been suggested to be the critical aspect for underlying this process (Jin and Maren, 2015). Working memory refers to a system of limited capacity that temporally stores information, which is fundamental for the process of human thought or, more generally, the ability for animals to successfully complete complex tasks (Baddeley, 2003). A common behavioural paradigm for rodents tasks spatial working memory by requiring animals to maintain the location of a food reward in mind throughout a delay, in order to successfully navigate to that location afterwards. Asymmetrically inactivating either mPFC or HPC impaired performance on the task, particularly at longer delay latencies (Churchwell and Kesner, 2011). Interactions between mPFC and HPC are as such fundamentally required to successfully complete such tasks. Moreover, increasing the delay length (*i.e.*, requiring the animal to maintain a memory for longer) similarly increases the demand on the functional interactions between HPC and mPFC (Lee and Kesner, 2003).

Perhaps the involvement of HPC in spatial navigation should not be so surprising, given its storied history in navigationally-relevant tasks. A formative study in the field published 50 years ago showed that hippocampal neurons fired selectively whenever a freely-moving rat visited a particular location (O'Keefe and Dostrovsky, 1971). This foundational work suggested that these "place cells" are the neuronal substrate of a cognitive map: a lasting and updatable representation of an animal's position in space (O'Keefe and Nadel, 1978). Further support for this cognitive map theory comes from the firing of place cells being unchanged in darkness (Quirk et al., 1990; Markus et al., 1994), and the ability of place cells to form even in the total absence of normal vision (Save et al., 1998). Animals must form some representation of their environment – regardless of the context in which they experience it – based on their own estimation of direction and distance relative to given landmarks. The hippocampus is as such ideally situated to serve a prominent role in navigation, as a key node in a path integration system (McNaughton et al., 1996). The parahippocampal formation has other useful tools for exploring and understanding spatial environments, including medial EC head-direction cells and speed cells (Sargolini et al., 2006; Kropff et al., 2015). These again indicate that internal representations of space are not purely derived from vision, but based on integration of the animal's own movements in terms of speed and direction.

This circuitry becomes somewhat more complicated considering mPFC-lesioned animals exhibit impaired navigational planning (Granon and Poucet, 1995). Rats in a water maze task could successfully navigate to a hidden platform from a start position they had experienced previously, but could not do so from novel start points. This provided early evidence that the mPFC may be important for supplying the hippocampus with flexible route planning, updating the required spatial representation as a function of the animal's current context (Ito, 2018).

Consistent with this, in a human patient with prefrontal cortical damage, the patient can successfully navigate to a target location only if they are repeatedly reminded of, or asked to recall, their goal while navigating (Ciaramelli, 2008). Successful navigation may therefore require keeping the goal location in mind – a working memory task reliant on the PFC continually communicating with HPC (Spiers, 2008).

One idea is that the prospective activity of the hippocampus is supplied by afferents from elsewhere in the brain: primarily, mPFC (Ito, 2018). Inactivating mPFC (PL and IL specifically) reduces the selectivity of rule-based object associations (*i.e.,* impairs goal representations), and even directly modifies place cell firing variability (Hok et al., 2013; Navawongse and Eichenbaum, 2013). More generally, mPFC appears to accumulate information about the context of inter-related memories and can therefore control the specificity of memory retrieval (Preston and Eichenbaum, 2013). For instance, in a paired-associate learning task, participants learn a list of word pairs (A-B). Subsequently, the cue words are repeated, but are associated with different response words (A-C). Patients with prefrontal damage are fully capable of learning the lists, but are severely impaired in learning the new associates of the original cue words (A-C) (Shimamura et al., 1995). In fact, even if both lists are comprised of unrelated associations, patients with prefrontal damage exhibit compromised memory for one of the lists because of interference from the other (Depue, 2012). In other words, mPFC guides memory retrieval by selecting memories appropriate to the current context or set of rules, while also acting to suppress irrelevant memories. This is consistent with a general schema of the hippocampus rapidly encoding novel information, and the mPFC assisting in guiding the organization, consolidation, and flexible retrieval of memories (Preston and Eichenbaum, 2013).

A descriptive metaphor for this interaction likens the brain to a set of railroad tracks (Miller and Cohen, 2001). The hippocampus lays down new tracks for information, while the mPFC acts as the switch operator, determining which set of tracks is appropriate for optimal and efficient functioning (Preston and Eichenbaum, 2013). Consistently, inactivation of or damage to the mPFC (again, in particular PL and IL) impoverishes the ability of rats to shift from or between "odor" and "place" discriminations (Ragozzino et al., 2003); impairs their performance on a spatial memory task by making it difficult to switch between "place" versus "response" strategies (Rich and Shapiro, 2007); and blocks their ability to shift to the appropriate attentional set (for example, choosing which bowl to select for a food reward based on its odor, what was in the bowl, or the texture of its surface) (Birrell and Brown, 2000). The mPFC and HPC thereby serve complimentary roles in mnemonic functioning, with the mPFC guiding the retrieval of hippocampally-encoded memories appropriate to the current context, while simultaneously resolving conflicts between related and competing memories (Preston and Eichenbaum, 2013).

Perhaps unsurprisingly, both sites have established roles in memory consolidation (Laroche et al., 2000). Directly after learning in a variety of tasks, engagement of the HPC is high, while activation of the mPFC is comparatively low (Eichenbaum, 2017). However, these levels of engagement reverse over the course of several days such that the mPFC (and other cortical areas) become more activated when retrieving remotely acquired memories, and the HPC relatively less so (Eichenbaum, 2017). Damage to or inactivation of mPFC at this point selectively blocks retrieval of remotely acquired memories (Bontempi et al., 1999; Frankland et al., 2004; Maviel et al., 2004). Other work has also shown that, during initial learning, several markers of plasticity are evident in mPFC, despite the temporal delay typically required for mPFC to become critical for representing memories (Lesburgueres et al., 2011; Kitamura et al.,

2017). In other words, mPFC neurons are selected in an activity-dependent "tagging" process upon memory encoding, which critically assists in their maturation and the progressive HPC-driven rewiring of cortical networks (Lesburgueres et al., 2011). This process is consistent with the previously described role of the mPFC in guiding retrieval, as the mPFC becomes increasingly important with time for integrating remotely acquired memories with other contextual and representational information (Eichenbaum, 2017). Consolidation of episodic memories requires a time-dependent dialogue between HPC and mPFC. This dialogue eventually enables distributed cortical networks to both mediate mnemonic recall, as well as independently store remotely-acquired memories (Maviel et al., 2004).

1.2.4 Prefronto-hippocampal neuronal activity and synchrony

Another indicator of the functional relevance for memory and behavior served by the mPFC-HPC circuitry arises when electrophysiological recordings are made from both sites simultaneously. Inter-areal recordings are commonly performed to assess whether fluctuations in neuronal activity are correlated in time – in other words, to measure neural synchrony (Sigurdsson and Duvarci, 2015). Specifically, it becomes possible to assess the degree of cross-correlation of neuronal spike trains, with greater coupling indicative of some degree of inter-regional dialogue. This type of approach revealed temporal correlations between hippocampal ripples and cortical spindles (see section 1.1; Siapas and Wilson (1998)). Moreover, it showed that hippocampal CA1 and mPFC neurons typically spike within ~100 ms of each other during ongoing theta oscillations, and that this correlated firing is enhanced during behaviours which task spatial working memory (Jones and Wilson, 2005; Siapas et al., 2005). The potential leading or lagging of mPFC neurons with respect to HPC neurons is thought to be important for gating

and determining the directionality of information flow through the circuit, in turn guiding the plastic changes required to store information (*i.e.,* form and maintain memories) (Siapas et al., 2005).

Synchrony between mPFC and HPC can also be measured using coherence, which assesses the consistency of fluctuations in phase over time – in other words, how well the phase of one signal predicts the phase of the other. For instance, mPFC-HPC coherence typically increases during performance of a working memory task (Sigurdsson et al., 2010). However, in a genetic mouse model of schizophrenia where mice are impaired in the acquisition of the task, PFC-HPC coherence at theta frequencies was drastically reduced (Sigurdsson et al., 2010). Intriguingly, the magnitude of PFC-HPC coherence at the beginning of training was a reliable predictor of subsequent performance on the task, suggesting that efficient, rhythmic coupling of prefrontal and hippocampal sites is required for optimal behavioral and mnemonic performance. Increased PFC-HPC coherence was similarly shown to be predictive of performance on a spatial memory task (Siapas et al., 2005). Correlated fluctuations in amplitude, or "power correlations" are also a useful measure of inter-regional dialogue, and have been used to demonstrate a role for theta-frequency synchronization between ventral HPC and mPFC in mediating anxiety (Adhikari et al., 2010).

Both the prefrontal cortex and the hippocampus exhibit SO activity. The cortical SO originates most commonly at prefrontal-orbitofrontal regions and migrates caudally towards the hippocampus (Massimini et al., 2004; Greenberg et al., 2016). It has been shown that during SO UP state time frames, the replay of previously learned events occurs in a temporally compressed manner with cortical frames leading hippocampal frames by ~50 ms (Ji and Wilson, 2007b). That considered, task-related firing sequences still appeared in the HPC first, suggesting that the

propagation of the cortical SO to HPC signals that a specific replay event should be relayed back to cortex. Slow oscillatory states may be especially well-suited for this type of interaction, particularly given that hippocampal sharp wave/ripple bursts during slow-wave sleep (SWS) appear to drive PFC neurons to fire consistently within 100ms of HPC cells, while this pattern is sharply attenuated during REM sleep (Wierzynski et al., 2009).

One model that encapsulates this SWS-specific relevance for memory proposes that the cortical SO synchronizes information transfer between neocortex, thalamus, and hippocampus (Born, 2010; Diekelmann and Born, 2010). As briefly mentioned in section 1.1, the SO provides a platform for grouping neuronal activity into temporally coherent bins: UP states of enhanced activity, and DOWN states of neuronal silence. This grouping extends beyond just the cortical SO, into thalamocortically generated spindles (McCormick and Bal, 1997; Staresina et al., 2015) and hippocampally-generated sharp wave/ ripple complexes. These sharp-wave/ ripples accompany the replay of memory events during slow-wave sleep, signaling the transfer of information with the neocortex. As such, the cortical SO can nest both sharp-wave/ ripples from the hippocampus, as well as thalamocortical spindles arriving at the neocortex at the same time in a temporally contiguous manner, optimal for efficient transfer and storage of mnemonically-relevant information (Born, 2010; Diekelmann and Born, 2010).

Concurrently, the UP- and DOWN-states inherent to neocortical slow oscillation provide a window for global synaptic downscaling, preventing an oversaturation of the synaptic networks involved in memory formation (Diekelmann and Born, 2010). This synaptic homeostasis hypothesis was first put forward as a possible explanation for the necessity of sleep, and of slow-wave sleep in particular (Tononi and Cirelli, 2003). Effectively, the longer an animal is awake, cortical circuits get synaptically potentiated by the constant influx of information and novel

demands. This synaptic potentiation is coupled to homeostatically regulating slow-wave sleep, and consequently slow-wave sleep is maximal at the beginning of the sleep episode. The slow oscillations during this stage of sleep provide an opportunity to synaptically downscale these circuits, which in turn leads to the myriad benefits of sleep on performance (Tononi and Cirelli, 2003).

Other oscillatory patterns of activity are common across the mPFC-HPC circuitry. For instance, mPFC neurons preferentially fire more rapidly at certain phases of the ongoing theta rhythm, a phenomenon known as phase locking (Hyman et al., 2005; Siapas et al., 2005). Prefrontal neurons are apparently capable of being more strongly phase-locked to either the past or future phases of the ongoing theta rhythm, suggesting that the directionality of information transfer may be modifiable (Jones and Wilson, 2005). However, phase-locking to the past phases is typically stronger, which may be a consequence of the direct monosynaptic input from ventral HPC to mPFC (Sigurdsson and Duvarci, 2015). Coherence in theta oscillations between PFC and HPC peaks at the choice point in a spatial working memory task, and simultaneously reorganizes the phase of PFC pyramidal neurons to concentrate at the trough of hippocampal theta (Benchenane et al., 2010). The interplay between PFC and HPC is as such capable of dynamically modulating success in a behavioral task, while simultaneously modulating memory performance as a function of inter-regional synchrony.

The comprehensive, behaviorally- and mnemonically-relevant functional interactions between mPFC and HPC are made more intriguing by the total lack of return projections directly from mPFC to HPC (see section 1.2.2; Vertes et al. (2007)). To this end, a wealth of research over the past 15 years has indicated the paramount role that an interposed node may play, in terms of anatomy, electrophysiology, and behavior: the thalamic nucleus reuniens.

1.3 The thalamic nucleus reuniens

1.3.1 History

The term "nucleus reuniens" (RE) ostensibly first appeared in a pair of manuscripts from Edward Malone (Malone, 1910, 1912), in which the diencephalon was divided into "primary nuclei" based on circumscribed groupings of cells with identical histological characteristics. However, these, as well as a later publication (Winkler and Potter, 1914) described the RE as a bundle of cells in the cat thalamus at its most dorsal point, extending across a medial-to-lateral component. The first description of the RE as it is known today came from Gurdjian (1927), who so named the ventral, midline collection medium-sized cells the nucleus reuniens, forgoing the previous name of the structure provided by Winkler and Potter (1914) of "nucleus centralis a." The description and borders of the RE were subsequently further defined in other mammals, and it became noted as one of the most prominent nuclei in the rostral aspect of the thalamus (Rioch, 1929).

1.3.2 Anatomy

The nucleus reuniens lies in a privileged position to underlie reciprocal communication between the medial prefrontal cortex and hippocampus. The RE is a circumscribed body that lies along the midline of the ventral thalamus, and has reciprocal connections to both the mPFC and HPC (Figure 1.3) (Vertes et al., 2007; Varela et al., 2014; Vertes, 2015). In the rat, the RE is approximately 2 mm long and 0.6 mm wide (Wouterlood et al., 1990). The HPC sends direct projections to the mPFC, but there exist no direct reciprocal connections from mPFC to the HPC (Goldman-Rakic et al., 1984; Sesack et al., 1989; Buchanan et al., 1994; Carmichael and Price,

1995; Vertes et al., 2007), although a recent paper has posited the existence of a return pathway from anterior cingulate cortex (Rajasethupathy et al., 2015). Indeed, the dense, monosynaptic HPC-mPFC pathway is important for working memory and memory consolidation, but a different pathway must be engaged for reciprocal communication from mPFC to HPC (Laroche et al., 2000). More recent considerations of neocortico-hippocampal dynamics have discussed the role of the RE in mediating them (Figure 1.4) (Hallock et al., 2016; Ferraris et al., 2018).

In general, the output of the RE is far more circumscribed than are its many and varied inputs (McKenna and Vertes, 2004) (for a comprehensive list, see Wheeler et al. (2013)). The RE projects largely ipsilaterally to CA1 of the HPC (Yanagihara et al., 1987; Wouterlood et al., 1990). Efferents ascend to the genu of the corpus callosum, turn caudally in the cingulate fasciculous/ bundle (CB) before curving around the callosal splenium and forming a massive fibre sheet which innervates the molecular layer of the subiculum; layers I - IV of dorsal lateral entorhinal cortex, layers I - VI of ventral lateral and medial entorhinal cortex; and in the HPC is remarkably restricted to the stratum lacunosum moleculare (SLM) of CA1 (Herkenham, 1978; Yanagihara et al., 1987; Wouterlood et al., 1990; Wouterlood, 1991; Cassel et al., 2013). Indeed, there is a striking absence of projections to CA3 (Herkenham, 1978; Wouterlood et al., 1990). Projections to the HPC are also much stronger from the rostral half of the RE (Wouterlood et al., 1990). While ostensibly different populations of RE neurons innervate the entorhinal cortex, CA1, and subiculum, these groupings are morphologically indistinguishable (Dolleman-Van Der Weel and Witter, 1996). Neurons projecting to the HPC largely arise from clusters in the dorsolateral aspect of RE, while medial septum-projecting cells are distributed primarily in the ventromedial portion of the nucleus (Bokor et al., 2002). These projections are all putatively

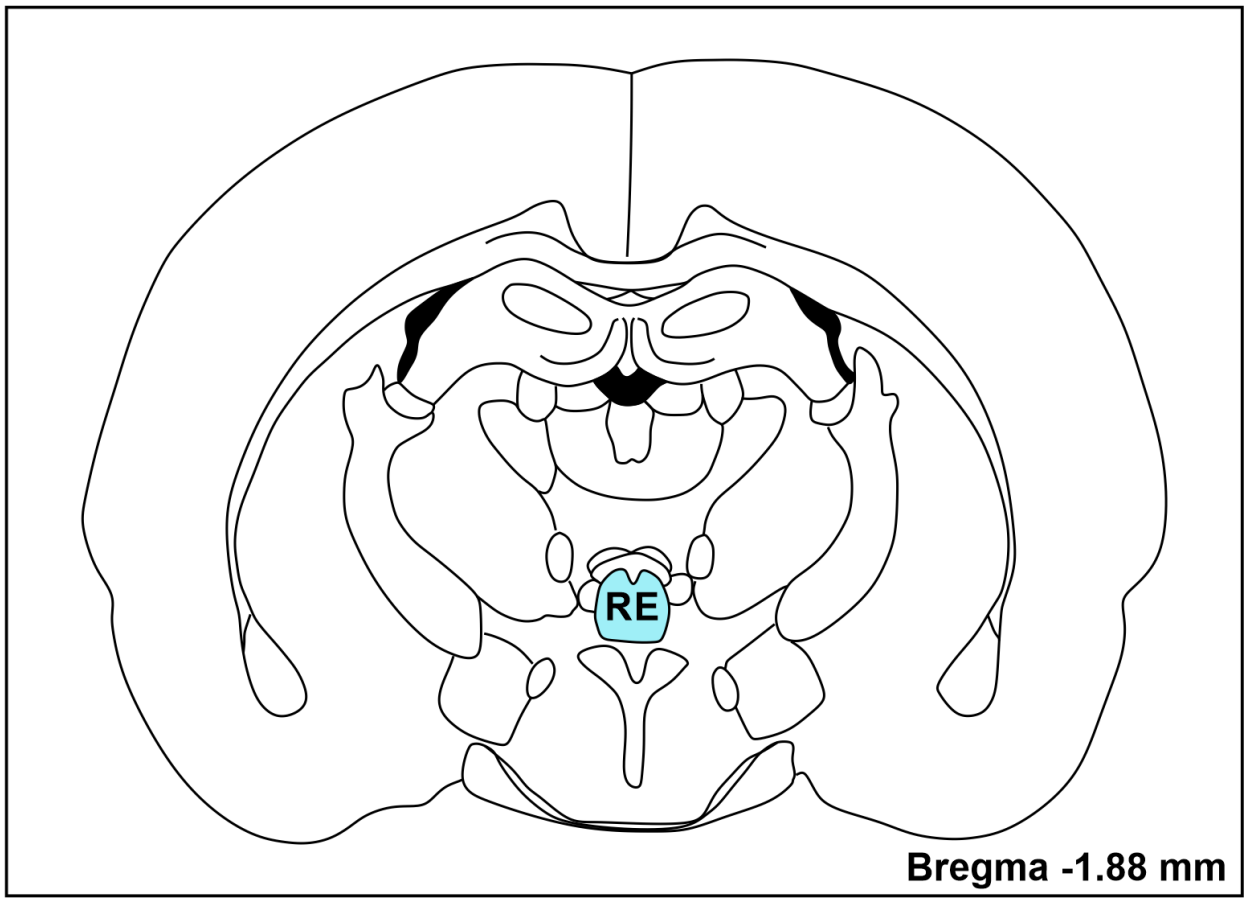

Figure 1.3 Coronal location of the RE.

A schematic depiction of a coronal section of rat brain approximately -1.88 mm from bregma, reproduced from Paxinos and Watson (1998). The RE lies along the ventral midline of the thalamus, and is highlighted in light blue.

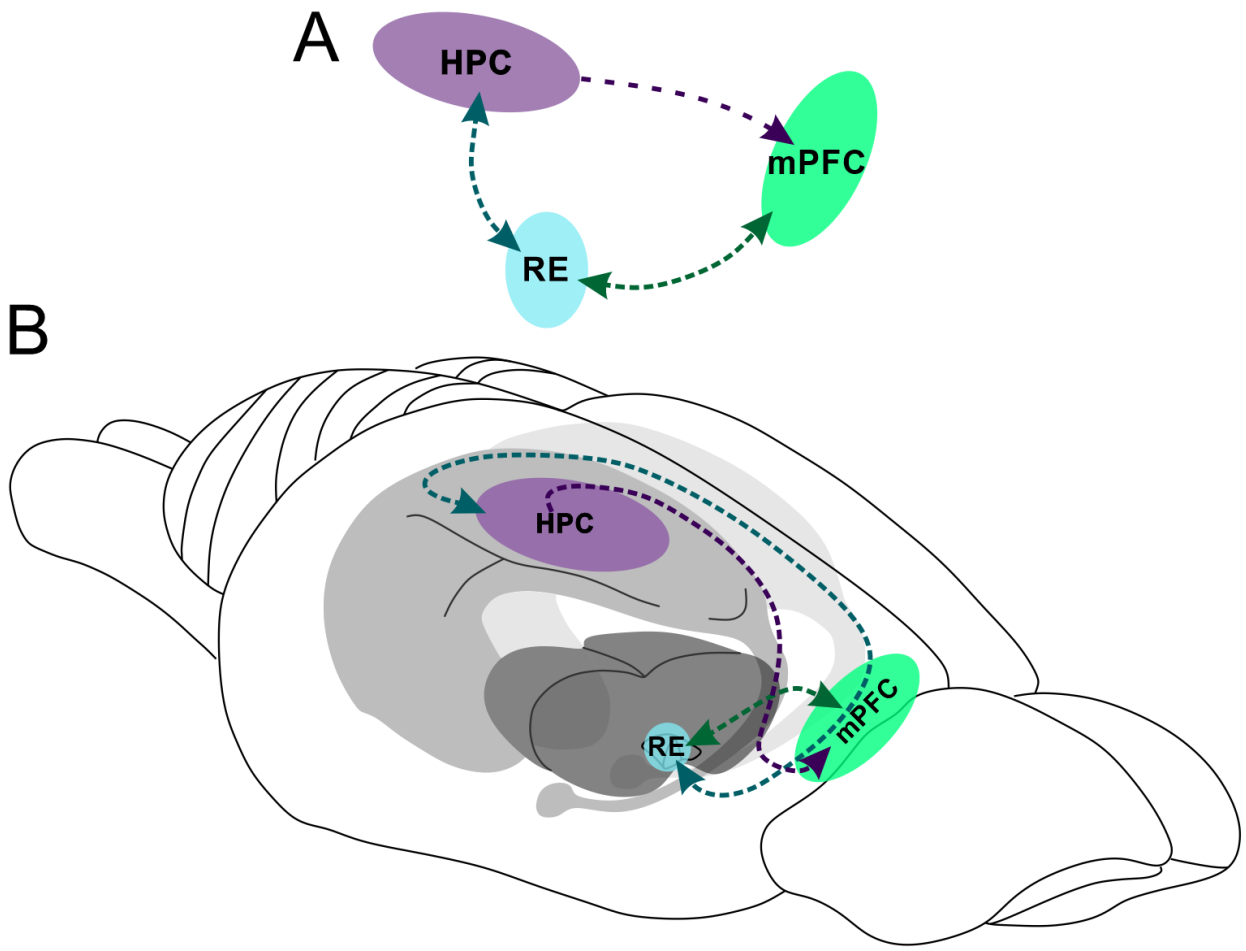

Figure 1.4 Prefrontal-hippocampal connections via the anatomically interposed RE

A. A simplified schematic of the bidirectional connections between RE and mPFC, and between RE and HPC, with the unidirectional input from HPC to mPFC indicated at the top. The RE lies in an ideal anatomical location to mediate a dialogue between these sites. **B.** A 3D schematic rat brain modified from Amaral and Witter (1995), showing the relative locations of each site with a rough approximation of the pathways by which they interconnect.

aspartatergic/ glutamatergic (Bokor et al., 2002), and synapses at the level of HPC are all of the asymmetric type (Wouterlood et al., 1990). The RE is also densely populated with both muscarinic (Frey et al., 1985; Frey and Howland, 1992) and nicotinic (Clarke et al., 1985) cholinergic receptors.

Nucleus reuniens fibers innervate the dendrites of principal cells in both layers II and III of EC (Wouterlood, 1991). RE fibres terminate preferentially on the dendrites of either sparsely spiny or spiny multipolar or pyramidal neurons, and seldom innervate the perikarya, primary dendrites, or axons of these cells (Wouterlood, 1991). These synapses are exclusively of the asymmetric (excitatory) type (Colonnier, 1968; Wouterlood, 1991). The layer I terminating fibers appear to form clusters, and may contact the extensive dendritic arbor of HPC-projecting cells that are located in EC layers II and III (Steward and Scoville, 1976; Wouterlood, 1991). RE fibers projecting to EC layers III and IV are most prominent in the medial subdivision. Layer IV medial EC (MEC) cells primarily distribute their fibers within the EC, suggesting that the RE may have a role in modifying the intrinsic activity and connectivity of the EC (Witter et al., 1989). The RE has a rostro-caudal organization of cortical projections: MEC is innervated primarily by rostral RE; lateral entorhinal cortex (LEC) by caudal RE; and the perirhinal cortex receives fibers primarily from the perireuniens (Vertes et al., 2006).

Projections from EC layer III terminate in the same HPC lamina that the RE itself does, the stratum lacunosum-moleculare (Witter et al., 1988; Wouterlood et al., 1990; Vertes et al., 2007). The RE, as such, is capable of influencing the transmission of cortical information into the HPC at the site of its termination in CA1 (Wouterlood et al., 1990). The exact nature of this influence, and how it may alter forebrain activity dynamics, have only recently begun to be explored (Dolleman-van der Weel et al., 2017; Vu et al., 2020). It is apparent that the RE-CA1

synapse is capable of displaying paired pulse facilitation, long term potentiation, and gamma oscillations more readily than the EC-CA1 synapse, suggesting a specialized role of the RE circuitry in memory processing (Vu et al., 2020). Additionally, an anatomical projection from caudal to rostral RE has been demonstrated (Dolleman-Van der Weel et al., 1997). This suggests that an entire, closed loop circuitry exists as: rostral RE → CA1 → subiculum → caudal RE → rostral RE, which could modulate CA1 activity directly as a function of hippocampal output (Dolleman-van der Weel et al., 2019).

The RE receives input from the mPFC throughout its dorsal-ventral extent, with particularly dense projections arising from prelimbic (PL) and infralimbic (IL) cortices (McKenna and Vertes, 2004; Vertes et al., 2006; Vertes et al., 2007). Most mPFC inputs to the RE arise from layer VI, with some additional inputs from layer V (Mathiasen et al., 2019). Between 3-9% of RE cells have collateral projections to both mPFC and HPC (Hoover and Vertes, 2012; Varela et al., 2014).

1.3.3 Electrophysiology

Midline thalamic nuclei first began to attract the attention of electrophysiologists when electrically stimulating nonspecific regions of a cat thalamus produced widespread disruptions in ongoing cortical activity (Jasper, 1949). Stimulation of midline thalamic nuclei produced an initially surface-positive wave, followed by a larger surface-negative wave. Repeated stimulation facilitated cortical responding, which Arduini and Terzuolo (1951) attributed to increased recruitment of thalamic neurons. Further, the authors described a slow, periodic fluctuation in the excitability of either the cortex or of the thalamo-cortical system; an idea that would be pursued decades later in the foundational work of Mircea Steriade. Thalamic nuclei strongly influence

cortical activity by modulating UP and DOWN states, and indeed, "to a large extent, what goes on in the cortex depends on state-related alterations in thalamic activity" (Steriade and Llinas, 1988).

The RE constitutes the principal source of excitatory thalamic input to the HPC (Vertes et al., 2007), forming a disynaptic link between mPFC and HPC (McKenna and Vertes, 2004; Prasad and Chudasama, 2013). Despite the rapidly increasing interest in the role of RE in the context of a mPFC-HPC circuit, very few electrophysiological studies have assessed RE-mediated responses in either mPFC or HPC. Perhaps the first to directly assess this showed RE stimulation generates a subthreshold depolarization of CA1 pyramidal cells, with a suprathreshold excitation of inhibitory interneurons in the alveus, *stratum oriens*, and *stratum radiatum* (Dolleman-Van der Weel et al., 1997). A follow-up to this work showed that both RE and EC axons form synapses onto the same dendritic compartments of CA1 (Dolleman-van der Weel et al., 2017). This suggests that the RE-CA1 synapse is capable of directly modulating the entorhino-hippocampal dialogue via their common inputs at the *stratum lacunosum-moleculare*, helping to synchronize inputs across the circuit. RE stimulation was also compared against CA3 stimulation for its ability to excite CA1, and exhibited a powerful monosynaptic influence capable of bypassing the classic trisynaptic circuit (see section 1.2.2; Bertram and Zhang (1999)). Similarly prominent, monosynaptic excitation was observed in the amygdala and entorhinal cortex as well, suggesting a potentially significant role in regulating and synchronizing limbic physiology (Zhang and Bertram, 2002).

More recently, Di Prisco and Vertes (2006) recorded electrophysiological activity along the dorsoventral axis of the mPFC, while simultaneously stimulating either the RE or the nearby interoanteromedial nucleus (IAM). They found that RE stimulation produced the most profound

field potentials at both the IL and PL, while stimulation of the IAM did not produce any robust potential. This confirmed the authors' hypotheses both that the IAM is a "null zone" and that the RE has a strong, monosynaptic excitatory influence on the mPFC. Direct, monosynaptic release of glutamate onto mPFC neurons by RE efferents has also been shown, providing more evidence of excitatory control by RE within the context of this circuit (Pirot et al., 1994; Hur and Zaborszky, 2005).

1.4 Role of the nucleus reuniens in memory

The RE is increasingly being implicated in a host of behavioural and memory-relevant tasks and conditions. While the central role of the RE in many of these processes is encouraging for the future of the field, the focus of this thesis is on types of behavior and memory in particular that are known to require an active dialogue between mPFC and HPC. While by no means exhaustive, the following sections are designed to highlight the robust role played by RE in mediating communication between mPFC and HPC, as evidenced by the remarkable impact it has on behaviors and memory of different types. Generally speaking, any task or type of memory known to be impaired by a compromised dialogue between mPFC and HPC will show that a similar pattern emerges following inactivation or lesioning of the RE, at least in tasks where the role of the RE has been thoroughly investigated so far. The RE, in particular, appears to have a critical role in memory retrieval and encoding processes, and these will be highlighted across various behavioral paradigms and memory types.

1.4.1 Behavioral flexibility

One of the most widely studied and consistent phenomena in RE-centric behavioral assays is its pronounced role in behavioral flexibility. This is perhaps an expected outcome considering 1) the pronounced role of the mPFC in allowing animals to flexibly switch rulesets in response to changing context via its interactions with the HPC (see section 1.2.3), and 2) the robust monosynaptic input RE receives directly from mPFC (see section 1.3.2). The first behavioral RE lesion study described a role for the RE in the inhibitory control of impulsive, anticipatory behavior in rats in a jumping test (Flamig and Klingberg, 1978). Similarly, the first RE lesion study to be conducted using a water maze task examined a dissociation between medial thalamic and hippocampal involvement in spatial navigation (Cain et al., 2006). Rats had to remember and utilize spatial cues in the environment to successfully escape a pool, and were either non-spatially pre-trained or not. Pre-training involved rats being placed in the pool with the platform visible and without surrounding environmental cues. This both reduced stress during subsequent experimental testing while also allowing animals to learn the required behavioral strategies for navigating the task, with the end result being that the authors could separate the behavioral strategies-learning component from the actual spatial learning component. They found that naïve rats were significantly impaired with either medial thalamic or HPC lesions, but that both groups could complete the task if they had been pre-trained. This demonstrated an impairment of naïve medial thalamic-lesioned animals to acquire necessary behavioral strategies to complete the task, as indicated by a severe inability to find a visible platform throughout 3 days of training, even when they began by facing it. However, if they could learn the required behavioral strategy before testing (as in the pre-trained animals) they performed as well as controls and quickly learned to find the hidden platform. Pre-trained HPC-lesioned animals used appropriate strategies, but were impaired in place responding, consistent

with previous literature (O'Keefe and Nadel, 1978; Morris et al., 1982). This highlights a dissociation between the tested structures, with a clear role of the midline thalamus in learning water maze behavioral strategies, and the HPC in spatial mapping and memory.

A subsequent paper examined the role of the RE specifically for its role in strategy shifting and behavioral flexibility, again using the water maze task (Dolleman-van der Weel et al., 2009). Again, the RE did not appear to be critical for learning and memory in the water maze task *per se*, but contributed to non-mnemonic strategy shifting. RE-lesioned rats rapidly learned the task and swam directly to the platform, but on subsequent platform-removed probe trials, they would swim to its location but not stop and explore locally. Indeed, the RE appeared to have a unique role among those structures studied, separate from HPC-related spatial learning and mPFC-related strategies in a water maze task (i.e., RE-lesioned rats also did not perseverate, a hallmark of mPFC-lesioned animals (Baddeley, 2003)). Its function instead appeared to be suppressing inappropriate or impulsive strategy shifting, which was the opposite of mediodorsal nucleus lesioned animals in the same study, who regularly perseverated with inappropriate responses. It would appear, then, that there is an impaired mPFC-HPC dialogue in RE-lesioned animals, where the RE-deficient animal is able to switch its strategy rapidly, but ineffectively given the spatial memory info provided by the HPC. The RE is a critical link in a HPC-mPFC-RE-HPC circuit that, behaviourally, suggests that the RE lesions do not impact tasks thought only to task the HPC, but *do* impact tasks thought only to rely on the mPFC.

Consistent with this, rats with local infusions of $GABA_A$ agonist muscimol into the RE and adjacent rhomboid (Rh) nuclei did not impair rats' capacity to find the platform in a similar water maze task (Cholvin et al., 2013). Muscimol infusions were also made into the mPFC and dorsal HPC on different days within the same animals, and only those with dorsal HPC lesions

showed spatial memory deficits. This was compared against a novel paradigm, the double-H maze, wherein rats made either right-left or left-left turns for a small food reward, and then in a misleading probe, had to switch their strategy from a previously effective but now ineffective strategy based on spatial memory. The authors found that bilateral muscimol infusions into either the mPFC or HPC induced major deficits in strategy shifting or spatial memory, respectively. Inhibiting the RE produced as large deficits in both strategy shifting and spatial memory, suggesting that all three structures participate in behavioral adaptations invoking a place strategy. The authors suggest that RE inactivation impairs the shift-triggering process when a previously useful strategy is no longer appropriate. In essence, the RE relays set (or strategy) shifting information from the mPFC to the spatial memory substrate of the HPC to update a strategy in response to changing environmental demands. This effect was also seen in rats with lesions to the RE/Rh, who were impaired on an attentional set shifting task, which is designed to test prefrontal function (recall the importance of mPFC-HPC interactions for attentional set shifting in section 1.2.3; Linley et al. (2016)). More specifically, lesioned rats were impaired on reversal learning (*i.e.,* they could not efficiently switch strategies and showed deficits in their capacity to transfer or generalize rules of the task). Again, the authors conclude that the RE contributes to flexible goal-directed behavior.

As a further demonstration of the involvement of RE in behaviors that almost solely enlist the mPFC, Prasad et al. (2013) lesioned the RE and demonstrated an increase in premature responding in the 5-choice serial reaction task, a prefrontal-dependent test of visuospatial attention and inhibitory control. Interestingly, the impairment was only observed with a variable intertrial interval schedule on the task, which had animals remember the location of a visual stimulus in a delayed non-matching to position paradigm. Rats then had to inhibit premature

responding in anticipation of the next stimulus (which RE-lesioned rats were significantly impaired at), as well as inhibit responding to a previously correct choice (*i.e.*, perseveration, which RE-lesioned rats performed similarly to controls at). The failure of impulse control/ inhibition observed in these animals is comparable to animals with lesions to the infralimbic cortex (Chudasama et al., 2003), which projects robustly to the RE (section 1.3.2; Vertes (2002, 2004)). The striking absence of perseverative errors in a task known to tax the mPFC is consistent with Dolleman-van der Weel et al. (2009), who would predict an increase in perseveration only with mediodorsal nucleus ablation, but not RE.

In contrast to previous literature, a recent study from this same group made excitotoxic lesions in the RE and assessed subsequent performance on a host of prefrontal-dependent tasks (Prasad et al., 2017). Interestingly, the authors found that lesioning the RE *enhanced* executive functioning by improving several cognitive operations including attention, response control, and some aspects of learning. They attribute this to a role of the RE in balancing a circuit involved in arousal and alertness because of ascending afferents from the brainstem. Crucially however, these attentional improvements did not extend into memory function or cognitive or behavioral flexibility. Indeed, RE-lesioned rats were impaired on a radial arm maze task, making repeated perseverative errors only when tasked with no delay. This also directly opposes their earlier findings (Prasad et al., 2013) in which RE-lesioned animals did not perseverate with incorrect responses, and equally opposes literature highlighting the importance of delay in behavioral tasks (Davoodi et al., 2009; Davoodi et al., 2011; Loureiro et al., 2012; Barker and Warburton, 2018). However, that RE lesions impair optimal searching of spatial contexts, rather than impacting spatial memory *per se* is consistent with other literature (Dolleman-van der Weel et al., 2009; Hembrook and Mair, 2011; Cholvin et al., 2013).

A recent study examining reversible inactivation of the RE on a spatial alternation T-maze task produced a failure in win-shift strategy as well as severe spatial perseveration (Viena et al., 2018). Muscimol-induced RE inactivation impaired behavioral flexibility and impaired successful response strategy selection at 30, 60, and 120 s delays, demonstrating that the RE is involved not only in spatial working memory, but guides goal-directed behavior and executive functioning. Interestingly, when procaine, a sodium channel blocker, was used to inactivate the RE instead, impairments were only noted at the longest delay condition, which the authors speculate is a consequence of being shorter acting than muscimol, having a different effective diffusion/ spread, or that an inadequate concentration was used. Regardless, they attribute the surprising perseverative behaviors to an impaired dialogue between the HPC and the orbital cortex, a circuit which is also mediated by the RE. Future work will continue to elucidate the role of RE vs mediodorsal nucleus vs orbital cortex in the perseverative deficits observed in some studies (Prasad et al., 2017; Viena et al., 2018) but not others (Dolleman-van der Weel et al., 2009; Prasad et al., 2013).

The observed impairment in win-shift strategies as a consequence of RE/Rh lesions also extends to other behavioral paradigms, including the radial arm maze (Hembrook and Mair, 2011) and delayed non-match to position tasks in general (Hembrook et al., 2012). Critically, for impairment to be observed, the task must rely jointly on activity from both the mPFC and HPC, and not just the HPC (if mPFC tasks alone are impacted by RE lesions is still a matter of debate; cf. Dolleman-van der Weel et al. (2009)). Rats with local infusions of muscimol into the RE were tested on two different delayed conditional discriminations (Hembrook et al., 2012): a delayed non-match to position task, known to depend on interactions between mPFC and HPC; and a varying choice delayed non-matching paradigm, which is affected by HPC lesions but not

by mPFC lesions (Porter et al., 2000). RE lesioned animals were impaired on the delayed non-match to position task, but not on the varying choice task. This, again, indicates that the RE affects measures of spatial working memory that depend on interactions between HPC and mPFC, but not on measures that depend on the HPC alone.

1.4.2 Delay length is critical

An important consideration in determining the extent of behavioral changes invoked by an inactivated or lesioned RE is whether a delay is introduced and how long it lasts. Delayed alternation tasks refer to a spatial working memory paradigm in rodent research wherein the animal must remember and alternate its response on each subsequent trial, with a delay of variable length imposed between trials (Dudchenko, 2004). This task has been demonstrated to rely on the dorsal HPC (Ainge et al., 2007; Czerniawski et al., 2009), as well as the mPFC (Kolb et al., 1994). The delay aspect appears to be critical for determining the relative involvement of the HPC or mPFC; at short delays, the structures may operate independently of each other, but HPC-mPFC communication is critical with longer delays (Churchwell and Kesner, 2011). Consistently, a recent study demonstrated a role of the RE in the delayed alternation task, with more pronounced deficits from RE-inactivation observed with longer delays (Layfield et al., 2015). This highlights a recurrent and key finding in the RE memory literature: behavioural paradigms that task both the mPFC and HPC also involve the RE in some capacity, suggesting that the RE is a critical node in normal mnemonic processes.

A pair of studies examined the importance of timing when inactivating the RE in a water maze (Davoodi et al., 2009) and passive avoidance task (Davoodi et al., 2011). In the former, the RE was inactivated with tetracaine before or immediately after training, or before the probe trial in subsequent retrieval tests. RE inactivation before training impaired learning of the task, and

inactivation immediately after learning impaired consolidation as evidenced by impaired performance in the probe trial. Similarly, inactivation directly before the probe trial impaired retrieval, suggesting that the RE is involved in spatial reference memory and working memory at all time points. This result has been contested by numerous subsequent studies, including a follow-up by the same group wherein the RE was again transiently inactivated using tetracaine 5 minutes before acquisition of a passive avoidance task, or 5, 90, or 360 minutes after acquisition (Davoodi et al., 2011). Here, inactivation prior to training did not impact acquisition, but impacted memory retention 24 hours later. Interestingly, inactivating the RE 5 minutes after training also impaired consolidation, but inactivation after 90 or 360 minutes did not have an impact, suggesting that the RE's involvement in a limbic memory circuit is biased toward the onset of memory formation. However, as with their previous study, inactivating the RE before the probe trial impaired retrieval. This is directly at odds with work demonstrating that a lidocaine infusion into the RE 15 minutes before the probe trial in a water maze task did not impact memory retrieval at all (Loureiro et al., 2012). Interestingly, excitotoxic but fiber-sparing NMDA lesions of the RE had no impact on probe trial performance 5 days after training, but caused a significant impairment in performance 25 days later (Loureiro et al., 2012). This was supported by c-Fos expression in the RE in a group of non-lesioned animals, which showed no change in expression 5 days after water maze training, but a stark increase 25 days later. Compared with Davoodi et al. (2009), whose animals could not learn a water maze task at all without the continuous online involvement of the RE, these discrepant findings are hard to rectify. These authors however did not test animals in the maze at any time point greater than 24 hours post-training, and the nature of their inactivation may also have important ramifications for the involvement of the RE. Note that Viena et al. (2018) also used a local sodium channel

blocker to inactivate the RE and found differential results from a $GABA_A$ agonist in the same behavioral paradigm, suggesting that fibres of passage may be critically important in the mPFC-RE-HPC circuit.

A recent study demonstrated a role of the RE in encoding and retrieval long-term object-in-place (associative recognition) memory, but not for remembrance of an individual place or object (Barker and Warburton, 2018). Consistent with Davoodi et al. (2009) and Davoodi et al. (2011) infusion of muscimol into the RE 15 minutes before the test phase impaired performance on the object-in-place task. Moreover, the authors found that encoding (but not retrieval) was dependent on muscarinic and nicotinic cholinergic neurotransmission, whereas NMDA receptor neurotransmission was unaffected. They argue based on these delay-dependent deficits that the RE actively modulates information processing during long-term associative memory formation and is not just a simple relay node (Barker and Warburton, 2018). Concordantly, the RE was further shown to be critical for memory retrieval in a spatial paradigm (Mei et al., 2018). Inactivating the RE with muscimol immediately following training sessions did not impact acquisition of the spatial task, nor memory retention of it 20 days later. However, inactivating the RE in already well-trained rats immediately before maze exposure significantly impaired task performance, highlighting once more a vital role of the RE in memory retrieval in this PFC-HPC dependent pathway (Mei et al., 2018). It is curious that these authors did not show an effect of "offline" mnemonic processing, at least in the time window immediately following learning. It will be vitally important for future researchers to carefully consider the time windows for interventions or modulations of RE activity, especially as they pertain to consolidating memories during offline states between PFC and HPC. That is, interrogating the distinction between the

RE's involvement in "early" versus "late" mnemonic processing will have profound implications for memory consolidation in general.

1.4.3 Spatial working memory

As discussed in section 1.2.3, the mPFC and HPC have cooperative but distinct roles in spatial working memory tasks. Their interaction is fundamentally required to successfully navigate an environment with changing contexts, rules, or contingencies (Churchwell and Kesner, 2011). Requiring the animal to maintain their memory of the environment or the appropriate rule-set for exploring it for longer durations increases the demand on the functional interactions between mPFC and HPC (Lee and Kesner, 2003). The interposed RE as such emerges as a likely candidate for maintaining, modulating, and supporting this type of memory.

While a role in spatial working memory has been repeatedly demonstrated, the specialized role of the RE and its cells in assisting with a host of spatial memory tasks has only recently been assessed. One of the first publications to highlight the involvement of the RE specifically in a spatial memory task used a modification of the 8 arm radial maze paradigm (Vann et al., 2000). Two groups of rats were trained to visit each of the 8 arms in a maze for a small food reward in one of two distinct rooms. Then, on the testing day, the experimenters brought the maze into a room that the rats had not been trained in, providing them an entirely new set of cues to use in navigation. They found significant increases in c-Fos expression in the anterior thalamic nuclei, as well as in the RE and rostral reticular nucleus over rats who were tested in the same room that they were trained in. Moreover, they found c-Fos increases in the PL, providing evidence for a group of anatomically related structures (recall the robust connectivity between PL and RE; Vertes (2002, 2004)) that work cooperatively during

allocentric spatial working memory tasks, thus providing some of the first evidence for a role of the RE specifically in spatial memory. Subsequent work also found a role for the RE in spatial memory in a water maze task, though the results and implications of this work have been disputed (Davoodi et al. (2009), see discussion in section 1.4.2).

A more recent paper was the first to describe a population of head directions cells in the RE (Jankowski et al., 2014). These cells, previously demonstrated in the dorsal tegmental and lateral mammillary nuclei (the latter of which innervates the RE) behaved like previously described head direction cells. They signaled head direction in the horizontal plane, established directionality rapidly upon entering an environment, maintained that directionality during dark-light transitions, did not re-map across days, and were unaffected by arena shape. This group subsequently described both place cell and perimeter/border cell populations within the RE (Jankowski et al., 2015). The authors suggest that the RE represents a special case among structures with direct HPC afferents, given that similar sites do no exhibit similar spatial properties and relatively lack place cells. They discuss potential roles for the RE in providing spatial input to the HPC to aid in spatial computations, or that the RE may reflect an entirely parallel spatial system in the brain (Jankowski et al., 2015). In any case, the RE is evidently part of a signalling cascade that can directly modulate CA fields in the HPC and, as such, spatial processing. Indeed, RE activity modulates firing rates of CA1 cells as a function of prospective trajectory in a spatial navigation task (Ito et al., 2015). Interestingly, the CA3 subfield demonstrated almost no goal-directed firing, which the authors posit is due to a complete lack of RE input. Projections from the mPFC via the RE to CA1 are critical for representing a rat's future path for goal-directed behavior.

The RE is also critical for the long-term spatial stability of CA1 place fields (Cholvin et al., 2018). Lesions of the RE and adjacent rhomboid nucleus in rats produced a pronounced and long-lasting decrease in place field stability, and altered firing rate variability in place cells. It appears that in rats without a functional RE/Rh, exploring a novel environment interferes with the representation of a familiar one, decreasing the place field stability in both (Cholvin et al., 2018). Similar implications for the RE in mediating long-term spatially-related memories were supported by increased c-Fos expression in the RE specifically 25 days after training in a water maze task, but not after 5 days (Loureiro et al., 2012). As mentioned briefly above, this supported findings from RE lesions impoverishing probe trial performance at 25 days, but not at 5 days. The authors conclude that the RE is a necessary component of a circuit underlying long-term systems consolidation via its modulation of dorsal HPC CA1 fields. Recent work has continued to demonstrate that the RE contributes to memory by modulating spatial information processing in HPC. Electrolytics lesions of the RE and Rh impaired performance on a novel object place task, but only in the latter half of the exploration period, which the authors attribute to RE/Rh contributing to the between-session similarity of CA1 place maps (Jung et al., 2019).

1.4.4 Fear memory specificity

The RE has a role in determining the generalization and specificity of contextual fear memories (Xu and Sudhof, 2013). Inactivating either RE or mPFC enhanced fear memory generalization to unconditioned contexts in a contextual fear memory discrimination task. This was a direct follow-up to an earlier study from the same group, wherein impairing synaptic transmission in the mPFC unexpectedly caused over-generalization of fear memories (Xu et al., 2012). Considered together, these studies led the authors to propose that the mPFC modulates

memory trace representation in the HPC via the RE. A captivating finding from their work also highlighted that not only is the presence or absence of the RE important for fear memory generalization, but that direct optogenetic activation of RE had a differential effect as a function of the stimulation parameters (Xu and Sudhof, 2013). Phasic (30 Hz pulses for 0.5 s every 5 s) activation of RE during memory acquisition produced over-generalization of fear memory, while tonic (stimulus trains at 4 Hz) activation reduced fear generalization. This suggests that the activity states of the RE are integral for optimal memory function, and that different states may serve different functions.

Further evidence for a role of the midline thalamus in mediating fear memory networks came from a brain-wide activity-dependent c-Fos labelling study (Wheeler et al., 2013). Similar to the previous work of Vann et al. (2000) wherein the involvement of the midline thalamus in a host of spatial tasks was implicated using activity-dependent neuronal tagging, a functional connectome for long-term fear memory was assessed using c-Fos expression, though this time in mice and on a much wider scale (Wheeler et al., 2013). Mice were trained in a contextual fear conditioning paradigm, and then sacrificed and histologically analyzed either 1 day or 36 days post-training. The authors found that memory organization changed as a function of age, and implicated the RE (along with the ACC and PL) as connector hubs positioned to mediate global connectivity. This again highlights a potential role of the RE in systems consolidation, given that mPFC became increasingly correlated with cortical, thalamic, and HPC networks at 36 days post-training. Indeed, they conclude by saying the RE is "ideally positioned to influence network functions," especially in fear memory-relevant circuitry (Wheeler et al., 2013). A direct follow-up to this work used both *in silico* and *in vivo* methods of either deleting or chemogenetically inhibiting various nodes involved in the fear memory network (Vetere et al., 2017).

Consolidation was impaired by the chronic chemogenetic inhibition of only 4 (of 21) tested nodes, two of which were CA1 and the RE. This shows decisively that neural activity in the RE is important for consolidation, in this case for fear memories in particular (Vetere et al., 2017).

1.4.5 Consolidation

Throughout the preceding sections, I have described the role of the RE in mediating memory performance in a host of "online" behavioural tasks. I have also highlighted the important function of the RE in "offline" mnemonic processing, particularly for consolidation. In this section, I will synthesize the body of behavioural work which indicates a crucial role of the RE in offline memory consolidation.

Some of the early behavioural work assayed the function of the RE in a classic episodic (spatial) memory paradigm, as well as a passive avoidance task. Inactivation of the RE immediately after learning the location of the goal platform in a water maze task impaired consolidation, indicated by impaired performance on the probe trial (Davoodi et al., 2009). Consistent with this, inactivating the RE immediately before or after acquisition of a passive avoidance task impaired its consolidation, decrementing memory retention 24 hours later (Davoodi et al., 2011). Inactivation after 90 or 360 minutes did not impact consolidation, suggesting that the RE's role in episodic memory consolidation is biased towards the onset of memory formation and may be a key mediator in the HPC-mPFC memory dialogue (see section 1.2.3). Interestingly, lesioning the RE before acquisition of a water maze task caused significant performance deficits 25 days later, but not 5 days later (Loureiro et al., 2012). The authors also show increased c-Fos expression at the 25 day mark, compared to no change at 5 days. This, too, is consistent with other work showing increased c-Fos expression in the RE 36 days post-training

in a contextual fear paradigm, suggesting the RE may be important for the long-term formation of mPFC-HPC dependent episodic memories (Wheeler et al., 2013). Indeed, a recent study also showed that the RE is important for the offline consolidation of contextual fear memories (Quet et al., 2020).

Infusion of the protein synthesis inhibitor anisomycin into RE impaired memory performance in an associative recognition task after a 24 hour but not 3 hour delay, suggesting that the RE participates in long-term object-in-place memory consolidation (Barker and Warburton, 2018), An important caveat is that anisomycin profoundly suppresses neural activity (Sharma et al., 2012) and has been shown to disrupt basic neuronal membrane properties (Scavuzzo et al., 2019). These findings (Barker and Warburton, 2018) however are consistent with our schema that it is the activity of the RE which is critical for mediating the mPFC-HPC dialogue, particularly as it pertains to the offline consolidation of episodic memories. Consistently, down-regulating RE activity using an inhibitory chemogenetic approach immediately after training in a spatial working memory paradigm impaired consolidation (Schwabe et al., 2021). RE inactivation also reduced the cellular activity marker and immediate early gene EGR-1 in the RE 1 hour after learning, which supports the notion that reduced RE activity impairs the formation of object location memories (Schwabe et al., 2021).

Mechanistically, the RE may be involved in mPFC-HPC-related memory consolidation by directly modifying hippocampal connectivity and prefrontal spinogenesis following learning (Klein et al., 2019). Lesions were made to the RE and adjacent rhomboid nucleus (Rh) before training in a water maze, with a probe trial performed 5 or 25 days post-acquisition. Spatial learning significantly increased dendritic spines in dorsal CA1 which were persistent at both delays in sham animals, but not in RE/Rh lesioned animals. In mPFC, dendritic spines had

robustly increased 25 days post-acquisition in sham animals, but not in those with RE/Rh lesions. Expression of c-Fos was also significantly lower in the mPFC following RE/Rh lesions (Klein et al., 2019). Together, these data indicate that the RE is key participant and mediator in the mPFC-HPC memory consolidation dialogue (Ferraris et al., 2021).

1.5 The role of the nucleus reuniens in coordinating PFC-HPC interactions – summary of findings

In Chapter II, I investigate the role of the RE in potentially mediating slow oscillatory coordination between PFC and hippocampus. Our lab has previously shown that the neocortical and HPC SO's are dynamically coordinated, with a potential local generation of SO hinted at in SLM in particular (Wolansky et al., 2006). We investigated the role of the RE in mediating that coordination, as one of only two inputs (the other being EC layer III via the temporoammonic pathway) to directly innervate SLM. It was first necessary to describe the single unit activity of the RE to provide the first clues that it may have relevance for SO timing. Indeed, I show that RE alternates between two primary activity states as a function of global forebrain state: a rhythmic ~1 Hz firing mode that is dynamically coupled to the PFC SO, and a tonic firing mode during theta. Subsequently, I show that optogenetic stimulation of RE as well as of its HPC-afferents coursing through the cingulum bundle reliably produce a robust excitation of SLM. Taking a step back in the circuitry, I show that electrical stimulation of IL similarly evokes a HPC response that is maximal at SLM. Finally, I show that chemogenetically inactivating the RE selectively decrements SO coherence between PFC and HPC, and abolishes the robust current sink at SLM following IL stimulation. This indicates that the RE plays a key role in mediating the SO

dialogue between these two critical memory centers, and as such may be well-positioned to modulate or partially underlie the offline consolidation of memory.

Chapter III investigates a peculiarity first noted while conducting the experiments in Chapter II: Namely, that the HPC response achieved in response to either RE or mPFC stimulation appeared markedly different depending on brain state. I first show that the magnitude of responding in HPC to optogenetic stimulation is markedly greater during SO states. I also show this is the case with CB stimulation, further suggesting it is a specific state-dependent effect of the RE-SLM synapse. The cortex shows a similarly greater magnitude of excitability during SO states. Electrical stimulation of IL shows a markedly different pattern of responding in HPC as a function of state, suggesting that during SO, a direct RE-HPC route may be preferred, while during theta a cortico-entorhino-hippocampal circuit is used for information transfer. Stimulation of both IL and RE shows a modulation of excitability as a function of where in the ongoing rhythmic cycle stimulation occurs. This is the first demonstration of phasic and, more generally, state-based modulation of excitability in the PFC-RE-HPC circuitry which may have marked implications for memory encoding versus retrieval.

In Chapter IV, I assay the role that the intrinsic activity states of RE neurons have in mediating mPFC-HPC dialogue, particularly during SO states. I first demonstrate the persistent optogenetic excitation of the RE tonically upregulates its multiunit activity, akin to that observed during spontaneous theta states. Tonically upregulating RE activity decrements the influence of mPFC stimulation on HPC only during SO states. Consistently, long-duration upregulation of RE activity decreases SO coherence between mPFC and HPC. As such, it appears that during SO states, the RE is primed to both receive and transmit SO related information in the mPFC-HPC circuitry, while the intrinsic activity states of RE neurons enable it to fulfill that role. It is the

rhythmically mPFC SO-coupled activity of RE neurons that underlie efficient informational exchange with the HPC, rather than just the integrity of the RE *per se*.

Finally, in Chapter V, I demonstrate that brief optogenetic excitation of the RE is sufficient to reset the ongoing HPC theta rhythm. Moreover, this effect could be achieved via stimulation of the ipsilaterally HPC-projecting fiber bundle from RE, the CB. The RE is therefore capable of fundamentally affecting the internal oscillator of the HPC. Resetting the spontaneous theta rhythm may mechanistically underlie the capacity of the RE to synchronize mPFC and HPC at theta frequencies and therefore augment activity-dependent mnemonic processes.

Taken all together, these findings decisively demonstrate that the thalamic nucleus reuniens – an often-ignored and ostensibly unassuming brain region – has a critical role in mediating the effective dialogue and coordination of prefrontal and hippocampal sites. The RE as such lies in a privileged position to modulate, facilitate, or constrain mnemonic processing, particularly as it pertains to memories requiring contributions from both the prefrontal cortex and hippocampus. Chapter VI presents a summary and synthesis of these findings, and offers potential avenues for future research in this tremendously exciting circuitry.

2 The reuniens nucleus of the thalamus has an essential role in coordinating slow wave activity between neocortex and hippocampus

Brandon E. Hauer[1], Silvia Pagliardini[1,2], Clayton T. Dickson[1,2,3]

[1]Neuroscience and Mental Health Institute, University of Alberta, Edmonton, Alberta T6G 2E9, Canada,

[2]Department of Physiology, University of Alberta, Edmonton, Alberta T6G 2E9, Canada, and

[3]Department of Psychology, University of Alberta, Edmonton, Alberta T6G 2E9, Canada

Acknowledgements: This work was supported by Natural Sciences and Engineering Research Council of Canada (NSERC) Discovery grants 249861 and 2016-06576 to C.T.D, and NSERC grant 435843 to S.P. B.E.H. was supported by an NSERC Doctoral Postgraduate Scholarship.

https://doi.org/10.1523/ENEURO.0365-19.2019

2.1 Abstract

Sleep is a period of profound neural synchrony throughout the brain, a phenomenon involved in various physiological functions. The coordination between neocortex and hippocampus, in particular, appears to be critical for episodic memory, and, indeed, enhanced synchrony in this circuit is a hallmark of slow-wave sleep. However, it is unclear how this coordination is mediated. To this end, we examined the role of the thalamic nucleus reuniens (RE), a midline body with reciprocal connections to both prefrontal and hippocampal cortices. Using a combination of electrophysiological, optogenetic, and chemogenetic techniques in the urethane-anesthetized rat (a model of forebrain sleep activity), we directly assessed the role of the RE in mediating slow oscillatory synchrony. Using unit recording techniques, we confirmed that RE neurons showed slow rhythmic activity patterns during deactivated forebrain states that were coupled to ongoing slow oscillations. Optogenetic activation of RE neurons or their projection fibers in the cingulum bundle caused an evoked potential in hippocampus that was maximal at the level of stratum lacunosum-moleculare of CA1. A similar but longer-latency response could be evoked by stimulation of the medial prefrontal cortex that was then abolished by chemogenetic inhibition of the RE. Inactivation of the RE also severely reduced the coherence of the slow oscillation across cortical and hippocampal sites, suggesting that its activity is necessary to couple slow-wave activity across these regions. These results indicate an essential role of the RE in coordinating neocortico-hippocampal slow oscillatory activity, which may be fundamental for slow-wave sleep-related episodic memory consolidation.

2.2 Significance Statement

Off-line reactivation of neural activity patterns occurring during previous waking periods might provide further activity-dependent solidification of the synaptic connections that would allow this neural information to be encoded more permanently. In other words, brain activity during sleep might benefit memory permanence. In this work, we show how two distant memory-related areas in the brain, the medial prefrontal cortex, and the hippocampus might coordinate their activity during slow-wave activity via an interposed thalamic structure, the nucleus reuniens. This circuit has already been suggested to play an important role during on-line memory processing; here, we show its potential relevance to off-line memory consolidation via its powerful ability to coordinate two episodic memory structures during slow-wave activity.

2.3 Introduction

Although a lack of behavioral responsiveness during sleep suggests neural inactivity, the complicated and orchestrated dynamics of ongoing brain activity during this state entirely contradicts this assumption. Indeed, sleep is a period of profound and dynamic neuronal synchrony, and few activity patterns are better suited to coordinate widespread forebrain networks than the slow oscillation (SO) (Cox et al., 2014). A major constituent of non-rapid eye movement (NREM) sleep, the SO is characterized by large-amplitude, ~1 Hz rhythmic activity patterns in both neocortex (nCTX) (Steriade et al., 1993a; Amzica and Steriade, 1997) and hippocampus (Isomura et al., 2006; Wolansky et al., 2006). The coordinated slow activity apparent during NREM sleep specifically has been shown to benefit HPC-dependent memory consolidation (Steriade and Timofeev, 2003; Molle et al., 2004; Marshall et al., 2006). This coordination across nCTX and HPC may be a platform for staged synchronization of neuronal ensembles important for a memory trace, suggesting that the SO in particular may at least partially underlie sleep-dependent memory consolidation (Buzsaki, 1996, 1998; Dickson, 2010). Coordinated and repetitive activity may also be an excellent platform for enhancing synaptic efficacy, an important factor in memory formation (Lee and Wilson, 2002; Dan and Poo, 2004; Buzsaki and Watson, 2012).

Despite its eminent importance for memory, how the SO is coordinated across the nCTX and HPC remains a mystery. Recording activity throughout HPC cell laminae revealed that SO power was maximal at stratum lacunosum-moleculare (SLM) for both field (voltage) and current source density (CSD) measures (Isomura et al., 2006; Wolansky et al., 2006).. In addition, the SO peak shows a good degree of coherence between nCTX and the HPC at the level of SLM, which is the site of termination of the temporoammonic pathway from layer III of the entorhinal

cortex (EC). It has been widely assumed that this entorhinal input is the main source of the phasing, coordination, and perhaps even the generation of the HPC SO (Isomura et al., 2006; Wolansky et al., 2006). However, a second major input to the SLM also exists, distinct from the multisynaptic corticoentorhinal–HPC pathway, that arises from the midline thalamic nucleus reuniens (RE) (Herkenham, 1978). The RE constitutes a robust anatomic link between medial prefrontal cortex (mPFC) and HPC (Vertes et al., 2006; Vertes et al., 2007), with a population of cells that project via axon collaterals to both structures, providing a direct disynaptic link between these two important episodic memory regions (Hoover and Vertes, 2012; Varela et al., 2014). While the output of the RE is wholly excitatory (Wouterlood et al., 1990), the input at the level of SLM also activates local inhibitory interneurons, such that the RE can yield both feedforward excitation and inhibition to influence HPC population activity (Dolleman-Van der Weel and Witter, 2000).

Considering this strong disynaptic connection between mPFC and HPC, the dialogue between which is critical for episodic forms of memory (Damasio, 1989; Laroche et al., 2000; Jin and Maren, 2015), more recent work has theorized a role for the RE in coordinating cortico-hippocampal SO activity (Hallock et al., 2016; Dolleman-van der Weel et al., 2017; Ferraris et al., 2018) which is itself important for memory consolidation (Steriade and Timofeev, 2003; Dickson, 2010; Niethard et al., 2018). In this regard, the RE has been implicated more directly in the consolidation of long-term, episodic forms of memory (Loureiro et al., 2012; Pereira de Vasconcelos and Cassel, 2015; Troyner et al., 2018).

It is clear that the neocortical SO is closely related to hippocampal SO during sleep and sleep-like states (Wolansky et al., 2006; Sharma et al., 2010). What is not clear, however, is how this correspondence is mediated. Here, using state-of-the-art multisite recording techniques,

together with optogenetic and chemogenetic manipulations in an in vivo rat preparation, we demonstrate that the RE is critically involved in coordinating SO activity between nCTX and HPC. This has marked implications for slow-wave sleep-dependent episodic memory consolidation.

2.4 Methods

2.4.1 Animals

Experiments were conducted on 33 male Sprague Dawley rats obtained from the Sciences Animal Support Services and/or Health Sciences Laboratory Animal Services of the University of Alberta with a mean (± SEM) final weight of 426.85 ± 14.41 g. Of these, 7 were used for single- and multiunit recordings; 11 were used for RE and cingulum bundle (CB) stimulation; and 15 were used for chemogenetic inhibition of RE. All animals were provided with food and water ad libitum and were maintained on a 12 h light/dark cycle, with lights on at 7:00 A.M. All procedures conformed to the guidelines of the Canadian Council on Animal Care and were approved by the Biological Sciences and/or Health Sciences Animal Policy and Welfare Committees (AUP 092 and AUP 461) of the University of Alberta.

2.4.2 Materials and Methods

Electrodes

Bipolar recording electrodes with tip length separation between 0.5 and 1.3 mm were constructed using Teflon- coated stainless steel wire (bare diameter, 125 μm; A-M Systems).

Electrodes were implanted using predetermined coordinates from a stereotaxic atlas, using bregma as a landmark (Paxinos and Watson, 1998). Electrodes were cemented in place using dental acrylic and jeweller's screws fastened into the skull.

For spatial profile field potential recordings in the HPC, we used a linear 16-contact (100 μm separation) microprobe arranged in a vertical linear array (U-probe, Plexon). The final depth of the probe was determined using the well-established electrophysiological profile of theta field activity (Bland and Bland, 1986; Buzsaki, 2002). The position of the multiprobe was histologically confirmed in every experiment by analyzing its track in relation to recorded field activity.

Viral Vectors

One primary viral vector was used for optogenetic experiments, an adeno-associated virus (AAV; serotype 2/2), expressing a channelrhodopsin-2 variant (ChR2/ H134R). It was conjugated with enhanced yellow fluorescent protein (EYFP) and driven by the synapsin promoter (hSyn-ChR2-EYFP). The virus was produced, characterized, and titrated at the University of North Carolina Virus Vector Core Facility (Chapel Hill, NC; ChR2: 3.9×10^{12} molecules ml^{-1}).

Chemogenetic experiments also used an AAV vector (serotype 2/5) that was also driven by the same synapsin promoter. However, the vector expressed a Gi-coupled DREADD (designer receptor exclusively activated by designer drug; hM4Di) and was conjugated with both the mCitrine fluorescent protein and a human influenza hemagglutinin (HA) tag (hSyn-hM4Di-HA-mCitrine; 3.5×10^{12} molecules ml^{-1}; UNC Virus Vector Core Facility).

Additionally, control experiments were conducted by using a virus with the same promoter (hSyn) and AAV serotype (5) that was coupled only to a fluorescent vector, without any opsin or DREADD (hSyn-mCherry; UNC Virus Vector Core Facility).

Photostimulation

An optic fiber (tip diameter, 200 μm) connected to a 473 nm laser (Laserglow Technologies) and calibrated to deliver light at 10–12 mW was positioned to deliver light at intracranial locations. Photostimulation events were driven by a pulse stimulator (Model 2100, A-M Systems) connected to the laser power supply as well as to the analog-to-digital board and PC acquiring data to mark each event (see below).

2.4.3 Procedures

Viral injections and recovery

Rats were initially anaesthetized in a sealed chamber with gaseous isoflurane (4% induction, 1.5% maintenance, in 100% O_2). After loss of righting reflexes, rats were given an intraperitoneal injection of a ketamine/ xylazine cocktail (90 and 10 mg/kg, respectively; Bimeda- MTC, Animal Health; and Rompun, Bayer). Supplemental doses (10% of original) of the ketamine/xylazine cocktail were administered as required to maintain a surgical anesthetic plane. Body temperature was maintained at 37°C following anesthesia using a homeothermic monitoring system (Harvard Apparatus).

Rats were placed into a stereotaxic apparatus (Model 900, David Kopf Instruments) and, using aseptic techniques, were prepared for intracranial injections. A single incision was made along the midline of the scalp, and the skin flaps were pinned back. The skull was leveled by adjusting lambda and bregma to be in the same horizontal plane. Holes were drilled in the skull at predetermined coordinates from a stereotaxic rat atlas (Paxinos and Watson, 1998). Micropipettes (tip diameter, 30 μm) loaded with hSyn-ChR2-EYFP (optogenetic experiments), hSyn-hM4Di-HA-mCitrine (chemogenetic experiments), or hSyn-mCherry (control experiments) were attached to a holder (EHW-2MS, A-M Systems) and lowered using a micropositioner into the brain. Injections targeted either the midline of the nucleus reuniens thalami [anteroposterior (AP), -2.0; mediolateral (ML), +1.9 mm] at an angle 16° oblique to the vertical line to avoid the midline sinus and advanced 6.4 –7.2 mm from the brain surface (infusion volume, 400–500 nl) or the infralimbic medial prefrontal cortex [AP, +2.8 to +3.2 mm; ML, +0.7 to +1.1 mm; dorsoventral (DV), -4.4 to -5.8 mm; infusion volume, 300 nl].

Injections were made using a microinjector (PMI-100, Dagan) connected via tubing (PVC, 2.79 x 4.5 mm; Gilson) to the holder, using a pressure of 40 psi and 15 ms pulse length, at a rate of ~100 nl/min. Micropipettes were left in place for 5–10 min following the injection to allow for adequate diffusion of the virus and to prevent unintended backflow of the viral vector up the pipette track.

Following injection procedures, the scalp was then sutured, and rats were given 0.5 ml of the local anesthetic Marcaine (5 mg/ml, s.c.) around the incision site. Animals were provided with pain medication (meloxicam, 1–2 mg/kg in oral suspension, Boehringer Ingelheim Vetmedica) over a 24 h period postsurgery. Food and water were provided ad libitum, and

animals were allowed to recover for 2–4 weeks before acute experimentation (see below). Neither the viral injection nor the surgical procedures produced any observable long-term issues.

Acute urethane-anesthetized recordings

Rats were initially anaesthetized in a gas chamber with isoflurane in medical oxygen (4% induction, 1.5% maintenance). A catheter was inserted into the femoral vein, and isoflurane was discontinued. General anesthesia was obtained by slow (~0.03–0.08 ml/min) incremental administrations of urethane (0.4 g/ml) via the catheter. Urethane was chosen because it promotes an unconscious state that closely mimics the typical activity dynamics present during natural sleep, both in terms of brain state alternations as well as in terms of physiologic correlates (Clement et al., 2008; Pagliardini et al., 2013b).

Rats were placed into a stereotaxic apparatus. The cranium was exposed by making a single long incision along the scalp and pinning back the skin flaps. The skull was leveled by adjusting lambda and bregma to be in the same horizontal plane. Body temperature was maintained at 37°C using a homeothermic monitoring system (Harvard Apparatus).

Unit recording procedures. Bipolar electrodes for recording local field potentials (LFPs) were positioned in the mPFC [AP, +3.2 mm; ML, 0.7 mm; DV (tip of long electrode), -1.2 to -1.8 mm], and straddling the pyramidal layer of CA1 of the dorsal HPC (AP, -3.5 mm; ML, -2.4 mm; DV, -2.5 to -3.5 mm). Our primary index for brain state was determined by the neocortical electrode, but dorsal HPC activity was recorded as an additional confirmation of state. A fine glass micropipette filled with either 1.0 M sodium chloride or 2.0 M sodium acetate, mixed with 2% pontamine sky blue for recording unit activity (resistance ranging from 2 to 10 MΩ) targeted

the RE (AP, -2.0 mm; ML, +1.9 mm) at an angle 16° oblique to the vertical line. Micropipettes were mounted on a single-axis fine hydraulic micromanipulator (Model 2660, David Kopf Instruments) that was positioned over the brain with a coarse three-axis manual manipulator (Märzhäuser) and were advanced at a variable rate, as follows: 10–20 μm/s for the first 5 mm; 2–5 μm/s for 5–6 mm; and finally at a rate of 1 μm/s until a final depth typically between 7.5 and 8 mm. The intrapipette solution was in contact with a silver chloride electrode connected to our amplification system.

Local field potentials were amplified in bipolar differential mode at a gain of 1000 and filtered between 0.1 and 500 Hz using a differential AC amplifier (Model 1700, A-M Systems). Single- and multiunit signals were initially amplified at a gain of 10 using a DC amplifier (Neuro Data IR283A, Cygnus Technology). This signal was further amplified using an AC amplifier (Model 1700, A-M Systems) at a gain of 1000 and bandpass filtered between 0.3 and 20 kHz. All signals were digitized and sampled at 20 kHz using a Digidata 1322A analog-to-digital board (Molecular Devices) connected to a PC running the Axoscope acquisition program (Molecular Devices). Unit activity was recorded along the dorsal–ventral axis throughout the RE. At the end of recording sessions, pontamine sky blue was iontophoresed for 5–10 min (+0.4 μA; 7 s on, 7 s off) or pressure injected using a microsyringe attached by tubing to the back end of the pipette.

Nucleus reuniens stimulation procedures. Bipolar recording electrodes were positioned in either the anterior frontal cortex (FC) or mPFC (FC: AP, +2.5 mm; ML, -1.2 mm; DV, -0.7 to -1.4 mm; mPFC: AP, +3.2 mm; ML, -0.7 mm; DV, -1.2 to -1.8 mm), as well as in the ipsilateral HPC (AP, -5.5 mm; ML, -4.5 mm). The linear multiprobe was positioned in the contralateral HPC (AP -5.5 mm; ML, +4.5 mm; DV, -3.3 to -4.5 mm) to straddle the CA1 pyramidal layer. Importantly, for monitoring the effects of RE and mPFC stimulation and/or inhibition, the intermediate HPC was

consistently targeted using the linear probe (rather than the dorsal HPC in unit experiments; see above), given the prominent projection patterns from RE to this septotemporal region of the HPC (Hoover and Vertes, 2012). Similar to the local field potential recording procedures described above, bipolar recordings were amplified in differential mode at a gain of 1000 and filtered between 0.1 and 500 Hz using an AC- coupled amplifier (Model 1700, A-M Systems). Multiprobe signals were referenced to ground, filtered between 0.1 and 500 Hz, and amplified at a final gain of 1000 via a 16-channel headstage (unity gain) and amplifier (X1000, Plexon). Signals were digitized at a sampling frequency of 1000 Hz with antialias filtering at 500 Hz using a Digidata 1440A Analog-to-Digital Board (Molecular Devices) connected to a PC running Axoscope (Molecular Devices).

On the right side, an optic fiber attached to a 473 nm laser was positioned first above the RE (AP, -2.0 mm; ML, +1.9 mm; DV, -6.4 mm) at an angle 16° oblique to the vertical line. Following stimulation (described below), the optic fiber was removed and repositioned to target the CB (AP, -2.5 mm; ML, +2.7 mm), angled at 40° oblique to the vertical line and advanced 2.6 –3.4 mm from the brain surface.

Evoked potentials were produced using 10 ms laser pulses delivered at 1.25 Hz to the RE and then subsequently to the CB, and were averaged over 64 trials. Stimulation trains were delivered during equivalent brain states, specifically during clear deactivated periods characterized by ongoing high power in the 1 Hz signal. This was ensured (1) by noting the ongoing brain state when delivering stimulation trains, and (2) afterward by concatenating all the individual sweeps together, and both visually and spectrally analyzing the underlying baseline activity as a definitive measure of the ongoing brain state.

Medial prefrontal cortex stimulation. In a subset of animals (n = 8), we used a paired-pulse stimulation paradigm in mPFC sites, with the goal of evoking HPC potentials. The surgical preparation was identical to that used for RE stimulation (see above), except that, instead of targeting an optic fiber over RE or CB, a bipolar stainless steel (0.08 inch bare; 0.11 inch Teflon coated) stimulating electrode was lowered into IL (infralimbic prefrontal cortex) (AP, +2.8 to +3.2 mm; ML, +0.7 to +1.1 mm; DV, -4.4 to -5.8 mm). Following the mPFC stimulation paradigm used by Gemmell and O'Mara (2000), 50–150 μA biphasic current pulses 0.5 ms in duration were delivered with a 30 ms interstimulus interval, every 8 s using a constant current stimulator (Model 2100, A-M Systems). Stimulation epochs were averaged over 32 trials and were always delivered during equivalent brain states.

Nucleus reuniens chemogenetic inactivation. In all experiments with mPFC stimulation, rats had been pretreated to express either hSyn-hM4Di-HA-mCitrine or hSyn-mCherry in the RE via our injection procedures above. Subsequent to evoked potential analysis, and after a suitable period of spontaneous recordings, the DREADD agonist clozapine *N*-oxide (CNO; Cayman Chemical) was administered intraperitoneally at a dose of 3 mg/kg (MacLaren et al., 2016). Activity was then recorded for ~2 more hours, followed by the same mPFC stimulation paradigm described above. This allowed for characterization of the HPC response evoked by mPFC stimulation before and after RE inactivation. We could also then compare baseline activity/coordination between the HPC and mPFC with an intact versus inactive RE within the same recording period.

2.4.4 Perfusion and Histology

Following experimental recordings, 5 s DC pulses of 1 mA using an isolated current pulse generator (Model 2100, A-M Systems) were passed through bipolar recording and stimulating electrodes to generate small electrolytic lesions at their tips. These lesions allowed for subsequent verification of recording and stimulation sites. Rats were then transcardially perfused with 0.9% saline and 4% paraformaldehyde in saline (Thermo Fisher Scientific). The brain was then removed and placed into a 4% formalin and 20% sucrose solution for at least 48 h. Brains were flash frozen using compressed CO_2 and sectioned with a rotary microtome (1320 Microtome, Leica) at a width of 60 μm. Tissue was countersectioned, with one-third of sections being mounted on gelatin-coated microscope slides for subsequent Thionin staining; another third being mounted on slides and immediately covered using a fluorescence preserving reagent and mounting medium (FluorSave, EMD Millipore); and a third of the tissue saved for immunoreaction for detection of specific neuronal markers.

Immunohistochemistry was performed according to the following protocol. Free-floating sections were rinsed three times using PBS and incubated with 10% normal donkey serum (NDS) and 0.3% Triton X-100 for 60 min to reduce nonspecific staining and increase antibody penetration. Sections were left to incubate overnight with primary antibodies diluted in PBS containing 1% NDS and 0.3% Triton X-100. The following primary antibodies were used: green fluorescent protein (dilution, 1:1000; raised in chicken; Aves Labs); red fluorescent protein (mCherry; dilution, 1:800; raised in rabbit; Millipore); human influenza HA (1:800; raised in rabbit; Cell Signaling Technology); and neuronal-specific nuclear protein (1:800; raised in mouse; Millipore). The following day, tissue was again washed three times with PBS, incubated with secondary antibodies conjugated to the specific fluorescent proteins in each viral construct (Cy2-conjugated donkey antichicken; Cy3-conjugated anti-rabbit; Cy5-conjugated anti- mouse;

1:200; Jackson ImmunoResearch), and diluted in PBS and 1% NDS for 2 h. Sections were again washed three times with PBS, mounted, and coverslipped with Fluorsave (EMD Millipore). Microscopic inspection of tissue was used to verify electrode recording loci, optic fiber tracks, and the expression of viral constructs using a Leica DM5500B Fluorescent Microscope.

2.4.5 Data Processing and Analysis

Signals were first examined visually using AxoScope 10.6 (Molecular Devices) to choose data segments for further analyses. Analyses were computed and visualized using custom-written code in MATLAB (version R2015b, MathWorks), before being processed with CorelDRAW X6 (Corel). Data analyses included the following: zero phase delay digital filtering, evoked potential averaging, power and phase profile and spectral analyses, coherence, current source density, single- and dual-channel spectra, auto- and cross-correlations, spike-triggered averaging (STA), and spike phase preference. Spectral analysis was used to confirm brain state in chosen segments before conducting other analyses.

Field recordings. Autopower, cross-power, coherence, and cross-phase spectra were computed and plotted for both individual and pairs of field signals (details further below). Spectra were estimated from a series of 6-s-long, Hanning-windowed samples with 2 s overlap using Welch's periodogram method. Power spectrograms (Wolansky et al., 2006; Whitten et al., 2009) were computed using a sliding window procedure, allowing discrete spectra to be calculated at specific time points across the entire time segment. Windows were 30 s in duration, and slid across the entire file in 6 s increments. These discrete spectra were then analyzed as described above. Spectral profiles were also created for activity recorded with the linear multiprobe in the

same way, except that each multiprobe channel was compared against a fixed (nCTX or HPC) bipolar reference, and then power values at spectral peak frequency values for both SO and theta states were extracted. The spatial locations of the channels were then estimated based on the power profile for theta (Wolansky et al., 2006), with the phase reversal point being at the interface between stratum pyramidale and stratum radiatum, and the theta maximum being at stratum lacunosum moleculare.

For chemogenetic experiments, 3 min samples of SO activity were extracted based on the analysis of cortical power spectrograms pre- and post-CNO. This duration was selected as a balance between a long-term, stable SO sample, without being compromised by potential nonstationarities. SO time points were all chosen at least 30 min post-CNO injection to ensure adequate time for the ligand or its metabolites to enter the brain (Whissell et al., 2016). A profile of the power at the peak SO frequency for each sample was then created for each channel across the linear multiprobe in the HPC. Using this, we could determine the channel of maximal SO power, which has been previously demonstrated to be the relative location of the SLM (Wolansky et al., 2006). The CSD (described below) profile of the linear multiprobe was then computed. Spectral (particularly power and coherence) estimates were computed as described above, comparing the CSD of the SLM channel to a fixed nCTX or HPC electrode.

Single-unit activity. The relationship between neocortical and hippocampal field with RE spikes was assessed by STA. The preferred phase of the unit to the field was computed separately by filtering the field within a specific bandwidth (0.5–1.5 Hz for SO; and 3–5 Hz for HPC theta), and then computing the time points of negative to positive zero crossings. Unit activity was binned (bin size, 18°) according to the phase of the field cycle, from 0° to 360° (from one zero

crossing to the next). Spike rates, interspike intervals, and autocorrelation histograms (10–100 ms bin size) were computed to analyze spike train dynamics.

STA significance was computed by comparison with the distribution of STAs using a series (n = 100–1000) of randomized (shuffled) spike trains derived from the original data. Spike trains were shuffled using random assignment based on the actual interspike intervals computed for the original spike train. The resulting STA distribution had a variance that was proportional to the amplitude of the original field signal, but that was lower than the original fluctuations for signals with a strong correspondence.

Significance for autocorrelation histograms was computed in a similar way, using the average bin value of individual point processes (single-unit activity) and their fluctuations within a randomized distribution (n = 100–1000). The 99% confidence limits were computed as the average value ± 2.6 SEM. We classified units with systematic and periodic fluctuations beyond this window as being rhythmic. Rayleigh statistics for circular data were used to statistically evaluate phase histograms (Zar, 1999).

Multiunit activity. Root mean square (rms) envelopes were created for multiunit RE activity by using a 200 ms window slid by 50 ms increments. The resulting envelope was inverted by multiplying by -1 to ensure that it was not antiphase to the ongoing SO. Power, coherence, and phase estimates were computed as described above for field signals. The peak cross-power and coherence frequency was used to estimate the spectral phase angle between the RE rms and field signal. Coherence between the signals was used as a measure of phase preference (radius). To determine a 99% confidence limit for coherence estimates, a series of time-reversed coherence spectra were computed, and the distribution of values across the entire spectrum was assessed.

Current source density analysis. CSD analysis was conducted on spontaneously collected field samples or evoked potential averages recorded using the linear multiprobe, following the assumptions of Freeman (1975), Rodriguez and Haberly (1989), and Ketchum and Haberly (1993). Briefly, CSD was computed by estimating the second spatial derivative of adjacent multiprobe voltage traces.

2.5 Results

2.5.1 Nucleus reuniens neurons phase lock with the slow oscillation during deactivated states

Striking changes in spike train dynamics of verified RE single unit recordings (n = 7 rats) were observed across activated (theta) and deactivated (SO) states (Fig. 1). Every RE neuron sampled across both states (10 of 10) changed its pattern of activity concomitantly with forebrain state (Fig. 1A, see example). During activated states, neuronal discharge was consistently elevated (average frequency, 4.86 ± 0.47 spikes/s; Fig. 1Biii) and was significantly higher than that observed during SO states (1.83 ± 0.27 spikes/s; $p < 0.0001$, two-tailed paired t test; Fig. 1Bi,C). In addition to firing frequency, the pattern of discharge appeared to be tonic during theta and rhythmic during SO. Using autocorrelation analysis, we observed that in all cells recorded during the SO state (n = 14), there was clear rhythmicity (average, 0.86 ± 0.06 Hz), which was highly similar (p = 0.97, two-tailed paired t test) to the average frequency (0.86 ± 0.05 Hz) of the cortical SO. No such rhythmicity was apparent in the randomized (spike-shifted) distribution. In the 10 cells recorded across both states, no rhythmicity was observed during the theta state (Fig. 1D, inset). Indeed, and as shown in Figure 1D, the randomized (spike-shifted) distribution was

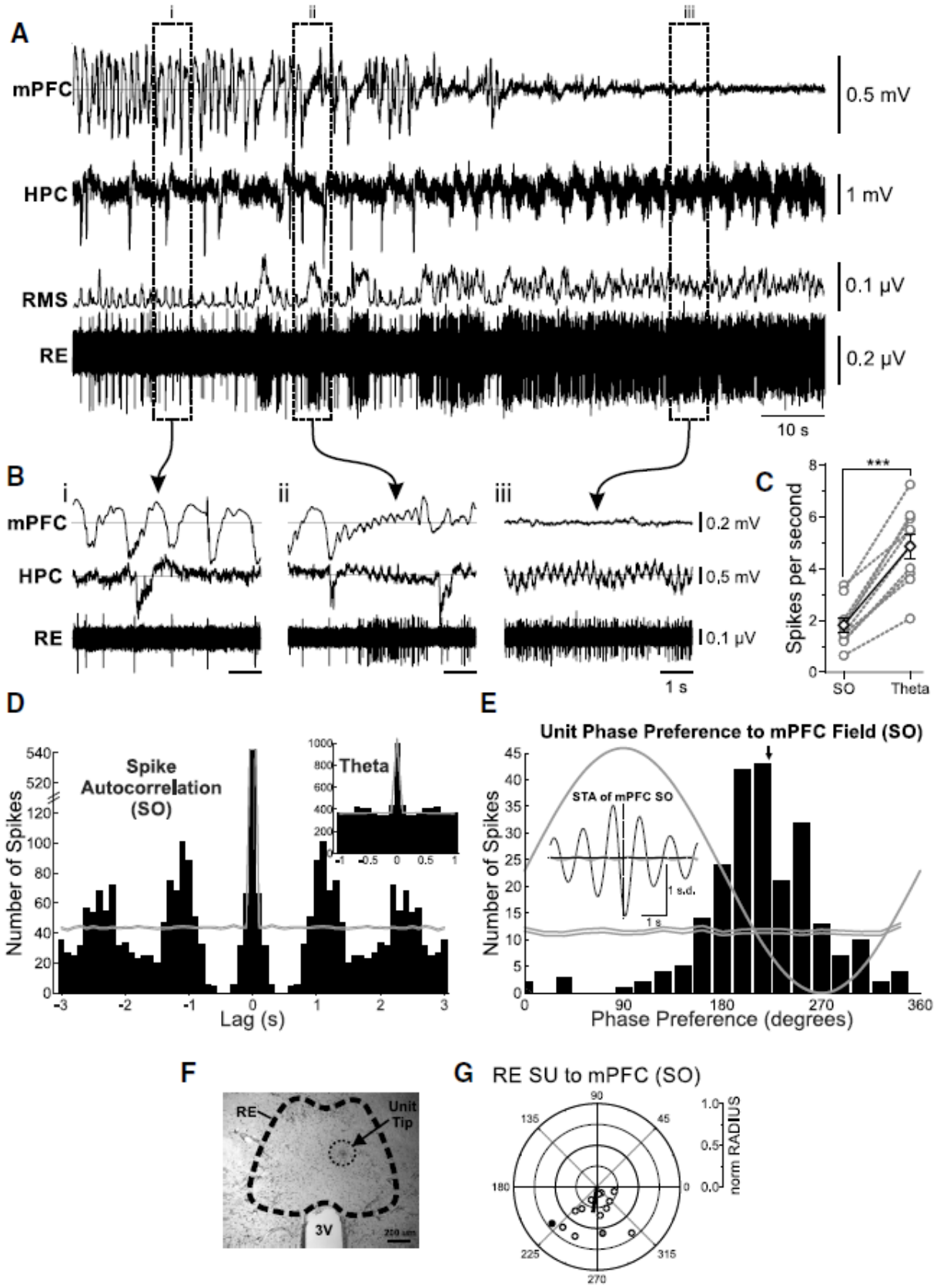

Figure 2.1 RE units are phase coupled to the forebrain SO.

Figure 2.1 RE units are phase coupled to the forebrain SO. A. Simultaneous field recordings in mPFC and HPC, with glass micropipette single-unit recording in RE, and rms envelope (200 ms window, slid by 10 ms) of RE single-unit recording, during a spontaneous deactivated-to-activated field state change. **B.** Bracketed segments correspond to expansions, which highlight the features of field and RE unit activity across states. **Bi.** Deactivated (SO) state showing a slow, rhythmic firing of a representative RE unit, coupled to the negative phase of the mPFC SO. **Bii.** Transitionary state illustrating the tonic firing of an RE unit only during prolonged activated forebrain activity. **Biii**. Activated (theta) state illustrating tonic firing of the RE unit. **C**. Spike frequency measures for RE neurons that were recorded across both deactivated and activated states, showing a prominent increase in firing rate during theta states for individual units (gray hollow circles and dashed gray lines), and on average (black hollow diamonds and solid black lines; Error bars represent SEM. ***$p < 0.001$). **D.** Spike train autocorrelation histograms of a representative RE unit during SO and theta (inset), demonstrating significant state-dependent rhythmicity (bin size, 100 ms). Gray lines represent 99% confidence intervals from randomized distributions. **E.** Phase histogram for this unit during SO, showing a strong preference for the descending/negative phase of the mPFC SO (bin size, 18°). Black arrow indicates mean phase preference. Inset, Spike-triggered average of the RE unit firing to mPFC field during SO. **F.** Photomicrograph of a representative coronal tissue section, showing the expression of pontamine sky blue localized to the RE, indicating the tip of the single-unit recording pipette. **G.** Circle plot of the preferred phase of RE units to mPFC SO cycle. The black line indicates the mean angle (°) and strength of phase preference (Rayleigh statistics). Gray, filled circle corresponds to the unit shown in **A** and **B**. Black, filled circle corresponds to the unit shown in **D** and **E**. SU, Single unit.

highly similar to the original histogram.

To determine whether there was any relationship between RE unit activity and the ongoing SO, we performed a cycle-by-cycle field potential phase analysis of spiking behavior as well as spike-triggered averaging of the local field potential at both mPFC and HPC sites. Using the phase of the ongoing cortical SO LFP to organize unit activity (Fig. 1E), we observed a prominent and highly significant degree of phase coupling of unit discharge to the field potential oscillation (for this example, the average preferred angle, 219°; Rayleigh distribution, z = 110.75; n = 229, $p < 0.0001$). This relationship was not at all apparent in the randomized (spike-shifted) distribution. Across all RE cells, there was significant (as determined by Rayleigh statistics) coupling in 12 of the 14 total cells, and the average preferred angle was also consistent across cells at a phase just before the negative peak of the SO (overall average angle, 261.59°; overall average radius, 0.31; $F_{(2,12)} = 17.61$, $p < 0.001$; Fig. 1G). A similar degree of coupling was observed to the ongoing HPC SO, although only eight cells showed a significant phase preference (overall average angle, 14.07°; overall average radius, 0.086; $F_{(2,12)} = 4.17$, $p < 0.05$). The HPC analysis was complicated by the fact that the bipolar montage was optimized for theta, and not for local SO, which minimized this latter signal in many of our experiments (also shown by lower than usual coherence analysis with the neocortical SO).

We confirmed the same phasic relationship using spike-triggered averaging (Fig. 1E, inset). The field potential average, organized by RE unit spiking, was highly rhythmic and showed a prominent negativity time locked to RE unit discharge. This relationship was flat when the averaging was done with randomized spike-shifted timing (Fig. 1E, inset). In 12 of the 14 recorded units, a similar phasic relationship to the HPC SO was found. In the remaining two examples, the hippocampal LFP site was not optimized for SO (as above).

In another nine recording situations, we were able to record multiunit activity (MUA) from the RE to gather a population index of unit activity (Fig. 2). Similar to the single-unit data, MUA tended to show tonic, high-frequency patterns during theta (Fig. 2A,Bii), and slow, rhythmic bursts during SO (Fig. 2A,Bi). By using the rms envelope of this activity (Fig. 2A; see Materials and Methods), we were able to compare it to the ongoing forebrain SO using spectral analysis. In nine of nine cases, and as shown in Figure 2C–E, we determined that the MUA had a significant phase relationship to ongoing mPFC SO by coherence analysis at the frequency peak demonstrated in the cross-power spectrum (values > 0.18 were determined to be significant via time-shifted randomizations; see Materials and Methods). By examining the cross-phase spectrum at this coherent frequency, we could determine the average preferred phase of the peak positivity of the MUA rms to the ongoing phase of the mPFC SO (Fig. 2E). On average, and as shown in Figure 2F, this occurred just after the peak negativity in the cortical field oscillation (average angle, 340.34°; radius, 0.68; $F_{(2,7)} = 141.11$, $p < 0.001$; Fig. 1H). There was also a slight phase preference of the peak positivity of the RE MUA rms to the negative trough of HPC SO activity (average angle, 248.35°; radius, 0.12).

Our unit recordings showed that the RE does exhibit SO-related activity that was correlated to ongoing forebrain SO, and could thus carry this signal between cortex and hippocampus.

2.5.2 Optogenetically stimulating the nucleus reuniens generates an evoked potential with maximal current sink in the stratum lacunosum moleculare of hippocampus

Having determined that RE neurons themselves displayed prominent SO activity and

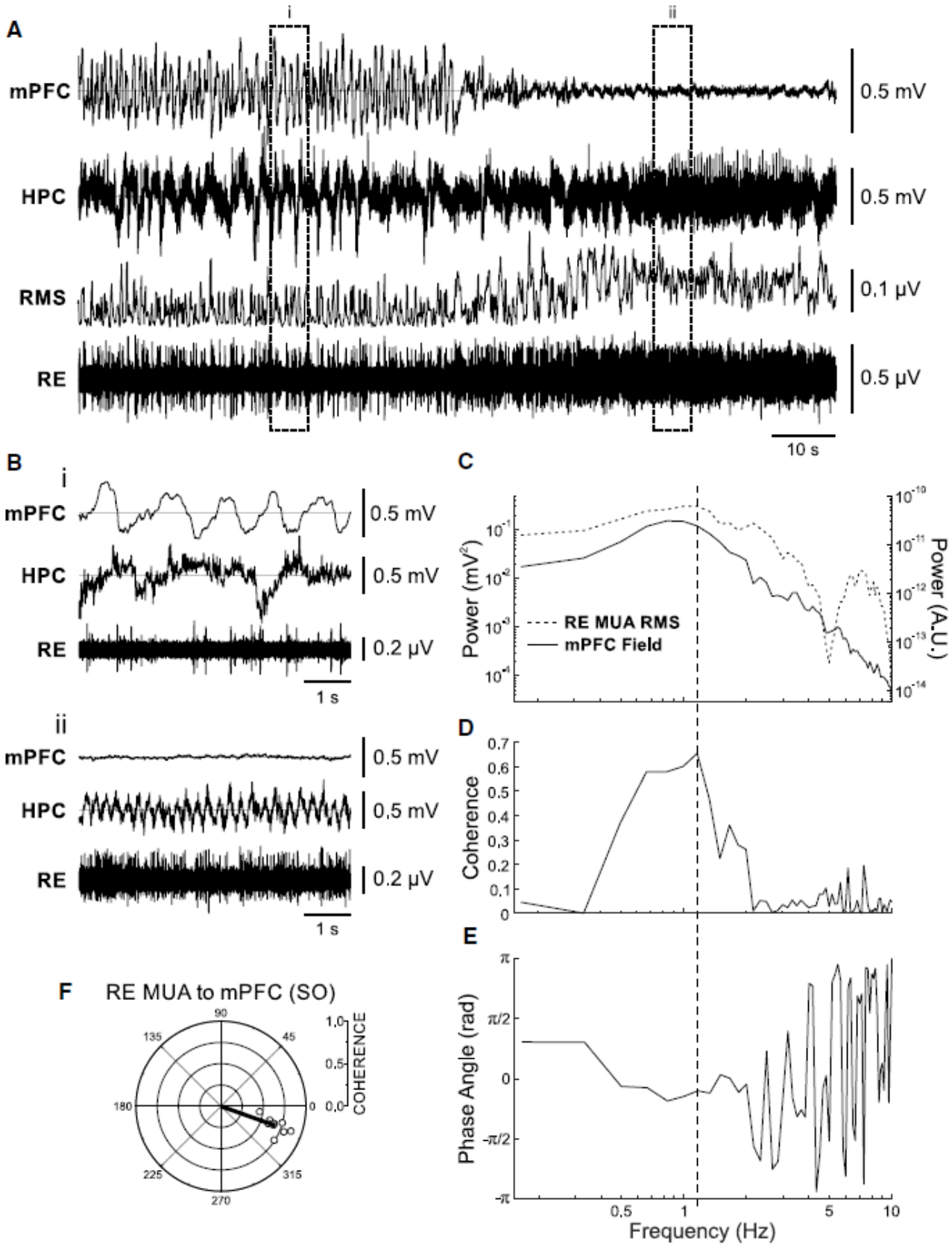

Figure 2.2 RE MUA is phase coupled to the forebrain SO.

Figure 2.2 RE MUA is phase coupled to the forebrain SO. A. Simultaneous field recordings in mPFC and HPC, with glass micropipette multiunit recording in RE, with rms envelope (200 ms window, slid by 50 ms) of RE multiunit recording above, during a spontaneous deactivated-to-activated field state change. Bracketed segments correspond to expansions in **B**, which highlight the features of field and RE unit activity across states. **Bi.** Deactivated (SO) state showing a slow, rhythmic firing of representative RE multiunit activity, coupled to the negative phase of the mPFC SO. **Bii.** Activated (theta) state illustrating tonic firing of RE units. **C.** Autospectral power of mPFC field (black line, left axis) and of the rms envelope of RE MUA (dashed black line, right axis) during SO. **D**, **E.** Coherence (**D**) and phase spectra (**E**) across the two signals shown in **C**. Vertical dashed line through **C–E** indicates SO frequency extracted from spectra. **F.** Circle plot of preferred phase as measured by coherence (radia) and phase angles (°) obtained from spectra of RE multiunit activity compared to the mPFC SO cycle. Shaded gray circle corresponds to the multiunit activity illustrated in all panels of this figure.

were coupled to ongoing SO, we next wanted to assess the influence of stimulating RE neurons on HPC activity. To do this, we adopted an optogenetic approach that involved targeted stereotaxic viral delivery to the RE and then subsequent simultaneous depth potential recording in the HPC during light stimulation directed at either the RE or its specific unilateral pathway to the HPC via the cingulum bundle (Fig. 3).

Following hSyn-ChR2-EYFP viral infection in the RE in nine rats, a series of optical pulses was delivered (see Materials and Methods) directly to the RE, during 14-channel linear probe recording through the CA1 region of HPC together with bipolar LFP recordings from the contralateral HPC and frontal cortices (Fig. 3A). Viral infection and electrode placements were histologically confirmed following every experiment (Fig. 3B). In all cases reported, viral infection was largely confined to the RE, with occasional minimal expression in the dorsally adjacent rhomboid nucleus. This, in part, motivated our subsequent stimulation of the CB, which confirmed that the evoked response in HPC was truly RE-mediated. All electrode tracks were localized to CA1, extending through stratum pyramidale and SLM and into the molecular layer of the dentate gyrus. The resulting evoked potential in the HPC was averaged over 64 individual stimulations and revealed a large negative potential that was maximal at a depth corresponding to the SLM (Fig. 3C,D). CSD analysis revealed a prominent sink (-7.89 ± 2.44 mV/mm^2) at an average latency of 25.00 ± 1.60 ms from the onset of stimulation at the level of the SLM (Fig. 3E,F). This potential profile is consistent with previous reports of RE-mediated potentials in the HPC (Dolleman-Van der Weel et al., 1997) and is also consistent with the projections of the RE to the HPC, which synapse on the distal dendrites of CA1 pyramidal cells (Herkenham, 1978).

To isolate this input more specifically, we directed optical stimuli at the level of the

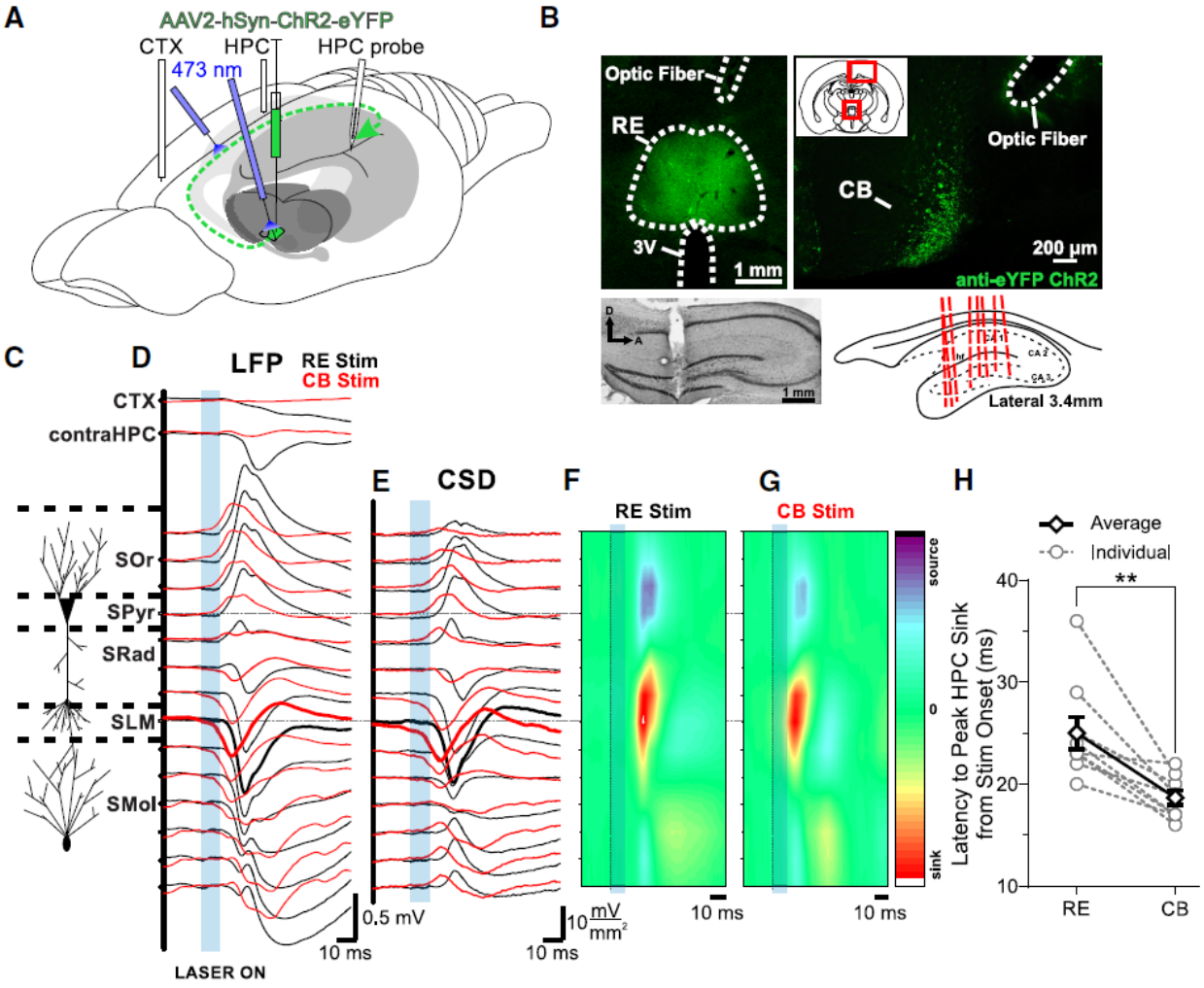

Figure 2.3 Optogenetic stimulation of the RE/CB reliably produces an evoked potential in the HPC.

A. Schematic illustration of the injection, stimulation, and recording procedures. Schema modified from Amaral and Witter (1995). **B.** Top left, Representative coronal tissue section showing the expression of hSyn-ChR2-EYFP virus localized to RE, with optic fiber track positioned dorsal to RE. Top right, hSyn-ChR2-EYFP viral expression in the CB from a single injection into RE, with optic fiber track. Inset, Schematic of relative locations of top two images. Bottom left, Nissl-stained sagittal section of HPC illustrating multiprobe track penetrating cell lamina perpendicularly. Bottom right, Schematic sagittal illustration of all (except one)

multiprobe tracks through the HPC. **C.** Schematic depiction of HPC cell lamina as determined by theta profiles. **D.** Local field potentials evoked in frontal CTX, contralateral HPC, and in the ipsilateral HPC via the multiprobe. Laser light delivery (10 ms pulse at 473 nm wavelength; blue rectangle) to the RE (black lines) produced a response in CTX and contralateral HPC, as well as a profile that reversed from dorsal-to-ventral locations through the ipsilateral CA1 region of the HPC, with a maximal amplitude at a depth corresponding to SLM (which was also the power maximum of the SO and theta profiles). Identical stimulation of the CB (red lines) produced a similar but lower latency profile in ipsilateral HPC, but largely eliminated the evoked response in CTX and contralateral HPC, indicative of the specificity of the ipsilateral RE pathway through the CB. **E.** Current sink/source density line plots illustrating net synaptic current flow at each ipsilateral hippocampal recording site, showing a maximal sink at SLM following both RE (black) and CB (red) stimulation (sinks are shown by downward or negative deflections, sources by upward or positive deflections). **F**, **G.** Color contour plot of the CSD traces in **E** following RE (**F**) and CB (**G**) stimulation (marked by a dashed line and blue box), depicting a large sink centered on SLM, with a corresponding source in basilar regions of CA1. CSD scales are -17 to 17 mV/mm^2 for RE stimulation, and -11 to 11 mV/mm^2 for CB stimulation. **H.** Latency from the end of the 10 ms optical stimulation to peak HPC sink, which in every case was at SLM, for individual animals (gray hollow circles and dashed gray lines), and on average (black hollow diamonds and solid black lines). Error bars represent SEM. (**$p < 0.01$). SOr, Stratum oriens; SPyr, stratum pyramidale; SRad, stratum radiatum; SMol, stratum moleculare.

ipsilateral CB, the pathway by which the RE projects to the HPC (Herkenham, 1978; Wouterlood et al., 1990). The evoked LFP profile during CB stimulation closely resembled the direct RE stimulation, again showing a maximal negativity at SLM (Fig. 3D). This evoked potential was limited to the ipsilateral hippocampus, and any influence of RE stimulation on contralateral HPC and neocortical potentials was markedly reduced or completely eliminated (contralateral HPC amplitude decreased 90.8%, $p = 0.0035$; neocortical amplitude decreased 93.0%, $p = 0.0051$; two-tailed paired *t* tests) using this procedure. Subsequent CSD analysis revealed a sink in the SLM similar to that evoked by RE stimulation, albeit at a significantly reduced latency of 18.67 ± 0.69 ms ($p = 0.0020$, compared with RE stimulation, two-tailed paired *t* test) and magnitude (-4.51 ± 1.36 mV/mm^2; $p = 0.024$, two-tailed paired *t* test with respect to Fig. 3E,G,H).

2.5.3 Stimulating the medial prefrontal cortex generates an evoked potential in the hippocampus that is mediated via the nucleus reuniens

Given the dense projections from PL and IL to RE (Vertes, 2002; Mathiasen et al., 2019), we targeted these sites in $n = 7$ rats (verified histologically; Fig. 4B) using a paired-pulse stimulation paradigm to record its influence in the HPC (Fig. 4A). In $n = 4$ animals, a Gi-coupled DREADD, hM4Di virus (Armbruster et al., 2007; Atasoy and Sternson, 2018) was preinjected into the RE 3 weeks before experimentation; in the remaining three animals, a control mCherry vector was used. This allowed us to evaluate the influence of chronic silencing of RE neurons following systemic CNO administration (Whissell et al., 2016; Aldrin-Kirk and Bjorklund, 2019). We then evaluated the evoked potential profile pre- and post-CNO administration. As with direct RE stimulation, we limited our analysis to those trials occurring during deactivated brain states.

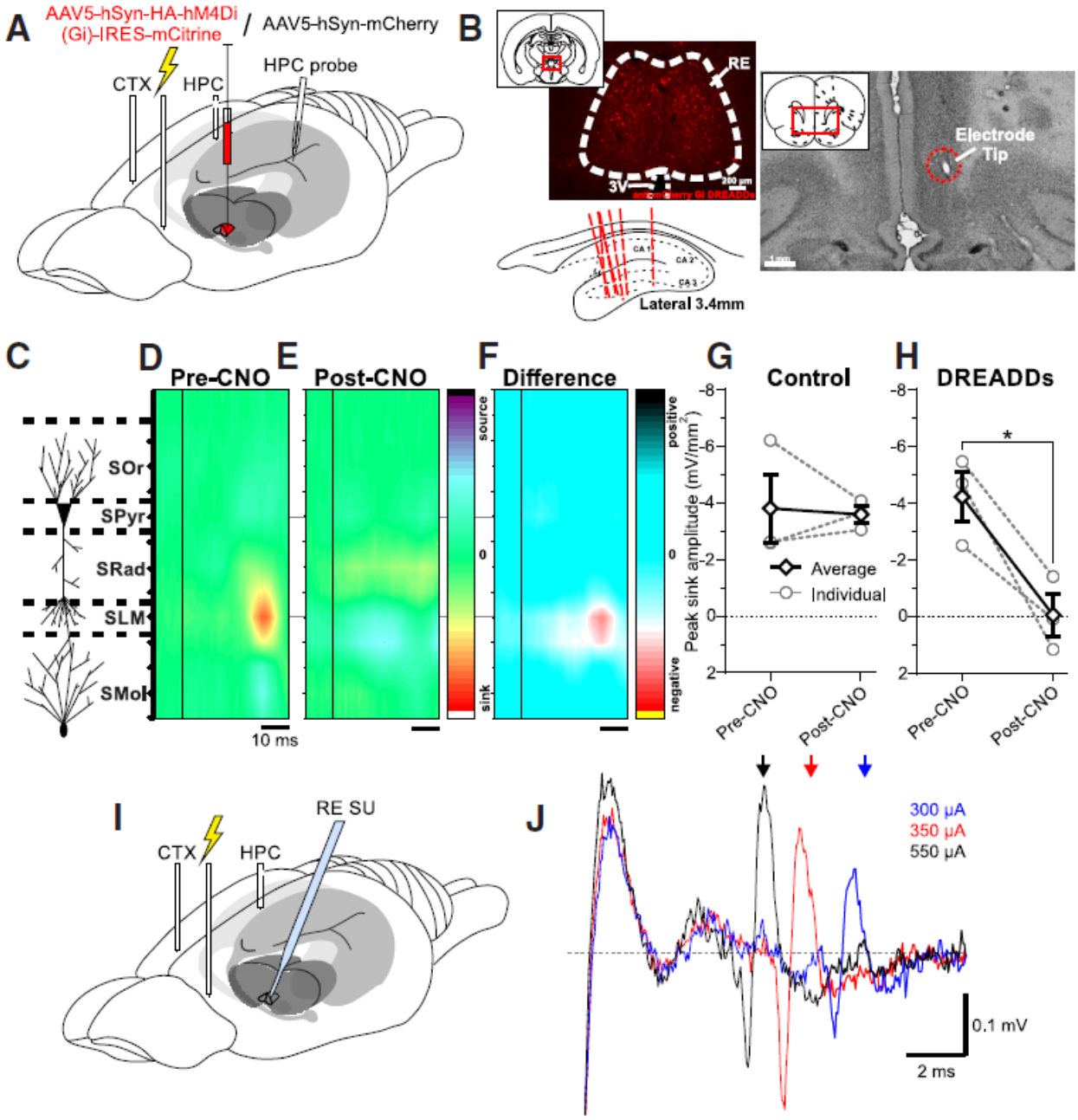

Figure 2.4 Stimulation of the mPFC produces an evoked response in the HPC that can be blocked by selective RE inhibition.

A. Schematic illustration of the injection, stimulation, inhibition, and recording procedures. **B.** Top left, Representative coronal tissue section showing expression of hSyn- hM4Di-HA-mCitrine virus localized to RE. Scale bar, 200 m. Inset, Schematic of relative location of image.

Top right, Representative coronal Nissl-stained tissue section showing the tip of a stimulating electrode in IL. Inset, Schematic of relative location of image. Bottom left, Schematic sagittal illustration of all (except one) multiprobe track through HPC. **C.** Schematic depiction of HPC cell lamina. **D.** Color contour plot of ipsilateral HPC CSD following the second pulse of paired-pulse stimulation (dashed vertical line) in IL before CNO administration, illustrating a prominent sink localized to SLM. CSD scales are -6 to 6 mV/mm^2. **E.** Color contour plot of CSD following identical IL stimulation paradigm (dashed vertical line), post-CNO administration in a DREADDs animal, illustrating a disappearance of the SLM sink. CSD scales are -6 to 6 mV/mm^2. **F.** Difference contour plot created by subtracting the post-CNO CSD in **E** from the pre-CNO CSD in **D** from the same animal, illustrating that the difference between the two conditions is limited and localized to the SLM sink. Difference scales are -7.4 to 7.4 mV/mm^2. **G.** Peak sink amplitude pre-CNO and post-CNO in control (hSyn-mCherry) animals (individuals: gray hollow circles and gray dashed lines; average: black hollow diamonds and solid black lines), showing no significant difference in amplitude between conditions. **H.** Peak sink amplitude pre-CNO and post-CNO in DREADDs (hSyn-hM4Di-HA-mCitrine) animals (individuals: gray hollow circles and gray dashed lines; average: black hollow diamonds and solid black lines), illustrating a robust decrement in sink amplitude after CNO administration in all animals (Error bars represent SEM. $*p < 0.05$). **I.** Schematic illustration of the mPFC stimulation and RE single-unit (SU) recording procedures. **J.** Increasing stimulation intensity (blue trace, 300 A; red, 350 A; black, 550 A) in IL decreases the latency of responding in RE single-unit and multiunit activity, indicating direct mPFC–RE orthodromic excitation. Arrows, Average spike latency over 10 stimulation trials.

Stimulating IL yielded an evoked potential profile in the HPC that, following CSD analyses, resembled that evoked by RE and CB stimulation (Fig. 4C,D). In control (mCherry) animals, a maximal current sink was observed at 17.67 ± 0.88 ms pre-CNO and at 17.67 ± 1.76 ms post-CNO. This latency is shorter when compared with the RE or CB stimulations as a consequence of using electrical, rather than optogenetic, stimulation. In a pilot chemogenetic inactivation experiment, the IL was optogenetically stimulated and evoked a response in HPC with a latency of 52 ms. Neither the latency to the peak sink ($p = 1.00$, two-tailed paired t test) nor the magnitude ($p = 0.84$, two-tailed paired t test; -3.79 ± 1.20 mV/mm^2 pre-CNO, and -3.57 ± 0.30 mV/mm^2 post-CNO) across conditions was significantly different (Fig. 4G).

In DREADD-expressing animals, the maximal sink amplitude was significantly ($p = 0.048$, two-tailed paired t test) decreased following CNO administration, from -4.22 ± 0.89 to -0.034 ± 0.75 mV/mm^2 (Fig. 4E,H). Given the robust diminution of the sink post-CNO, the current flow at an equivalent time point to that chosen pre-CNO was selected for comparison. Subtracting the entire evoked CSD potential post-CNO from that pre- CNO revealed an obvious abolition of the effect of prefrontal stimulation on the HPC (Fig. 4F).

These results imply that SO-related activity in the mPFC is actively transmitted to the HPC via excitation of RE neurons. To show this directly, we recorded single-unit and multiunit unit activity in RE during mPFC stimulation ($n = 6$). Indeed, we found that mPFC stimulation evoked orthodromic excitation in RE units (Fig. 4I,J).

2.5.4 Chemogenetic silencing of the nucleus reuniens impairs prefrontal-hippocampal SO coordination

In the same animals expressing a Gi-coupled DREADD virus in the RE (n = 9) or control vector (mCherry n = 4; Fig. 5A), we evaluated the coordination of the SO across mPFC and HPC sites pre-CNO and post-CNO administration. To minimize any contamination of the hippocampal signal by volume conduction from overlying cortex, we used the continuous CSD signal at the SO maximal contact on the linear probe (Wolansky et al., 2006). The average coherence of the SO signal during baseline recordings was 0.50 ± 0.09 in controls and 0.57 ± 0.05 in DREADD-infected animals (Fig. 5C). This was significantly reduced following CNO administration in every animal in the DREADD-infected group (0.38 ± 0.04; $p < 0.0011$, two-tailed paired t test; Fig. 5B, see example), while no significant difference was observed in the control group (0.48 ± 0.08; $p = 0.35$, two-tailed paired t test; Fig. 5B,C). As coherence can be influenced by the relative power of the frequency of interest at the two sites (Srinath and Ray, 2014), we ensured that there were no reductions of SO power in either the mPFC or HPC sites. There was no reduction of field SO power in the mPFC across these time points (control, p = 0.24; DREADDs, $p = 0.26$; two-tailed paired t tests; Fig. 5B,D). Interestingly, CSD SO power in the HPC increased post-CNO (control, $p = 0.023$; DREADDs, $p = 0.010$; two-tailed paired t tests) between pre-RE and post-RE inhibition conditions (Fig. 5E). This increase at SO frequencies in the CSD signal from the linear probe was also present in three additional experiments in which no CNO was administered and was likely a nonspecific result related to the passage of time itself, since we also observed a nonspecific increase in broadband (0–500 Hz) power as well.

In four animals, we could relate the drop in SO coherence to the reduction of the evoked sink from mPFC stimulation. The degree of suppression in the evoked potential was positively related to the reduction in coherence, with an R^2 value of 0.88 (Fig. 5F). Thus, any reduction of

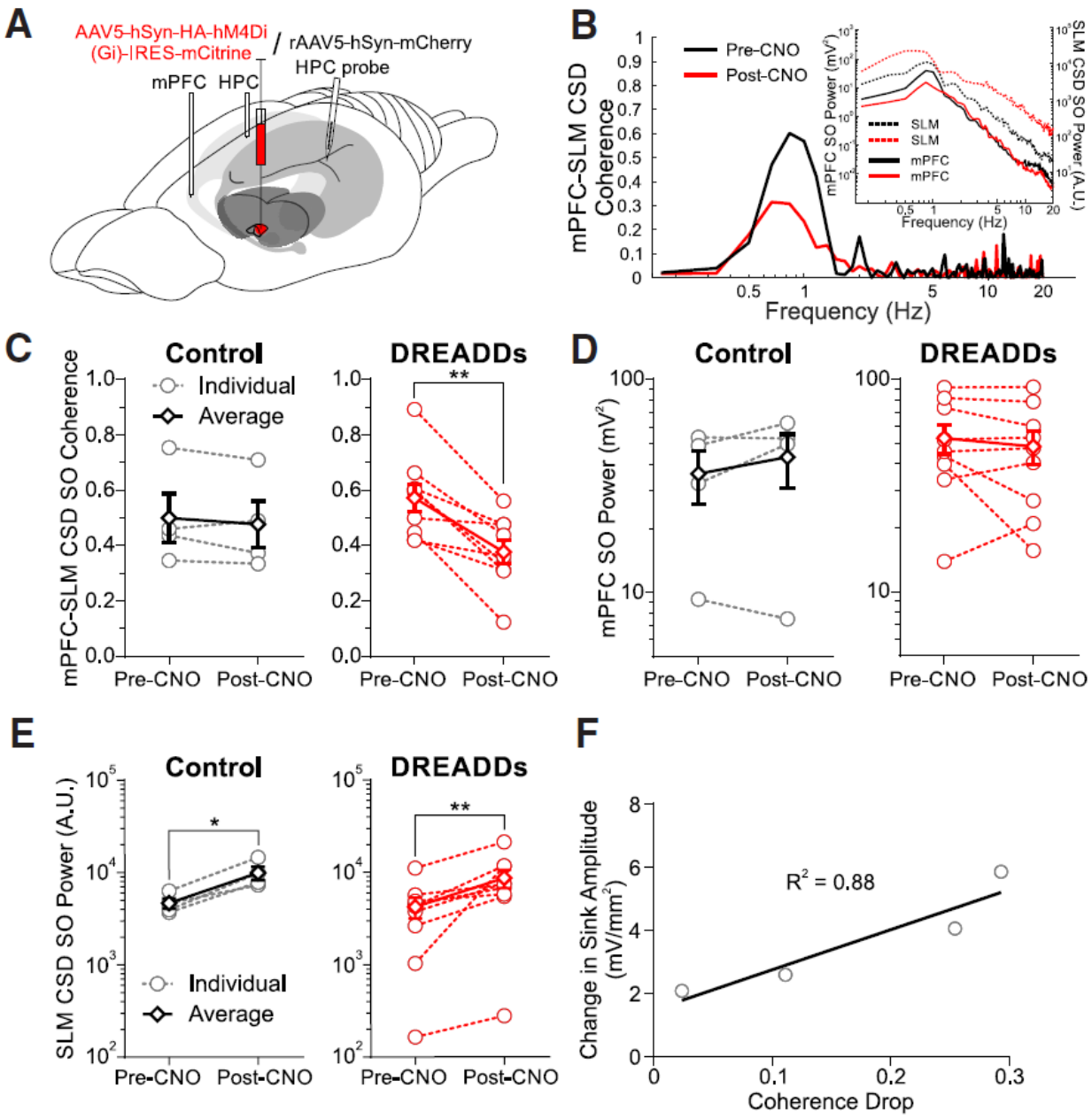

Figure 2.5 RE inhibition decreases mPFC–HPC SO synchrony.

Figure 2.5 RE inhibition decreases mPFC–HPC SO synchrony. A. Schematic illustration of the injection, inhibition, and recording procedure. Either a hSyn-hM4Di-HA-mCitrine (DREADDs) or an hSyn-mCherry (CONTROL) virus was injected into RE 3 weeks before experimentation. **B.** Example difference in mPFC-SLM CSD coherence pre-CNO and post-CNO in a representative DREADDs animal. Black lines, pre-CNO; red lines, post-CNO. Inset, Autospectral power of mPFC field (solid lines, left axis) and SLM CSD (dashed lines, right axis). **C.** Coherence between mPFC bipolar field and HPC CSD (selecting the SLM depth trace in particular) in both control (left: individuals: gray hollow circles and gray dashed lines; average: black hollow diamonds and solid black lines) and DREADDs (right: individuals: red hollow circles and red dashed lines; average: red hollow diamonds and solid red lines) groups, showing a significant drop in every DREADDs animal, but not in controls. **D.** Autospectral power in mPFC at the peak SO frequency in CONTROL (left) and DREADDs (right) groups, showing no significant difference in either. **E.** SLM CSD power at the peak SO frequency in CONTROL (left) and DREADDs (right) groups, showing an increase in power across both conditions. **F.** Scatterplot of the reduction in evoked sinks via mPFC stimulation as a function of the drop of SO coherence following chemogenetic RE inhibition. Solid line indicates least-squares regression fit ($R^2 = 0.88$). Error bars represent SEM. $*p < 0.05$; $**p < 0.01$.

the RE-mediated mPFC stimulation effects on the HPC was directly related to the subsequent reduction in SO coordination across mPFC and the HPC.

2.6 Discussion

Our data show that the connections mediated between medial prefrontal cortex and the hippocampus via the nucleus reuniens appear to be necessary for coordination of the slow oscillation between these structures. Indeed, we showed that RE neurons track the ongoing slow oscillation and that they have consistent phase relationships to both the neocortical and hippocampal expression of this activity. When RE cells are inactivated, communication between the mPFC and HPC is disrupted, and so too is the coherence of the cortico-hippocampal SO. Given the role of slow-wave sleep, and in particular the SO, in memory consolidation, we feel that the RE is in a prime position to influence the coordination of cellular ensembles that would be relevant for the solidification of episodic memories.

2.6.1 Urethane anesthesia and natural sleep

Spontaneous, rhythmic brain state alternations under urethane anesthesia bear more than a passing resemblance to those across REM and NREM sleep. Field potential recordings from neocortical and hippocampal sites demonstrate transitions between an activated pattern composed of low-power, high-frequency cortical activity together with rhythmic hippocampal theta frequency (3–4 Hz) activity versus a deactivated pattern of high amplitude, slow-frequency (~1 Hz) activity at both sites. The timing of these alternations overlaps very well with those observed in natural sleep, and concomitant with these state alternations are peripheral

physiologic changes, including respiratory rate, heart rate, muscle tone, and temperature. These correspond well to observed changes across natural REM and NREM states (Clement et al., 2008; Whitten et al., 2009; Pagliardini et al., 2012). Urethane-anesthetized mice also show these same alternations (Pagliardini et al., 2013b). As we have also reviewed recently (Ward-Flanagan and Dickson, 2019), other central and peripheral changes observed across these state changes also correspond well to those noted for natural sleep. As such, the urethane-anesthetized rodent is a highly tractable model that is widely used to study central and peripheral dynamics of natural sleep.

2.6.2 Activity states of nucleus reuniens neurons

The activity of RE neurons has been previously examined almost exclusively during theta. Consistent with previous work (Morales et al., 2007; Lara-Vasquez et al., 2016; Walsh et al., 2017), we found that during activated/ theta brain states, RE units showed high-frequency tonic activity that had no rhythmicity or oscillatory LFP correlates. During transitions to deactivated states, and especially during strong forebrain SO, however, the activity of all RE neurons recorded developed striking phase rhythmicity, strongly coupled to ongoing SO. Not only does this suggest a strong state-dependent modulation of information processing by the RE but also implicates it in following and potentially transmitting SO rhythmicity from the mPFC to the HPC.

The RE sits in a nodal region interfacing mPFC and HPC. RE neurons receive input from mPFC and, in turn, send a dense excitatory projection to SLM of CA1 (Herkenham, 1978; Yanagihara et al., 1987; Wouterlood et al., 1990). Previous work (Isomura et al., 2006;

Wolansky et al., 2006) has demonstrated that HPC SO potentials and current sink–source alternations have the strongest power at the level of the SLM. These results suggest that inputs arriving at the SLM are the source of phasing, coordination and, perhaps, the generation of the SO in the HPC. Although previous work implicated layer III neurons of the entorhinal cortex in mediating this SO activity, via the densely SLM-innervating temporoammonic pathway (Isomura et al., 2006; Wolansky et al., 2006; Sullivan et al., 2011; Hahn et al., 2012; Taxidis et al., 2013), our present data suggest a more important role for the RE. Indeed, the RE may well integrate SO activity at both the level of HPC and EC through its additional prominent connections to EC layer III. This latter idea remains to be tested.

Our unit findings are also consistent with other work conducted during SO activity facilitated by ketamine anesthesia (Angulo-Garcia et al., 2018; Ferraris et al., 2018). This work also showed strong SO coupling of RE units but was focused more specifically on examining ON-phase gamma coupling between the HPC and mPFC that might be mediated by the return projections of the RE. Indeed, the grouping of ensemble activity into the active (ON) phase of the SO would be a powerful way to enhance synaptic coupling between sets of neurons in disparate episodic memory regions, and this may be the exact mechanism by which SO activity enhances episodic memory consolidation. Although Ferraris et al. (2018) suggested that the RE mediated coupling between the HPC and the mPFC (i.e., in the opposite direction to what we propose), it very well may be the case that it does both, and thereby could mediate continuing reverberative activity in this bidirectional circuit. Of course, this would presumably strengthen cellular assemblies to an even greater degree across mPFC and HPC.

The mPFC (and the IL in particular) has also been shown to alter the firing of RE cells (Zimmerman and Grace, 2018). Our findings suggest that the mPFC provides a rhythmic input to

RE during SO states, the timing of which is then relayed to CA1. As such, it is likely that the RE is entrained by slow, rhythmic stimulation via the mPFC, which could subsequently entrain the HPC. Indeed, we observed that increased forebrain deactivation predicted increased rhythmicity in the RE, suggesting that SO activity in mPFC is reliably transmitted to, and likely entrains, RE units to the cortical SO ON phase. Moreover, we also showed that mPFC stimulation orthodromically excited RE neurons. In our model, we regard the RE as a rhythmic mediator in a disparate slow-wave circuit, not responsible for generating the SO in either mPFC or HPC per se, but rather for maintaining synchronous coordination between them through an SO-driven clock-like mechanism.

2.6.3 Disrupting mPFC coupling to the HPC by RE inactivation decouples forebrain SO coordination

We confirmed that optogenetic activation of RE inputs to HPC evoked an excitatory sink at the level of the SLM, similar to previous electrical stimulation studies (Dolleman-Van der Weel et al., 1997; Bertram and Zhang, 1999; Morales et al., 2007; Dolleman-van der Weel et al., 2017). Furthermore, stimulation of mPFC itself could also produce this same pattern of activation in the HPC, which was then abolished by chemogenetic inactivation of RE neurons. In the same inactivation experiments, this reduction of the evoked response was strongly related to a marked decrease in mPFC–HPC SO phase coherence, but without any loss of SO power at either site. Altogether, our experiments strongly suggest that SO coupling (but not power) across mPFC and HPC is mediated by the interfacing activity of RE neurons.

Of interest here is the mediation of remaining slow power at the level of the HPC following RE inactivation. The power profile of SO activity remained similar, suggesting that activity at SLM continues to drive slow oscillatory activity within the hippocampal circuit. With the RE inactive, the only other input would be the temporoammonic pathway from EC. Further work will determine the role of the layer III input from EC and how it integrates with RE activity.

It is possible that RE activation (either directly or via mPFC stimulation) evokes a response in the HPC via a complex interaction with the entorhinal cortex. Anterograde tracing of outputs from the RE showed not only dense labeling in the SLM, but in the medial entorhinal cortex as well (Wouterlood et al., 1990). In this study, transecting the CB showed large numbers of degenerating axon terminals present in medial entorhinal cortex, suggesting that the RE may simultaneously influence the parent cell bodies of the perforant pathway, as well as target neurons in CA1. More recent work has examined the effect of coincidental stimulation of both RE and entorhinal cortex (Dolleman-van der Weel et al., 2017). Stimulating both sites produced a nonlinear interaction throughout the HPC evoked potential, suggesting that RE and EC axons synapse, at least partly, onto the same dendritic sites in CA1 pyramidal cells. The authors posit that the role of the RE in a slow-wave-related circuit may be to facilitate an entorhinal–HPC dialogue, and that is what may be responsible for coordinating and synchronizing the SO between frontal cortical and HPC sites (Dolleman-van der Weel et al., 2017). A natural follow-up to the present study then, is to assess any changes in SO coherence between the entorhinal cortex and HPC following RE inactivation or excitation. What we can conclude from our work is that the RE certainly has an excitatory influence on the HPC, and that without that input, prefrontal– HPC SO synchrony is considerably impaired.

2.6.4 The RE as a nodal hub between mPFC and HPC for synchrony and memory

Consistent with the idea of the RE acting as a gate or nodal hub for information flow between mPFC and HPC (Vertes et al., 2007; Cassel et al., 2013; Varela et al., 2014), the role of the RE in a host of memory tasks is being increasingly recognized. RE lesions or inactivation have a particularly detrimental effect on spatial working memory tasks requiring interactions between mPFC and HPC, but not those that only require HPC activity alone (Davoodi et al., 2009; Hembrook and Mair, 2011; Hembrook et al., 2012). The RE also has a described role in determining the generalization and specificity of contextual fear memories (Xu and Sudhof, 2013). A critical role of the RE in forming long-term (>24 h) memories, but not acquisition or short term memories, has also been demonstrated (Loureiro et al., 2012; Barker and Warburton, 2018). Importantly, however, many studies have used behavioral tasks that assess influences of RE impairments at only short delays or periods in which animals may not have slept, highlighting that the RE is not solely involved in slow-wave coordination for off-line memory consolidation, but may also be involved in memory during on-line theta states (Hallock et al., 2016; Maisson et al., 2018). Together, these results demonstrate a role for the RE in the integration of HPC and mPFC-mediated memory function.

More recent considerations of nCTX–HPC dynamics have discussed the role of the RE in mediating widespread coordination (Hallock et al., 2016; Dolleman-van der Weel et al., 2017; Ferraris et al., 2018). Specific studies have intimated that the directionality of information transfer in this tripartite circuit depends on the specific stage of the task involved (Spellman et al., 2015; Hallock et al., 2016). For instance, in a delayed alternation T-maze task HPC theta activity led and organized both unit and theta activity in the mPFC during the delay period between trials (Hallock et al., 2016). Conversely, during choice point traversals, slow gamma

activity in the mPFC led and predicted slow gamma activity in the HPC. Effective performance of the task as such requires an interplay between the mPFC relaying choice information to the HPC, which stores and subsequently relays this information back to mPFC to guide future decision-making. Critically, communication in either direction was eliminated following RE inactivation. Interestingly, and in support of our directional model of SO influence from the mPFC to the HPC, another recent study demonstrated that statistical (using partial correlation analysis) or pharmacological removal of the RE impaired PFC–HPC coherence in a 2–5 Hz bandwidth, but had minimal effect on theta coupling, which the authors posit is because of a strong, intact connection directly from HPC to mPFC (Roy et al., 2017). In contrast, Ferraris et al. (2018) describe an HPC-to-mPFC directionality during slow gamma activity that is disrupted by muscimol infusion into the RE. Interestingly, the authors also describe a diminished degree of coupling of HPC (but not mPFC) gamma to the SO phase following RE inhibition, suggesting that the opposite of their conclusion may be the case (i.e., the off-line, slow-wave pathway operates to synchronize activity in a mPFC-to-HPC-dependent manner). One point to highlight in this regard that may be relevant to the results reported by Ferraris et al. (2018) during anesthesia is that they evoked SO activity by supplementing urethane anesthesia with ketamine-xylazine. Ketamine–xylazine anesthesia is known to inflate SO-related coherence between neocortex and hippocampus compared with urethane alone (Sharma et al., 2010). In addition, ketamine–xylazine anesthesia is also known to alter the dynamics of SO-related neocortical unit activity (Chauvette et al., 2011) compared with natural sleep. Finally, ketamine–xylazine anesthesia inflates SO-related gamma activity in the forebrain (Hong et al., 2010; Shaw et al., 2015; Furth et al., 2017), but also specifically in the hippocampus compared directly with

urethane anesthesia (Sharma et al., 2010). In this respect, we feel that urethane-alone experiments more closely resemble natural sleep.

Slow-wave sleep and, indeed, the SO itself have been implicated in off-line memory consolidation (Steriade and Timofeev, 2003; Stickgold, 2005; Dickson, 2010). Transcranial stimulation at SO frequencies enhanced the retention of declarative memories in a human population (Marshall et al., 2006). Slow-wave sleep appears to be especially well suited for facilitating spike timing-dependent plasticity processes that are critical for memory formation (Gonzalez-Rueda et al., 2018). Moreover, the negative trough of the SO is ideally suited for optimizing synaptic plasticity within local circuits (Molle et al., 2011; Niethard et al., 2018). Synaptic excitability in general is enhanced during SO (compared with theta) states, but this is especially prominent during the falling phase (positive to negative) of the SO (Schall et al., 2008). This is the precise timing we found that RE units were phase coupled to, with respect to the mPFC SO. The SO, as such, represents an excellent platform for coordinating communication across large and disparate cortical sites (Buzsaki, 1996, 1998; Steriade and Timofeev, 2003; Dickson, 2010; Cox et al., 2014), and the RE is an ideal mediator for exactly this activity pattern.

2.7 Conclusion

Here we show that selective inhibition of the thalamic RE impairs slow oscillatory coordination between neocortical and hippocampal sites. We first demonstrated that RE neurons were strongly and rhythmically coupled to the negative phase of the neocortical SO. Stimulating either directly at the level of the RE or its axonal projection bundle, or even at the level of the

mPFC, reliably produced an evoked HPC potential maximal at the level of SLM. Chemogenetic inhibition of the RE abolished the HPC potential evoked by mPFC stimulation, demonstrating that we could functionally impair this disynaptic circuit. Doing so caused a robust decrease in mPFC–HPC synchronization at SO frequencies. Together, our data demonstrate that the RE has a critical role in mediating frontal cortical–HPC coordination, particularly during slow-wave/off-line states. This has marked implications for sleep-dependent memory consolidation and highlights the RE as an exciting avenue for future study.

3 Prefrontal-hippocampal communication through the nucleus reuniens is biased by brain state

Brandon E. Hauer[1], Silvia Pagliardini[1,2,3], Clayton T. Dickson[1,2,3,4]

[1]Neuroscience and Mental Health Institute, University of Alberta, Edmonton, Alberta T6G 2E9, Canada,

[2]Department of Physiology, University of Alberta, Edmonton, Alberta T6G 2E9, Canada,

[3]Department of Anesthesiology and Pain Medicine, Edmonton, Alberta T6G 2E9, Canada,

[4]Department of Psychology, University of Alberta, Edmonton, Alberta T6G 2E9, Canada

Acknowledgements: This work was supported by Natural Sciences and Engineering Research Council of Canada (NSERC) Discovery grants 2016-06576 and 2021-02926 to C.T.D, and NSERC grant 435843 to S.P. B.E.H. was supported by an NSERC Doctoral Postgraduate Scholarship.

3.1 Abstract

Circuit-level communication between disparate brain regions is fundamental for the complexities of central nervous system operation. Co-ordinated bouts of rhythmic activity between prefrontal cortex (PFC) and hippocampus (HPC), in particular, are important for mnemonic processes. This is true during awake behaviour, as well as during offline states like sleep. We have recently shown that the anatomically interposed thalamic nucleus reuniens (RE) has a role in coordinating slow-wave activity between PFC and HPC. Here, we took advantage of spontaneous brain state changes occurring during urethane anesthesia in order to assess if PFC-HPC communication was modified during activated (theta) versus deactivated (slow oscillation: SO) states. These forebrain states are highly similar to those expressed during REM and nonREM stages of natural sleep, respectively. Evoked potentials and excitatory current sinks in HPC were consistently larger during SO states, regardless of whether PFC or RE afferents were stimulated. Interestingly, PFC stimulation during theta appeared to preferentially use a cortico-cortical pathway, presumably involving the entorhinal cortex as opposed to the more direct RE to HPC conduit. Optogenetic and chemogenetic manipulations of the RE suggested that this state-dependent biasing was mediated by responding in the RE itself. Finally, the phase of both ongoing rhythms also appeared to be an important factor in modulating HPC responses, with maximal field EPSPs occurring during the negative-going phase of both rhythms. Thus, forebrain state plays an important role in how communication takes place across the PFC and HPC, with the RE as a determining factor in how this is shaped. Furthermore, ongoing sleep-like rhythms influence the coordination and perhaps potentiate excitatory processing in this extended episodic memory circuit. Our results have direct implications for activity-dependent processes relevant to sleep-dependent memory consolidation.

3.2 Contribution to the Field Statement

Forebrain communication is fundamentally important for mnemonic processes. Reverberant activation of neural circuitries important for a memory trace during subsequent offline states like sleep is potentially important for consolidating memory. In this work, we show that two disparate episodic memory-related areas in the brain, the medial prefrontal cortex and the hippocampus, communicate in a fundamentally different fashion as a function of ongoing brain state. Moreover, we demonstrate that the interposed thalamic nucleus reuniens is a key mediator of this state-dependent modulation of cortico-hippocampal communication. As such, the nucleus reuniens is poised to be a key modulator in timing-dependent mnemonic processes, helping to gate information flow between frontal cortices and the hippocampus.

3.3 Introduction

Coordinated neural activity is vital for mnemonic processes (Buzsaki, 1996; Siapas and Wilson, 1998). One of the most widely studied phenomena in memory-relevant brain areas is the emergence (and prevalence) of collective oscillatory activity. These rhythmic patterns and their inter-regional synchrony are thought to modulate and constrain information processing, especially in key memory centers including the hippocampus (HPC) and medial prefrontal cortex (mPFC). Decades of research have indicated a decisive role of both HPC and mPFC in episodic mnemonic processes (Jin and Maren, 2015). Indeed, communication between these disparate structures is essential for the proper encoding and retrieval of episodic memories (Simons and Spiers, 2003; Preston and Eichenbaum, 2013). Conceptually, mPFC may be directing the retrieval of episodic memories from HPC, based on the current context (Navawongse and Eichenbaum, 2013). In other words, information relayed from mPFC to HPC aids in guiding both memory acquisition and retrieval, while in turn, the HPC sends signals to mPFC to provide remembered episodes with goals, rules, and procedural representations (Morris, 2001; Dolleman-van der Weel et al., 2019).

There exists a robust and direct connection from the HPC to mPFC which strongly targets infralimbic (IL) and prelimbic (PL) cortices (Hoover and Vertes (2007), yet the reverse is not true (Sesack et al., 1989; Laroche et al., 2000), however, *cf*. Rajasethupathy et al. (2015). Instead, a small midline thalamic body, the nucleus reuniens (RE) lies anatomically interposed between mPFC and HPC (Vertes et al., 2006; Vertes et al., 2007). Within the RE is a population of neurons that project via axon collaterals to both mPFC and HPC, providing a direct disynaptic link between these two important structures (Hoover and Vertes, 2012; Varela et al., 2014). The RE as such is a key node for return projections from mPFC to HPC, completing a loop circuit

capable of bridging executive functioning and memory: HPC → mPFC → RE → HPC (Dolleman-van der Weel et al., 2019).

Broadly speaking, the most predominant (and widely-studied) activity-dependent oscillatory patterns in these two sites are slow oscillations (SO, ~1 Hz) and the theta rhythm (~3-12 Hz). Slow oscillations are known to nest other mnemonically-relevant activity patterns, including spindles (~12-16 Hz), beta/gamma (25-100 Hz), and sharp wave/ ripple complexes (transient, irregularly-occurring high frequency: 150-250 Hz oscillations) (Staresina et al., 2015; Oyanedel et al., 2020). The importance of these rhythms for memory processes has been demonstrated during waking (Sauseng et al., 2009; Buzsaki and Watson, 2012), as well as during offline states like sleep (Puentes-Mestril et al., 2019; Marshall et al., 2020).

Recently, we have demonstrated that the RE has an essential role in coordinating SO activity between the PFC and HPC (Hauer et al., 2019). However, less clear is how the ongoing dialogue between these structures changes as a function of ongoing shifts in brain state. Moreover, it is unclear how the role of the RE may change during activated (theta) states, and how its activity (or inactivity) may modulate cortico-hippocampal information exchange. To this end, we performed a sequence of multisite recordings, along with opto- and chemogenetic circuit perturbations in an *in vivo* rat preparation, while stimulating both RE and IL across SO and theta states. Our results demonstrate that PFC-HPC communication is fundamentally different between states, and that the RE has a critical role in mediating this disparity. Different circuitry is recruited as a function of ongoing forebrain state, but both states show a rhythmical modulation of excitability dependent on the oscillatory phase of the ongoing rhythm.

3.4 Materials and Methods

3.4.1 Animals

Experiments were conducted on 22 male Sprague Dawley (SD) rats obtained from the Sciences Animal Support Services and/or Health Sciences Laboratory Animal Services of the University of Alberta with a mean (± standard error of the mean; SEM) final weight of 453.09 ± 9.40 g. Of these, 14 were used for electrical or optical stimulation of RE, cingulum bundle (CB), and PFC; and 8 were used for chemogenetic inhibition of RE. Some of these data (n = 8 rats for DREADDs experiments; n = 3 for RE and CB optogenetic stimulation) were used in a prior study from our laboratory (Hauer et al., 2019), while the rest (n = 11) constitute entirely original data. All animals were provided with food and water *ad libitum* and were maintained on a 12 h light/dark cycle, with lights on at 7:00 am. All procedures conformed to the guidelines of the Canadian Council on Animal Care (CCAC) and were approved by the Biological Sciences and/or Health Sciences Animal Policy and Welfare Committees (AUP 092 and AUP 461) of the University of Alberta.

3.4.2 Materials

Bipolar recording electrodes with tip length separation between 0.4-0.9 mm were constructed using Teflon-coated stainless steel wire (bare diameter 125 μm; A-M Systems Inc.). We also used a linear 16-contact (100 μm separation) multiprobe arranged in a vertical linear array (U-probe, Plexon Inc., Dallas, TX) to assess spatial profile field potential recordings in the HPC.

One primary viral vector was used for optogenetic experiments: an adeno-associated virus (AAV, serotype 2/2), expressing a channelrhodopsin-2 variant (ChR2/H134R). The vector was conjugated with enhanced yellow fluorescent protein (EYFP), and driven by the synapsin promoter (hSyn-ChR2-EYFP). They were produced, characterized, and titrated at the University of North Carolina Virus Vector Core Facility, Chapel Hill, NC, USA (ChR2: 3.9 x 10^{12} molecules ml^{-1}).

Chemogenetic experiments also used an AAV vector (serotype 2/5) that was also driven by the same synapsin promoter. However, the vector expressed a Gi-coupled DREADD (designer receptor exclusively activated by designer drug; hM4Di), and was conjugated with both the mCitrine fluorescent protein and a human influenza hemagglutinin (HA) tag (hSyn-hM4Di-HA-mCitrine; 3.5 x 10^{12} molecules ml^{-1} ; UNC Virus Vector Core Facility).

Additionally, chemogenetic control experiments were conducted by using a virus with the same promoter (hSyn) and AAV serotype (5) that was coupled only to a fluorescent vector, without any opsin or DREADD (hSyn-mCherry; UNC Virus Vector Core Facility).

3.4.3 Procedures

Viral injections

Rats were initially anesthetized in a sealed chamber with gaseous isoflurane (4% induction, 1.5% maintenance, in 100% O_2). After loss of righting reflexes, rats were given an intraperitoneal injection of a ketamine/xylazine cocktail (90 and 10 mg/kg, respectively; Bimeda-MTC; Animal Health Inc., Cambridge, ON, Canada; and Rompun; Bayer Inc., Mississauga, ON, Canada). Supplemental doses (10% of original dose) of the ketamine/xylazine cocktail were

administered as required to maintain a surgical anesthetic plane. Body temperature was maintained at 37°C following anesthesia using a homeothermic monitoring system (Harvard Apparatus, Holliston, MA, USA).

Rats were placed into a stereotaxic apparatus (Model 900, David Kopf Instruments, Tujunga, CA, USA) and using aseptic techniques, were prepared for intracranial injections. A single incision was made along the midline of the scalp, and the skin flaps were pinned back. The skull was levelled by adjusting lambda and bregma to be in the same horizontal plane. Holes were drilled in the skull at pre-determined coordinates from a stereotaxic rat atlas (Paxinos and Watson, 1998).

Micropipettes (tip diameter, 30 μm) loaded with either hSyn-ChR2-EYFP (optogenetic experiments), hSyn-hM4Di-HA-mCitrine (chemogenetic experiments), or hSyn-mCherry (control experiments) were attached to a holder (EHW-2MS; A-M Systems Inc., Carlsborg, WA, USA) and lowered using a micro-positioner into the brain. Injections targeted the midline of the nucleus reuniens thalami (AP -2.0; ML +1.9 mm) at an angle 16° oblique to the vertical line to avoid the midline sinus and advanced 6.8 mm from the brain surface (infusion volume 400 nl). Injections were made using a micro-injector (PMI-100; Dagan, Minneapolis, MN, USA) connected via tubing (PVC, 2.79 mm x 4.5 mm; Gilson Inc., Middleton, WI, USA) to the holder, using a pressure of 40 psi and 15 ms pulse length, at a rate of approximately 100 nl/min. Micropipettes were left in place for 7 – 10 min following the injection to allow for adequate diffusion of the virus, and to prevent unintended backtravel of the injected solution up the pipette track.

Following injection procedures, the scalp was then sutured, and rats were given 0.5 ml of the local anesthetic bupivacaine (5 mg/ml s.c.) around the incision site. Animals were provided

with pain medication (meloxicam, 1-2mg/kg in oral suspension; Boehringer Ingelheim Vetmedica, Ingelheim, Germany) over a 24 hour period post-surgery. Food and water were provided *ad libitum* and animals were allowed to recover for 3 weeks before acute experimentation (see below). Neither the viral injection nor the surgical procedures produced any observable long-term issues.

Acute urethane anesthesia and general experimental procedures

For acute anesthetized recordings, rats were initially anesthetized in a gas chamber with isoflurane in medical oxygen (4% induction, 1.5% maintenance). A catheter was inserted into the femoral vein, and isoflurane was discontinued. General anesthesia was obtained by slow (~0.03 – 0.08 ml/min) incremental administrations of urethane (0.4 g/ml) via the catheter (final dose across all rats: 1.33 ± 0.05 g/kg). Urethane was chosen because it promotes an unconscious state that closely mimics the typical dynamics present during natural sleep, both in terms of brain state alternations as well as in terms of their typical physiological correlates (Clement et al., 2008; Pagliardini et al., 2013b).

Rats were placed back into the stereotaxic apparatus and once again the cranium was exposed by making a single long incision along the scalp and pinning back the skin flaps. As before, the skull was levelled by adjusting lambda and bregma to be in the same horizontal plane. Body temperature was maintained at 37°C using the same homeothermic monitoring system. Intracranial implantations were made using pre-determined coordinates from a stereotaxic atlas, using bregma as a landmark (Paxinos and Watson, 1998).

In all experiments, bipolar electrodes for recording local field potentials were positioned in the PFC (AP +3.2; ML 0.7; DV (tip of long electrode) -1.1 to -1.8 mm), and were also placed in the HPC, straddling the pyramidal layer of CA1 (AP -5.5; ML -4.5 mm; DV -2.2 to -3.2 mm). These electrodes were cemented in place using dental acrylic and jeweller's screws fastened into the skull. Local field potentials from bipolar wire electrodes were amplified in differential mode at a gain of 1000 and filtered between 0.1 to 500 Hz using a differential AC amplifier (Model 1700, A-M Systems Inc.).

Photostimulation

An optic fibre (tip diameter 200 μm) connected to a 473 nm laser (Laserglow Technologies, Toronto, ON, Canada), calibrated to deliver light at 10 – 12 mW, was positioned in order to deliver light at intracranial locations. Photostimulation events were driven by a pulse stimulator (Model 2100; A-M Systems Inc.) connected to the laser power supply as well as to the analog-to-digital board and PC acquiring data to mark each event (see below).

Nucleus reuniens stimulation procedures. In addition to bipolar local field potential recordings of PFC and HPC, we also used the linear multiprobe in the contralateral HPC (AP -5.5; ML +4.5; DV -3.3 to 4.5 mm), which was positioned in order sample activity throughout the vertical extent of CA1. Importantly, for monitoring the effects of RE and mPFC stimulation and/or inhibition, the intermediate HPC was consistently targeted using the linear probe given the prominent projection patterns from RE to this septo-temporal region of the HPC (Hoover and Vertes, 2012). Local field potentials from the multiprobe were referenced to stereotaxic ground, passed through a unity gain headstage and then amplified at a gain of 1000 and filtered between 0.1 to 500 Hz

(X1000: Plexon, Dallas, TX, USA). Signals were digitized at a sampling frequency of 1000 Hz using a Digidata 1440A analog to digital board (Molecular Devices) connected to a PC running Axoscope (Molecular Devices). The final depth of the probe was determined using the well-established electrophysiological profile of theta field activity (Bland and Bland, 1986; Buzsaki, 2002). The position of the multiprobe was histologically confirmed in every experiment by analyzing its track in relation to recorded field activity.

The optic fibre was first positioned above the RE (AP -2.0; ML +1.9; DV -6.4 mm) at an angle 16° oblique to the vertical line. Following sufficient optic stimulation (described below), the optic fibre was removed and re-positioned to target the CB (AP -2.5; ML +2.7 mm), angled at 40° oblique to the vertical line and advanced 2.6 to 3.4mm from the brain surface. Evoked potentials were produced using 10 ms laser pulses delivered every 5 s to the RE and then subsequently, the CB, and were averaged over 32-64 trials. Stimulation trains were delivered during equivalent brain states, specifically during either clear deactivated periods characterized by ongoing high power in the 1 Hz signal, or while prominent theta (~4 Hz) activity could be observed in HPC with concomitant low voltage, higher frequency activity in PFC. Stimulation during particular states was confirmed by monitoring ongoing brain state when delivering stimulation trains; and subsequently by both visual and spectral examination of individual recorded sweeps. For the purposes of assessing phase preference, optical stimuli were also delivered every 5 s during continuous field recordings, with the goal of delivering stimuli at random phases of the oscillatory cycle.

Medial prefrontal cortex stimulation. In a subset of animals (n = 18), we employed either a single or paired pulse stimulation paradigm in mPFC sites, with the goal of evoking HPC potentials. The surgical preparation was identical to that employed for RE stimulation (see

above), except that instead of targeting an optic fibre over RE or CB, a bipolar stainless steel (0.08” bare, 0.11” Teflon coated) stimulating electrode was lowered into IL (AP +2.8 to +3.2; ML +0.7 to +1.1; DV -4.0 to -4.5 mm). Following the mPFC paired pulse stimulation paradigm used by Gemmell and O'Mara (2000), 100 – 500 μA biphasic current pulses 0.5 ms in duration were delivered with a 30 ms inter-stimulus interval, every 8 s using a constant current stimulator (Model 2100; A-M Systems Inc.). In some instances, current pulses were also delivered with a 50 ms inter-stimulus interval, or as single, stand-alone pulses. Stimulation epochs were averaged over 32 trials, and were always delivered during a consistent brain state, either theta or SO. Epochs containing trials with electrophysiological artifacts or with sudden, brief state transitions were removed from the analyses on an individual, trial-by-trial basis. Similarly to the optical stimuli delivered to RE and CB during continuous recordings, electrical pulses were delivered to the IL for the purposes of assessing phase preference. Single pulse stimuli were delivered every 8 s during continuous field recordings, with the goal of delivering stimuli at completely random phases of the oscillatory cycle.

Nucleus reuniens chemogenetic inactivation. In 8 experiments with IL stimulation, rats had been pre-treated to express either hSyn-hM4Di-HA-mCitrine or hSyn-mCherry in the RE via our viral injection procedures as described above. Subsequent to baseline evoked potential analysis, and after a suitable period of spontaneous recordings, the DREADD agonist clozapine *N*-oxide (CNO; Cayman Chemical, Ann Arbor, MI, USA) was administered *i.p.* at a dose of 3mg/kg (MacLaren et al., 2016). Activity was then recorded for ~2 more hours, followed by the same IL stimulation paradigm described above. Evoked potentials were performed at least 30 min post *i.p.* CNO injection to ensure adequate time for the ligand or its metabolites to enter the brain (Whissell et al., 2016). This allowed for characterization of the HPC response evoked by IL

stimulation before and after RE inactivation. We could also then compare the evoked response profile in the HPC with an intact vs inactive RE within the same animals and recording period.

3.4.4 Perfusion and Histology

Following experimental recordings, 5 s DC pulses of 1 mA using an isolated current pulse generator (Model 2100; A-M Systems Inc.) were passed through bipolar recording and stimulating electrodes to generate small electrolytic lesions at their tips. These lesions allowed for subsequent verification of recording and stimulation sites. Rats were then transcardially perfused with 0.9% saline and 4% paraformaldehyde in saline (Fisher Scientific, Toronto, ON, Canada). The brain was then removed and placed into a 4% formalin and 20% sucrose solution for at least 48 h. Brains were flash frozen using compressed CO_2 and sectioned with a rotary microtome (1320 Microtome; Leica, Vienna, Austria) at a width of 60 μm. Tissue was counter-sectioned, with one third of sections being mounted on gelatin-coated microscope slides for subsequent thionin staining; another third being mounted on slides and immediately covered using a fluorescence preserving reagent and mounting medium (FluorSave; EMD Millipore, Darnstadt, Germany); and a third of the tissue saved for immunohistochemistry for detection of specific neuronal markers.

Immunohistochemistry was performed according to the following protocol. Free-floating sections were rinsed three times using phosphate-buffered saline (PBS) and incubated with 10% normal donkey serum (NDS) and 0.3% Triton X-100 for 60 min to reduce non-specific staining and increase antibody penetration. Sections were left to incubate over night with primary antibodies diluted in PBS containing 1% NDS and 0.3% Triton X-100 at room temperature.

Primary antibodies used detected: green fluorescent protein (GFP; dilution 1:1000; raised in chicken; Aves Labs, Tigard, OR, USA); red fluorescent protein (mCherry; dilution 1:800; raised in rabbit; Millipore); human influenza hemagglutinin (HA; 1:800; raised in rabbit; Cell Signaling Technology, Danvers, MA, USA); and neuronal nuclear marker (NeuN; 1:800; raised in mouse; Millipore). The following day, tissue was again washed three times with PBS, incubated with secondary antibodies conjugated to the specific fluorescent proteins in each viral construct (Cy2-conjugated donkey anti-chicken; Cy3-conjugated anti-rabbit; Cy5-conjugated anti-mouse; 1:200; Jackson ImmunoResearch, West Grove, PA, USA) diluted in PBS and 1% NDS for 2 h. Sections were again washed three times with PBS, mounted, and coverslipped with Fluorsave (EMD Millipore). Microscopic inspection of tissue was used to verify electrode recording loci, optic fibre tracks, and expression of viral constructs using a Leica DM5500B fluorescent microscope.

3.4.5 Data Processing and Analysis

All signals were acquired with Axoscope 10.6 (Molecular Devices) and were first examined visually to choose data segments for further analyses. Computation and analyses were conducted using custom-written code, as well as the Circular Statistics Toolbox (Berens, 2021) in MATLAB (version R2015b, Mathworks). Analyses were further processed with CorelDRAW X6 (Corel). Data analyses are highly similar to those described in Hauer et al. (2019) and, briefly, included the following: zero phase delay digital filtering, evoked potential averaging, power and phase profile and spectral analyses, coherence, current source density, single- and dual-channel spectra, auto- and cross-correlations, and circular (Rayleigh) statistics.

Field recordings. Autopower, crosspower, coherence, and cross-phase spectra were computed and visualized for both individual, as well as pairs of field signals. Spectra were estimated using a series of 6-s-long, Hanning-windowed samples with 2 s overlap using Welch's periodogram method. Power spectrograms (Wolansky et al., 2006; Whitten et al., 2009; Hauer et al., 2019) were calculated with a sliding window procedure, enabling discrete spectra to be computed and visualized at specific time points across the duration of the recording. These windows were 30 s in duration, slid across the file in 6 s increments. These discrete spectra were then visualized and analyzed as described above. Spectral profiles from multiprobe recordings were created in the same manner for the activity recorded at each channel of the multiprobe, except that each channel was compared against a fixed (either PFC or HPC) bipolar reference, enabling extraction of power, phase, and coherence information at spectral peak frequencies for both SO and theta states. The spatial locations of the multiprobe channels were estimated based on the well-described theta power profile (Bland and Bland, 1986; Buzsaki, 2002; Wolansky et al., 2006), with the phase reversal point corresponding to the interface between *stratum pyramidale* and *stratum radiatum*, and the maximal theta channel located at *stratum lacunosum moleculare* (SLM).

Current source density analysis. CSD analysis was performed on both spontaneously recorded (gap free) field samples, or on evoked potential sweeps and averages recorded using the multiprobe. Briefly, CSD was computed by estimating the second spatial derivative of adjacent multiprobe voltage traces, following the assumptions of Freeman (1975), Rodriguez and Haberly (1989), and Ketchum and Haberly (1993). An advantage of this analytical technique is that it eliminates potential contamination from volume conducted fields at distant sites, because it estimates the volume density of the net current entering or leaving the extracellular space at a

particular site (Buzsaki et al., 2012). Spectral (particularly power and coherence) estimates of the CSD were computed as described above, comparing the CSD of individual multiprobe channels against each other, or against fixed PFC or HPC bipolar electrodes. This technique enabled visualization and analysis of the magnitude of current sinks and sources as a function of space.

Slope and Hilbert phase analysis. To compare the degree of excitatory input across states, we first examined the negative slopes of the evoked field EPSPs due to stimulation of either IL or RE. Using ClampFit 10.7 (Molecular Devices), we manually defined the beginning and end points of the initial negative-going portion of the evoked potential to compute the max slope on an individual, sweep-by-sweep basis, as well as on average. For determining the phase value at which the evoked potential was triggered, we computed the Hilbert transform of the ongoing band-passed rhythm (0.5 – 1.5 Hz for SO and 3 – 6 Hz for theta). This analytic approach enabled the computation of instantaneous amplitude and phase for each type of signal (Le Van Quyen et al., 2001; Bruns, 2004). Phase values were standardized to their sine equivalents by adjusting resultant cosine equivalent values by 90° degrees so that positive-going zero crossings were at phase 0°, 90° the positive peak, 180° the negative-going zero crossing, 270° the negative peak, and 360° the final positive zero crossing and thus, the complete cycle. This allowed us to define the exact phase at which stimulation occurred and then later subcategorize it as occurring during either the rising (270° - 90°) or falling (90° - 270°) phase of the ongoing oscillation.

To assess the relationship between evoked potential slope and the neocortical and hippocampal field, we subdivided evoked potentials across cycles into 20 (18°-wide) bins according to the phase of the field cycle at which they occurred. Since individual slope values could be variable, especially considering the large amplitude of ongoing potentials, we applied an adjacent-averaging (3 bin-wide) smoothing function to these values. This provided an

estimate of the relative magnitude of evoked potential responding as a function of the ongoing oscillation during SO versus during theta, for both IL and RE stimulation. Rayleigh statistics for circular data were used to statistically evaluate the significance of average phase preference on an experiment-by-experiment basis (Zar, 1999). Only experiments where stimuli were delivered with a relatively uniform distribution across all phases of the cycle (i.e., across all 20 phase bins) were included.

3.5 Results

3.5.1 Histological findings

In every experiment, we confirmed the location of all recording and stimulation electrodes, as well as the positioning of the optic fibre. Using immunohistochemistry we also confirmed the location of viral vector expression (Figure 1). Bipolar electrodes were successfully placed in their respective positions (mPFC or HPC) in all cases. As well, all linear multiprobe tracks were localized to CA1, spanning from *stratum pyramidale* through SLM, and into the molecular layer of DG. Localized viral expression was largely confined to the RE, with occasional expression in the adjacent rhomboid and ventral anteromedial nuclei. Any experiments in which viral expression was not localized appropriately to the RE showed a lack of electrophysiological responsiveness to optogenetic stimulation, and were excluded from any further analysis. Placement of the optic fiber was also verified in the immuno-labeled slices, and in all RE-targeting experiments, was positioned just dorsal to the RE, approximately on the midline. Similarly, in experiments where CB stimulation was performed, the optic fiber tip was just dorsolateral relative to the CB at an angled approach. The tip of the stimulation electrode

targeting IL was found to consistently be located within IL, just ventral to prelimbic cortex and above dorsal peduncular cortex, and always medial relative to the basal ganglia.

3.5.2 Nucleus reuniens stimulation produces a stronger hippocampal response during deactivated states

Following viral infection of the RE with hSyn-ChR2-EYFP in eight rats, optical pulses were delivered to the RE (Figure 1). To confirm the observed effects were not due to off-target expression in other nuclei, we additionally stimulated the isolated primary efferent from RE to CA1 in the CB (see below). Evoked potentials were averaged over between 32 and 64 individual stimulations, delivered within each state. Our primary index for brain state was determined by the neocortical electrode, but HPC activity was recorded as an additional confirmation of state.

As we have previously shown (Hauer et al., 2019), opto-stimulation of the RE evoked a prominent negative-going potential peaking at a latency of 24.75 ± 0.73 ms from laser onset in both bipolar and multiprobe recordings from the HPC. In multiprobe recordings the maximum negativity was observed at the approximate level of the SLM. Current source density profiles confirmed that the shortest latency sink (peaking at a similar latency of 22.94 ± 0.60 ms) was indeed centered at the SLM.

When comparing responses across states we observed a consistently larger evoked response (in all 8 of 8 experiments) when light pulses were delivered during ongoing slow oscillation (deactivated) states as compared to theta (activated) states. Stimulation during SO states produced a significantly larger current sink (-10.03 ± 1.82 mV/mm^2) that was maximal at SLM than did stimulation during theta states (-4.48 ± 1.13 mV/mm^2; p = 0.00060, two-tailed

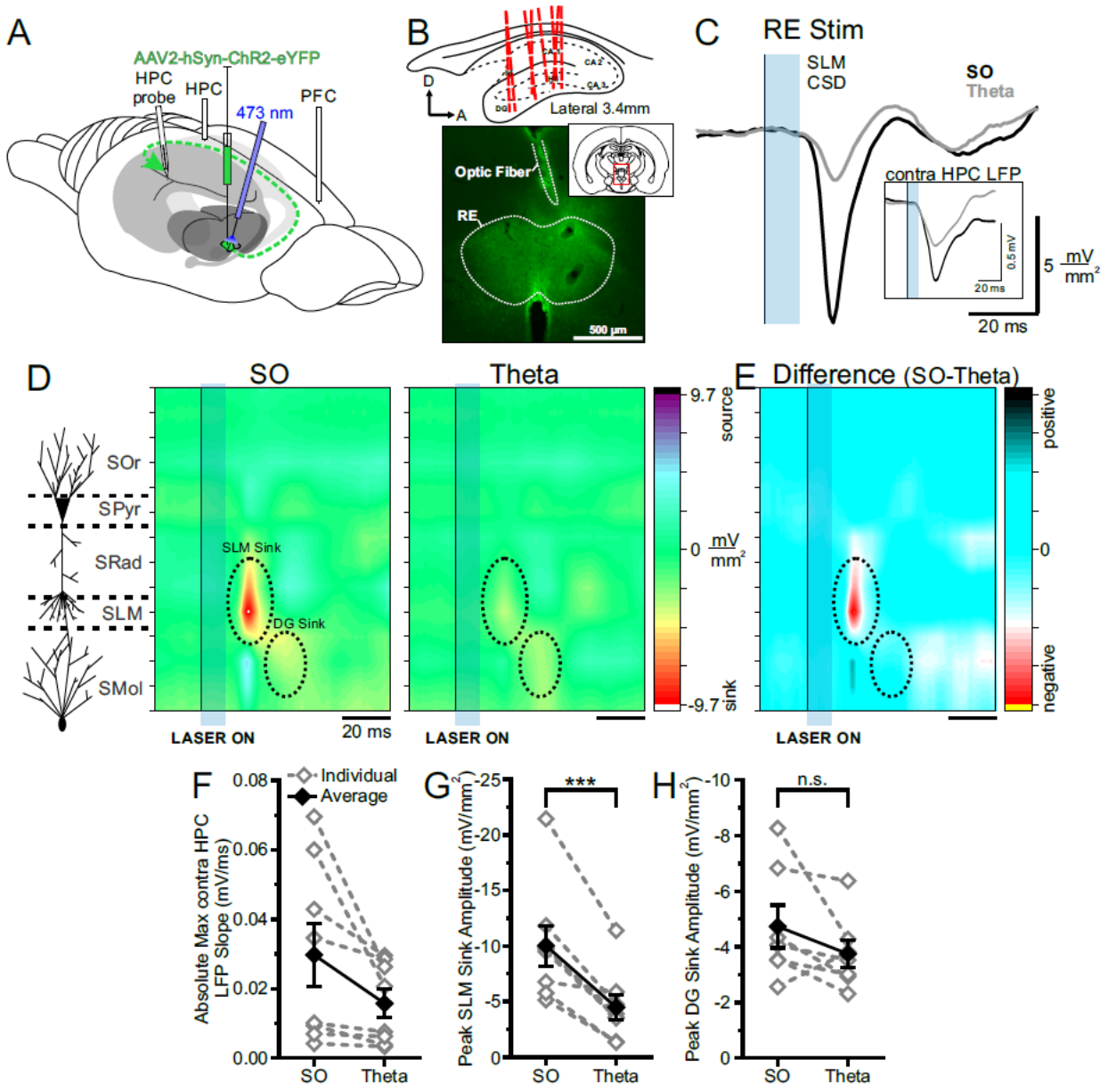

Figure 3.1 Optogenetic stimulation of RE evokes a much larger response in HPC during SO.

A. Schematic illustration of the recording, injection, and stimulation sites. Schema modified from Amaral and Witter (1995). **B.** Top, Schematic sagittal illustration of all multiprobe tracks through HPC. Bottom, Representative coronal tissue section depicting the expression of hSyn-ChR2-EYFP virus localized largely to RE, with optic fiber track positioned dorsal to RE. Inset,

Coronal schematic of the relative location (red box) of the image. Histology corresponds to the same animal whose data are depicted throughout this figure. **C.** Current sink/source density traces evoked in SLM following optogenetic stimulation (10 ms pulse at 473nm wavelength; blue rectangle) of RE during SO (black line) and theta (grey line), averaged over 64 trials. Stimulation of RE during SO produces a much larger current sink in HPC than does stimulation during theta. Inset, Local field potentials recorded from the contralateral HPC following the same optogenetic stimulation of RE during SO (black line) and theta (grey line), showing a larger response during SO. **D.** Left, Schematic depiction of HPC cell lamina as determined by theta profile. Colour contour plot of CSD values just before and following 10ms optogenetic stimulation of RE (black line and blue rectangle) during SO (middle) and during theta (right). RE stimulation produces a large current sink centered around SLM (with a corresponding current source in DG) which is of much greater magnitude during SO compared to during theta. A later DG sink is also evoked by RE stimulation, that does not significantly differ in amplitude between states. CSD scales for both contour plots are identical, from -9.7 to 9.7 mV/mm^2. **E.** Difference contour plot created by subtracting the theta CSD (**D**, right) from the SO CSD (**D**, middle) in the same animal, illustrating that the difference between the two states is largely confined to the SLM sink. Scale of difference contour plot is -6.4 to 6.4 mV/mm^2. **F.** Absolute value of the maximum local field potential slope evoked in contralateral HPC following optogenetic stimulation of RE averaged over 32-64 trials, for individual rats (grey, hollow diamonds and dashed grey lines) and on average (black, filled diamonds and solid black line). Stimulation during SO evokes a slope of greater magnitude than stimulation during theta in every case, although this difference is not significant overall ($p = 0.057$). **G.** Peak SLM sink amplitude evoked by optogenetic stimulation of RE during SO and theta in the same individual animals

(grey, hollow diamonds and dashed grey lines) and on average (black, filled diamonds and solid black line). A significantly larger sink at SLM is evoked during SO than during theta. **H.** Peak DG sink amplitude evoked by optogenetic RE stimulation across both states, in individuals (grey, hollow diamonds and dashed grey lines) and on average (black, filled diamonds and solid black line), showing no significant difference across states. Error bars represent SEM. ***$p <$ 0.001. SOr, Stratum oriens; SPyr, stratum pyramidale; SRad, stratum radiatum; SLM, stratum lacunosum-moleculare; SMol, stratum moleculare.

paired *t* test; Fig. 1D,G). Similarly, optogenetic activation of RE during SO evoked a larger local field potential (averaged over 32-64 stimulation trials per animal) in the contralateral HPC bipolar recording than did excitation during theta. This was a consistent effect in every animal, however the magnitude was not statistically significant overall (SO: 0.030 ± 0.0091 mV/ms; theta: 0.016 ± 0.0041 mV/ms; $p = 0.057$, two-tailed paired *t* test; Fig. 1C,F).

No significant difference in latency to the maximal SLM sink was observed across states (SO: 23.63 ± 0.96 ms; theta: 22.25 ± 0.70 ms; $p = 0.29$, two-tailed paired *t* test). As such, the overall pattern of current sinks and sources was otherwise consistent across both states (Fig. 1E), and with previous literature (Dolleman-Van der Weel et al., 1997, 2017; Hauer et al., 2019; Vu et al., 2020). In 7 rats, we compared the somewhat later evoked sink in DG across states, and all but one showed a greater sink magnitude during SO states (-4.74 ± 0.77 mV/mm^2) compared to during theta (-3.76 ± 0.50 mV/mm^2; Fig. 1H). However, this difference was not significant ($p = 0.15$, two-tailed paired *t* test). Unlike the SLM sink however, the peak of the DG sink occurred slightly later during SO (39.29 ± 1.66 ms) than during theta (35.57 ± 0.81 ms; $p = 0.031$, two-tailed paired *t* test). As such, the primary difference between the states was the amplitude of the current sink at SLM, where RE projections synapse on distal apical dendrites of CA1 pyramidal cells (Herkenham, 1978) (Fig. 1E).

Optogenetic stimulation of the RE also produced an evoked potential in frontal cortex, which similarly was modulated by state (Figure 2). Stimulation during SO states evoked a significantly greater absolute maximum evoked potential slope than did stimulation during theta (SO: 0.0077 ± 0.0024 mV/ms; theta: 0.0047 ± 0.0016 mV/ms; $p = 0.015$, two-tailed paired *t* test; Fig. 2A,B). The latency to the peak negativity was not significantly different between states (SO: 43.00 ± 7.54 ms; theta: 37.00 ± 3.79 ms; $p = 0.37$, two-tailed paired *t* test; Fig. 2A).

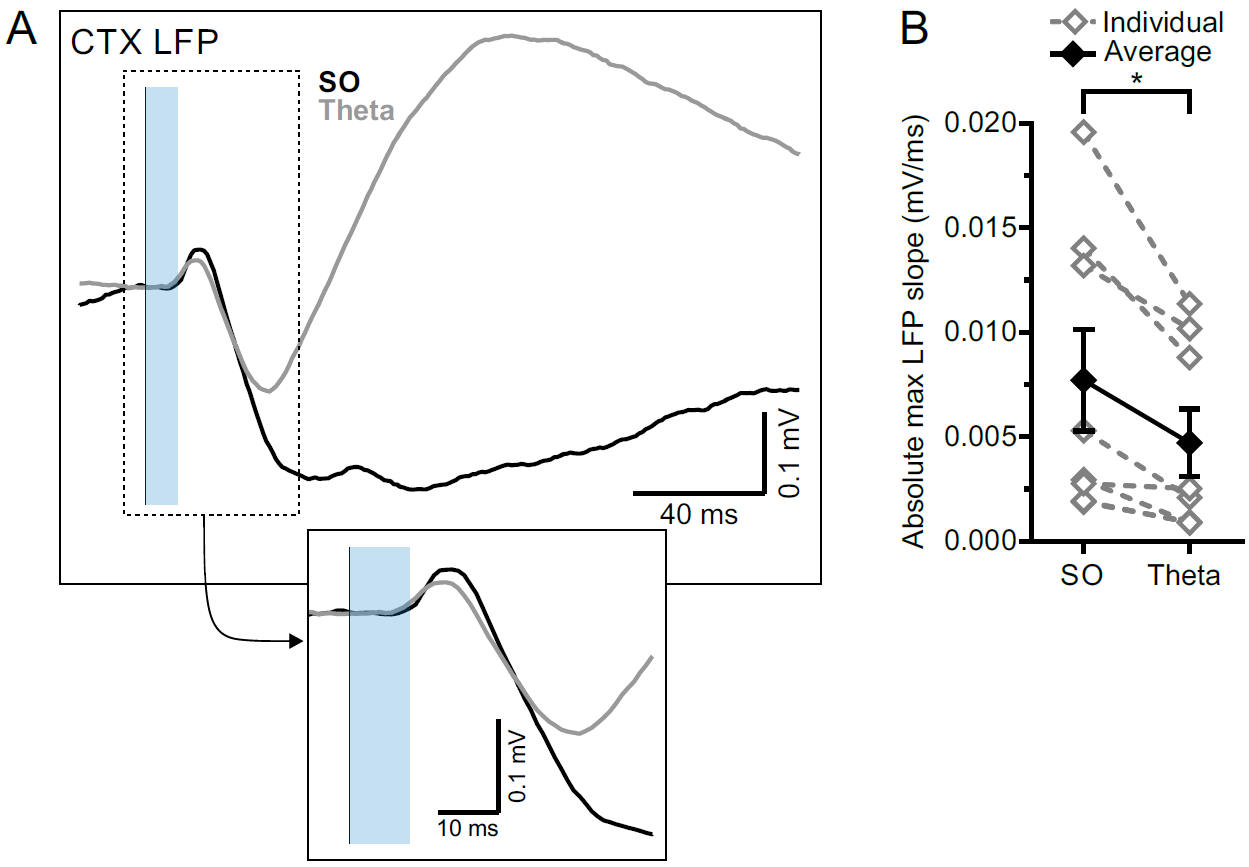

Figure 3.2 RE-evoked cortical field potentials are modulated by state.

A. Cortical local field potential evoked by 10ms optogenetic stimulation of RE (blue transparent rectangle), averaged over 64 trials in both SO (black) and theta (grey) states. Inset: Magnified representation of the box in the main panel, highlighting the initial slope of the evoked response. **B.** Absolute maximum slope of the initial cortical potential in **A** across both states, in individuals (grey, hollow diamonds and dashed grey lines) and on average (black, filled diamonds and solid black line). *$p < 0.05$.

In 7 of the above 8 rats, we also successfully delivered optical stimulation to the cingulum bundle in order to activate RE efferents to the HPC. In this way we were able to isolate and verify the RE-mediated component of this pathway (Figure 3). As we have previously shown (Hauer et al., 2019), the pattern of evoked field and sink/source activity in HPC evoked by this stimulation was virtually indistinguishable to that evoked by direct RE activation (compare responses across Figures 1 and 3 conducted in the same animal). Light delivery to the CB evoked a prominent negative-going potential peaking at a latency of 18.43 ± 0.83 ms in multiprobe recordings from the HPC. As with direct RE stimulation, the maximum negativity in multiprobe recordings was observed at the level of the SLM, and again, current source density profiles confirmed that the shortest latency sink (peaking at a similar latency of 18.00 ± 0.64 ms) was indeed centered at the SLM.

When comparing responses across states, we again observed a robust difference in the magnitude of responses of CB stimulation. As with RE, CB excitation yielded a much larger current sink during SO (-6.30 ± 1.53 mV/mm^2) compared to during theta (-3.90 ± 1.00 mV/mm^2; $p = 0.042$, two-tailed paired *t* test; Fig. 3D,F). As with direct RE stimulation, no significant difference in latency to the peak SLM sink was observed between states (SO: 18.29 ± 0.92 ms; theta: 17.71 ± 0.97 ms; $p = 0.44$, two-tailed paired *t* test). As previously shown (Hauer et al., 2019), no response was observed in the contralateral HPC, consistent with the unilateral projection pattern via the CB (Fig. 3C).

As with RE stimulation, no amplitude difference was observed in terms of the later DG sink evoked by optic stimulation (SO: -2.47 ± 1.01 mV/mm^2; theta: -3.11 ± 0.82 mV/mm^2; $p = 0.17$, two-tailed paired *t* test; Fig. 3G). Although the latency to the peak DG sink was similarly

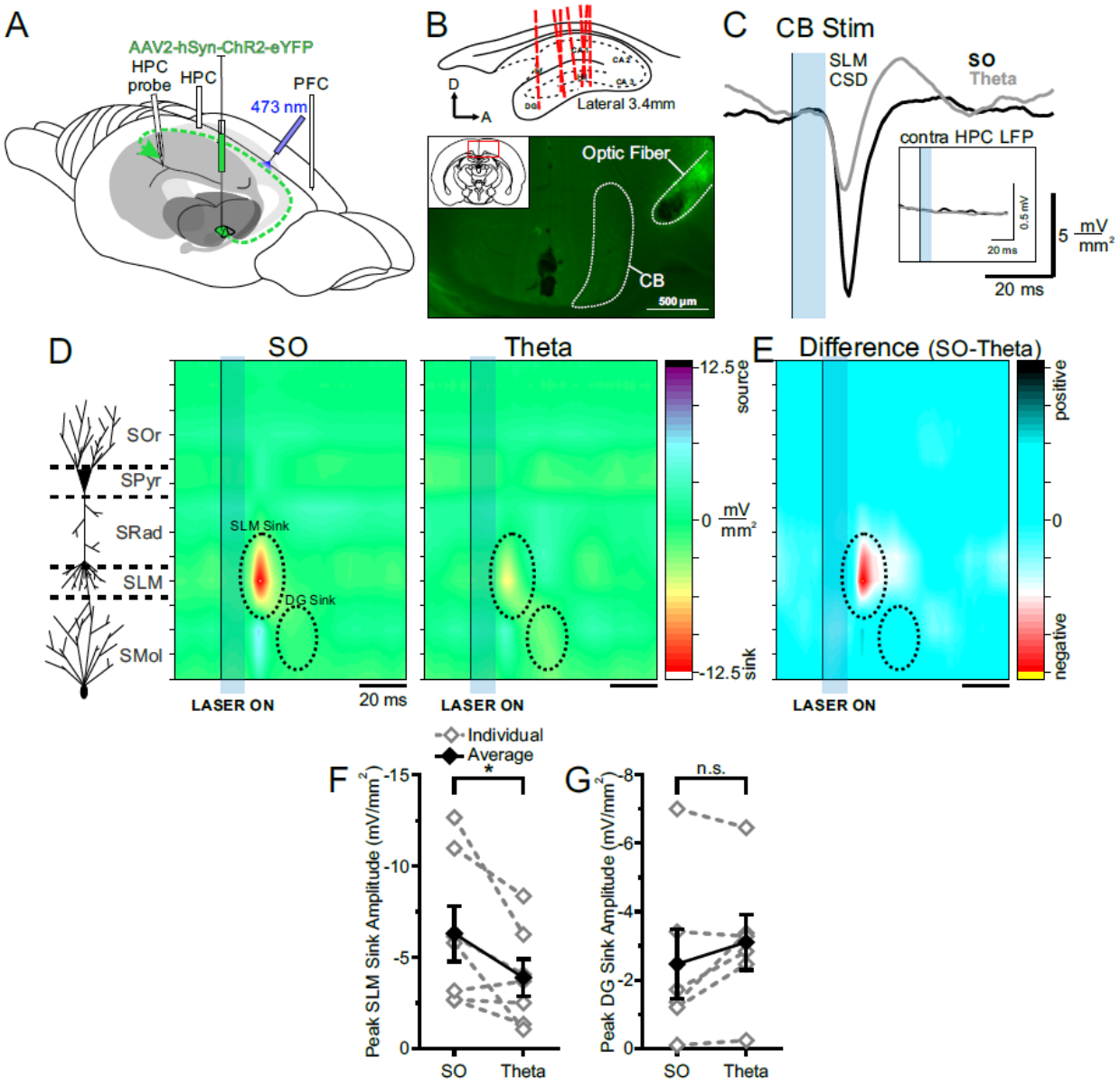

Figure 3.3 Optogenetic stimulation of CB evokes a larger response in HPC during SO.

A. Schematic illustration of the recording, injection, and stimulation sites. Schema modified from Amaral and Witter (1995). **B.** Top, Schematic sagittal illustration of all multiprobe tracks through HPC. Bottom, Representative coronal tissue section depicting hSyn-ChR2-EYFP viral expression in CB following a single injection in RE, with optic fiber track positioned dorsolateral to CB. Inset, Coronal schematic of the relative location (red box) of the image. Histology corresponds to the same animal whose data are depicted throughout this figure. **C.** Current

sink/source density traces evoked in SLM following optogenetic stimulation (10 ms pulse at 473nm wavelength; blue rectangle) of CB during SO (black line) and theta (grey line), averaged over 64 trials. Stimulation of CB during SO produces a much larger current sink in HPC than did stimulation during theta. Inset, Local field potentials recorded from the contralateral HPC following the same optogenetic stimulation of CB during SO (black line) and theta (grey line). There is a total lack of response in the contralateral HPC regardless of state given the ipsilateral projection pathway of RE-to-HPC via the CB. **D.** Left, Schematic depiction of HPC cell lamina as determined by theta profile. Colour contour plot of CSD values just before and following 10ms optogenetic stimulation of CB (black line and blue rectangle) during SO (middle) and during theta (right). CB stimulation produces a large current sink centered around SLM (with a corresponding current source in DG) which is of greater magnitude during SO compared to during theta. A later DG sink is also evoked by CB stimulation that does not significantly differ in amplitude between states. The overall pattern of responding is effectively identical to that evoked by RE stimulation. CSD scales for both contour plots are identical, from -12.5 to 12.5 mV/mm^2. **E.** Difference contour plot created by subtracting the theta CSD (**D**, right) from the SO CSD (**D**, middle) in the same animal, illustrating that the difference between the two states is largely confined to the SLM sink. Scale of difference contour is -6.8 to 6.8 mV/mm^2. **F.** Peak SLM sink amplitude evoked by optogenetic stimulation of CB during SO and theta in the same individual animals (grey, hollow diamonds and dashed grey lines) and on average (black, filled diamonds and solid black line). A significantly larger sink at SLM is evoked during SO than during theta. **G.** Peak DG sink amplitude evoked by optogenetic CB stimulation across both states, in individuals (grey, hollow diamonds and dashed grey lines) and on average (black, filled diamonds and solid black line), showing no significant difference across states. Error bars

represent SEM. *$p < 0.05$. SOr, Stratum oriens; SPyr, stratum pyramidale; SRad, stratum radiatum; SLM, stratum lacunosum-moleculare; SMol, stratum moleculare.

longer during SO as opposed to theta states with CB stimulation, this difference was not significant (SO: 35.50 ± 2.64 ms; theta: 31.33 ± 1.41 ms; $p = 0.19$, two-tailed paired t test).

3.5.3 Forebrain state biases the pattern of hippocampal responding to medial prefrontal cortex stimulation

In 6 rats, we electrically stimulated the infralimbic (IL) zone of the medial prefrontal cortex, and monitored evoked HPC potentials across deactivated and activated brain states. We were especially interested in the contributions of the interposed RE in this communication (Vertes, 2002; Mathiasen et al., 2019). We first verified that IL stimulation could evoke a potential in the hippocampus by monitoring field responses at both the bipolar and multiprobe sites. A short latency (20.50 ± 0.67 ms at peak) and prominent negative-going potential was observed in both hemispheres that appeared to be maximal at the level of the SLM in the linear multiprobe recordings. In order to maximize this response, we used a paired-pulse paradigm that was designed to produce strong paired-pulse facilitation at the level of the HPC. In addition, we computed CSDs of the evoked potential responses when elicited during either SO or theta. We then assessed the pattern of IL-evoked HPC responses across deactivated and activated states, both pre- and post-CNO.

Stimulating IL yielded a remarkably distinct pattern of HPC excitation as a function of brain state. Across both states, prominent current sinks were observed at the level of SLM. However, the timing of these sinks was markedly different between SO and theta states (Fig. 4C,D). During SO, the first stimulus yielded a maximal sink at SLM with a latency of 13.50 ± 0.85 ms, while the second stimulus prompted another SLM sink at a latency of 20.17 ± 3.11 ms. This contrasted sharply with stimulation delivered during theta, which produced sinks at

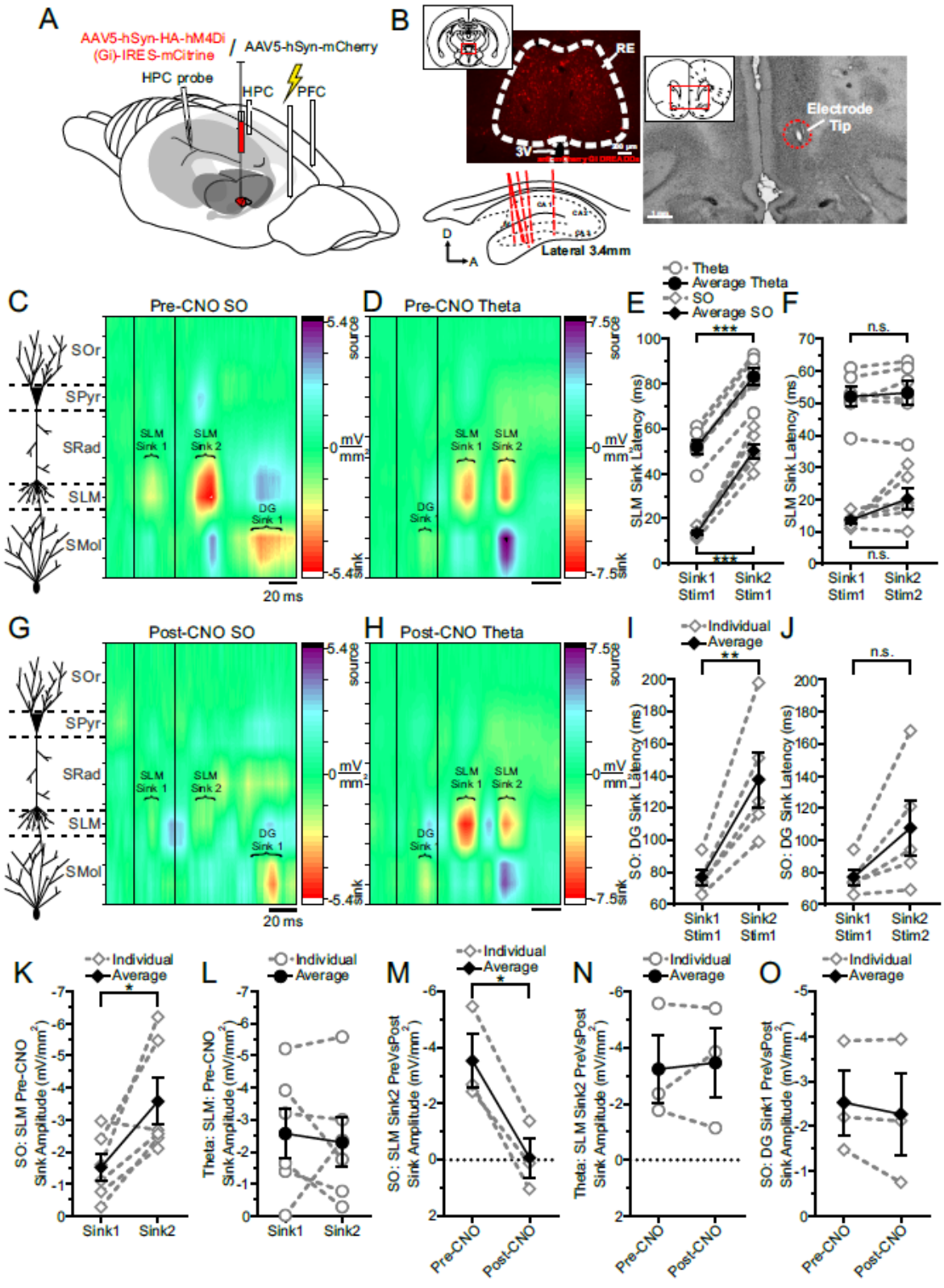

Figure 3.4 Infralimbic stimulation evokes a different pattern of responding in HPC as a function of state, which RE mediates.

Figure 3.4 Infralimbic stimulation evokes a different pattern of responding in HPC as a function of state, which RE mediates. A. Schematic illustration of the recording, injection, stimulation, and inhibition sites. Schema modified from Amaral and Witter (1995). **B.** Originally published in Hauer et al. (2019), with modifications. Representative coronal tissue section showing expression of hSyn-hM4Di-HA-mCitrine virus localized to RE. Inset, Schematic of relative location of image. Top right, Representative coronal Nissl-stained tissue section showing the tip of a stimulating electrode in IL. Inset, Schematic of relative location of image. Bottom left, Schematic sagittal illustration of all (except one) multiprobe tracks through HPC. **C.** Left, Schematic depiction of HPC cell lamina as determined by theta profile. Right, Colour contour plot of CSD values just before and following 30ms inter-stimulus interval paired pulse stimulation of IL. During SO, each pulse evokes a prominent current sink that is maximal around SLM, with a corresponding DG source. The second SLM sink is noticeably facilitated. A late DG sink can be observed well after the SLM sinks that correspond to each pulse. **D.** During theta, each pulse evokes a current sink that is maximal at SLM, but with a considerably longer latency than during SO. A small initial DG sink can be observed following the first pulse, which is obscured following the second pulse by a larger current source. **E.** Latency to peak SLM sinks relative to the first pulse across both states. The second SLM sink is maximal after a consistent latency difference (~30 ms) in both states. Latency to both maximal SLM sinks is much longer when stimulation is delivered during theta, compared to SO. **F.** Latency to peak SLM sinks, relative to the pulse each putatively corresponds to (*i.e.*, subtracting 30 ms from the latency to the second SLM sink). Accounting for the inter-stimulus interval demonstrates that each sink corresponds to each pulse. **G.** Left, Schematic depiction of HPC cell lamina as determined by theta profile. Right, Chemogenetically inhibiting RE and then delivering the same paired pulse

stimulation to IL produces an obviously different pattern of responding in HPC. The SLM sinks corresponding to each pulse are severely diminished, and no facilitation can be seen in the second sink as such. The late DG sink remains unaffected. **H.** Paired pulse stimulation of IL during theta with RE chemogenetically inhibited does not change the pattern of responding in HPC. Both SLM sinks remain intact, and so too does the initial DG sink. **I.** Latency to the peak DG sink evoked during SO when IL is stimulated, with RE intact, showing a more variable latency to the second sink. **J.** Latency to peak DG sinks during SO relative to the pulse each putatively corresponds to (*i.e.*, subtracting 30 ms from the latency to the second SLM sink) shows there is no significant difference in latency, indicating that each DG sink corresponds to each IL pulse. **K.** Peak SLM sink amplitudes during SO with RE intact, showing a larger response in the second sink, indicating paired-pulse facilitation is occurring. **L.** Peak SLM sink amplitudes during theta with RE intact, showing no difference in sink magnitude, indicating paired-pulse facilitation is not occurring. **M.** Amplitude of the second peak SLM sink SO comparing stimulation with RE intact (pre-CNO) against stimulation while RE is chemogenetically inactivated (post-CNO). Following RE inhibition, the second SLM sink during SO is almost entirely abolished. **N.** Amplitude of the second peak SLM sink during theta, comparing stimulation with RE intact (pre-CNO) against stimulation while RE is chemogenetically inactivated (post-CNO). There is no difference in second SLM peak sink amplitude during theta when RE is inhibited. **O.** Amplitude of the first peak DG current sink is unchanged during SO regardless of whether RE is inactivated or not. In all panels, diamonds represent stimulation during SO; circles represent stimulation during theta; grey, hollow symbols and dashed grey lines represent individual animals; black, filled symbols and solid black lines represent the average. *$p < 0.05$; **$p < 0.01$; ***$p < 0.001$.

latencies of 52.00 ± 3.12 ms and 53.17 ± 3.87 ms following the first and second stimuli, respectively. Latency values of these two sinks from their respective stimuli were not significantly different within states (SO: $p = 0.095$; theta: $p = 0.46$, two-tailed paired t tests; Fig. 4F). Indeed, the differences observed in absolute latency (relative to the timing of the first stimulus in the pair, Fig. 4E) is entirely attributable to the 30 ms inter-stimulus interval, with the second sink following the first by ~30 ms in both states.

A sink in the molecular layer of DG was evoked following stimulation across states as well (Fig. 4C,D). During SO, a maximal sink could be observed 76.80 ± 4.66 ms following the first stimulus, with a second DG sink occurring at a more variable latency, 107.60 ± 17.28 ms following the second stimulus (not shown). Comparing these sinks to their respective stimuli in the pair showed no significant difference in timing ($p = 0.073$, two-tailed paired t test; Fig. 4J) suggesting that each DG sink corresponds to one of the stimulus pulses. As with the SLM sinks, the significant difference in absolute latency relative to the first stimulus in the pair (Fig. 4I) is attributable to the 30 ms ISI. Interestingly, unlike during SO, stimulation during theta states yielded only one prominent DG sink 22.00 ± 1.15 ms after the initial stimulus. A second DG sink may be occurring at a similar latency following the second stimulus, but it is apparently obscured by the prominent current source in DG that corresponds to the evoked SLM sink (Fig. 4D).

We observed paired-pulse facilitation of the SLM sink only when stimulating during SO states (Fig. 4K). Maximal SLM sink amplitude increased from -1.52 ± 0.41 to -3.58 ± 0.72 mV/mm^2 ($p = 0.029$, two-tailed paired t test) between pulses during SO (Fig. 4K), while remaining unchanged during theta (sink 1: -2.57 ± 0.77; sink 2: -2.30 ± 0.77 mV/mm^2; $p = 0.69$ two-tailed paired t test; Fig. 4L). This further suggests that fundamentally distinct circuits are being activated as a function of ongoing brain state: likely a direct input to HPC routing through

the RE during SO states which shows facilitation, and an indirect cortico-entorhinal cortical route that ultimately activates EC III inputs to SLM. DG sinks showed no facilitation either during SO or theta. (SO: sink 1: -3.63 ± 0.90; sink 2: -3.80 ± 0.66 mV/mm^2; $p = 0.72$; two-tailed paired *t* test).

In order to test the idea of alternate pathways that didn't involve the RE (both within and across states) we used chemogenetic means to inactivate the RE and assessed the subsequent influence on the IL-evoked potentials in HPC. Following systemic injections of CNO, and consistent with our prior work (Hauer et al., 2019), we observed an almost complete disappearance of both evoked current sinks at SLM during SO (post-CNO sink 1 amplitude: -0.12 ± 0.70 mV/mm^2, $p = 0.27$, two-tailed paired *t* test; post-CNO sink 2 amplitude: -0.084 ± 0.71 mV/mm^2; $p = 0.017$ two-tailed paired *t* test; Fig. 4 G,M). Although the depression of the first SLM sink was not significant, this was a likely consequence of the already low amplitude of this sink pre-CNO. In addition, we no longer observed any paired-pulse facilitation of the SLM sink post-CNO during SO ($p = 0.62$, two-tailed paired *t* test). Across these analyses, the hSyn-mCherry expressing control animals showed no differences pre- versus post-CNO administration. Taken all together, these data are consistent with the idea of a bisynaptic pathway from the mPFC to the HPC that is dependent on the integrity of the RE and that this pathway is functional during deactivated states.

In contrast to the disappearance of sinks at SLM, paired-pulse stimulation delivered during SO-states post-CNO continued to yield a prominent DG sink that was not significantly different to that evoked during control conditions pre-CNO in terms of either latency (pre-CNO: 84.00 ± 6.02 ms; post-CNO 87.33 ± 7.84 ms; $p = 0.55$, two-tailed paired *t* test) or amplitude (pre-CNO: -2.52 ± 0.72 mV/mm^2; post-CNO amplitude: -2.27 ± 0.92 mV/mm^2; $p = 0.39$, two-tailed

paired *t* test; Fig. 4G,O). We also continued to observe a second DG sink at a similar latency (113.33 ± 15.59 ms after the second stimulation) and with a similar amplitude (-2.90 ± 1.62 mV/mm^2) to that recorded pre-CNO. This non-RE-dependent pathway likely involved an alternative route from mPFC, perhaps via fronto-cortical circuits that ultimately terminate in layer II of EC which then profoundly innervates the DG via the perforant path.

Although marked alterations were observed at the level of SLM following inactivation of the RE during SO, this was not the case during theta. Indeed, the overall pattern of evoked responses during theta appear remarkably unchanged when comparing cases pre- to post-CNO (Fig. 4H). Neither the amplitudes nor latencies of the SLM sinks evoked during theta-states were significantly different post-CNO (post-CNO sink 1 amplitude: -4.22 ± 1.38 mV/mm^2, $p = 0.38$, two-tailed paired *t* test; post-CNO sink 2 amplitude: -3.46 ± 1.24 mV/mm^2; $p = 0.76$, two-tailed paired *t* test; Fig. 4H,N; sink 1 latency: 58.33 ± 4.18 ms, $p = 0.43$, two-tailed paired *t* test; sink 2 latency relative to stimulus 2: 54.33 ± 2.33 ms, $p = 0.50$, two-tailed paired *t* test). As with the pre-CNO case, no paired-pulse facilitation was observed for the SLM sinks during theta ($p = 0.53$, two-tailed paired *t* test). Furthermore, the initial DG sink observed pre-CNO was also unchanged (post-CNO amplitude: -1.02 ± 1.07 mV/mm^2; $p = 0.96$, two-tailed paired *t* test). Again, the hSyn-mCherry expressing control animals did not show any differences pre- versus post-CNO administration. This suggests that IL stimulation during theta is entirely routed through a pathway that specifically does not involve the RE. Indeed, in partial contrast to the case with SO, this circuit may be biased to another fronto-cortical circuit that activates both layers II and III of the EC at different latencies.

Together, these data demonstrate that RE inactivation selectively impoverishes the mPFC-RE-SLM connection specifically during SO states. Activation of the mPFC during theta appears to target the HPC by an entirely alternate route.

3.5.4 Hippocampal excitation is modulated by the ongoing phase of forebrain rhythms

By tracking the amplitude of field potential responses evoked during either RE or IL stimulation across random phases of the ongoing SO or theta rhythm we also noted a phase dependency of the HPC response at SLM (Fig. 5). This was first shown by separating stimuli occurring during either the falling or rising phase of the oscillation of interest (Fig. 5A,B). As shown for the example in Fig. 5D, the magnitude and slope of the evoked potential was greater when RE stimulation was delivered during the falling, as compared to the rising phase of the theta rhythm (falling: 0.048 ± 0.0018 mV/s; rising: 0.030 ± 0.0018 mV/s; $p < 0.0001$, two-tailed *t* test assuming equal variances; Fig. 5D,E). This was the also the case for stimulation of IL during theta (Fig. 5G) (falling: 0.055 ± 0.0026 mV/s; rising: 0.034 ± 0.0047 mV/s; $p < 0.001$, two-tailed *t* test assuming equal variances; Fig. 5G,H). Interestingly, the magnitude of the difference between the falling phase as compared to the rising phase during theta was similar whether stimuli were delivered to RE (0.017 mV/s) or IL (0.021 mV/s).

Although the amplitude and slope of evoked potentials recorded across different phases of the SO showed a similar direction, with the falling phase being larger than the rising phase (Fig 5C,F), these values on average were not significantly different with stimulation of either the RE (falling: 0.069 ± 0.0024 mV/s; rising: 0.064 ± 0.0021 mV/s; $p = 0.083$, two-tailed paired *t* test; Fig. 5C,E) or IL (falling: 0.079 ± 0.0044 mV/s; rising: 0.075 ± 0.0039 mV/s; $p = 0.55$, two-tailed paired *t* test; Fig. 5F,H). However, in all cases (rising or falling phase, with stimulation at

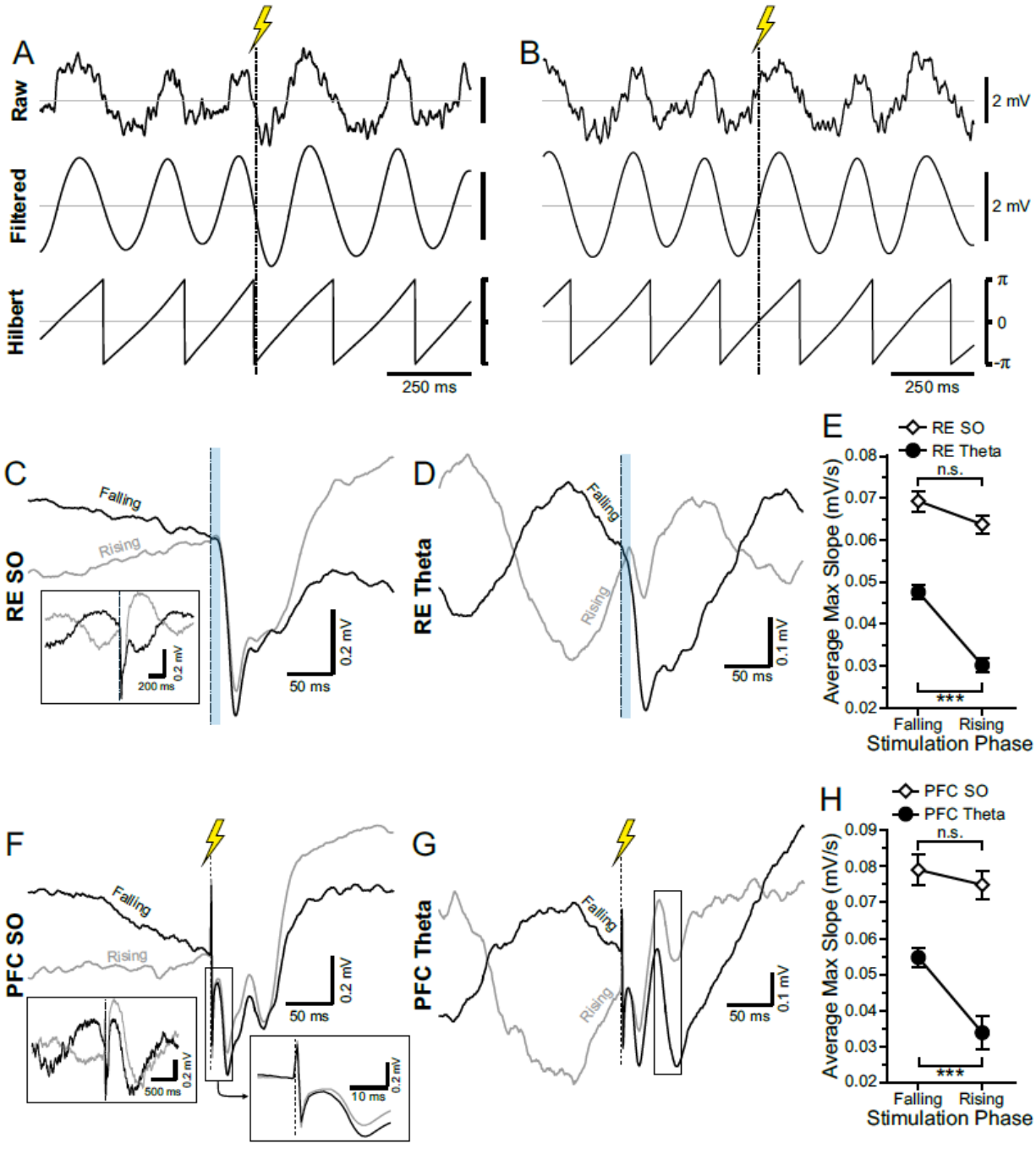

Figure 3.5 HPC is differentially excited by stimulation during the falling or rising phase of the theta and SO rhythms.

A. Raw local field potential recording, 3-6 Hz bandpass filtered signal, and Hilbert transformed signal of the same ~1.5 s of HPC theta. Stimulation is indicated by a vertical dashed line with a

lightning bolt above it. Stimulation is being delivered during the falling phase of the oscillatory cycle. **B.** Identical to **A** except that stimulation is being delivered on the rising phase of the oscillatory cycle. Scale bars are identical in **A**. **C, D.** RE stimulation (10 ms optical pulse) being delivered during the falling (black) or rising (grey) phase of the ongoing SO cycle (**C**) and theta cycle (**D**), with average evoked LFP at SLM shown. Stimulation in both states produces an obvious evoked response, which appears larger when stimulation is delivered on the falling phase of the rhythm. Inset in **C** provides a larger timescale for easier visualization of the rising or falling phase of the SO cycle. **E.** Maximum evoked slope averaged over every IL stimulation trial during SO (unfilled black diamonds) and during theta (filled black circles). Maximum slope is significantly greater during theta when stimulation is delivered on the falling phase, while no significant difference (n.s.) is observed during SO. However, regardless of phase, stimulation during SO always yields a larger response. **F, G.** The same as **C** and **D**, but with an electrical instead of optical pulse, to IL. Stimuli are delivered either on the falling (black) or rising (grey) phase of the SO (**F**) or theta (**G**) cycle. Dashed box in each corresponds to approximate time window for evoked potential analysis. **H.** As is the case with RE stim in **E**, IL stimulation delivered on the falling phase of theta (black, filled circles) produces a significantly larger maximum slope on average than equivalent stimulation delivered during the rising phase. No significant difference (n.s.) between stimulation phases is observed during SO (hollow black diamonds), although stimulation during SO always yields a larger response than stimulation during theta, regardless of oscillatory phase. Error bars represent SEM. ***$p < 0.001$.

either RE or IL), stimulation during SO yielded a much larger response than the equivalent stimulation during theta (Fig. 5E,H).

We expanded upon this analysis to determine on a stimulus-by-stimulus basis what particular phase might yield the greatest response across both stimulus locations and brain states (Fig. 6). To visualize the average phase preference, we further subdivided the occurrence of stimuli into 20 equally sized bins (18° wide) across the entire oscillatory cycle. To assist in smoothing the bin-to-bin comparisons (which could appear artificially noisy in the case of relatively few stimulations in a given bin), we computed the normalized average of three bins (the bin of interest, plus the bins on either side) and compared that with an idealized superimposed sine wave to represent the oscillatory cycle of ongoing rhythmic field activity (Fig 6, left column, normalized 3-bin average in blue, sine wave in grey).

As shown in Figure 6, we observed a prominent and significant degree of phase coupling of the maximum evoked slope to the ongoing field potential oscillation across stimulation sites and brain states. Stimulating RE during SO (Fig. 6A) showed a preference for responding during the positive rising phase of the field oscillation (in this example, angle: 348.68°; radius: 0.10; n = 105 stimuli; Rayleigh p = 0.58; Fig. 6Ai). The window for maximal slope of the evoked potential corresponded to the first prominent negative deflection at SLM (from 11.17 ± 1.64 ms to 25.50 ± 3.08 ms). Preference for the rising phase of the SO cycle was also observed on average (overall average preferred angle: 70.10°; overall average radius: 0.12; N = 6 experiments; Rayleigh p = 0.014; Fig. 6Aii). Conversely, stimulation of RE during theta (Fig. 6B) displayed a somewhat stronger phase preference for earlier in the field cycle, during the falling phase. This held true both in this example (angle: 186.73°; radius: 0.22; n = 150 stimuli; Rayleigh p = 0.013; Fig. 6Bi), and on average (overall average preferred angle: 169.95°; overall average radius: 0.20; N =

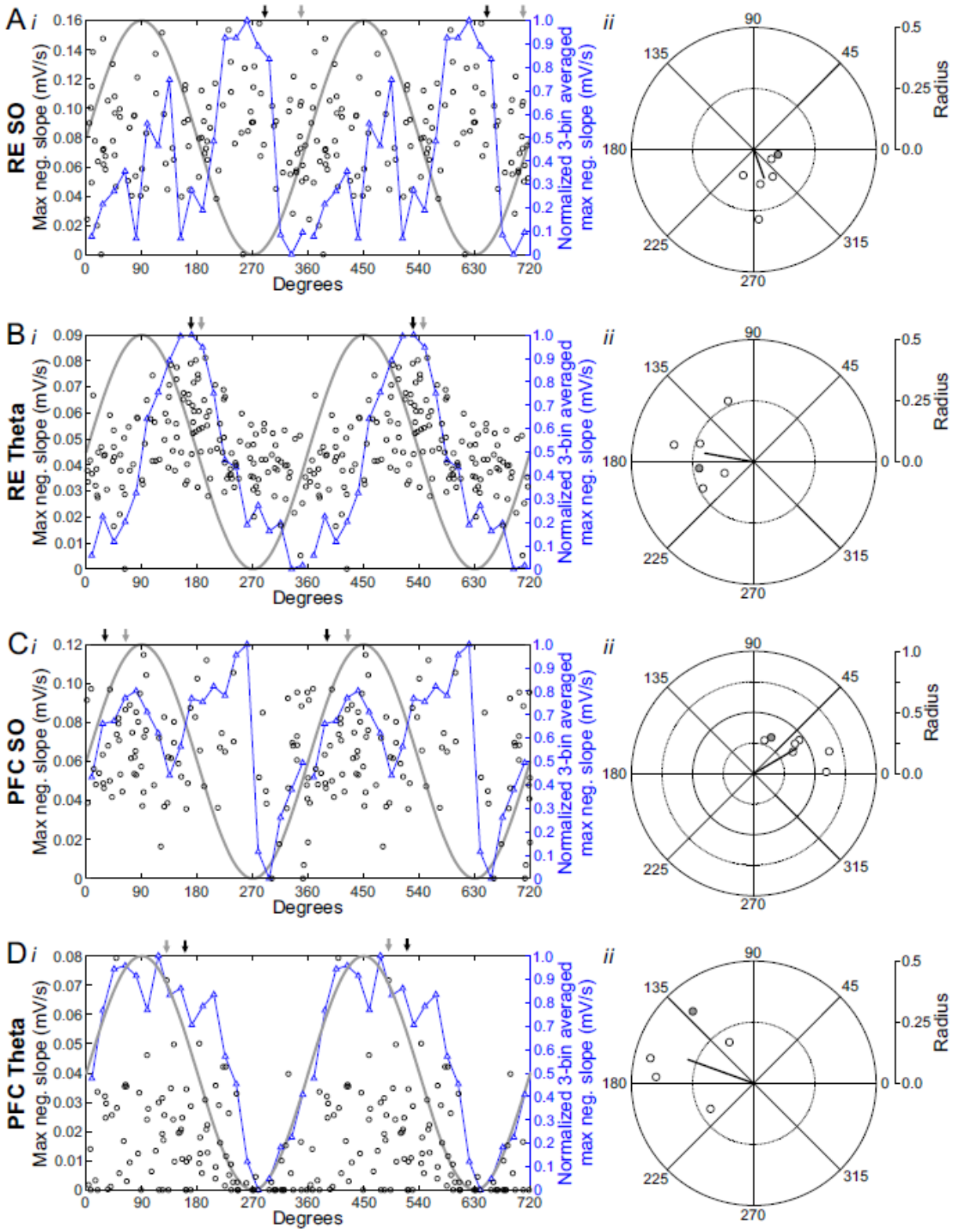

Figure 3.6 Hippocampal excitation is modulated by the phase of the ongoing forebrain rhythm.

Figure 3.6 Hippocampal excitation is modulated by the phase of the ongoing forebrain rhythm. Ai. Stimulating RE during SO evokes a HPC response with a variable maximum slope. Each black hollow circle represents the maximum negative slope evoked by stimulation of RE, which fluctuates as a function of the phase in the oscillatory cycle that the pulse was delivered at. Phase values were organized into 20 equivalent 18° bins, and the average maximum slope for each bin was calculated. The normalized 3-bin average (a rolling average of the centre bin and two flanking bins) was computed and plotted (hollow blue triangles and blue line). An idealized sine wave is overlaid (grey line) to aid in visualizing phase preference, as indicated by greater or lesser maximum evoked slope. All data (including the 3-bin average and the sine wave) are repeated a second time to illustrate two full cycles. Grey arrow indicates mean phase preference for this experiment; black arrow indicates mean phase preference across all experiments. **Aii**. Circle plot of preferred phase of HPC response (as measured by maximum evoked slope) to RE stimulation during SO. The thick, black line indicates the mean angle (°) and the strength of phase preference computed via circular Rayleigh statistics. Grey, filled circle corresponds to the data depicted in **Ai**. **B.** Identical to **A**, except that stimulation was delivered optogenetically to RE during theta. **C.** Identical to **A**, except that stimulation was delivered electrically to IL, during SO. **D.** Identical to **C**, except that electrical IL stimulation was delivered during theta.

6 experiments; Rayleigh $p = 0.016$; Fig. 6Bii). The window chosen for maximal slope similarly corresponded to the initial negativity at SLM (from 12.17 ± 2.40 ms to 23.00 ± 2.25 ms).

During SO, stimulation of IL (Fig. 6C) showed a prominent preference for responding during the positive rising phase of the cycle (in this example, average preferred angle: 64.19°; radius: 0.33; number of stimuli: 86; Rayleigh $p = 0.0061$; Fig. 6Ci). This was consistent across 7 of 7 rats (overall average preferred angle: 30.46°; overall average radius: 0.41; $N = 7$ experiments; Rayleigh $p = 0.00014$; Fig. 6Cii). Here again, the initial SLM negativity was chosen for slope analysis (from 11.43 ± 0.57 ms to 25.71 ± 3.08 ms). Phase preference was less obvious across ongoing theta, but still showed a pattern of maximal excitation similar to that observed during stimulation of RE. Stimulating IL during theta (Fig. 6D) yielded a maximal response during the falling phase of the cycle (in this example, angle: 130.22°; radius: 0.39; $n =$ 121 stimuli; Rayleigh $p = 0.047$; Fig. 6Di). This non-statistically significant pattern held true on average as well (overall average preferred angle: 160.15°; overall average radius: 0.29; $N = 5$ experiments; Rayleigh $p = 0.062$; Fig. 6Dii). Importantly, given the delayed maximal response at SLM following IL stim during theta specifically, the window for evoked potential analysis was later than for SO or RE stimulation (from 27.00 ± 1.18 ms to 39.40 ± 0.60 ms).

3.6 Discussion

Understanding the neural dialogue between extended brain regions that have parallel functional relationships for cognition is important for understanding integrative brain operation. Of particular interest for episodic memory are the connections between the mPFC and the HPC. Although much is known about the anatomy of their interactions, much less is known about their functional relationships during ongoing and shifting exigencies. In the present work, we have

demonstrated that global forebrain state fundamentally alters the way in which the mPFC and HPC interact. Furthermore, we have demonstrated that this state-dependent interaction is critically modulated by an interposed structure, the thalamic RE. Our study underscores the importance of delineating the ways in which brain circuitry might be modulated by shifts in overall state.

3.6.1 Prefrontal and thalamic excitation of hippocampus

Stimulating RE during baseline conditions reliably produced a hippocampal current sink that was maximal at SLM. This excitation of CA1 distal dendrites is consistent with previous reports (Dolleman-Van der Weel et al., 1997; Bertram and Zhang, 1999; Morales et al., 2007; Dolleman-van der Weel et al., 2017; Hauer et al., 2019; Vu et al., 2020). However, what is novel here is the demonstration of enhanced excitability during SO as compared to theta states. This was confirmed by stimulation of the RE-to-HPC afferent fibres in the CB, revealing the same pattern of enhanced excitation during SO. RE stimulation also produced a somewhat later sink in DG across both states, a finding that, again is consistent with past work (Hauer et al., 2019; Vu et al., 2020). While a direct route from RE to DG has not been demonstrated anatomically (Herkenham, 1978; Wouterlood et al., 1990) we suspect that this late DG sink arises from a likely disynaptic circuit involving RE projections to lateral and medial entorhinal cortices (EC), and subsequently to DG via the performant path (Yanagihara et al., 1987; Wouterlood, 1991). Indeed, and in line with preliminary studies in our own laboratory (Hauer, Pagliardini, and Dickson, unpublished observations), stimulation of ventral midline thalamus in urethane-anesthetized rats has been previously shown to evoke a significant monosynaptic excitatory potential in EC (Zhang and Bertram, 2002). Specifically, ventral midline thalamic stimulation

produced the largest amplitude responses in more lateral areas of EC layer II and III (Zhang and Bertram, 2002). Other work describing a significantly temporally delayed DG sink following RE stim also attributed it to layer II activation of both lateral and medial EC (Vu et al., 2020). This is further supported by anatomical work demonstrating that RE fibers innervate the dendrites of principal cells in both layers II and III of EC (Wouterlood, 1991). As such, an alternate (shorter and faster) ventral thalamo-temporal pathway presumably exists for RE-EC afferents to travel, creating a disynaptic RE-EC-DG circuit.

Stimulating IL similarly yielded a prominent sink at SLM during both SO and theta, although at a significant delay during the latter. We also observed a delayed DG sink during SO, but a temporally earlier sink during theta. Chemogenetic inactivation of RE only impacted responding during SO, robustly diminishing the SLM sink while leaving the DG sink unperturbed. The silencing of RE had no impact on HPC responses during theta, suggesting that an alternate circuitry is engaged for PFC-HPC dialogue during activated states. Past work has shown that ventromedial PFC stimulation modulates HPC LFPs and the coherence between PFC and HPC (Jia et al., 2019). Both IL and PL also densely innervate lateral and medial EC almost equally, particularly at the pyramidal cells of layer Vb (Witter et al., 2017). From here, information is outputted from layer Va to CA1/subiculum and beyond for further processing, while a hippocampally processed copy of the original input information is relayed back to layer Vb. Layer Vb as such may be well-positioned to integrate these inputs with additional sets of information, and send these representations to layers II and III (Witter et al., 2017). Layers II and III are also major modulators of HPC activity via the perforant pathway (layer II → DG) and temporoammonic pathway (layer III → SLM). Further study is required to precisely characterize the state-dependencies of EC cell lamina, both in terms of the layer II and III projections to HPC,

but also in terms of the potential role of layer Vb in modulating and integrating these inputs. Indeed, past work has demonstrated a differential responsiveness to slow rhythmic stimulation compared to theta burst stimulation in deep versus superficial layers of EC (Yun et al., 2002). It is likely that the DG sink that remains even after RE is chemogenetically inactivated is a consequence of these dynamic inputs, suggesting that the RE-SLM pathway may be the preferred access point to the HPC for cortico-thalamic information during SO.

3.6.2 Importance of state

It is well known that the intrinsic responsiveness of single neurons is subject to diverse neuromodulatory influences that are correlated themselves to brain state changes (Kaczmarek and Levitan, 1987; Steriade, 2001; Marder et al., 2014). It is also well known that local networks can modify their collective properties based on alterations in neuromodulatory influences again related to brain state changes (Steriade, 2001; Marder, 2012). Our present work documents how inter-areal forebrain circuit interactions are changed in fundamentally different ways based upon state. As such, our work further highlights the importance of both monitoring and reporting on brain state as a function of understanding brain operation since this is both a critical theoretical and experimental concern. In our present study, not only have we documented striking changes in terms of neural responding in the mPFC to HPC circuit that depend on state, but we have also shown that ongoing cycles of circuit rhythms expressed within these states is another significant aspect of altered responsiveness.

3.6.3 State-dependent modulation of mPFC-HPC circuitry

The interaction of mPFC and HPC is crucial for episodic mnemonic functions (Preston and Eichenbaum, 2013). It is important to note that these memory-related functions are not only engaged during wakefulness, when behavioral performance is required and learning can occur, but also during the subsequent offline periods that follow learning, such as sleep (Eichenbaum, 2004; Stickgold, 2005; Dickson, 2010). The distinct and dynamic electrographic patterns of activity that occur during sleep, especially within and between the cycles of REM and non-REM periods, are likely candidates for examining the interactions between mPFC and HPC that might facilitate long-term storage and consolidation of declarative memories (Marshall et al., 2006; Klinzing et al., 2019).

Urethane anesthesia is an ideal model for studying brain-wide interactions that occur during sleep given how closely it resembles the natural central patterns of unconsciousness (Ward-Flanagan and Dickson, 2019). To date, only urethane allows for spontaneous and dynamic changes in brain state that parallel the alternations between REM and non-REM sleep. Not only are individual electrographic states similar to each of these respective stages of sleep, but also the timing of alternations and other corresponding peripheral physiological changes mimic those of natural sleep (Clement et al., 2008; Whitten et al., 2009; Pagliardini et al., 2012). Indeed, these same alternations are also observed in urethane-anesthetized mice (Pagliardini et al., 2013a). The urethane model is therefore ideally suited to study the central and peripheral dynamics of natural sleep, particularly with respect to the spontaneous alternation between distinct activity states.

Our findings here demonstrate that the spontaneously expressed and state-dependent patterns of activity across the forebrain appear to differentially engage memory-relevant circuitry and, moreover, regulate hippocampal excitability. Despite apparent tonic excitation of RE cells

during theta (Morales et al., 2007; Hauer et al., 2019), optogenetic activation of RE produced a smaller SLM response as compared to SO. Perhaps more surprising was that the pattern of responding in this same region following mPFC stimulation was entirely different across states and furthermore, suggestive of an alternate re-routing of inputs. Stimulation of mPFC during SO produced a large-amplitude SLM-located excitation at short latencies that displayed clear paired-pulse facilitation. This response was eliminated following chemogenetic RE inactivation. In contrast, during theta states, we observed a significantly longer latency excitation, which failed to show paired-pulse facilitation. This latter response remained intact following RE inactivation. Our results suggest that the more direct influence of the mPFC input to HPC via the RE was greatly impoverished during theta states and that mPFC-HPC interactions were mediated instead through a cortico-entorhinal circuit. Altogether, this indicates that the RE is ideally situated to modulate the flow of information from mPFC to HPC across deactivated and activated states such that during slow oscillatory states, responding through this bi-synaptic circuit is optimized, whereas during theta, this circuit is bypassed in favour of a cortico-entorhinal circuit. It is worth emphasizing that the role of the RE in mediating this long-range information transfer during theta is still important, as its intrinsic activity appears to select for a different circuitry to be engaged which may be vital for waking behavioral or mnemonic processes.

The short- and long-term plasticity of these synapses was recently assessed in urethane-anesthetized mice (Vu et al., 2020). Consistent with what we have shown here, the authors showed that RE stimulation produces an SLM sink, and a later DG sink. Moreover, RE stimulation could produce gamma oscillations at the level of SLM. Intriguingly, paired-pulse facilitation was found more readily after RE than medial perforant path stimulation, a result that was common across comparisons of RE and EC inputs. The RE→CA1 circuit had a propensity

to show paired-pulse facilitation, LTP, and gamma oscillations more so than the EC input to CA1, all of which are relevant for memory processing. This is consistent with the data presented here, wherein we found that paired pulse facilitation occurred only at the RE-SLM synapse, and only during SO. The authors also showed periodic fluctuations with time of both the magnitude of evoked responses, and of the induction of either LTP or LTD (particularly in the medial perforant path to the middle molecular layer of DG). We posit that these fluctuations reflect the modulation of excitability across natural state transitions, which we have directly shown in the present work. We would further suggest that different circuitry is preferentially engaged as a function of state, with the RE-SLM synapse being particularly well-suited for information exchange during SO.

We have previously shown that during SO states, the RE exhibits slow, rhythmic single unit firing that is coupled to the ongoing mPFC SO (Hauer et al., 2019). Conversely, we showed that during theta states, RE neurons fire tonically and arhythmically (also shown by Morales et al. (2007)). The differential activity and responding of the RE to mPFC inputs during theta could be related to the depolarizing influence of increased cholinergic neuromodulation during activated states (Hasselmo, 2006; Clement et al., 2008) With a profound tonic activation of RE neurons, it may well be the case that the influence of mPFC inputs are effectively filtered out. Cholinergic neuromodulation is also able to pre-synaptically depress excitatory transmission (Picciotto et al., 2012; Colangelo et al., 2019) which might work at both mPFC terminals in RE and/or RE terminals in HPC.

The relevance of advantaged RE-mediated inputs to the HPC during slow-wave states likely plays an important role in global SO synchronization. Indeed, based on the strong coupling of RE unit activity to mPFC slow waves, and the loss of synchronization of mPFC and

hippocampal SO activities with RE inactivation (Hauer et al., 2019), it would appear that the RE is an important conduit for mPFC information to arrive at the HPC during slow-wave states. With respect to SO-related coupling throughout the forebrain, the mPFC has been framed as a key player. It has been suggested to play a pacemaking role in forebrain SO coordination since it often appears as the source of propagating SO waves across the cortex that can additionally be entrained by electric or magnetic field stimulation delivered to frontal regions (Massimini et al., 2004; Marshall et al., 2006; Massimini et al., 2007; Greenberg and Dickson, 2013; Greenberg et al., 2016). Here we suggest that this potential mPFC pacemaking role can be extended to include coordination of the hippocampus, via the interposed RE.

3.6.4 Oscillatory phase preference as a mechanism for memory formation

Ongoing state was an obviously important modulator of HPC excitability and the pattern of responding, but so too was the phase of the oscillatory field cycle whether during SO or theta. This type of phase preference, or active modulation of responding as a function of the rhythmic cycle, provides the circuitry involved with an even more fine-grained temporal mechanism for influencing information processing (Jacobs et al., 2007; Sauseng and Klimesch, 2008; Schall et al., 2008; Cox et al., 2020). Stimulation of either IL or RE yielded a larger HPC evoked potential slope during the falling phase of the theta cycle compared to the rising phase. In both theta and SO, excitability was systematically modulated across the phase of the cycle. Regardless of phase, stimulation during SO produced a larger response than did stimulation during theta. Modulated CA1 responding by phase has been shown before during theta (Wyble et al., 2000), as well as during SO (Schall et al., 2008). However, we are the first to demonstrate that a cyclical modulation of excitability in the mPFC-RE-HPC circuitry specifically.

The rising and falling phases of the extracellular field potential rhythm are a consequence of net current flow entering or leaving the extracellular medium being recorded from, creating windows of enhanced synaptic efficacy (Buzsaki et al., 2012). Our results show that this type of rhythmic modulation is occurring across both states within the broad mPFC-RE-HPC circuitry. There is an optimal phase window during which stimulation of IL may most effectively relay information to HPC, presumably via the RE during SO, and via EC during theta. This is consistent with our schema of the RE as a key relay node for (in particular) slow oscillatory information, where the precise, phase-dependent timing of inputs from mPFC to RE, and from RE to HPC is reliant on the SO-coupled unit activity of RE (Hauer et al., 2019). Moreover, we suggest here that forebrain state may differentially bias this circuitry during theta, engaging an alternative entorhinal pathway.

While we observed a degree of modulation of excitability through the circuit as a function of oscillatory phase, we saw a much greater modulation by global forebrain state. In all cases, stimulation during SO yielded a larger response than did stimulation during theta. It is possible the greater variability in excitability we observed as a function of phase particularly during theta represents a fundamentally different type of processing occurring at these inputs. Subthreshold oscillatory phase preference during theta may be a useful tool to maintain coordinated rhythmic discharge across sites as disparate as HPC and mPFC, particularly with tonic, arrhythmic firing in RE. Conversely, during SO, a much more efficient and reliable rhythmic transfer of information from mPFC to HPC via RE can occur, with the relative phase of inputs becoming less important.

It is difficult to surmise the full implications of this state- and phase-dependent modulation in the mPFC-RE-HPC circuitry, although certainly the relative timing of discharging

neurons in this circuit would have marked functional implications for synaptic plasticity and memory formation as a whole (Hyman et al., 2003; Dolleman-van der Weel et al., 2017; Vu et al., 2020).

3.6.5 Functional relevance of state-dependent modulation of mPFC-HPC inputs

Conventional models of frontal-hippocampal interplay in episodic memory describe the HPC as forming and replaying episodes, while the mPFC engages contextual representations that link related memories, in order to retrieve memories appropriate for any given context (Preston and Eichenbaum, 2013). One likely mechanism by which these disparate sites could communicate most effectively is by coordinated SO activity (Born, 2010). Given the prominence of the SO during the deep stages of slow-wave sleep, and how CA1 excitability to both RE and mPFC stimulation is maximal during this form of activity, we suggest that the circuitry corresponding to both the input and output of this hippocampal region is preferentially biased during SO states as compared to during theta (Schall et al., 2008). As we have previously reported, spontaneous slow-wave activity between frontal neocortical regions and the HPC is dynamically coordinated during SO states (Wolansky et al., 2006), which supports the idea that neural interactions between these disparate structures could be systematically synchronized or de-synchronized on a cycle by cycle basis. This coupling (and, indeed, de-coupling) of cortical and hippocampal ensembles during SO is an ideal platform for the associative and activity-dependent processes of both long-term potentiation (LTP) and long-term depression (LTD), respectively (Dickson, 2010). In this way, neural activity during the SO can provide a dynamic window for the process of declarative memory consolidation to occur in a spike-timing-dependent manner (Dan and Poo, 2004).

In this context, the SO itself has been recognized as an important element in sleep-dependent memory consolidation (Born, 2010; Diekelmann and Born, 2010). It is thought that it temporally organizes both local (intra-areal) and global (inter-areal) replay of newly-formed neural ensembles (Diekelmann and Born, 2010; Staresina et al., 2015; Miyamoto et al., 2017; Klinzing et al., 2019). Indeed, replay is most intensive during slow-wave states (Pavlides and Winson, 1989; Ji and Wilson, 2007b; Born, 2010). As alluded to above, in this way, SO-dependent reactivation of neural sequences corresponding to recently-experienced episodic memory representations could be synchronized in a fashion that would lead to further activity-dependent synaptic facilitation. This type of "neural rehearsal" would further strengthen connections between ensemble elements to promote "to-be-remembered" episodic representations. Consistently, we also demonstrated that the frontal cortex shows an enhanced response to RE stimulation during the SO as well. The phase-dependent coordinated replay of related cellular ensembles in both mPFC and HPC could serve as a reverberative strategy to enhance activity-dependent coupling of these neural representations. Having the return loop back to the mPFC from the HPC (Jay et al., 1989; Hoover and Vertes, 2007) involved as well might create a self-sustaining and repetitive reverberation that would be well positioned to either strengthen or weaken a set of neuronal assemblies in both the mPFC and HPC, depending upon the relative phasing of activations. Although untested in our study, it would be of significant interest to understand how hippocampal output, either via CA1 or subiculum, is modulated by brain state at the level of the mPFC.

A further, and contrasting, way in which the SO could play a role in maintaining relevant memories is through an activity-dependent pruning of older and inconsequential episodic mnemonic representations. This could occur through an opposing neural replay mechanism that

involves active desynchronization of activity in cellular assemblies in a fashion that decreases the strength of their synaptic connections via activity-dependent synaptic depression (Tononi and Cirelli, 2003; Lubenov and Siapas, 2008; Tononi and Cirelli, 2014). In this way, "to-be-forgotten" episodic representations would be more likely to be eliminated. Indeed, it has been strongly suggested that the metabolic limitations of central nervous system operation would fundamentally require this kind of synaptic pruning since synapses are so energy expensive (Attwell and Gibb, 2005; Tononi and Cirelli, 2014).

Regardless of how memory representations might be solidified across slow-wave states, the synchronized coupling of SO activity between prefrontal cortical regions and the HPC is primarily dependent upon the interposed activity in the RE, as we have previously shown (Hauer et al., 2019). In this way, the RE is vitally positioned to either synchronize or desynchronize cellular assemblies across the mPFC and HPC during slow-wave states. Indeed, it would also appear that phasic information from the RE is rhythmically biased in this circuit with maximal excitability at very nearly the exact phase of the SO (~270°) at which RE units show their maximal discharge preference (Hauer et al., 2019). This means that RE input is optimized for maximal hippocampal effect during the SO and it is likely that this is what allows it to coordinate and synchronize hippocampal slow oscillatory activity during slow-wave states.

We feel that the functional relevance of the theta state in the mPFC-RE-HPC circuitry may be related to the increased influence of cholinergic modulation present. Brain-wide release of acetylcholine has been suggested as a signal to update existing memories with new relevant information, or to encode new memories entirely (Hasselmo et al., 1996; Hasselmo, 2006). In this way, the RE could act as a switch, biasing information to be relayed through a cortico-entorhinal route during high acetylcholine, theta rhythmic "encoding" states for new memories

or for updating existing ones. This is consistent with the RE being an integral mediator of prefronto-hippocampal theta synchrony during behavioral tasks, such as spatial working memory paradigms (Hallock et al., 2016; Maisson et al., 2018). Conversely, during SO, the lower levels of acetylcholine in the extracellular *milieu*, combined with the slow rhythmic firing of RE units that are coupled to the ongoing mPFC SO (Hauer et al., 2019) promotes a "consolidating" state, updating representations in the HPC with new rules and binding related episodes together for easier retrieval. Modulation of CA1 inputs by acetylcholine has recently been demonstrated in feedforward inhibitory circuits from the EC (Palacios-Filardo et al., 2021). We posit that a similar modulatory mechanism could be occurring from RE inputs. Indeed, cholinergic neurotransmission in the RE has been previously shown to be crucial for encoding and retrieving long-term object-in-place memories (Barker and Warburton, 2018). The way RE and HPC interact is completely different between states, not only because of the activity of RE itself, but because the entire prefronto-thalamo-hippocampal circuitry is changing as well. Cholinergic modulation of the strength of afferent input relative to feedback likely has an important role at all nodes of this memory-relevant circuit (Hasselmo, 2006).

In the context of understanding interactions in the opposite direction (HPC to mPFC via RE) it would be of interest to test the state-dependency of mPFC responding to HPC stimulation across states as well. Any kind of reverberatory interactions within any particular state could likely aid in activity-dependent neuroplasticity and thus, mnemonic processes.

It is our idea that the RE constitutes a vital element in terms of the reactivation of mnemonic representations. This has been shown in behavioural studies. For instance, the RE has been identified as a critical connector hub for facilitating and influencing network function in the context of long-term fear memory (Wheeler et al., 2013). Similarly, reversible inactivation of RE

immediately after spatial memory learning sessions did not appear to affect task acquisition nor memory retention (Mei et al., 2018). However, RE inactivation in already trained rats immediately before performing the task impaired performance, suggesting that RE has a key role in memory retrieval. Other work showed a crucial role for RE in both the encoding and retrieval of long-term object-in-place (associative recognition) memories (Barker and Warburton, 2018). Lesions to RE impaired long-term memories only, without impacting short-term memories. Consistently, infusing muscimol into RE 15 minutes before testing rats on the associative recognition task impaired performance, demonstrating an important role in mnemonic retrieval. The authors conclude that the RE actively modulates information processing during long-term associative memory formation, and is not just a simple relay (Barker and Warburton, 2018). These findings are all indicative of a key, albeit complicated, role for the RE in effective memory formation and retrieval.

3.7 Conclusion

Here we show that that PFC-HPC communication is fundamentally different between states, and that the anatomically interposed thalamic RE has a critical role in mediating this disparity. Distinct circuits can be engaged as a function of this ongoing forebrain state, with slow oscillatory states likely being ideal platforms for forebrain information exchange. To this end, the RE reliably produces a larger response in the CA1 during SO activity, and is critical in the standard PFC-to-HPC circuitry. During activated theta states, a cortico-cortical circuit via the EC may instead be the preferred pathway of information transfer. However, both states show a rhythmical modulation of excitability dependent on the oscillatory phase of the ongoing rhythm. Together, our data demonstrate that the RE has a critical role in mediating PFC-HPC information

transfer during slow oscillatory states, and that the neural circuitry engaged during theta states is fundamentally different. This has marked implications for the circuitry involved in memory formation, and how the RE may be differentially engaged across deactivated and activated states to underlie it.

4 Tonic excitation of nucleus reuniens decreases prefrontal-hippocampal coordination during slow-wave states

Brandon E. Hauer[1], Silvia Pagliardini[1,2,3], Clayton T. Dickson[1,2,3,4]

[1]Neuroscience and Mental Health Institute, University of Alberta, Edmonton, Alberta T6G 2E9, Canada,

[2]Department of Physiology, University of Alberta, Edmonton, Alberta T6G 2E9, Canada,

[3]Department of Anesthesiology and Pain Medicine, Edmonton, Alberta T6G 2E9, Canada,

[4]Department of Psychology, University of Alberta, Edmonton, Alberta T6G 2E9, Canada

Acknowledgements: This work was supported by Natural Sciences and Engineering Research Council of Canada (NSERC) Discovery grants 2016-06576 and 2021-02926 to C.T.D, and NSERC grant 435843 to S.P. B.E.H. was supported by an NSERC Doctoral Postgraduate Scholarship.

4.1 Abstract

The nucleus reuniens of the thalamus (RE) is an important node between the medial prefrontal cortex (mPFC) and the hippocampus (HPC). Previously, we have shown that its mode of activity and its influence in mPFC – HPC communication is dependent upon brain state. During slow-wave states, RE units are closely and rhythmically coupled to the ongoing mPFC slow oscillation (SO), while during activated (theta) states, RE neurons fire tonically. Inactivating the RE selectively impoverishes coordination of the SO between mPFC and HPC and interestingly, both mPFC and RE stimulation during the SO cause larger responses in the HPC than during theta. It is unclear if the activity patterns within the RE across states may play a role in both phenomena. Here, we optogenetically excited RE neurons to assess the impact on mPFC-HPC coupling. Tonic excitation decreased the influence of mPFC stimulation in the HPC during SO states, in a manner similar to what is observed across state changes into theta. Importantly, tonic excitation of the RE also decreased mPFC-HPC SO coherence. Thus, it is not the integrity of the RE *per se* that is responsible for efficient communication between mPFC and HPC, but rather the particular state in which RE neurons find themselves. Our results have direct implications for how distant brain regions can communicate most effectively, an issue that is ultimately important for activity-dependent processes occurring during slow-wave sleep-dependent memory consolidation.

4.2 Introduction

The medial prefrontal cortex (mPFC) and hippocampus (HPC) have very well established roles in memory (Preston and Eichenbaum, 2013). The mPFC has been classically associated with cognitive control processes like selection, engagement, monitoring, and inhibition while the HPC has a demonstrated role in the encoding, storage, and retrieval of long-term episodic memories (Simons and Spiers, 2003). Somewhat more recently, the ongoing dialogue between these two sites has been increasingly recognized as critical for a host of mnemonic functions. For instance, it appears that mPFC may be a key afferent to HPC for prospection, updating goal representations, and potentially even spatial representations (Hok et al., 2013; Navawongse and Eichenbaum, 2013; Ito, 2018). One important anatomical intermediary between these spatially removed sites is the interposed thalamic nucleus reuniens (RE). A small, midline body, the RE has robust bidirectional projections to both mPFC and HPC (Vertes et al., 2007; Varela et al., 2014; Vertes, 2015). It has previously been shown to have a role in behavioural/mnemonic tasks requiring mPFC to HPC interactions (Dolleman-van der Weel et al., 2019). The critical function of an intermediary node such as this may be to maintain the timing and coordination between the two sites. This would be expected to have functional consequences including timing-dependent mechanisms for synaptic plasticity and, consequently, memory formation and maintenance.

Oscillatory activity and rhythmic spiking are common across neuronal populations across even disparate regions. The emergence of oscillatory synchrony is thought to be a useful information processing tool, and one essential for cognitive function (Wang, 2010; Voytek and Knight, 2015). The precise timing of rhythmic fluctuations of membrane excitability create temporally distinct windows for communication (Fries, 2005; Buzsaki et al., 2012). More specifically, it is thought that only subgroups of neurons exhibiting coherent oscillatory activity

can interact effectively, given that their respective windows for input and output (*i.e.*, information exchange) are accessible at similar times (Fries, 2005). Perturbations to this rhythmic synchrony can result in aberrant information exchange, a hallmark of neurological disorders like epilepsy, schizophrenia, and Parkinson's disease (Winterer et al., 2004; Wang, 2010; Warren et al., 2010; Voytek and Knight, 2015; Dolleman-van der Weel and Witter, 2020).

During sleep, the slow oscillation (SO, ~ 1 Hz) is particularly well-suited to organize these types of contemporaneous interactions. The SO nests faster rhythms (like thalamocortical spindles and gamma oscillations), as well as punctate physiological events like sharp-wave/ ripple complexes within the HPC (Sirota et al., 2003; Steriade, 2006; Molle et al., 2009; Staresina et al., 2015). The SO, as such, has a unique ability to coordinate sequences of activity across large swaths of the forebrain – including the mPFC and HPC in particular – and may therefore allow for the types of associative and activity-dependent synaptic modifications important for memory consolidation (Dan and Poo, 2004; Dickson, 2010).

We have previously shown that chemogenetically inactivating the RE impairs SO coherence between mPFC and HPC (Hauer et al., 2019). However, it is unclear how the activity states of the RE modulate mPFC-HPC dialogue. Our aim was to assess if it is simply the integrity of the RE that is required for efficient information exchange, or if attempting to mimic the state-dependent discharge apparent during theta states might have a similar deleterious effect on mPFC-HPC SO coordination. To this end, we optogenetically stimulated the RE during trials of electrical stimulation of mPFC, as well as during longer continuous field recordings to assess the electrographic consequences of activity manipulations on spontaneous mPFC-HPC dialogue. Our results demonstrate that up-regulation of RE activity is sufficient to diminish mPFC-evoked potentials in HPC (during SO states specifically) and that this same manipulation also

specifically decrements mPFC-HPC coherence at SO frequencies. Ours is the first demonstration that mimicking the spike train dynamics of activated states in the RE can functionally decrease the communication through this nodal structure.

4.3 Materials and Methods

4.3.1 Animals

Experiments were conducted on 16 male Sprague Dawley (SD) rats obtained from the Sciences Animal Support Services and/or Health Sciences Laboratory Animal Services of the University of Alberta with a mean (± standard error of the mean; SEM) final weight of 427.25 ± 7.65 g. Of these, 6 were used for multiunit recording experiments with optogenetic excitation of RE, and 10 were used for optogenetic excitation of RE both short- and long-term. All but the 6 rats used in the multiunit experiments additionally received electrical stimulation of mPFC. Some of these data (n = 10 rats for optogenetic activation of RE) were used in a prior study from our laboratory (Hauer et al., 2022; Chapter 3), while the rest (n = 6) constitute entirely original data. All rats were provided with food and water *ad libitum* and were maintained on a 12 h light/dark cycle, with lights on at 7:00 am. All procedures conformed to the guidelines of the Canadian Council on Animal Care (CCAC) and were approved by the Biological Sciences and/or Health Sciences Animal Policy and Welfare Committees (AUP 092 and AUP 461) of the University of Alberta.

4.3.2 Materials

Bipolar recording electrodes with tip length separation between 0.4-0.9 mm were constructed using Teflon-coated stainless steel wire (bare diameter 125 μm; A-M Systems Inc.).

We also used a linear 16-contact (100 μm separation) multiprobe arranged in a vertical linear array (U-probe, Plexon Inc., Dallas, TX) to assess spatial profile field potential recordings in the HPC.

One viral vector was used for optogenetic experiments, an adeno-associated virus (AAV, serotype 2/2) expressing a channelrhodopsin-2 variant (ChR2/H134R). It was conjugated with enhanced yellow fluorescent protein (EYFP), and driven by the synapsin promoter (hSyn-ChR2-EYFP). It was produced, characterized, and titrated at the University of North Carolina Virus Vector Core Facility, Chapel Hill, NC, USA (ChR2: 3.9 x 10^{12} molecules ml^{-1}).

4.3.3 Procedures

Viral injections

Viral injection procedures very closely match those reported in (Hauer et al., 2019). Rats were first anesthetized with gaseous isoflurane (4% induction, 1.5% maintenance, in 100% O_2) in a sealed chamber. After losing righting reflexes, rats were given an intraperitoneal injection of a ketamine/xylazine cocktail (90 and 10 mg/kg, respectively; Bimeda-MTC; Animal Health Inc., Cambridge, ON, Canada; and Rompun; Bayer Inc., Mississauga, ON, Canada). Supplemental doses (10% of original dose) of the ketamine/xylazine cocktail were administered as required to maintain a surgical anesthetic plane. Body temperature was maintained at 37°C following anesthesia using a homeothermic monitoring system (Harvard Apparatus, Holliston, MA, USA).

Rats were placed into a stereotaxic apparatus (Model 900, David Kopf Instruments, Tujunga, CA, USA) and prepared for intracranial injections, using aseptic techniques. One long incision was made along the midline of the scalp, and the skin flaps were pinned back. The skull

was levelled by adjusting lambda and bregma to be in the same horizontal plane. Holes were drilled in the skull at pre-determined coordinates from a stereotaxic rat atlas (Paxinos and Watson, 1998).

Micropipettes (tip diameter, 30 μm) loaded with hSyn-ChR2-EYFP were attached to a holder (EHW-2MS; A-M Systems Inc., Carlsborg, WA, USA) and lowered using a micro-positioner into the brain. Injections targeted the midline of the nucleus reuniens thalami (AP -2.0; ML +1.9 mm) at an angle 16° oblique to the vertical line to avoid the midline sinus and advanced 6.8 mm from the brain surface (infusion volume 400 - 500 nl). Injections were made using a micro-injector (PMI-100; Dagan, Minneapolis, MN, USA) connected via tubing (PVC, 2.79 mm x 4.5 mm; Gilson Inc., Middleton, WI, USA) to the holder, using a pressure of 40 psi and 15 ms pulse length, at a rate of approximately 100 nl/min. Micropipettes were left in place for 7 – 10 min following the injection to allow for adequate diffusion of the virus, and to prevent unintended backtravel of the injected solution up the pipette track.

Following injection procedures, the scalp was then sutured, and rats were given 0.5 ml of the local anesthetic bupivacaine (5 mg/ml s.c.) around the incision site. Animals were provided with pain medication (meloxicam, 1-2mg/kg in oral suspension; Boehringer Ingelheim Vetmedica, Ingelheim, Germany) over a 24 hour period post-surgery. Food and water were provided *ad libitum* and animals were allowed to recover for 3 weeks before acute experimentation (see below). Neither the viral injection nor the surgical procedures produced any observable long-term issues.

Acute urethane anesthesia and general experimental procedures

For acute anesthetized recordings, rats were initially anesthetized in a gas chamber with isoflurane in medical oxygen (4% induction, 1.5% maintenance). A catheter was inserted into the femoral vein, and isoflurane was discontinued. General anesthesia was obtained by slow (~0.03 – 0.08 ml/min) incremental administrations of urethane (0.4 g/ml) via the catheter (final dose across all rats: 1.22 ± 0.047 g/kg). Urethane was chosen for anesthesia because it promotes an unconscious state that mimics the typical dynamics of natural sleep, both in terms of brain state alternations and in terms of their typical physiological correlates (Clement et al., 2008; Pagliardini et al., 2013b).

Rats were placed back into the stereotaxic apparatus and once again a single long incision was made along the scalp to expose the cranium, with the skin flaps again pinned back. As before, the skull was levelled by adjusting lambda and bregma to be in the same horizontal plane. Body temperature was maintained at 37°C using the same homeothermic monitoring system (Harvard Apparatus). Intracranial implantations were made using pre-determined coordinates from a stereotaxic atlas, using bregma as a landmark (Paxinos and Watson, 1998).

In all experiments, bipolar electrodes for recording local field potentials were positioned in the PFC (AP +3.2; ML 0.7; DV (tip of long electrode) -1.1 to -1.8 mm), and were also placed in the HPC, straddling the pyramidal layer of CA1 (AP -5.5; ML -4.5 mm; DV -2.2 to -3.2 mm). These electrodes were cemented in place using dental acrylic and jeweller's screws fastened into the skull. Local field potentials from bipolar wire electrodes were amplified in differential mode at a gain of 1000 and filtered between 0.1 to 500 Hz using a differential AC amplifier (Model 1700, A-M Systems Inc.).

Photostimulation

An optic fibre (tip diameter 200 µm) connected to a 473 nm laser (Laserglow Technologies, Toronto, ON, Canada), calibrated to deliver light at 10 – 12 mW, was positioned in order to deliver light intracranially. Photostimulation events were driven by a pulse stimulator (Model 2100; A-M Systems Inc.) connected to the laser power supply as well as to the analog-to-digital board and PC acquiring data to mark each event (see below).

Nucleus reuniens stimulation procedures. In addition to bipolar local field potential recordings of PFC and HPC, we also used the linear multiprobe in the contralateral HPC (AP -5.5; ML +4.5; DV -3.3 to 4.5 mm), which was positioned in order sample activity throughout the vertical extent of CA1. Importantly, for monitoring the effects of RE and mPFC stimulation, the intermediate HPC was consistently targeted using the linear probe given the prominent projection patterns from RE to this septo-temporal region of the HPC (Hoover and Vertes, 2012). Local field potentials from the multiprobe were referenced to stereotaxic ground, passed through a unity gain headstage and then amplified at a gain of 1000 and filtered between 0.1 to 500 Hz (X1000: Plexon, Dallas, TX, USA). Signals were digitized at a sampling frequency of 1000 Hz using a Digidata 1440A analog to digital board (Molecular Devices) connected to a PC running Axoscope (Molecular Devices). The final depth of the probe was determined using the well-established electrophysiological profile of theta field activity (Bland and Bland, 1986; Buzsaki, 2002). The position of the multiprobe was histologically confirmed in every experiment by analyzing its track in relation to recorded field activity.

In a subset of initial pilot experiments (n = 6), a 12 mΩ tungsten electrode (AM Systems) was lowered into RE to record multiunit activity in response to optogenetic stimulation. The electrode was mounted on a One Axis IVM Scientifica micromanipulator and advanced at a

variable rate: 10–20 μm/s for the first 5 mm; 2–5 μm/s for 5–6 mm; and finally at a rate of 1 μm/s until reaching a final depth typically between 6.8 and 7.8 mm. Positioning of the electrode was confirmed by histological examination of post-fixed tissue.

The optic fibre was positioned above the RE (AP -2.0; ML +1.9; DV -6.4 mm) at an angle 16° oblique to the vertical line. Optogenetic evoked potentials were produced using 10 ms laser pulses delivered every 5 s to the RE and were averaged over 32-64 trials. During multiunit recording experiments, square wave pulses of varying length (from 10 ms – 1 s) were delivered sporadically to assess RE responding. During continuous field recordings without multiunit recordings, stimulation was delivered tonically (10 ms square wave pulses delivered every 25 ms (40 Hz) for 30 – 90 s). Brain state was always considered during stimulation of any kind, with equivalent stimulation given during both states: during either clear deactivated periods characterized by high power in the 1 Hz signal in PFC and HPC (deactivated/ SO state), or while prominent theta (~4 Hz) activity could be observed in HPC with concomitant low voltage, higher frequency activity in PFC (activated/ theta state). Stimulation during particular states was confirmed by monitoring ongoing brain state when delivering stimulation trains; and subsequently by both visual and spectral examination of individual recorded sweeps.

Medial prefrontal cortex stimulation. In most rats (n = 10) we delivered electrical stimuli to the mPFC, specifically targeting IL, with the goal of evoking HPC potentials. The surgical preparation was identical to that employed for RE stimulation (see above), except that instead of targeting an optic fibre over RE, a bipolar stainless steel (0.08” bare, 0.11” Teflon coated) stimulating electrode was lowered into IL (AP +2.8 to +3.2; ML +0.7 to +1.1; DV -4.0 to -4.5 mm). Electrical stimuli (1 ms long, 200 μA biphasic current pulses, every 5 s) were delivered with a constant current stimulator (Model 2100; A-M Systems Inc.). Prior to the onset of each

electrical pulse, the RE was optogenetically stimulated (from 1 full second before the electrical pulse, continuously for 2 s). The objective was to robustly up-regulate RE activity during transmission of an electrical pulse from IL to HPC. Optogenetic stimulation onset and offset flanking the electrical pulse by a full second was chosen to prevent unintended excitation of RE by the optogenetic vectors (*i.e.*, excitation that was not due to the electrical pulse alone). Control experiments were performed identically, except that the laser was turned off. Stimulation epochs were averaged over 32 trials, and were always delivered during a consistent brain state, either theta or SO. Epochs containing trials with electrophysiological artifacts or with sudden, brief state transitions were removed from the analyses on an individual, trial-by-trial basis.

4.3.4 Perfusion and Histology

Following experimental recordings, 5 s DC pulses of 1 mA using an isolated current pulse generator (Model 2100; A-M Systems Inc.) were passed through bipolar recording and stimulating electrodes to generate small electrolytic lesions at their tips. These lesions allowed for subsequent verification of recording and stimulation sites. Rats were then transcardially perfused with 0.9% saline and 4% paraformaldehyde in saline (Fisher Scientific, Toronto, ON, Canada). The brain was then removed and placed into a 4% formalin and 20% sucrose solution for at least 48 h. Brains were flash frozen using compressed CO_2 and sectioned with a rotary microtome (1320 Microtome; Leica, Vienna, Austria) at a width of 60 μm. Tissue was counter-sectioned, with one third of sections being mounted on gelatin-coated microscope slides for subsequent thionin staining; another third being mounted on slides and immediately covered using a fluorescence preserving reagent and mounting medium (FluorSave; EMD Millipore,

Darnstadt, Germany); and a third of the tissue saved for immunohistochemistry for detection of specific neuronal markers.

Immunohistochemistry was performed according to the following protocol. Free-floating sections were rinsed three times using phosphate-buffered saline (PBS) and incubated with 10% normal donkey serum (NDS) and 0.3% Triton X-100 for 60 min to reduce non-specific staining and increase antibody penetration. Sections were left to incubate over night with primary antibodies diluted in PBS containing 1% NDS and 0.3% Triton X-100. Primary antibodies used detected: green fluorescent protein (GFP; dilution 1:1000; raised in chicken; Aves Labs, Tigard, OR, USA); and neuronal nuclear marker (NeuN; 1:800; raised in mouse; Millipore). The following day, tissue was again washed three times with PBS, incubated with secondary antibodies conjugated to the specific fluorescent proteins in each viral construct (Cy2-conjugated donkey anti-chicken; Cy5-conjugated anti-mouse; 1:200; Jackson ImmunoResearch, West Grove, PA, USA) diluted in PBS and 1% NDS for 2 h. Sections were again washed three times with PBS, mounted, and coverslipped with Fluorsave (EMD Millipore). Microscopic inspection of tissue was used to verify electrode recording loci, optic fibre tracks, and expression of viral constructs using a Leica DM5500B fluorescent microscope.

4.3.5 Data Processing and Analysis

All signals were acquired with Axoscope 10.6 (Molecular Devices) and were first visually assessed to select data segments for further analyses. Computation and analyses were conducted using custom-written MATLAB code (version R2021b, Mathworks). Further analyses and graphical processing were performed with CorelDRAW X6 (Corel). Data analyses are

highly similar to those described in Hauer et al. (2019) and, briefly, included the following: zero phase delay digital filtering, evoked potential averaging, power and phase profile and spectral analyses, coherence, current source density, single- and dual-channel spectra, auto- and cross-correlations, and spectral analyses using wavelets, including wavelet coherence.

Field recordings. Autopower, crosspower, coherence, and cross-phase spectra were computed and visualized for both individual, as well as pairs of field signals. Spectra were estimated using a series of 6-s-long, Hanning-windowed samples with 2 s overlap using Welch's periodogram method. Power spectrograms (Wolansky et al., 2006; Whitten et al., 2009; Hauer et al., 2019) were calculated with a sliding window procedure, enabling discrete spectra to be computed and visualized at specific time points across the duration of the recording. These windows were 30 s in duration, slid across the file in 6 s increments. These discrete spectra were then visualized and analyzed as described above. Spectral profiles from multiprobe recordings were created in the same manner for the activity recorded at each channel of the multiprobe, except that each channel was compared against a fixed (either PFC or HPC) bipolar reference, enabling extraction of power, phase, and coherence information at spectral peak frequencies for both SO and theta states. The spatial locations of the multiprobe channels were estimated based on the well-described theta power profile (Bland and Bland, 1986; Buzsaki, 2002; Wolansky et al., 2006), with the phase reversal point corresponding to the interface between *stratum pyramidale* and *stratum radiatum*, and the maximal theta channel located at *stratum lacunosum-moleculare* (SLM). All statistical comparisons between pre-, during-, and post-stimulation were computed using repeated-measures one-way ANOVAs with Geisser-Greenhouse correction to account for sphericity.

Multiunit activity. Root mean square (RMS) envelopes were created for multiunit activity (MUA) in the RE by using a 200 ms window slid by 50 ms increments. The resulting envelope was inverted by multiplying by -1 to ensure that it was not antiphase to the ongoing SO. We used RMS envelopes to better visualize changes in RE multiunit activity during stimulation of hSyn-ChR2-EYFP, as well as to visualize changes in cellular activity correlated to spontaneous forebrain state transition.

Current source density analysis. CSD analysis was performed on both spontaneously recorded (gap free) field samples, and on evoked potential sweeps and averages recorded using the multiprobe. Briefly, CSD was computed by estimating the second spatial derivative of adjacent multiprobe voltage traces, following the assumptions of Freeman (1975), Rodriguez and Haberly (1989), and Ketchum and Haberly (1993). This technique eliminates potential contamination from volume conducted fields at distant sites, because it estimates the volume density of the net current entering or leaving the extracellular space at a particular site (Buzsaki et al., 2012). Spectral (particularly power and coherence) estimates of the CSD were computed as described above, comparing the CSD of individual multiprobe channels against each other, or against fixed PFC or HPC bipolar electrodes. This technique enabled visualization and analysis of the magnitude of current sinks and sources as a function of space.

Wavelet Analysis. Wavelet analysis was performed on continuous field recordings. Wavelet coherence was chosen as an analytical technique for two primary reasons. First, to ensure that the short sample length (one minute pre-, during-, and post-stimulation) used in traditional, fast Fourier transform (FFT) based spectral analysis methods was not biasing the resulting coherence, given the relatively fewer number of cycles with which coherence can be computed across. Second, the enhanced time-frequency resolution offered by wavelet analysis enabled us to assess

transient shifts in the magnitude of the signal with excellent resolution in both time and frequency. Using the Wavelet Toolbox in MATLAB, coherence was assessed using default settings (analytic Morlet wavelet, 12 voices per octave, 9 octaves, and smooths 12 scales). Computations were done on ~ 3 minutes of continuous field recordings, with equivalent 1 minute pre-, during-, and post-stimulation epochs. Continuous wavelet transforms were also performed to assess the magnitude of the signal, using default settings (analytic Morse wavelet with the symmetry parameter set to 3, and the time-bandwidth product equal to 60, using 10 voices per octave). Magnitude was compared in two ways: 1) in terms of the raw magnitude of the signal, averaged across all frequencies in the frequency band of interest, and 2) by calculating the standard deviation of the entire epoch, again across all frequencies in the band, to get an estimate of the overall RMS. The latter was performed to assess overall fluctuations in amplitude with time. Coherence estimates were performed between the CSD of the signal corresponding to SLM and the LFP from mPFC, as well as between the SLM CSD and the contralateral HPC LFP. Both wavelet coherence and power were assessed across a band corresponding to SO (0.5 – 1.5 Hz) as well as a band corresponding to theta (3.0 – 5.5 Hz). The average across all frequencies within each band was taken to generate an overall estimate of the magnitude or the coherence within the band of interest. All statistical comparisons between pre-, during-, and post-stimulation were computed using repeated-measures one-way ANOVAs with Geisser-Greenhouse correction to account for sphericity.

4.4 Results

4.4.1 Histological findings

In all experiments, we confirmed the location of all recording and stimulation electrodes, as well as the positioning of the optic fibre. We also localized viral vector expression using immunohistochemistry. Bipolar electrodes were successfully placed in their respective positions (mPFC or HPC) in all cases. All linear multiprobe tracks were localized to CA1, spanning from *stratum pyramidale* through SLM, with the tip extending into the molecular layer and/or granule cell layer of DG. Localized viral expression was largely confined to the RE, with occasional expression in the adjacent rhomboid and ventral anteromedial nuclei. Any experiments in which viral expression was not localized appropriately to the RE showed a lack of electrophysiological responsiveness to optogenetic stimulation, and were excluded from any further analysis. Placement of the optic fiber was also verified in the immuno-labeled slices, and in all RE-targeting experiments, was positioned just dorsal to the RE, approximately on the midline. The tip of the stimulation electrode targeting IL was found to consistently be located within IL, just ventral to prelimbic cortex and above dorsal peduncular cortex, and was always medial relative to the basal ganglia.

4.4.2 Optogenetic excitation of the RE increases multiunit activity

Following viral infection of the RE with hSyn-ChR2-EYFP in 6 rats, optical pulses were delivered to the RE during continuous field recordings in mPFC and HPC with a concomitant MUA recording in RE (Figure 1). We first verified that optogenetic stimulation of the RE evoked a similar pattern of local field potential and CSD responses to what we have previously shown. As shown previously (Hauer et al., 2019) (Hauer et al., 2022; Chapter 3), laser pulse applications evoked maximal negative-going field potentials and current sinks at the level of SLM in HPC

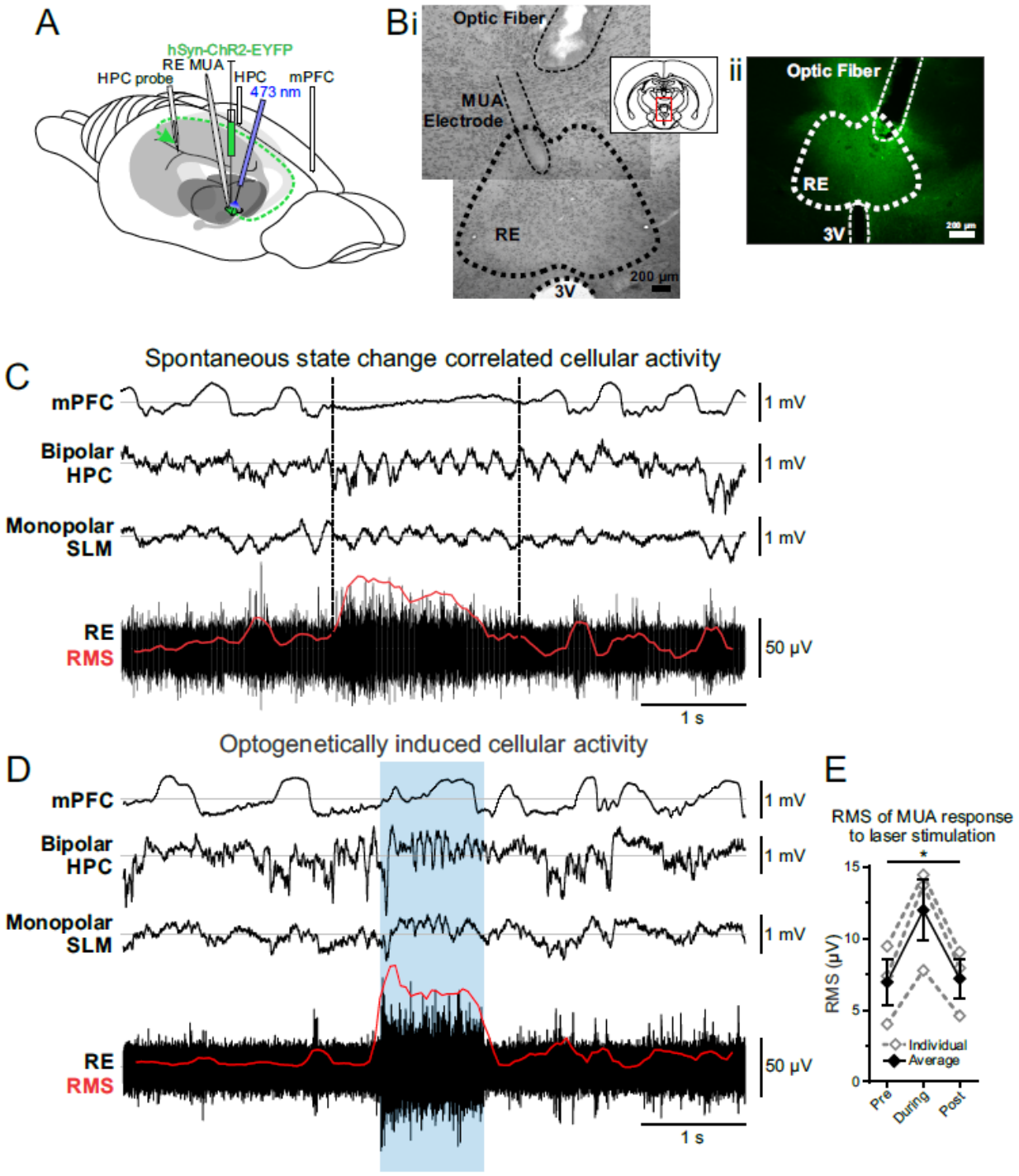

Figure 4.1 Optogenetic stimulation of RE increases multiunit activity while the laser is on.

Figure 4.1 Optogenetic stimulation of RE increases multiunit activity while the laser is on. **A.** Schematic illustration of the recording, injection, and stimulation sites. Schema modified from Amaral and Witter (1995). **Bi.** Left, Representative coronal tissue section depicting a multiunit recording electrode track (MUA Electrode), optic fiber track, and the relative locations of the RE and third ventricle (3V). Inset, Coronal schematic of the relative location (red box) of the image. **Bii.** Representative coronal section showing the expression of hSyn-ChR2-EYFP virus localized largely to RE, with optic fiber track positioned dorsal to RE. **C.** Simultaneous bipolar field recordings in PFC and HPC, monopolar HPC signal corresponding to SLM from the linear multiprobe recording, with tungsten electrode multi-unit recording in RE, and RMS envelope (200 ms window, slid by 50 ms) of RE multi-unit recording during a brief spontaneous transition from SO to theta and back**. D.** Similar recording to that in **C**, but during a consistent SO state with 473 nm laser stimulation (1 s duration) of RE in the middle (indicated by transparent blue box). Optogenetic stimulation consistently and robustly increases RE multi-unit activity only while the laser is on, evident in both the RE MUA recording and the RMS envelope. The increase in RE MUA during optogenetic stimulation is comparable to that observed during a spontaneous transition into an activated (theta) state (as in **C**). Approximately 5 ms of data were blanked at laser onset to eliminate the photoelectrical stimulation artifact. **E.** Average RMS pre-, during-, and post-optogenetic stimulation of RE. Individual rats (grey, hollow diamonds and dashed grey lines) and on average across all rats (black, filled diamonds and solid black line). Optogenetic stimulation of RE significantly increases its MUA. Error bar represents SEM. $*p < 0.05$.

which closely resembles that resulting from electrical stimulation of RE (Dolleman-Van der Weel et al., 1997; Morales et al., 2007; Dolleman-van der Weel et al., 2017; Vu et al., 2020). Indeed, we were also able to observe evoked potentials in mPFC as well (Hauer et al., 2022; Chapter 3).

We also ensured that laser applications evoked MUA responses that were similar to those exhibited during spontaneous transitions into theta. As we have previously described (Hauer et al., 2019), the RE exhibits distinct activity states as a function of ongoing forebrain state. Multiunit activity in the RE during SO is closely and rhythmically coupled to the ongoing mPFC SO, while during transitions into theta states or theta states in general, the RE adopts a tonic, arrhythmic firing pattern (Fig. 1C). Our objective with multiunit recordings in conjunction with optical RE excitation was to show that hSyn-ChR2-EYFP stimulation reliably boosts RE activity into a tonic firing mode regardless of forebrain state, mimicking that observed during natural theta states. Indeed, we observed that stimuli of varying length effectively and rapidly increased RE MUA and consequently the RMS of the signal (Fig. 1D). Tonic firing persisted throughout the duration of laser stimulation, and halted abruptly immediately following laser offset. Across 3 animals with continuous 1 s stimulations given during SO, RMS robustly increased selectively during laser activation (pre: 6.95 ± 1.58 μV; during: 11.97 ± 2.11 μV; post: 7.19 ± 1.34 μV; p = 0.015; Fig. 1E).

4.4.3 Upregulating RE activity diminishes PFC-HPC communication

In 9 rats expressing hSyn-ChR2-EYFP in the RE, we co-delivered electrical stimuli to the IL together with optogenetic excitation of the RE (Figure 2). We have previously shown that IL stimulation produces an evoked response in HPC that is modulated in an RE-dependent fashion

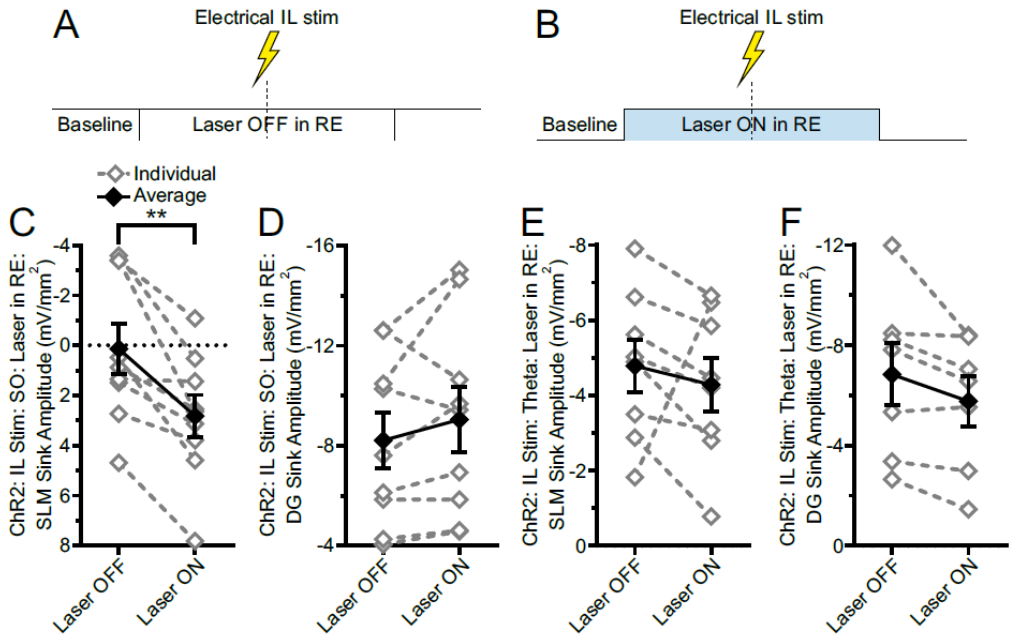

Figure 4.2 Short term tonic activation of RE is sufficient to impoverish mPFC-HPC input.

A. Schematic diagram of the stimulation procedures. Briefly, optical stimulation is delivered to the RE for two continuous seconds to excite an excitatory hSyn-ChR2-EYFP virus, from 1 before electrical stimulation of IL up to 1 s post-stimulation. The procedure was repeated in every animal with the laser turned off as a control. The evoked response was averaged over 32-64 trials. **B.** Averaged peak sink magnitude at SLM following electrical IL stimulation with the laser in RE either off or on, during SO. Individual rats (grey, hollow diamonds and dashed grey lines) and on average across all rats (black, filled diamonds and solid black line). Tonic optogenetic activation of RE significantly reduces the peak sink magnitude at SLM. **C.** The same as **B**, but comparing the peak DG sink amplitude evoked by IL stimulation during SO, showing no change regardless of laser activation. **D.** The same as B, but during theta states, showing no difference in SLM response with the laser off or on. **E.** The same as C, but during theta states, showing no difference in SLM response with the laser off or on. Error bars represent SEM. $^{**}p < 0.01$.

across SO and theta states (Hauer et al., 2022; Chapter 3). We hypothesized that it might not be the integrity of the RE *per se* that is responsible for mediating effective PFC-HPC communication during SO, but rather the state of excitation of the entire RE network (Hauer et al., 2019). To this end, we delivered electrical stimuli to IL while concurrently delivering laser pulses to the RE to selectively and robustly upregulate RE activity in a temporally discrete window (Fig. 2A,B).

As previously reported (Hauer et al., 2019), stimulation of IL evokes a consistent response in HPC that overlaps with the location of the excitatory response evoked by direct RE stimulation. In 9 of 9 rats, IL stimulation produced a current sink localized to SLM when delivered without laser illumination. Crucially, however, tonically activating the RE using laser stimulation that flanked the IL stimulation by one second on each side, significantly diminished the magnitude of the current sink at SLM during SO states (laser on sink reduced by 2.69 ± 0.61 mV/mm^2; $p = 0.0024$, two-tailed paired *t* test). This laser-induced diminution was specific to trials during SO states, with no significant differences in SLM sink amplitudes observed during theta ($n = 8$, 1 animal excluded because of insufficient stimuli delivered during the theta state). The sink produced during theta while the laser was on was reduced on average by 0.50 ± 0.76 mV/mm^2 ($p = 0.54$, two-tailed paired *t* test).

Also consistent with our previous work (Hauer et al., 2022; Chapter 3), we observed no change, either across state or across laser delivery, in the magnitude of the evoked DG sink to mPFC stimulation. During SO, IL stimulation produced a DG sink that did not significantly change in magnitude regardless of laser activation (laser on sink increased by 0.83 ± 0.61 mV/mm^2, $p = 0.21$, two-tailed paired *t* test). During theta, IL stimulation in 7 rats (one rat was excluded because of insufficient stimuli delivered during the theta state, and another was

excluded because of a shift in multiprobe placement resulting in insufficient traces from the DG) yielded a current sink in DG that also did not change in magnitude regardless of laser activation (laser on sink reduced by 1.07 ± 0.47 mV/mm^2; $p = 0.063$, two-tailed paired t test).

4.4.4 Coherence between PFC and HPC decreases as RE activity is modulated

In 4 of the same rats expressing hSyn-ChR2-EYFP which were used in the preceding evoked potential experiments, we successfully delivered high frequency tonic optical stimulation to RE, designed to induce tonic activity, for continuous 60 s epochs (Figure 3). The stimulation was designed to tonically upregulate RE activity, in contrast to the typical pace-keeping SO activity (Hauer et al., 2019). Both the power/ magnitude of the signals, as well as the coherence between pairs of signals were assessed by spectral (FFT-based) means, as well as using wavelet-based methods. Optogenetic stimulation did not appear to affect the amplitude of the SO signal. The CSD power of the channel corresponding to SLM at the peak SO frequency (1 Hz in all 4 experiments) did not significantly change as a function of stimulation (pre: 12.81 ± 1.60 A.U.; during: 8.67 ± 2.39 A.U.; post: 11.39 ± 2.69 A.U.; $p = 0.057$; Fig. 3B), and neither did the mPFC LFP signal at 1 Hz (pre: 0.054 ± 0.012 mV^2; during: 0.026 ± 0.0097 mV^2; post: 0.047 ± 0.0078 mV^2; $p = 0.11$; Fig. 3C). However, the coherence between these signals (CSD of SLM and mPFC LFP) was significantly reduced by tonic RE stimulation (pre: 0.38 ± 0.044; during: 0.10 ± 0.031; post: 0.17 ± 0.019; $p = 0.0034$; Fig. 3D).

Re-analysis of these data using continuous wavelet transforms (CWT) to assess signal magnitude, as well as assessing the coherence of pairs of signals at frequency bands of interest re-capitulated exactly the results observed using spectral analyses (Figure 4). RMS of the

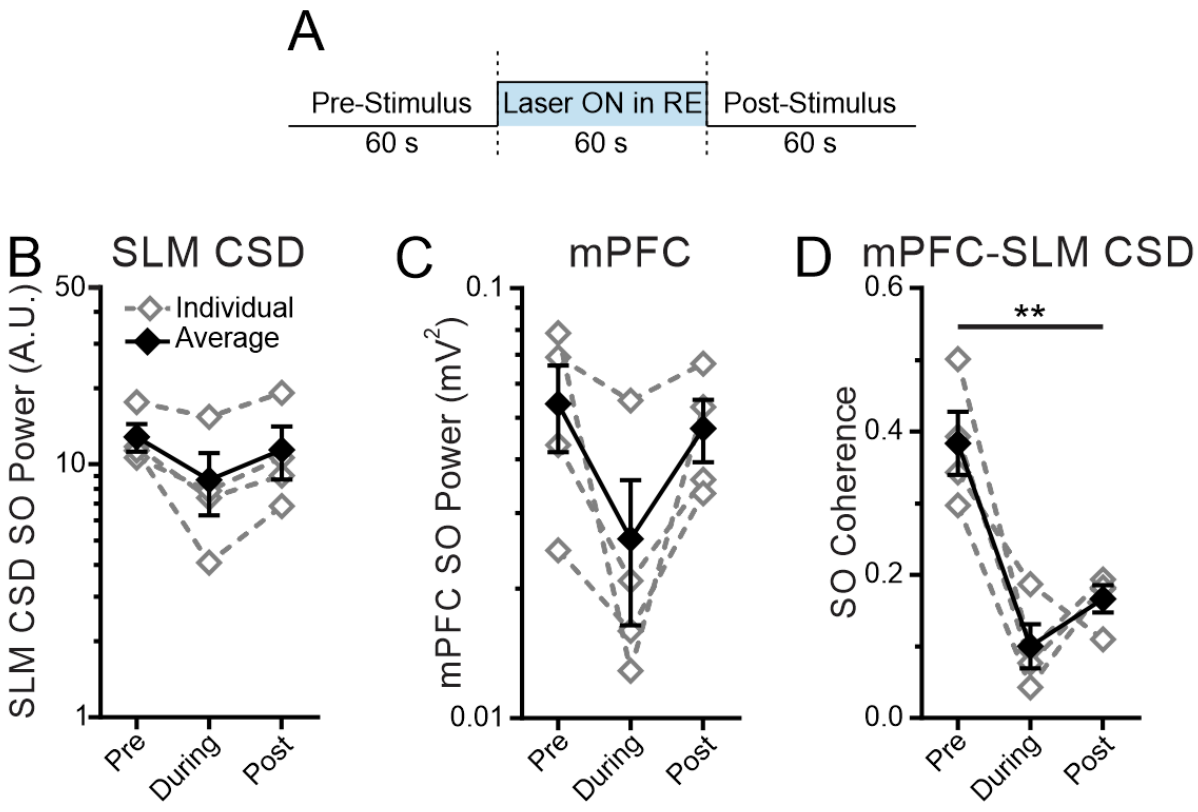

Figure 4.3 Tonic activation of RE reduces mPFC-HPC SO coherence.

A. Schematic representation of the recording and stimulation procedures. Briefly, in both forebrain activity states, 3 min of continuous field recordings were obtained. The first 60 s acted as a pre-stimulation control, the second 60 s involved the RE being tonically stimulated throughout at 40 Hz, and the last 60 s comprised the post-stimulation baseline comparison. **B, C.** Average (± SEM) power at the peak SO frequency (1 Hz) for the CSD of SLM (**B**) and for the mPFC (**C**), pre-, during-, and post-stimulation, showing no significant difference in power across conditions. Individual rats (grey, hollow diamonds and dashed grey lines) and on average across all rats (black, filled diamonds and solid black line). **D.** Coherence at 1 Hz between the CSD of the SLM signal and mPFC during SO, comparing pre-, during-, and post-stimulation of RE. Tonic optogenetic activation of RE significantly reduces the SO coherence between SLM and mPFC. Error bars represent SEM. $^{**}p < 0.01$.

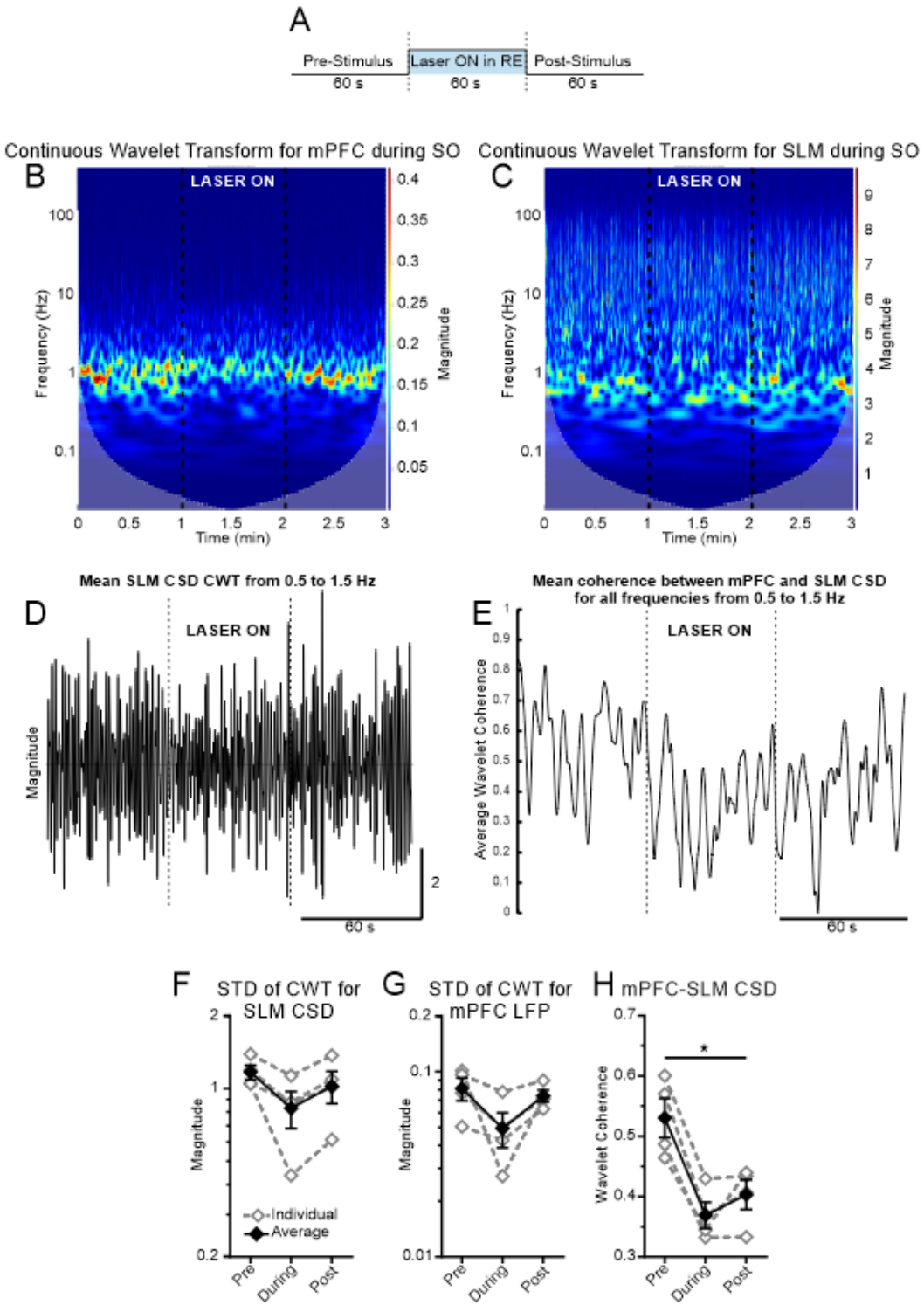

Figure 4.4 Tonic activation of RE reduces wavelet coherence between mPFC and HPC during SO.

Figure 4.4 Tonic activation of RE reduces wavelet coherence between mPFC and HPC during SO. A. Schematic representation of the recording and stimulation procedures. Briefly, in both forebrain activity states, 3 min of continuous field recordings were obtained. The first 60 s acted as a pre-stimulation control, the second 60 s involved the RE being tonically stimulated throughout at 40 Hz, and the last 60 s comprised the post-stimulation baseline comparison. **B, C.** Example continuous wavelet transform (CWT) spectrograms of a full 3 min recording from mPFC (**B**) and from SLM (**C**) during SO, showing a relatively consistent band of activity between 0.5 and 1.5 Hz (SO activity). The white dashed line and area depicts the cone of influence for the CWT computation. **D.** The extracted magnitude of the CWT of the SLM CSD between 0.5 and 1.5 Hz, averaged across all frequency bands within. This SO magnitude shows quick fluctuations that are consistent throughout the 3 min recording, without any obvious drop off in magnitude pre-, during-, or post-stimulation. **E.** The wavelet coherence averaged across all analyzed frequencies in the 0.5 to 1.5 Hz band, between the CSD signal of the channel corresponding to SLM and the mPFC recording. Wavelet coherence rapidly and significantly drops off immediately following the onset of tonic optical stimulation, stays suppressed during stimulation, and only slowly starts to recover following laser offset. **F, G.** Average (± SEM) standard deviation (RMS) of mean CWT magnitude for the CSD of SLM (**F**) and for the mPFC (**G**), pre-, during-, and post-stimulation, showing no significant difference in magnitude across conditions. Individual rats (grey, hollow diamonds and dashed grey lines) and on average across all rats (black, filled diamonds and solid black line). **H.** Wavelet coherence between the CSD of the SLM signal and mPFC during SO, comparing pre-, during-, and post-stimulation of RE. Tonic optogenetic activation of RE significantly reduces the wavelet coherence between SLM and mPFC. Error bars represent SEM. $*p < 0.05$.

continuous wavelet transform (CWT) magnitude of the signal in the 0.5 – 1.5 Hz band did not change for the SLM CSD trace (pre: 1.17 ± 0.080; during: 0.83 ± 0.14; post: 1.02 ± 0.16; p = 0.060; Fig. 4C,F) or for the mPFC LFP signal (pre: 0.081 ± 0.012; during: 0.049 ± 0.011; post: 0.074 ± 0.0056; p = 0.10; Fig. 4B,G). There were no significant differences in the mean CWT magnitude for any of the signals (SLM CSD: p = 0.36; mPFC LFP: p = 0.48; contralateral HPC LFP: p = 0.72). Crucially, however, we again observed a robust decrement in coherence at SO frequencies between the SLM CSD signal and the mPFC LFP (pre: 0.53 ± 0.033; during: 0.37 ± 0.022; post: 0.40 ± 0.025; p = 0.012; Fig. 4E,H). This mirrors our previous finding in which chemogenetically inhibiting the RE specifically impoverished coherence at SO frequencies between SLM and mPFC (Hauer et al., 2019). In this case, however, the impairment of SO coherence was evoked by the exact opposite manipulation.

4.5 Discussion

The thalamic nucleus reuniens sits in an ideal position to influence communication between mPFC and HPC. We have previously shown that its mode of activity and ability to modulate mPFC-HPC dialogue is dependent upon forebrain state (Hauer et al., 2022; Chapter 3). Units in the RE are tightly and rhythmically coupled to the mPFC SO (Hauer et al., 2019). Perhaps not surprisingly, chemogenetically silencing RE neurons specifically decrements SO coupling between mPFC and HPC (Hauer et al., 2019). Evoked responses in the HPC by activation of either RE or mPFC are also larger during SO states than during theta (Hauer et al., 2022; Chapter 3). These findings suggest that it may be the activity state of the RE specifically that is important for mediating this dialogue. Here, we induced tonic neuronal firing in the RE using optogenetic methods during both SO and theta states. Despite the forebrain otherwise

being in a SO state, forcing the RE to adopt a tonic mode of firing appeared to impoverish the influence of mPFC stimulation on the HPC, similar to that typically observed during theta. Tonic activation of the RE during longer duration field recordings also decreased mPFC-HPC coherence at SO frequencies. We are the first to show that it is not the integrity of the RE *per se* that mediates the effective dialogue between mPFC and HPC, but rather the mode of operation of RE neurons. Altogether with our previous work, it is likely that during deactivated states, RE neurons are primed both to receive SO-related excitation from the mPFC and to transmit it advantageously to the HPC. This slow-wave pacing is likely fundamental for efficient information exchange in the prefrontal-hippocampal circuit, which has important implications for activity-dependent processes occurring during slow-wave sleep-dependent memory consolidation.

4.5.1 Tonic upregulation of RE activity filters out mPFC-SLM input

We first demonstrated that short term (2 s) continuous optogenetic activation of RE disrupts mPFC evoked potentials in the HPC. This effect was exclusively observed during SO states. The RE has an established role in mediating SO-related coordination between mPFC and HPC (Ferraris et al., 2018; Hauer et al., 2019). It has similarly been recognized as important for theta synchrony between mPFC and HPC, particularly in the context of spatial working memory (Hallock et al., 2016; Maisson et al., 2018; Griffin, 2021). However, RE units have not been shown to display theta rhythmicity, and rather appear to adopt an arrhythmic, tonic firing mode during theta states (Morales et al., 2007; Hauer et al., 2019; Viena et al., 2021). It is possible that this tonic activity may still have a key role in modulating field activity in the HPC not as a pacemaker necessarily, but in its ability to influence the phase of the oscillation. Such phasic

modulation from tonic RE input could help to synchronize HPC and mPFC during theta states. We theorize that the RE also assists in mediating synchrony during theta states (including during active/ waking exploration) by biasing a different route of mPFC-HPC information exchange (Hauer et al., 2022; Chapter 3) that instead involves the entorhinal cortex. Consistent with this, we found that tonic upregulation of RE activity only decreased the IL-induced current sink at SLM during SO, but that the temporally delayed DG sink was unaffected in either SO or theta. This response is likely a result of entirely different RE- and non-RE-dependent pathways by which the mPFC activates the HPC (Hauer et al., 2022; Chapter 3). The non-RE pathway likely involves an exclusive cortico-cortical circuit that ultimately activates superficial layer II neurons giving rise to the perforant path input to DG (Witter et al., 2017). As such, the RE may mediate differential communications across states, and its intrinsic activity patterns appear to be the critical element underlying this phenomenon.

The tonic firing mode of the RE during theta states and, indeed, during constant stimulation of hSyn-ChR2-EYFP would thus be expected to 1) filter out slow oscillatory rhythmic input from mPFC, and 2) bias a differential circuitry for information transfer. This is exactly what we have shown in the present study. Our schema of the RE during SO states is that of a pace-keeper or clock for carefully relaying the precise timings of the mPFC SO to the HPC. We have additionally showed here that the RE presumably engages in a type of processing role, given that its mode of neuronal firing can selectively gate information transfer from prefrontal to hippocampal cortices. Indeed, optogenetically forcing RE neurons to engage in activity dynamics typical for theta states compromises informational exchange, comparable to that observed during spontaneous theta.

The function of the RE as such is two-fold: during deactivated states, RE neurons are primed both to receive SO-related excitation from the mPFC and to transmit it in an optimized way to the HPC. In this state, the circuit is open and functionally transmitting. In contrast, during activated states, RE neurons are tonically excited and seem less responsive to mPFC input. Effectively, in this state, the mPFC-RE-HPC circuit is closed. As such, brain state modulation influences at the level of the RE appear to be primed to either pass or filter out information in this bisynaptic circuit. This likely reflects differential processing modes across these two mutually exclusive states where mPFC activity has more direct influence on the HPC during deactivated (non-REM-like states). As such, the RE is a nodal communications hub between mPFC and HPC which is independently capable of regulating their dialogue.

4.5.2 Tonic activation of RE decreases mPFC-HPC SO coupling

The slow oscillation ostensibly begins in prefrontal-orbitofrontal sites and propagates in a posterior direction, towards the hippocampus (Massimini et al., 2004). Suggestive evidence of the mPFC playing an important pace-making role for this rhythm has been shown by electrical or magnetic field stimulation of frontal sites effectively entraining cortical SO waves (Marshall et al., 2006; Massimini et al., 2007; Greenberg and Dickson, 2013; Greenberg et al., 2016). The HPC SO is dynamically coordinated with the mPFC SO, and shows a power maximum and phase shift at the level of SLM (Wolansky et al., 2006). This modulation and coordination has largely been assumed to be driven by temporoammonic input from layer III of the entorhinal cortex (Isomura et al., 2006; Wolansky et al., 2006). However, we have previously shown that not only are units in the interposed RE tightly and rhythmically coupled to the mPFC SO, but that chemogenetically inactivating the RE specifically decrements SO coordination between

mPFC and HPC (Hauer et al., 2019). Consistent with this, the RE constitutes the major source of thalamic afferents to HPC, and is the only other primary input to SLM specifically (aside from EC layer III via the temporoammonic pathway) (Steward and Scoville, 1976; McKenna and Vertes, 2004).

Having shown that the mode of activity in the RE alone was sufficient to modulate state dependent evoked potentials in the HPC, we turned our attention to the normal functional coupling of mPFC and HPC during SO states specifically. Tonic stimulation of RE over protracted durations (60 s) effectively reduced the coherence between mPFC and HPC, an effect which lasted beyond the stimulation period. We surmise that this is a consequence of interfering with the rhythmic, clock-like SO timing cues relayed from mPFC to HPC via RE, and that regaining coherent coupling between these sites takes an extended period of time. By filtering out the mPFC SO rhythmic timing cues in RE with tonic stimulation, that SO information is unable to be relayed to HPC and thus coupling decreases. Importantly, we do not see any decrement to SO power at either site, again consistent with the idea that some local generation of SO is occurring both at prefrontal and hippocampal sites (Massimini et al., 2004; Wolansky et al., 2006). By removing the clock-like timing of the RE however, these sites display a less-coordinated SO. The lack of changing power is also important to note given that coherence estimates between two sites can be influenced by the relative power of the frequency of interest at each site (Srinath and Ray, 2014). Varying amplitude correlations can bias estimates of coherence, resulting in either an under- or over-estimation of the true degree of phase coherence (Srinath and Ray, 2014). We are the first to demonstrate that tonic upregulation of RE – pushing it into an activity state akin to that observed during endogenous theta – impoverishes coordination between mPFC and HPC.

We expect that the entorhinal cortex plays a role in coordinating mPFC and HPC as well (particularly during theta states; Hauer et al., 2022; Chapter 3). This role may likely be cooperative with the RE given that they synapse on the same distal dendritic compartments at SLM (Dolleman-van der Weel et al., 2017). Indeed, neither chemogenetic silencing of the RE nor the tonic activation performed here completely remove all SO coherence (Hauer et al., 2019). Presumably, the remaining mPFC-HPC SO coherence is provided by temporoammonic input from EC layer III (Isomura et al., 2006; Wolansky et al., 2006) Exhaustive study of the precise contributions of the EC as compared to the RE in mediating such rhythmic coordination remains an open area of research.

4.5.3 Functional consequences of impoverished SO coordination

We conceive of the RE as having an important role in timing the dialogue between prefrontal and hippocampal sites during SO specifically. By forcing the RE into a tonically active state akin to that observed naturally during theta, the timing mechanism supplied by the RE to keep slow oscillatory rhythms locked between mPFC and HPC is eliminated. Impoverishing the SO dialogue between these sites likely has marked functional implications. For instance, the SO temporally organizes faster rhythms and oscillatory events, aiding in the replay of newly-formed neuronal ensembles (Ji and Wilson, 2007a; Diekelmann and Born, 2010; Staresina et al., 2015; Miyamoto et al., 2017). Inactivating the RE with muscimol disrupts gamma burst synchronization during SOs between mPFC and HPC, suggesting the RE is important for creating an optimal window for information exchange/ memory formation (Ferraris et al., 2018). Behavioral work has showed that the uninterrupted function of the RE is required for spatial memory consolidation, a process dependent on mPFC-HPC SO synchronization

(Loureiro et al., 2012). Indeed, chemogenetic RE inactivation in female mice before or immediately following object training blocked object placement memory formation (Schwabe et al., 2021). The role of the RE in offline memory consolidation is increasingly being appreciated (Barker and Warburton, 2018; Klein et al., 2019; Quet et al., 2020; Ferraris et al., 2021). Prefrontal-hippocampal interactions are vital for normal memory functioning, and the RE is an essential mediator of them (Preston and Eichenbaum, 2013; Eichenbaum, 2017; Dolleman-van der Weel et al., 2019).

Activity states in the RE have been previously intimated to have differential roles in memory processing. The RE has been previously characterized as important for fear memory generalization (Xu and Sudhof, 2013). However, it was shown that not only is the presence or absence of the RE important for fear memory generalization, but that direct optogenetic activation of RE produced differential effects based on the stimulation parameters (Xu and Sudhof, 2013). Phasic (30 Hz pulses for 0.5 s every 5 s) activation of RE during memory acquisition produced over-generalization of fear memory, while tonic (stimulus trains at 4 Hz) activation reduced fear generalization. This was perhaps the first evidence that activity states of the RE have crucial but potentially dissociable implications for memory function, and that tonic upregulation of its activity may have behavioral consequences. The authors suggest that the RE may as such contribute to the mPFC-HPC dialogue and consequent memory consolidation.

A recent pre-print examined the role of chemogenetically upregulating RE activity in two mouse models of Alzheimer's disease, and failed to show any rescue of memory impairments (Kohli et al., 2021). This result would be expected by our model, which predicts that the SO-related rhythmic function of the RE is integral for its role in this memory circuitry. We feel our

present work provides important insights for mechanistically how the RE may be underlying coordinated information exchange between PFC and HPC particularly during SO states.

It will be of interest for future researchers to examine closely the role of RE activity in behavioural and memory-relevant paradigms, particularly as they concern tonic upregulation of activity. For instance, Gq-coupled chemogenetic approaches may be compared to inhibitory or lesioning approaches for silencing the RE, with potentially dissociable effects observed in terms of behaviour and memory.

4.6 Conclusion

Here we show that the endogenous activity of the thalamic nucleus reuniens exerts a state-dependent influence on information processing and exchange between mPFC and HPC. Short-term continuous optogenetic excitation of RE neurons compromised mPFC-to-HPC information flow only during SO. During slow oscillatory states, the RE is primed to receive SO-related excitation from mPFC and relay it to HPC. In addition, during SO states, RE neurons appear to serve a clock-like, pace-keeping function, intimately coupled to the ongoing mPFC SO. Tonically upregulating the activity of the RE such that those timing cues are obliterated (as is the case during spontaneous theta) significantly impairs SO coherence between mPFC and HPC. It is as such not the overall integrity of the RE *per se* that is required for efficient information transfer in this circuit, but rather the mode of its firing and the precise timing during deactivated states that orchestrates SO coordination. The RE lies optimally positioned as a nodal communications and processing hub between mPFC and HPC, which can regulate their dialogue via its activity state.

5 Brief activation of the nucleus reuniens resets the hippocampal theta rhythm

Brandon E. Hauer[1], Silvia Pagliardini[1,2,3], Clayton T. Dickson[1,2,3,4]

[1]Neuroscience and Mental Health Institute, University of Alberta, Edmonton, Alberta T6G 2E9, Canada,

[2]Department of Physiology, University of Alberta, Edmonton, Alberta T6G 2E9, Canada,

[3]Department of Anesthesiology and Pain Medicine, Edmonton, Alberta T6G 2E9, Canada,

[4]Department of Psychology, University of Alberta, Edmonton, Alberta T6G 2E9, Canada

Acknowledgements: This work was supported by Natural Sciences and Engineering Research Council of Canada (NSERC) Discovery grants 2016-06576 and 2021-02926 to C.T.D, and NSERC grant 435843 to S.P. B.E.H. was supported by an NSERC Doctoral Postgraduate Scholarship.

5.1 Abstract

Spontaneous neural rhythms like hippocampal theta have been suggested to be important for mnemonic processing. A potential mechanism by which it may update information is via phase resetting in response to novel stimuli or inputs. Here, we show that optogenetic activation of a midline thalamic input to the hippocampus results in a robust resetting of ongoing theta rhythms. This has important mechanistic implications for how the thalamic nucleus reuniens mediates theta synchrony across memory processing areas in both the hippocampus and across the brain, and furthermore for its role in its role in memory.

5.2 Introduction

The hippocampal (HPC) theta rhythm is one of the most widely studied neural phenomena. One of the most prominent oscillations in the mammalian brain (Bland, 1986), theta (~3 – 12 Hz) occurs during both active exploration as well as during rapid eye movement (REM) sleep or REM-like states under certain anesthetics (Jouvet, 1969; Buzsaki, 2002). Theta emerges as a consequence of synchronizing rhythmic intrinsic cellular properties, and can readily be entrained by other sources of theta oscillations throughout the brain (Colgin, 2013). One theory for how HPC theta may enhance cognitive processing and memory, in particular, is via a resetting of the theta rhythm, wherein ongoing theta becomes phase-locked to either incoming stimuli or rhythmic input from other neural oscillators (Williams and Givens, 2003).

Resetting the phase of a given oscillation facilitates coordinated transfer of information both within circuits and across distributed brain regions (Voloh and Womelsdorf, 2016). Theta itself can be reset by exogenous stimuli (e.g., light pulses), and by electrical stimulation of various foci including the fornix and perforant pathway (Williams and Givens, 2003). Indeed, the resetting of theta produces optimal conditions for long term potentiation, important for memory-relevant processes (McCartney et al., 2004).

Here, we show that optogenetically stimulating the nucleus reuniens (RE), a midline node that comprises the majority of thalamic afferents to HPC (McKenna and Vertes, 2004), is capable of resetting the ongoing theta rhythm. The RE is known to be important for mediating prefrontal-HPC theta synchrony (Griffin, 2021). Here, we provide the first mechanistic evidence for how this process may be occurring. The RE lies in a nodal position to modulate hippocampal theta and thus mPFC-HPC coupling which has important implications for activity-dependent mnemonic processing.

5.3 Materials and Methods

5.3.1 Animals

Experiments were conducted on 4 male Sprague Dawley (SD) rats obtained from the Sciences Animal Support Services and/or Health Sciences Laboratory Animal Services of the University of Alberta with a mean (± standard error of the mean; SEM) final weight of 422.50 ± 21.88 g.. All rats were provided with food and water *ad libitum* and were maintained on a 12 h light/dark cycle, with lights on at 7:00 am. All procedures conformed to the guidelines of the Canadian Council on Animal Care (CCAC) and were approved by the Biological Sciences and/or Health Sciences Animal Policy and Welfare Committees (AUP 092 and AUP 461) of the University of Alberta.

5.3.2 Procedures

Viral injections

Rats were anesthetized with an intraperitoneal injection of a ketamine/xylazine cocktail (90 and 10 mg/kg, respectively; Bimeda-MTC; Animal Health Inc., Cambridge, ON, Canada; and Rompun; Bayer Inc., Mississauga, ON, Canada). Rats were then placed into a stereotaxic apparatus (Model 900, David Kopf Instruments, Tujunga, CA, USA). One long incision was made along the midline of the scalp, and the skin flaps were pinned back. The skull was levelled by adjusting lambda and bregma to be in the same horizontal plane. A single hole were drilled in the skull at pre-determined coordinates from a stereotaxic rat atlas (Paxinos and Watson, 1998).

Micropipettes (tip diameter, 30 μm) loaded with an adeno associated virus expressing a channelrhodopsin-2 variant (ChR2/H134R) and driven by a synapsin promoter (hSyn-ChR2-

EYFP; University of North Carolina Virus Vector Core Facility, Chapel Hill, NC, USA; 3.9 x 10^{12} molecules ml^{-1}) were attached to a holder (EHW-2MS; A-M Systems Inc., Carlsborg, WA, USA) and lowered using a micro-positioner into the brain. Injections targeted the midline of the nucleus reuniens thalami (AP -2.0; ML +1.9 mm) at an angle 16° oblique to the vertical line to avoid the midline sinus and advanced 6.8 mm from the brain surface (infusion volume 400 nl). Injections were made using a micro-injector (PMI-100; Dagan, Minneapolis, MN, USA). Following injection procedures, the scalp was then sutured, rats were given 0.5 ml of the local anesthetic bupivacaine (5 mg/ml s.c.) around the incision site, and were allowed to recover for 3 weeks before acute experimentation.

Acute urethane anesthesia and general experimental procedures

For acute anesthetized recordings, rats were anesthetized via slow (~0.03 – 0.08 ml/min) incremental administrations of urethane (0.4 g/ml) via a catheter (final dose across all rats: 1.18 ± 0.033 g/kg). Urethane was chosen for anesthesia because it promotes an unconscious state that mimics the typical dynamics of natural sleep, both in terms of brain state alternations and in terms of their typical physiological correlates, and is stable over protracted recordings (Clement et al., 2008; Pagliardini et al., 2013b; Silver et al., 2021).

Rats were placed back into the stereotaxic apparatus and once again a single long incision was made along the scalp to expose the cranium. Body temperature was maintained at 37°C (Harvard Apparatus). Bipolar recording electrodes (tip separation 0.4-0.9 mm) were positioned in the PFC (AP +3.2; ML 0.7; DV -1.1 to -1.8 mm), and straddling the pyramidal layer of CA1 (AP -5.5; ML -4.5 mm; DV -2.2 to -3.2 mm), and were cemented in place. A linear 16-contact

(100 μm separation) multiprobe arranged in a vertical linear array (U-probe, Plexon Inc., Dallas, TX) was placed in the contralateral HPC (AP -5.5; ML +4.5; DV -3.3 to 4.5 mm). Local field potentials were amplified in differential mode at a gain of 1000 and filtered between 0.1 to 500 Hz using a differential AC amplifier (for bipolar electrodes: Model 1700, A-M Systems Inc.; for the multiprobe: X1000: Plexon, Dallas, TX, USA). Signals were digitized at a sampling frequency of 1000 Hz using a Digidata 1440A analog to digital board (Molecular Devices) connected to a PC running Axoscope (Molecular Devices).. The position of the multiprobe was histologically confirmed in every experiment by analyzing its track in relation to recorded field activity.

An optic fibre (tip diameter 200 μm) connected to a 473 nm laser (Laserglow Technologies, Toronto, ON, Canada), calibrated to deliver light at 10 – 12 mW, was positioned above RE. Optogenetic evoked potentials were produced using 10 ms laser pulses delivered every 5 s to the RE and were averaged over 32-64 trials during theta states.

5.3.3 Perfusion and Histology

Rats were transcardially perfused with 0.9% saline and 4% paraformaldehyde in saline (Fisher Scientific, Toronto, ON, Canada). The brain was then removed and placed into a 4% formalin and 20% sucrose solution for at least 48 h. Brains were flash frozen using compressed CO_2 and sectioned with a rotary microtome (1320 Microtome; Leica, Vienna, Austria) at a width of 60 μm. Tissue was counter-sectioned, with half of the sections mounted for thionin staining, and the other half saved for immunohistochemistry Briefly, the primary antibodies detected green fluorescent protein (GFP; dilution 1:1000; raised in chicken; Aves Labs, Tigard, OR,

USA), and the secondary antibodies were conjugated to that fluorescent protein (Cy2-conjugated donkey anti-chicken; 1:200; Jackson ImmunoResearch, West Grove, PA, USA). Microscopic inspection of tissue was used to verify electrode recording loci, optic fibre tracks, and expression of viral constructs using a Leica DM5500B fluorescent microscope.

5.3.4 Data Processing and Analysis

The spatial locations of the multiprobe channels were estimated based on the well-described theta power profile (Bland and Bland, 1986; Buzsaki, 2002; Wolansky et al., 2006), with the phase reversal point corresponding to the interface between *stratum pyramidale* and *stratum radiatum*, and the maximal theta channel located at *stratum lacunosum moleculare* (SLM). Evoked potentials were normalized to compute significance, and averages were created and compared against the 99% confidence limits (average value ± 2.6 SEM). Current source density (CSD) analysis was performed on both spontaneously recorded (gap free) field samples, and on evoked potential sweeps and averages recorded using the multiprobe. Briefly, CSD was computed by estimating the second spatial derivative of adjacent multiprobe voltage traces, following the assumptions of Freeman (1975), Rodriguez and Haberly (1989), and Ketchum and Haberly (1993).

5.4 Results

We first confirmed that optogenetic excitation of RE evoked a similar pattern of local field potential and CSD responses to what we have previously shown (Hauer et al., 2019). During trials in which we collected long-duration sweeps, we also saw evidence of theta rhythm

reset subsequent to stimulation (Figure 1). Stimulation was delivered at random phases of ongoing theta and traces were subsequently aligned by stimulation onset. Normalizing the traces by the average RMS of spontaneous theta recordings showed significant (> 2 S.D.) fluctuations in local field potential activity that aligned with each other across stimulation trials, regardless of the oscillatory phase at stimulus onset, which was random (Fig. 1A). Averaging these traces over many (in this case, 58) trials clearly showed an initial evoked potential followed by a regular ~ 4 Hz rhythm, which extended well beyond the 99% confidence limits of the randomized traces. Stimulating the ipsilateral fiber bundle by which RE projects to HPC (the cingulum bundle, CB) also reset the ongoing field activity and produced a ~ 4 Hz (theta) rhythm (Fig. 1B). The reset rhythm was larger and more obvious in the ipsilateral HPC, to which the lateralized fibres from RE independently projects.

Spontaneous theta evokes a regular, rhythmic pattern of sinks and sources between stratum lacunosum-moleculare (SLM) and stratum pyramidale of CA1 (Fig. 2A). Stimulation of either RE (Fig. 2B) or CB (Fig. 2C) creates a short latency evoked potential maximal at SLM, followed by an obvious ~4 Hz alternation of sinks and sources that closely mimics the spatial distribution during spontaneous theta. Using autocorrelation analysis, we observed that the average evoked field activity was rhythmic during theta, but not SO states (Fig. 2D). Examining the evoked CSD activity the same way showed prominent rhythmicity at theta frequencies resulting from both RE and CB stim, with CB stim leading slightly (Fig. 2E). Finally, autocorrelation analysis of the field evoked in both hippocampi from CB stim showed a larger rhythmic fluctuation at theta frequencies in the ipsilateral, as compared to the contralateral, HPC (Fig. 2F).

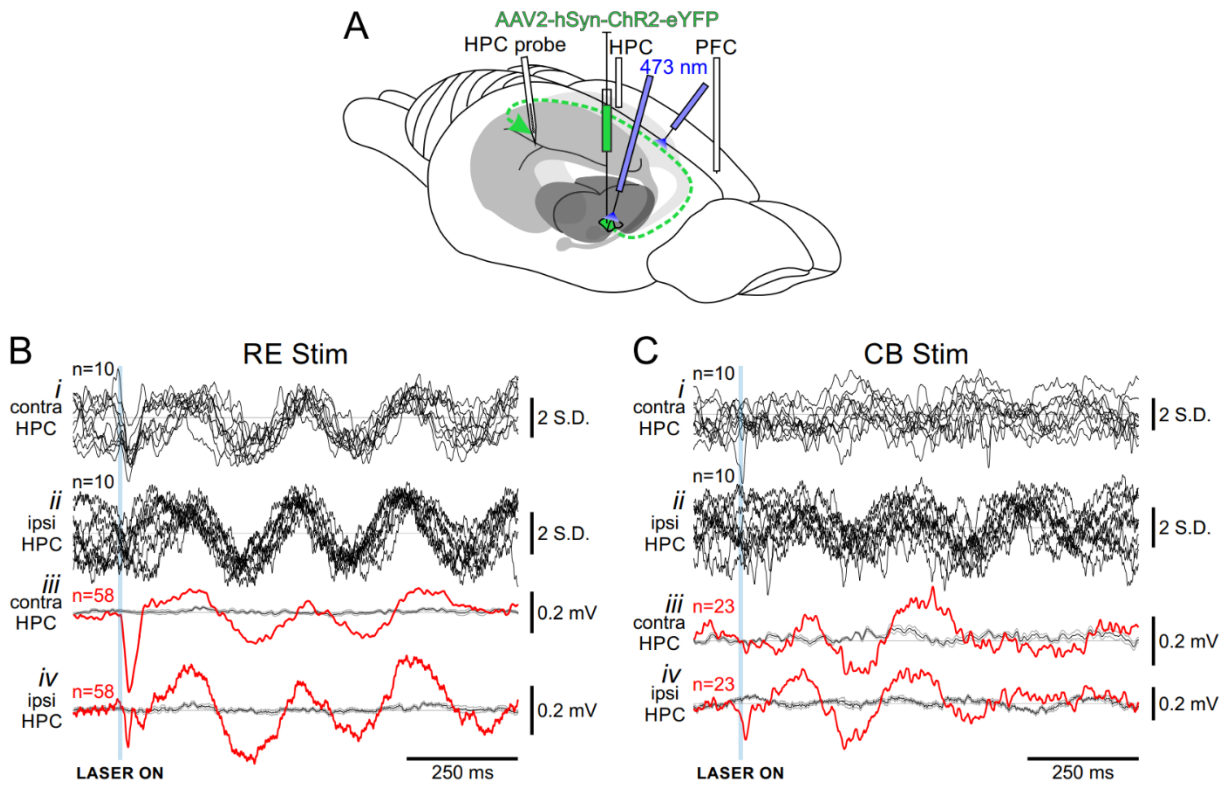

Figure 5.1 Optogenetic stimulation of RE or CB resets ongoing theta local field activity increases multiunit activity while the laser is on.

A. Schematic illustration of the recording, injection, and stimulation sites. Schema modified from Amaral and Witter (1995). **B, C.** Brief (10 ms) optogenetic pulses delivered to RE (**B**) or CB (**C**) at random phases of the HPC theta rhythm produce an initial evoked potential and subsequently reset theta in individual trials and on average. Grey lines represent 99% confidence limits.

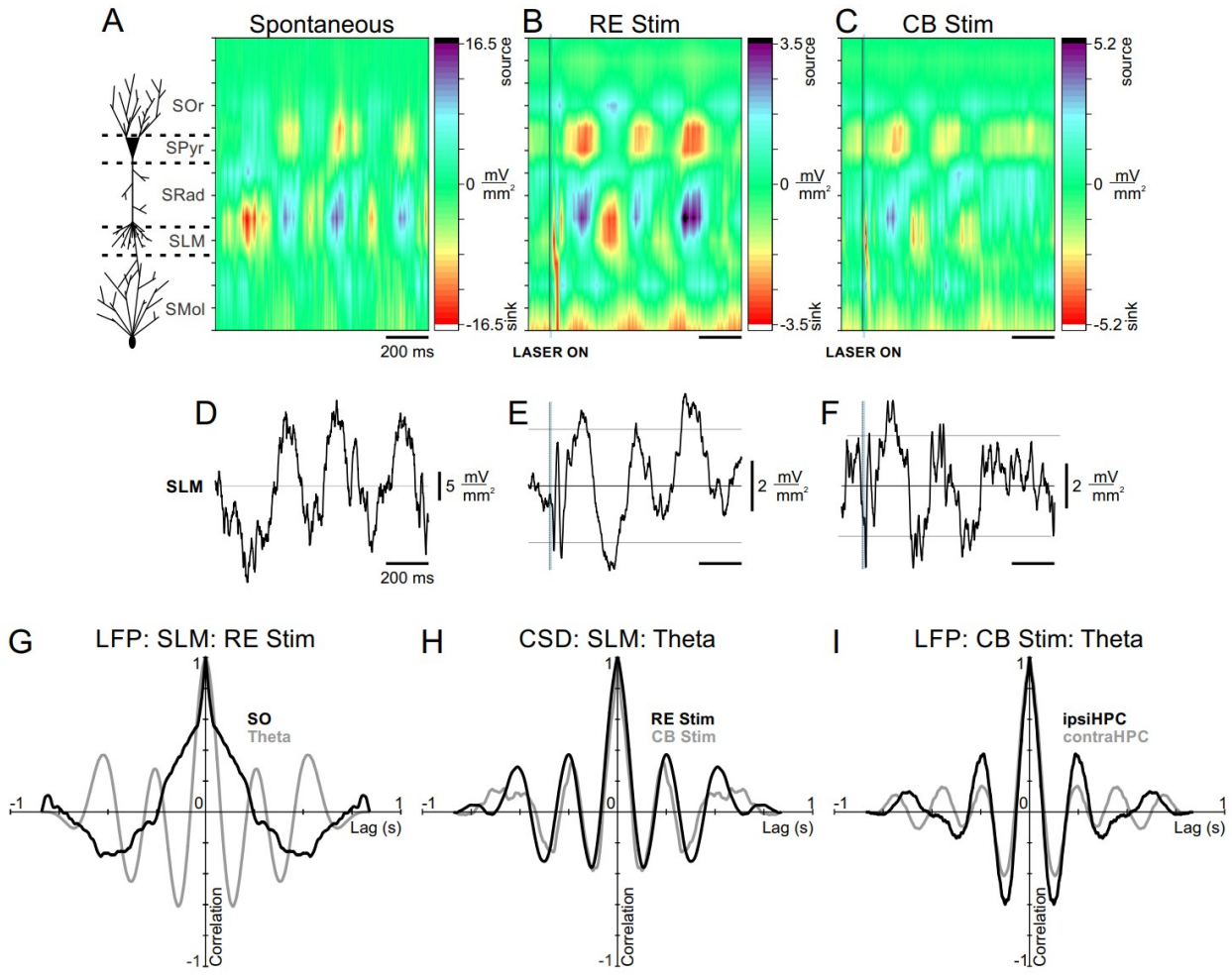

Figure 5.2 The optogenetically induced theta reset closely resembles spontaneous theta and is highly rhythmic at theta frequencies.

A, B, C. Colour contour plots visualizing the patterns of sinks and sources during spontaneous theta activity (**A**); resulting from RE stimulation (**B**); and resulting from CB stimulation (**C**). The pattern of sinks and sources evoked by optogenetic stimulation closely resembles spontaneous theta. **D, E, F.** CSD trace corresponding to the SLM channel in **A**, **B**, and **C**. In **E** and **F**, the trace is compared against the averaged baseline (0 - 100ms) across all channels (thin black line), ± 99% confidence limits (grey lines) based on the distribution of these baseline values. **G.** Autocorrelation of the field activity resulting from RE stim during SO (black) and during theta

(grey), showing prominent rhythmicity only during theta. **H.** Autocorrelation of t CSD of the signal corresponding to SLM, showing prominent rhythmicity resulting from both RE (black) and CB (grey) stimulation. **I.** Autocorrelation of the field activity in the ipsilateral HPC (black) and the contralateral HPC (grey) resulting from CB stimulation, showing more prominent rhythmicity generated in the ipsilateral HPC.

5.5 Discussion

Optogenetic stimulation of the thalamic nucleus reuniens during spontaneous theta is capable of resetting the HPC theta rhythm in urethane-anesthetized rats. Stimulating the ipsilateral fiber afferent by which it projects to HPC more effectively entrains that hemisphere as compared to the contralateral HPC. The RE as such has the ability to fundamentally affect the internal oscillator of the HPC. The RE has already been suggested to play an important role in mediating prefrontal-HPC theta synchrony (Griffin, 2021), and our results provide a mechanism by which this may occur. Theta reset creates optimal conditions for activity-dependent mnemonic processes (McCartney et al., 2004) and more generally facilitates efficient information transfer across local circuits and distributed brain networks alike (Voloh and Womelsdorf, 2016). In conclusion, the RE lies optimally positioned to augment the oscillatory theta activity of the HPC, providing a mechanism by which it can modulate forebrain synchrony and mnemonic processing.

6 Discussion

Discussion

The goal of this thesis was to explore the role of an understudied circuitry in facilitating efficient information exchange between medial prefrontal cortex and hippocampus; specifically, that interface provided by the anatomically interposed thalamic nucleus reuniens. The continued and synchronous dialogue between these two disparate sites is vital for many of the complexities of behavioral experience and memory. To this end, the nucleus reuniens provides a unique interface between these sites both anatomically and, as demonstrated throughout this thesis, in terms of its ability to process and relay information between them. I have shown that this unique node is modulated by the broader circuitry it connects, by forebrain state, and by its own patterns of neuronal activity, such that it may enable and facilitate the coordinated transfer of information between prefrontal and hippocampal sites, paramount for episodic memory processes. The nucleus reuniens is a nodal and state-variant processor that is optimized for mPFC-HPC directional communication, particularly during slow oscillatory states.

In Chapter 2, I explored the single- and multi-unit activity of the RE during natural forebrain state changes under urethane anesthesia. This work provided the first clues that the RE may be particularly well-suited to mediating the exchange of information between mPFC and HPC during SO states in particular. RE units were intimately coupled to the ongoing mPFC SO, firing preferentially during the ON state of the oscillation. Optogenetic stimulation of the RE further showed that it was a functionally active site in terms of exciting CA1. Critically, long-duration chemogenetic inhibition of RE significantly decremented SO coherence between mPFC and HPC sites. In Chapter 3, I expanded upon these findings by contrasting the two primary brain states observed under urethane, particularly in the context of how the activity of the RE may lead to differential responding in HPC. Not only was the magnitude of response to

stimulation consistently larger in SO as compared to theta states, but the pattern of responding in HPC to mPFC stimulation was fundamentally different as a function of state. The RE appeared to bias the preferred pathway of information transfer from mPFC to HPC, including itself preferentially during SO as the most direct access route to CA1. In Chapter 4, I showed that it was not the basic integrity of the RE *per se* that facilitates mPFC-HPC SO dialogue in particular, but rather the specific activity states of RE neurons that biases information exchange. Short term tonic upregulation of RE activity decreased the influence of mPFC stimulation in the HPC during SO states. Consistently, extended tonic upregulation of RE neurons decreased SO coherence between mPFC and HPC. Simply modulating the activity dynamics of the RE to mimic those observed during spontaneous theta was sufficient to disrupt SO coupling in particular. As such, it appears that during SO, the RE is primed by the mPFC-HPC circuitry to both receive and transmit SO information, while the rhythmically-coupled activity state of RE neurons enables them to fulfill this function. Finally, in Chapter 5, I showed that brief stimulation of the RE during spontaneous theta states is capable of resetting the hippocampal theta rhythm. The RE therefore has the ability to fundamentally affect the internal oscillator of the HPC, the resetting of which may mechanistically underlie its capacity to synchronize theta in the mPFC-HPC circuitry and augment activity-dependent mnemonic processes. Taken together, the results presented in this thesis indicate decisively a role of the RE in facilitating efficient information exchange between mPFC and HPC. This mechanistic capacity to underlie and maintain an oscillatory dialogue has important implications for activity-related processes including sleep-dependent memory consolidation.

6.1 The RE is important for coordinating forebrain slow oscillations

Despite the rapidly increasing appreciation for the RE's role in activity-dependent memory-related phenomena, exhaustive electrophysiological studies either *in vitro* or *in vivo*, as presented here, have remained curiously elusive. Previous work from our lab decisively showed that a local SO power maximum with a corresponding slight phase shift occurred at SLM, suggesting that some type of local generation of SO was going on at this level (Wolansky et al., 2006). Only two primary inputs synapse directly at SLM: one, a comparatively far more studied route arriving via the temporoammonic pathway from layer III of EC (Steward and Scoville, 1976; Ino et al., 1998; Kloosterman et al., 2004; Isomura et al., 2006); and the other, a thalamic input arising from the RE (Herkenham, 1978; Wouterlood et al., 1990; Dolleman-Van Der Weel and Witter, 1996; Vertes et al., 2006; Vertes et al., 2007; Varela et al., 2014; Vertes, 2015). The comparatively robust body of anatomical literature in terms of RE connectivity has outpaced the physiological research by such a degree that basic single- or multi-unit recordings in this structure have hardly ever been done.

The first clue that the RE may be involved *somehow* with the SO came from recording single units in the RE (Chapter 2). They were remarkably well-coupled to the ongoing mPFC SO, and showed an impressive modulation by state (Hauer et al., 2019). Even brief transitions into activated/ theta states yielded a substantial upregulation of activity, and an ostensible loss of rhythmic/ phasic input the HPC. This also suggested that the RE was not following the oscillatory activity of the HPC directly, given the lack of any theta-related coupling observed in the RE, but instead seemed to better track the activity of the frontal cortex. Indeed, we confirmed that stimulation of mPFC was orthodromically exciting RE units. Oscillatory coupling is an important mechanism for informational transfer, with coherent oscillations representing an ideal platform to precisely align windows for efficient dialogue (Fries, 2005; Voytek and Knight,

2015). Optogenetic stimulation of the RE showed robust excitation of HPC, consistent both with past literature (Dolleman-Van der Weel et al., 1997; Morales et al., 2007; Dolleman-van der Weel et al., 2017; Vu et al., 2020) and with the circuit being functionally excitable.

Critically, I showed that chemogenetic inactivation of the RE decreased SO coherence between mPFC and HPC. This was the first demonstration that, in urethane-anesthetized rats, the "other" input to the SLM (that is, from the RE instead of EC) actually had a substantial contribution to the oscillatory dynamics between mPFC and HPC. Coupled with my demonstration of mPFC-to-RE orthodromic excitation, I theorized from these results that that the mPFC may be entraining RE units to efficiently transfer information to the HPC, particularly during SO states. This SO coordination is likely to be an important factor in the offline consolidation of various types of memory (Loureiro et al., 2012; Klein et al., 2019; Quet et al., 2020; Ferraris et al., 2021).

6.2 State dependent transfer of information through the RE

It quickly became apparent that the evoked potentials being generated in HPC were considerably different based on whether stimulation was delivered during SO or theta states. In Chapter 3, I investigated these state-related differences in the mPFC-RE-HPC circuitry by comparing evoked potentials during both SO and theta states, and also assessed how chemogenetically inhibiting the RE modulated these responses with respect to state.

Optically stimulating either the RE or the CB reliably produced a much larger response in HPC if that excitation was delivered during SO as compared to theta states. This was also true of evoked potentials in PFC following RE stimulation. Similarly, we observed a distinct phase-

preference across states, with stimuli provided at any phase of the SO cycle generating a more robust response than during theta. This is noteworthy within the greater context of the mPFC-RE-HPC circuitry, because the phase-dependent coordinated replay of related cellular ensembles across both mPFC and HPC could serve as a reverberative strategy to enhance activity-dependent coupling of these neural representations (Hebb, 1949; Siapas and Wilson, 1998; Ji and Wilson, 2007b). The HPC projecting directly back to the mPFC (Jay et al., 1989; Hoover and Vertes, 2007) may create a "return loop," resulting in a self-sustaining and repetitive reverberation that could be well positioned to either strengthen or weaken a set of neuronal assemblies in both the mPFC and HPC, depending upon the relative phasing of activations. The RE lies critically interposed as a mediator of phase-dependent communications.

Also noteworthy is that the pattern of evoked responding in HPC following mPFC stimulation was considerably different based on brain state. This surprising finding suggests that the way information is processed in this mnemonically-relevant circuitry is considerably different based on forebrain state, whether the animal is sleeping/ anesthetized, or awake and behaving. Previous work from our lab has shown that synaptic excitability is enhanced in almost all HPC-projecting pathways during SO (Schall et al., 2008), but this is the first such demonstration in the RE-HPC synapse. The one exception to this augmented excitability was the EC layer II-originating medial perforant path to the DG, which showed enhanced excitability during theta (Schall et al., 2008). The temporally delayed DG sink we observed following stimulation of RE and mPFC did not show any variation by state (Chapters 3, 4). Given that the RE does not project directly to DG (Herkenham, 1978; Wouterlood et al., 1990), it must instead project via an alternate ventral pathway through the EC, which in turn provides a distinct access route to HPC (Wouterlood, 1991; Zhang and Bertram, 2002; Vu et al., 2020).

My theory of RE function in this circuit is that, during SO states, it becomes the preferred route of information transfer between mPFC and HPC, providing an ideal platform for offline memory consolidation (Laroche et al., 2000; Born, 2010; Eichenbaum, 2017). Conversely, during theta states, high levels of acetylcholine in the extracellular milieu of the forebrain provides an "encoding state" for processing newly acquired information as an animal explores its environment (Hasselmo et al., 1996; Hasselmo, 2006). Perturbations to the RE during offline states consistently impoverish consolidation (Loureiro et al., 2012; Klein et al., 2019; Quet et al., 2020), while RE perturbations during active choice points as an animal explores or completes a behavioural task impair theta synchrony and memory encoding (Hallock et al., 2016; Maisson et al., 2018). However, it was still unclear what the exact role of the differential activity modes of the RE across states was, and if mimicking one of those modes could alter mPFC-HPC communication in a manner comparable to endogenous state changes. To this end, we sought to mimic RE activity dynamics typical during theta states using tonic optogenetic stimulation (Chapter 4).

6.3 Activity states of the nucleus reuniens

The first electrophysiological assay of RE units was performed in rats under anaesthesia, with a particular focus on theta states (Morales et al., 2007). RE units exhibited a marked increase in firing rate during theta, but without showing any rhythmic patterns or bursting. Moreover, they displayed only negligible (10^{-3} – 10^{-4}) coherence with hippocampal theta. The authors concluded that the RE exerts a tonic (and not phasic/ rhythmic) influence on HPC during theta states (Morales et al., 2007). The increased activity observed during theta has been corroborated through histological means, by examining c-Fos expression across sleep and wake

states. During spontaneous or forced waking, the RE exhibited higher expression of c-Fos, indicative of greater cellular activation (Cirelli et al., 1995; Cirelli and Tononi, 2000). Indeed, within sleep itself, paradoxical (REM) sleep produced significantly more c-Fos immunopositive cells in the RE than during deep slow-wave sleep (Sastre et al., 2000). A recent study examined discharge characteristics of RE neurons across sleep and wake states, contrasting active waking versus REM in particular (Viena et al., 2021). The authors described a majority of RE cells exhibiting state-related changes in activity, consistent with our schema of RE as serving not only a nodal relay function, but as a critical thalamic processing link in this case for attentional networks and ascending arousal (Viena et al., 2021). Perhaps surprisingly, few studies have examined the physiological properties of the RE during offline, and in particular SO states. During both anesthetized and naturally sleeping preparations, the RE mediates mPFC-HPC coupling during SOs and slow-wave sleep by synchronizing gamma (30 – 90 Hz) bursts between them (Ferraris et al., 2018). Moreover, the same group later showed that the RE coordinates and stabilizes neuronal sequences between mPFC and HPC during SOs (Angulo-Garcia et al., 2020). The work presented in this thesis together suggests that the RE is an essential mediator of SO information in particular, but that so too does the RE have important ramifications for informational processing during activated states, even if that role is largely to bias the circuitry involved between mPFC and HPC.

My conception of the role of this SO-related coupling is that two primary functions are occurring which help to "select" the RE as the preferred access point to CA1 during SO specifically (Chapter 4). First, the mPFC-HPC circuitry appears biased during SO states to include the RE. RE neurons appear primed to both receive and subsequently transmit to HPC information that gets packaged across SO cycles, since its neurons exhibit robust coupling to the

mPFC SO. Conversely, during theta, the HPC exhibits a significantly diminished response to RE stimulation. Even more convincingly, stimulation of mPFC produced a remarkably different pattern of results between states, with a temporally-delayed and non-RE-modulated response observed in HPC during theta. This perhaps suggests that theta represents a non-preferred state for relaying information from mPFC through the RE. Second, the mode of firing – the overall activity state of RE neurons – enables them to serve this function. Even during a global SO forebrain state, selectively and tonically upregulating the activity of the RE is sufficient to 1) impoverish mPFC input to HPC, and 2) decrease SO coupling between the two sites (Chapter 4). That is, even when the RE would typically be engaged in the mPFC-HPC circuitry (during SO), simply tonically activating its activity (rather than lesioning or inactivating it) is sufficient to remove this important node from its role as an SO coupler. The rhythmic, clock-like activity of the RE during SO is thus fundamental for effective information transfer between mPFC and HPC during offline states, which is consistent with its increasingly appreciated role in offline activity-dependent memory consolidation (Ferraris et al., 2021).

6.4 The RE modulates ongoing HPC activity directly

The RE is known to have a role in mediating PFC-HPC synchrony at theta frequencies (Griffin, 2021). Behavioral tasks requiring the online participation of the RE for optimal memory performance are impaired by even temporary inactivation of the RE at decision critical time points, and also reduce theta synchrony between PFC and HPC (Hallock et al., 2013; Hallock et al., 2016; Maisson et al., 2018). Mechanistically how the RE underlies such synchrony is far less clear, however, given that RE neurons themselves do not oscillate at theta frequencies (Morales

et al., 2007; Viena et al., 2021). In Chapter 5, I showed, perhaps surprisingly, that brief optogenetic activation of the RE was sufficient to reset the ongoing theta rhythm in HPC.

Oscillatory resetting is a highly efficient mechanism for facilitating coordinated information transfer within and across circuits (Voloh and Womelsdorf, 2016). Theta, in particular, can be readily entrained by other sources of theta oscillations including from activity emanating from both the EC and the medial septum (Colgin, 2013), and direct excitation of HPC afferents has been shown to reliably reset the rhythm (Williams and Givens, 2003). Resetting of the theta rhythm allows other nodes in the HPC circuitry (for instance, the mPFC) to coordinate their inputs and information transfer, and creates optimal conditions for long term potentiation (McCartney et al., 2004). The RE therefore lies in a position to facilitate coordinated timing across mPFC and HPC both during SO (Chapter 2, 4), as well as potentially during activated theta states. This is the first such demonstration of the RE (and moreover, of RE efferents coursing through the CB to HPC) being able to reset the HPC theta rhythm. It remains unclear how exactly the tone of RE activity may help to set theta rhythmicity, or to what extent its influence modulates informational processing in the HPC. However, my hope is that the short communication presented in Chapter 5 provides a key mechanistic clue for how the RE serves its increasingly notable role in mediating theta synchrony and efficient mnemonic encoding during online tasks.

6.5 Future Directions

Many exciting potential avenues exist for investigations into this relatively novel but obviously important circuitry. For instance, both chemogenetic inhibition (Chapter 2) and

optogenetic tonic activation (Chapter 4) of the RE decreased mPFC-HPC SO coherence. However, in neither case was the coherence reduced to zero. That is, some degree of prefrontal-hippocampal SO coupling remained intact despite the functional removal of the RE from the circuit. It appears more likely that the remaining coherence is supplied by input from the EC, but future work must carefully disentangle these co-operative but distinct HPC inputs. Another curiosity would be to assess EC-HPC coherence at SO frequencies following down or up-regulation of RE activity. It is conceivable that SO coherence between these sites may actually increase following perturbations of the RE, in a compensatory mechanism to maintain effective SO discharge using an alternate circuitry.

Surprisingly, to my knowledge, no literature exists which clearly characterizes the effects of stimulating the RE on EC cell lamina. The RE innervates the dendrites of principal cells in both layers II and III of EC (Wouterlood, 1991), and may have other ramifications on deeper layers as well (Witter et al., 1989). However, the electrophysiological assay of RE-evoked potentials across EC lamina remains elusive. This study would be supremely useful for characterizing the complex interplay between the RE, EC, and HPC, and may lead to further insights for how exactly the DG sink following by RE stimulation is evoked (Dolleman-van der Weel et al., 2017; Vu et al., 2020).

Much of the work in this thesis has focused on an mPFC → RE → HPC directionality of informational transfer. It remains an open and captivating question how the HPC communicates with the mPFC (especially via the RE) during offline states. Retrograde approaches to selectively target mPFC-projecting HPC neurons and subsequently activating or inhibiting them during both brain states would provide valuable insight for the "return" function of this circuit. Further, stimulating RE-projecting HPC neurons (perhaps using a retrograde Cre recombinase approach)

and recording from the mPFC could reveal a differential pattern of excitability as a function of state, one which could be expected to modulate offline or sleep-dependent memory consolidation. I would expect that the magnitude of response in mPFC would be larger during SO states, mirroring the findings in this thesis that mPFC-to-HPC activation via the RE is larger during SO compared to theta. That is, this study could provide evidence of the specialized role of the RE in mediating SO coordination in both directions in the circuitry, important for the types of reverberatory circuit activity involved in memory consolidation. I would also be very curious to assess HPC-to-RE excitation during theta states. Would the phase of the theta oscillation modulate RE responding? Would entrainment of HPC theta at a slightly faster frequency modulate RE unit activity at all? Understanding how the RE may be poised to facilitate communication in both directions remains an open and fascinating area of potential study.

In considering the dynamics of mPFC inputs to this circuit, would entraining mPFC SOs to a different frequency alter the average firing frequency of RE units? I would theorize that this would indeed be the case, with RE units remaining locked to the predominant oscillation for effective transfer of information to HPC. An approach that would answer this would be to use a closed-loop optogenetic stimulation paradigm, selectively modulating SO activity at either mPFC or RE. The objective could be to forcibly increase SO coupling between mPFC and HPC by optogenetically driving RE units at precise times, theoretically augmenting activity-dependent mnemonic processes such that memory of a recently learned event could be facilitated. Indeed, exogenous augmentation of SOs has been previously shown to have beneficial effects for human memory (Marshall et al., 2006) Conversely, chronic upregulation of RE activity would be expected to decrease SO coupling, and consequently impair or impoverish the offline consolidation of episodic-like memories (Ferraris et al., 2021). The same closed-loop system

could be used to tonically drive RE neurons during SO or slow-wave sleep states specifically, theoretically abolishing the windows for offline, SO-related memory consolidation and therefore removing one of the most critical circuitries for mnemonically important information transfer between mPFC and HPC.

The exact role of the RE in mechanistically mediating theta synchrony between mPFC and HPC is another alluring angle for future study (Griffin, 2021). While we and others (Morales et al., 2007; Viena et al., 2021) have never demonstrated any theta rhythmicity in the tonic firing of RE during activated states, we have also shown that its tone may be important for HPC theta (Chapter 5). Being able to reset spontaneous HPC theta with only brief optical stimulation suggests that the RE has a potentially important role in modulating rhythmicity, and therefore synchronous information transfer, during online states. It is unclear if stimulation of the mPFC is similarly capable of resetting HPC theta, or how the tonic activity of RE may be subtly modulated to alter rhythmic HPC dynamics. Again, the directionality of this circuitry remains open for further study, as perhaps the RE allows for HPC stimulation to reset mPFC theta (or indeed, perhaps reset mPFC SO as well).

The work in this thesis is also, to my knowledge, the only to directly manipulate the cingulum bundle in the context of RE circuitry. I feel this is an exciting and heretofore un-utilized approach to attempt to disentangle ipsilateral HPC phenomena resulting from mPFC or more directly RE manipulations. It may be possible to alter the frequency or expression of either theta or SO rhythms in a single HPC by perturbing the CB, with the contralateral HPC presumably “catching up” or compensating at some point afterwards.

6.6 Conclusion

In the work described in this thesis, I have thoroughly investigated the role of the thalamic nucleus reuniens in facilitating communication between the prefrontal cortex and hippocampus. It has become abundantly clear that the RE is fundamentally required for effective information exchange between these mnemonically important sites, and lies as such in an ideal position to modulate activity-dependent memory consolidation processes.

It has been more than 70 years since the electrophysiological foray into the ventral midline thalamus first began (Jasper, 1949). In a sense, I consider the work within this thesis to be a continuation of these original pioneering studies. However, to my advantage, I have the many interposing decades of technological advancement that have resulted in toolboxes like optogenetics and chemogenetics, to be used at my disposal. While by no means experimentally easier nor more difficult, instead, I am but the latest in a long line of electrophysiologists, who just happened to be armed with new equipment, new capabilities, and new questions. It is a line of study, of scientific exploration, of pure unadulterated passion and curiosity, which I hope continues in perpetuity.

References

Adhikari A, Topiwala MA, Gordon JA (2010) Synchronized activity between the ventral hippocampus and the medial prefrontal cortex during anxiety. Neuron 65:257-269.

Ainge JA, van der Meer MA, Langston RF, Wood ER (2007) Exploring the role of context-dependent hippocampal activity in spatial alternation behavior. Hippocampus 17:988-1002.

Aldrin-Kirk P, Bjorklund T (2019) Practical Considerations for the Use of DREADD and Other Chemogenetic Receptors to Regulate Neuronal Activity in the Mammalian Brain. Methods Mol Biol 1937:59-87.

Amaral DG, Witter MP (1995) Hippocampal Formation. In: The Rat Nervous System, 2nd Edition (Paxinos G, ed), pp 443-493. San Diego, USA: Academic Press, Inc.

Amzica F, Steriade M (1995) Short- and long-range neuronal synchronization of the slow (< 1 Hz) cortical oscillation. J Neurophysiol 73:20-38.

Amzica F, Steriade M (1997) The K-complex: its slow (<1-Hz) rhythmicity and relation to delta waves. Neurology 49:952-959.

Angulo-Garcia D, Ferraris M, Ghestem A, Bernard C, Quilichini PP (2018) Spatio-temporal organization of cell assemblies in Nucleus Reuniens during slow oscillations. bioRxiv:474973.

Angulo-Garcia D, Ferraris M, Ghestem A, Nallet-Khosrofian L, Bernard C, Quilichini PP (2020) Cell Assemblies in the Cortico-Hippocampal-Reuniens Network during Slow Oscillations. J Neurosci 40:8343-8354.

Arantius G (1587) De humano foetu. Ejusdem anatomicorum observationum liber, etc. Venice.

Arduini A, Terzuolo C (1951) Cortical and subcortical components in the recruiting responses. Electroencephalogr Clin Neurophysiol 3:189-196.

Armbruster BN, Li X, Pausch MH, Herlitze S, Roth BL (2007) Evolving the lock to fit the key to create a family of G protein-coupled receptors potently activated by an inert ligand. Proc Natl Acad Sci U S A 104:5163-5168.

Atasoy D, Sternson SM (2018) Chemogenetic Tools for Causal Cellular and Neuronal Biology. Physiol Rev 98:391-418.

Attwell D, Gibb A (2005) Neuroenergetics and the kinetic design of excitatory synapses. Nat Rev Neurosci 6:841-849.

Azarfar A, Calcini N, Huang C, Zeldenrust F, Celikel T (2018) Neural coding: A single neuron's perspective. Neurosci Biobehav Rev 94:238-247.

Baddeley A (2003) Working memory: looking back and looking forward. Nat Rev Neurosci 4:829-839.

Barker GRI, Warburton EC (2018) A Critical Role for the Nucleus Reuniens in Long-Term, But Not Short-Term Associative Recognition Memory Formation. J Neurosci 38:3208-3217.

Battaglia FP, Sutherland GR, McNaughton BL (2004) Hippocampal sharp wave bursts coincide with neocortical "up-state" transitions. Learn Mem 11:697-704.

Benchenane K, Peyrache A, Khamassi M, Tierney PL, Gioanni Y, Battaglia FP, Wiener SI (2010) Coherent theta oscillations and reorganization of spike timing in the hippocampal-prefrontal network upon learning. Neuron 66:921-936.

Berendse HW, Groenewegen HJ (1991) Restricted cortical termination fields of the midline and intralaminar thalamic nuclei in the rat. Neuroscience 42:73-102.

Berens P (2021) Circular Statistics Toolbox (Directional Statistics). In, 1.21.0.0 Edition. https://www.mathworks.com/matlabcentral/fileexchange/10676-circular-statistics-toolbox-directional-statistics: MATLAB Central File Exchange.

Bertram EH, Zhang DX (1999) Thalamic excitation of hippocampal CA1 neurons: a comparison with the effects of CA3 stimulation. Neuroscience 92:15-26.

Birrell JM, Brown VJ (2000) Medial frontal cortex mediates perceptual attentional set shifting in the rat. J Neurosci 20:4320-4324.

Bland BH (1986) The physiology and pharmacology of hippocampal formation theta rhythms. Prog Neurobiol 26:1-54.

Bland SK, Bland BH (1986) Medial septal modulation of hippocampal theta cell discharges. Brain Res 375:102-116.

Bokor H, Csaki A, Kocsis K, Kiss J (2002) Cellular architecture of the nucleus reuniens thalami and its putative aspartatergic/glutamatergic projection to the hippocampus and medial septum in the rat. Eur J Neurosci 16:1227-1239.

Bontempi B, Laurent-Demir C, Destrade C, Jaffard R (1999) Time-dependent reorganization of brain circuitry underlying long-term memory storage. Nature 400:671-675.

Borbely AA (1976) Sleep and motor activity of the rat during ultra-short light-dark cycles. Brain Res 114:305-317.

Born J (2010) Slow-wave sleep and the consolidation of long-term memory. World J Biol Psychiatry 11 Suppl 1:16-21.

Boyce R, Glasgow SD, Williams S, Adamantidis A (2016) Causal evidence for the role of REM sleep theta rhythm in contextual memory consolidation. Science 352:812-816.

Bruns A (2004) Fourier-, Hilbert- and wavelet-based signal analysis: are they really different approaches? J Neurosci Methods 137:321-332.

Buchanan SL, Thompson RH, Maxwell BL, Powell DA (1994) Efferent connections of the medial prefrontal cortex in the rabbit. Exp Brain Res 100:469-483.

Buzsaki G (1996) The hippocampo-neocortical dialogue. Cereb Cortex 6:81-92.

Buzsaki G (1998) Memory consolidation during sleep: a neurophysiological perspective. J Sleep Res 7 Suppl 1:17-23.

Buzsaki G (2002) Theta oscillations in the hippocampus. Neuron 33:325-340.

Buzsaki G, Draguhn A (2004) Neuronal oscillations in cortical networks. Science 304:1926-1929.

Buzsaki G, Watson BO (2012) Brain rhythms and neural syntax: implications for efficient coding of cognitive content and neuropsychiatric disease. Dialogues Clin Neurosci 14:345-367.

Buzsaki G, Anastassiou CA, Koch C (2012) The origin of extracellular fields and currents--EEG, ECoG, LFP and spikes. Nat Rev Neurosci 13:407-420.

Cain DP, Boon F, Corcoran ME (2006) Thalamic and hippocampal mechanisms in spatial navigation: a dissociation between brain mechanisms for learning how versus learning where to navigate. Behav Brain Res 170:241-256.

Cajal SRy (1911) Histologie Du Système Nerveux De L'homme Et Des Vertébrés. Paris: Maloine.

Carmichael ST, Price JL (1995) Limbic connections of the orbital and medial prefrontal cortex in macaque monkeys. J Comp Neurol 363:615-641.

Carr DB, Sesack SR (1996) Hippocampal afferents to the rat prefrontal cortex: synaptic targets and relation to dopamine terminals. J Comp Neurol 369:1-15.

Carskadon MA, Dement WC (2005) Chapter 2 - Normal Human Sleep: An Overview. In: Principles and Practice of Sleep Medicine (Fourth Edition), pp 13-23. Philadelphia: W.B. Saunders.

Cassel JC, Pereira de Vasconcelos A, Loureiro M, Cholvin T, Dalrymple-Alford JC, Vertes RP (2013) The reuniens and rhomboid nuclei: neuroanatomy, electrophysiological characteristics and behavioral implications. Prog Neurobiol 111:34-52.

Chauvette S, Crochet S, Volgushev M, Timofeev I (2011) Properties of slow oscillation during slow-wave sleep and anesthesia in cats. J Neurosci 31:14998-15008.

Cholvin T, Hok V, Giorgi L, Chaillan FA, Poucet B (2018) Ventral Midline Thalamus Is Necessary for Hippocampal Place Field Stability and Cell Firing Modulation. J Neurosci 38:158-172.

Cholvin T, Loureiro M, Cassel R, Cosquer B, Geiger K, De Sa Nogueira D, Raingard H, Robelin L, Kelche C, Pereira de Vasconcelos A, Cassel JC (2013) The ventral midline thalamus contributes to strategy shifting in a memory task requiring both prefrontal cortical and hippocampal functions. J Neurosci 33:8772-8783.

Chudasama Y, Baunez C, Robbins TW (2003) Functional disconnection of the medial prefrontal cortex and subthalamic nucleus in attentional performance: evidence for corticosubthalamic interaction. J Neurosci 23:5477-5485.

Churchwell JC, Kesner RP (2011) Hippocampal-prefrontal dynamics in spatial working memory: interactions and independent parallel processing. Behav Brain Res 225:389-395.

Ciaramelli E (2008) The role of ventromedial prefrontal cortex in navigation: a case of impaired wayfinding and rehabilitation. Neuropsychologia 46:2099-2105.

Cirelli C, Tononi G (2000) On the functional significance of c-fos induction during the sleep-waking cycle. Sleep 23:453-469.

Cirelli C, Pompeiano M, Tononi G (1995) Sleep deprivation and c-fos expression in the rat brain. J Sleep Res 4:92-106.

Clarke PB, Schwartz RD, Paul SM, Pert CB, Pert A (1985) Nicotinic binding in rat brain: autoradiographic comparison of [3H]acetylcholine, [3H]nicotine, and [125I]-alpha-bungarotoxin. J Neurosci 5:1307-1315.

Clement EA, Richard A, Thwaites M, Ailon J, Peters S, Dickson CT (2008) Cyclic and sleep-like spontaneous alternations of brain state under urethane anaesthesia. PLoS One 3:e2004.

Colangelo C, Shichkova P, Keller D, Markram H, Ramaswamy S (2019) Cellular, Synaptic and Network Effects of Acetylcholine in the Neocortex. Front Neural Circuits 13:24.

Colgin LL (2013) Mechanisms and functions of theta rhythms. Annu Rev Neurosci 36:295-312.

Colonnier M (1968) Synaptic patterns on different cell types in the different laminae of the cat visual cortex. An electron microscope study. Brain Res 9:268-287.

Courtney SM, Petit L, Haxby JV, Ungerleider LG (1998) The role of prefrontal cortex in working memory: examining the contents of consciousness. Philos Trans R Soc Lond B Biol Sci 353:1819-1828.

Cox R, van Driel J, de Boer M, Talamini LM (2014) Slow oscillations during sleep coordinate interregional communication in cortical networks. J Neurosci 34:16890-16901.

Cox R, Ruber T, Staresina BP, Fell J (2020) Phase-based coordination of hippocampal and neocortical oscillations during human sleep. Commun Biol 3:176.

Czerniawski J, Yoon T, Otto T (2009) Dissociating space and trace in dorsal and ventral hippocampus. Hippocampus 19:20-32.

Damasio AR (1989) Time-locked multiregional retroactivation: a systems-level proposal for the neural substrates of recall and recognition. Cognition 33:25-62.

Dan Y, Poo MM (2004) Spike timing-dependent plasticity of neural circuits. Neuron 44:23-30.

Davoodi FG, Motamedi F, Naghdi N, Akbari E (2009) Effect of reversible inactivation of the reuniens nucleus on spatial learning and memory in rats using Morris water maze task. Behav Brain Res 198:130-135.

Davoodi FG, Motamedi F, Akbari E, Ghanbarian E, Jila B (2011) Effect of reversible inactivation of reuniens nucleus on memory processing in passive avoidance task. Behav Brain Res 221:1-6.

DeFelipe J, Farinas I (1992) The pyramidal neuron of the cerebral cortex: morphological and chemical characteristics of the synaptic inputs. Prog Neurobiol 39:563-607.

Depue BE (2012) A neuroanatomical model of prefrontal inhibitory modulation of memory retrieval. Neurosci Biobehav Rev 36:1382-1399.

Di Prisco GV, Vertes RP (2006) Excitatory actions of the ventral midline thalamus (rhomboid/reuniens) on the medial prefrontal cortex in the rat. Synapse 60:45-55.

Dickson CT (2010) Ups and downs in the hippocampus: the influence of oscillatory sleep states on "neuroplasticity" at different time scales. Behav Brain Res 214:35-41.

Diekelmann S, Born J (2010) The memory function of sleep. Nat Rev Neurosci 11:114-126.

Dolleman-Van Der Weel MJ, Witter MP (1996) Projections from the nucleus reuniens thalami to the entorhinal cortex, hippocampal field CA1, and the subiculum in the rat arise from different populations of neurons. J Comp Neurol 364:637-650.

Dolleman-Van der Weel MJ, Witter MP (2000) Nucleus reuniens thalami innervates gamma aminobutyric acid positive cells in hippocampal field CA1 of the rat. Neurosci Lett 278:145-148.

Dolleman-van der Weel MJ, Witter MP (2020) The thalamic midline nucleus reuniens: potential relevance for schizophrenia and epilepsy. Neurosci Biobehav Rev 119:422-439.

Dolleman-Van der Weel MJ, Lopes da Silva FH, Witter MP (1997) Nucleus reuniens thalami modulates activity in hippocampal field CA1 through excitatory and inhibitory mechanisms. J Neurosci 17:5640-5650.

Dolleman-van der Weel MJ, Morris RG, Witter MP (2009) Neurotoxic lesions of the thalamic reuniens or mediodorsal nucleus in rats affect non-mnemonic aspects of watermaze learning. Brain Struct Funct 213:329-342.

Dolleman-van der Weel MJ, Lopes da Silva FH, Witter MP (2017) Interaction of nucleus reuniens and entorhinal cortex projections in hippocampal field CA1 of the rat. Brain Struct Funct 222:2421-2438.

Dolleman-van der Weel MJ, Griffin AL, Ito HT, Shapiro ML, Witter MP, Vertes RP, Allen TA (2019) The nucleus reuniens of the thalamus sits at the nexus of a hippocampus and medial prefrontal cortex circuit enabling memory and behavior. Learn Mem 26:191-205.

Dudchenko PA (2004) An overview of the tasks used to test working memory in rodents. Neurosci Biobehav Rev 28:699-709.

Eacott MJ, Norman G (2004) Integrated memory for object, place, and context in rats: a possible model of episodic-like memory? J Neurosci 24:1948-1953.

Eichenbaum H (2004) Hippocampus: cognitive processes and neural representations that underlie declarative memory. Neuron 44:109-120.

Eichenbaum H (2017) Prefrontal-hippocampal interactions in episodic memory. Nat Rev Neurosci 18:547-558.

Ferraris M, Cassel JC, Pereira de Vasconcelos A, Stephan A, Quilichini PP (2021) The nucleus reuniens, a thalamic relay for cortico-hippocampal interaction in recent and remote memory consolidation. Neurosci Biobehav Rev 125:339-354.

Ferraris M, Ghestem A, Vicente AF, Nallet-Khosrofian L, Bernard C, Quilichini PP (2018) The Nucleus Reuniens Controls Long-Range Hippocampo-Prefrontal Gamma Synchronization during Slow Oscillations. J Neurosci 38:3026-3038.

Flamig R, Klingberg F (1978) [Participation of thalamic nuclei in the elaboration of conditioned avoidance reflexes of rats. IV. Lesions of the nucleus reuniens]. Acta Biol Med Ger 37:1779-1782.

Frankland PW, Bontempi B, Talton LE, Kaczmarek L, Silva AJ (2004) The involvement of the anterior cingulate cortex in remote contextual fear memory. Science 304:881-883.

Freeman WJ (1975) Mass Action in the Nervous System. New York: Academic Press.

Frey KA, Howland MM (1992) Quantitative autoradiography of muscarinic cholinergic receptor binding in the rat brain: distinction of receptor subtypes in antagonist competition assays. J Pharmacol Exp Ther 263:1391-1400.

Frey KA, Ehrenkaufer RL, Agranoff BW (1985) Quantitative in vivo receptor binding. II. Autoradiographic imaging of muscarinic cholinergic receptors. J Neurosci 5:2407-2414.

Fries P (2005) A mechanism for cognitive dynamics: neuronal communication through neuronal coherence. Trends Cogn Sci 9:474-480.

Furth KE, McCoy AJ, Dodge C, Walters JR, Buonanno A, Delaville C (2017) Neuronal correlates of ketamine and walking induced gamma oscillations in the medial prefrontal cortex and mediodorsal thalamus. PLoS One 12:e0186732.

Gemmell C, O'Mara SM (2000) Long-term potentiation and paired-pulse facilitation in the prelimbic cortex of the rat following stimulation in the contralateral hemisphere in vivo. Exp Brain Res 132:223-229.

Goldman-Rakic PS, Selemon LD, Schwartz ML (1984) Dual pathways connecting the dorsolateral prefrontal cortex with the hippocampal formation and parahippocampal cortex in the rhesus monkey. Neuroscience 12:719-743.

Gonzalez-Rueda A, Pedrosa V, Feord RC, Clopath C, Paulsen O (2018) Activity-Dependent Downscaling of Subthreshold Synaptic Inputs during Slow-Wave-Sleep-like Activity In Vivo. Neuron 97:1244-1252 e1245.

Granon S, Poucet B (1995) Medial prefrontal lesions in the rat and spatial navigation: evidence for impaired planning. Behav Neurosci 109:474-484.

Greenberg A, Dickson CT (2013) Spontaneous and electrically modulated spatiotemporal dynamics of the neocortical slow oscillation and associated local fast activity. Neuroimage 83:782-794.

Greenberg A, Whitten TA, Dickson CT (2016) Stimulating forebrain communications: Slow sinusoidal electric fields over frontal cortices dynamically modulate hippocampal activity and cortico-hippocampal interplay during slow-wave states. Neuroimage 133:189-206.

Griffin AL (2021) The nucleus reuniens orchestrates prefrontal-hippocampal synchrony during spatial working memory. Neurosci Biobehav Rev 128:415-420.

Gurdjian ES (1927) The diencephalon of the albino rat. Philadelphia, Pa.,: The Wistar institute press.

Hahn TT, McFarland JM, Berberich S, Sakmann B, Mehta MR (2012) Spontaneous persistent activity in entorhinal cortex modulates cortico-hippocampal interaction in vivo. Nat Neurosci 15:1531-1538.

Hallock HL, Wang A, Griffin AL (2016) Ventral Midline Thalamus Is Critical for Hippocampal-Prefrontal Synchrony and Spatial Working Memory. J Neurosci 36:8372-8389.

Hallock HL, Wang A, Shaw CL, Griffin AL (2013) Transient inactivation of the thalamic nucleus reuniens and rhomboid nucleus produces deficits of a working-memory dependent tactile-visual conditional discrimination task. Behav Neurosci 127:860-866.

Hasselmo ME (2006) The role of acetylcholine in learning and memory. Curr Opin Neurobiol 16:710-715.

Hasselmo ME, Wyble BP, Wallenstein GV (1996) Encoding and retrieval of episodic memories: role of cholinergic and GABAergic modulation in the hippocampus. Hippocampus 6:693-708.

Hauer BE, Pagliardini S, Dickson CT (2019) The Reuniens Nucleus of the Thalamus has an Essential Role in Coordinating Slow Wave Activity between Neocortex and Hippocampus. eNeuro 6:1-17. doi: 10.1523/ENEURO.0365-19.2019

Hauer BE, Pagliardini S, Dickson CT (2022) Prefrontal-hippocampal pathways through the nucleus reuniens are functionally biased by brain state. Front Neuroanat. In Press. doi: 10.3389/fnana.2021.804872

Hebb DO (1949) The organization of behavior; a neuropsychological theory. New York,: Wiley.

Hembrook JR, Mair RG (2011) Lesions of reuniens and rhomboid thalamic nuclei impair radial maze win-shift performance. Hippocampus 21:815-826.

Hembrook JR, Onos KD, Mair RG (2012) Inactivation of ventral midline thalamus produces selective spatial delayed conditional discrimination impairment in the rat. Hippocampus 22:853-860.

Herkenham M (1978) The connections of the nucleus reuniens thalami: evidence for a direct thalamo-hippocampal pathway in the rat. J Comp Neurol 177:589-610.

Hok V, Chah E, Save E, Poucet B (2013) Prefrontal cortex focally modulates hippocampal place cell firing patterns. J Neurosci 33:3443-3451.

Hong LE, Summerfelt A, Buchanan RW, O'Donnell P, Thaker GK, Weiler MA, Lahti AC (2010) Gamma and delta neural oscillations and association with clinical symptoms under subanesthetic ketamine. Neuropsychopharmacology 35:632-640.

Hoover WB, Vertes RP (2007) Anatomical analysis of afferent projections to the medial prefrontal cortex in the rat. Brain Struct Funct 212:149-179.

Hoover WB, Vertes RP (2012) Collateral projections from nucleus reuniens of thalamus to hippocampus and medial prefrontal cortex in the rat: a single and double retrograde fluorescent labeling study. Brain Struct Funct 217:191-209.

Hur EE, Zaborszky L (2005) Vglut2 afferents to the medial prefrontal and primary somatosensory cortices: a combined retrograde tracing in situ hybridization study [corrected]. J Comp Neurol 483:351-373.

Hyman JM, Zilli EA, Paley AM, Hasselmo ME (2005) Medial prefrontal cortex cells show dynamic modulation with the hippocampal theta rhythm dependent on behavior. Hippocampus 15:739-749.

Hyman JM, Wyble BP, Goyal V, Rossi CA, Hasselmo ME (2003) Stimulation in hippocampal region CA1 in behaving rats yields long-term potentiation when delivered to the peak of theta and long-term depression when delivered to the trough. J Neurosci 23:11725-11731.

Ino T, Kaneko T, Mizuno N (1998) Direct projections from the entorhinal cortical layers to the dentate gyrus, hippocampus, and subicular complex in the cat. Neurosci Res 32:241-265.

Isomura Y, Sirota A, Ozen S, Montgomery S, Mizuseki K, Henze DA, Buzsaki G (2006) Integration and segregation of activity in entorhinal-hippocampal subregions by neocortical slow oscillations. Neuron 52:871-882.

Ito HT (2018) Prefrontal-hippocampal interactions for spatial navigation. Neurosci Res 129:2-7.

Ito HT, Zhang SJ, Witter MP, Moser EI, Moser MB (2015) A prefrontal-thalamo-hippocampal circuit for goal-directed spatial navigation. Nature 522:50-55.

Jacobs J, Kahana MJ, Ekstrom AD, Fried I (2007) Brain oscillations control timing of single-neuron activity in humans. J Neurosci 27:3839-3844.

Jankowski MM, Islam MN, Wright NF, Vann SD, Erichsen JT, Aggleton JP, O'Mara SM (2014) Nucleus reuniens of the thalamus contains head direction cells. Elife 3.

Jankowski MM, Passecker J, Islam MN, Vann S, Erichsen JT, Aggleton JP, O'Mara SM (2015) Evidence for spatially-responsive neurons in the rostral thalamus. Front Behav Neurosci 9:256.

Jasper H (1949) Diffuse projection systems: the integrative action of the thalamic reticular system. Electroencephalogr Clin Neurophysiol 1:405-419; discussion 419-420.

Jay TM, Witter MP (1991) Distribution of hippocampal CA1 and subicular efferents in the prefrontal cortex of the rat studied by means of anterograde transport of Phaseolus vulgaris-leucoagglutinin. J Comp Neurol 313:574-586.

Jay TM, Glowinski J, Thierry AM (1989) Selectivity of the hippocampal projection to the prelimbic area of the prefrontal cortex in the rat. Brain Res 505:337-340.

Ji D, Wilson MA (2007a) Coordinated memory replay in the visual cortex and hippocampus during sleep. Nature neuroscience 10:100-107.

Ji D, Wilson MA (2007b) Coordinated memory replay in the visual cortex and hippocampus during sleep. Nat Neurosci 10:100-107.

Jia L, Sun Z, Shi D, Wang M, Jia J, He Y, Xue F, Ren Y, Yang J, Ma X (2019) Effects of different patterns of electric stimulation of the ventromedial prefrontal cortex on hippocampal-prefrontal coherence in a rat model of depression. Behav Brain Res 356:179-188.

Jin J, Maren S (2015) Prefrontal-Hippocampal Interactions in Memory and Emotion. Front Syst Neurosci 9:170.

Jones MW, Wilson MA (2005) Theta rhythms coordinate hippocampal-prefrontal interactions in a spatial memory task. PLoS Biol 3:e402.

Josselyn SA, Tonegawa S (2020) Memory engrams: Recalling the past and imagining the future. Science 367.

Josselyn SA, Kohler S, Frankland PW (2015) Finding the engram. Nat Rev Neurosci 16:521-534.

Jouvet M (1969) Biogenic amines and the states of sleep. Science 163:32-41.

Jung D, Huh Y, Cho J (2019) The Ventral Midline Thalamus Mediates Hippocampal Spatial Information Processes upon Spatial Cue Changes. J Neurosci 39:2276-2290.

Kaczmarek lK, Levitan IB (1987) Neuromodulation : the biochemical control of neuronal excitability, 1st Edition: Oxford University Press.

Ketchum KL, Haberly LB (1993) Synaptic events that generate fast oscillations in piriform cortex. J Neurosci 13:3980-3985.

Kitamura T, Ogawa SK, Roy DS, Okuyama T, Morrissey MD, Smith LM, Redondo RL, Tonegawa S (2017) Engrams and circuits crucial for systems consolidation of a memory. Science 356:73-78.

Klein MM, Cholvin T, Cosquer B, Salvadori A, Le Mero J, Kourouma L, Boutillier AL, Pereira de Vasconcelos A, Cassel JC (2019) Ventral midline thalamus lesion prevents persistence of new (learning-triggered) hippocampal spines, delayed neocortical spinogenesis, and spatial memory durability. Brain Struct Funct 224:1659-1676.

Klinzing JG, Niethard N, Born J (2019) Mechanisms of systems memory consolidation during sleep. Nat Neurosci 22:1598-1610.

Kloosterman F, van Haeften T, Lopes da Silva FH (2004) Two reentrant pathways in the hippocampal-entorhinal system. Hippocampus 14:1026-1039.

Kohli S, Andrianova L, Margetts-Smith G, Brady E, Craig MT (2021) Chemogenetic activation of midline thalamic nuclei fails to ameliorate memory deficits in two mouse models of Alzheimer's disease. BioRxiv.

Kolb B (1990) Animal models for human PFC-related disorders. Prog Brain Res 85:501-519.

Kolb B, Buhrmann K, McDonald R, Sutherland RJ (1994) Dissociation of the medial prefrontal, posterior parietal, and posterior temporal cortex for spatial navigation and recognition memory in the rat. Cereb Cortex 4:664-680.

Kropff E, Carmichael JE, Moser MB, Moser EI (2015) Speed cells in the medial entorhinal cortex. Nature 523:419-424.

Langston RF, Wood ER (2010) Associative recognition and the hippocampus: differential effects of hippocampal lesions on object-place, object-context and object-place-context memory. Hippocampus 20:1139-1153.

Lara-Vasquez A, Espinosa N, Duran E, Stockle M, Fuentealba P (2016) Midline thalamic neurons are differentially engaged during hippocampus network oscillations. Sci Rep 6:29807.

Laroche S, Davis S, Jay TM (2000) Plasticity at hippocampal to prefrontal cortex synapses: dual roles in working memory and consolidation. Hippocampus 10:438-446.

Laubach M, Amarante LM, Swanson K, White SR (2018) What, If Anything, Is Rodent Prefrontal Cortex? eNeuro 5.

Laurberg S, Sorensen KE (1981) Associational and commissural collaterals of neurons in the hippocampal formation (hilus fasciae dentatae and subfield CA3). Brain Res 212:287-300.

Layfield DM, Patel M, Hallock H, Griffin AL (2015) Inactivation of the nucleus reuniens/rhomboid causes a delay-dependent impairment of spatial working memory. Neurobiol Learn Mem 125:163-167.

Le Van Quyen M, Foucher J, Lachaux J, Rodriguez E, Lutz A, Martinerie J, Varela FJ (2001) Comparison of Hilbert transform and wavelet methods for the analysis of neuronal synchrony. J Neurosci Methods 111:83-98.

Lee AK, Wilson MA (2002) Memory of sequential experience in the hippocampus during slow wave sleep. Neuron 36:1183-1194.

Lee I, Kesner RP (2003) Time-dependent relationship between the dorsal hippocampus and the prefrontal cortex in spatial memory. J Neurosci 23:1517-1523.

Lesburgueres E, Gobbo OL, Alaux-Cantin S, Hambucken A, Trifilieff P, Bontempi B (2011) Early tagging of cortical networks is required for the formation of enduring associative memory. Science 331:924-928.

Linden H, Pettersen KH, Einevoll GT (2010) Intrinsic dendritic filtering gives low-pass power spectra of local field potentials. J Comput Neurosci 29:423-444.

Linley SB, Gallo MM, Vertes RP (2016) Lesions of the ventral midline thalamus produce deficits in reversal learning and attention on an odor texture set shifting task. Brain Res 1649:110-122.

Llinas RR (1988) The intrinsic electrophysiological properties of mammalian neurons: insights into central nervous system function. Science 242:1654-1664.

Lorente de Nó R (1934) Studies on the structure of the cerebral cortex. II. Continuation of the study of the ammonic system. J Psychol Neurol:113-177.

Loureiro M, Cholvin T, Lopez J, Merienne N, Latreche A, Cosquer B, Geiger K, Kelche C, Cassel JC, Pereira de Vasconcelos A (2012) The ventral midline thalamus (reuniens and rhomboid nuclei) contributes to the persistence of spatial memory in rats. J Neurosci 32:9947-9959.

Lubenov EV, Siapas AG (2008) Decoupling through synchrony in neuronal circuits with propagation delays. Neuron 58:118-131.

MacLaren DA, Browne RW, Shaw JK, Krishnan Radhakrishnan S, Khare P, Espana RA, Clark SD (2016) Clozapine N-Oxide Administration Produces Behavioral Effects in Long-Evans Rats: Implications for Designing DREADD Experiments. eNeuro 3.

Maisson DJ, Gemzik ZM, Griffin AL (2018) Optogenetic suppression of the nucleus reuniens selectively impairs encoding during spatial working memory. Neurobiol Learn Mem 155:78-85.

Malone EF (1910) Uber die Kerne des niensclilichen diencephalon. Abh Der Kgl Preuss Akademie der Wissenschaften.

Malone EF (1912) Observations concerning the comparative anatomy of the diencephalon. Anat Rec 6:281-290.

Marder E (2012) Neuromodulation of neuronal circuits: back to the future. Neuron 76:1-11.

Marder E, O'Leary T, Shruti S (2014) Neuromodulation of circuits with variable parameters: single neurons and small circuits reveal principles of state-dependent and robust neuromodulation. Annu Rev Neurosci 37:329-346.

Markus EJ, Barnes CA, McNaughton BL, Gladden VL, Skaggs WE (1994) Spatial information content and reliability of hippocampal CA1 neurons: effects of visual input. Hippocampus 4:410-421.

Marshall L, Helgadottir H, Molle M, Born J (2006) Boosting slow oscillations during sleep potentiates memory. Nature 444:610-613.

Marshall L, Cross N, Binder S, Dang-Vu TT (2020) Brain Rhythms During Sleep and Memory Consolidation: Neurobiological Insights. Physiology (Bethesda) 35:4-15.

Massimini M, Huber R, Ferrarelli F, Hill S, Tononi G (2004) The sleep slow oscillation as a traveling wave. J Neurosci 24:6862-6870.

Massimini M, Ferrarelli F, Esser SK, Riedner BA, Huber R, Murphy M, Peterson MJ, Tononi G (2007) Triggering sleep slow waves by transcranial magnetic stimulation. Proc Natl Acad Sci U S A 104:8496-8501.

Mathiasen ML, Amin E, Nelson AJD, Dillingham CM, O'Mara SM, Aggleton JP (2019) Separate cortical and hippocampal cell populations target the rat nucleus reuniens and mammillary bodies. Eur J Neurosci.

Maviel T, Durkin TP, Menzaghi F, Bontempi B (2004) Sites of neocortical reorganization critical for remote spatial memory. Science 305:96-99.

McCartney H, Johnson AD, Weil ZM, Givens B (2004) Theta reset produces optimal conditions for long-term potentiation. Hippocampus 14:684-687.

McCormick DA, Bal T (1997) Sleep and arousal: thalamocortical mechanisms. Annu Rev Neurosci 20:185-215.

McKenna JT, Vertes RP (2004) Afferent projections to nucleus reuniens of the thalamus. J Comp Neurol 480:115-142.

McNaughton BL, Barnes CA, Gerrard JL, Gothard K, Jung MW, Knierim JJ, Kudrimoti H, Qin Y, Skaggs WE, Suster M, Weaver KL (1996) Deciphering the hippocampal polyglot: the hippocampus as a path integration system. J Exp Biol 199:173-185.

Mei H, Logothetis NK, Eschenko O (2018) The activity of thalamic nucleus reuniens is critical for memory retrieval, but not essential for the early phase of "off-line" consolidation. Learn Mem 25:129-137.

Miller EK, Cohen JD (2001) An integrative theory of prefrontal cortex function. Annu Rev Neurosci 24:167-202.

Mirollo RE, Strogatz SH (1990) Synchronization of Pulse-Coupled Biological Oscillators. SIAM J Appl Math 50:1645-1662.

Miyamoto D, Hirai D, Murayama M (2017) The Roles of Cortical Slow Waves in Synaptic Plasticity and Memory Consolidation. Front Neural Circuits 11:92.

Molle M, Marshall L, Gais S, Born J (2004) Learning increases human electroencephalographic coherence during subsequent slow sleep oscillations. Proc Natl Acad Sci U S A 101:13963-13968.

Molle M, Bergmann TO, Marshall L, Born J (2011) Fast and slow spindles during the sleep slow oscillation: disparate coalescence and engagement in memory processing. Sleep 34:1411-1421.

Molle M, Eschenko O, Gais S, Sara SJ, Born J (2009) The influence of learning on sleep slow oscillations and associated spindles and ripples in humans and rats. Eur J Neurosci 29:1071-1081.

Molyneaux BJ, Arlotta P, Menezes JR, Macklis JD (2007) Neuronal subtype specification in the cerebral cortex. Nat Rev Neurosci 8:427-437.

Morales GJ, Ramcharan EJ, Sundararaman N, Morgera SD, Vertes RP (2007) Analysis of the actions of nucleus reuniens and the entorhinal cortex on EEG and evoked population behavior of the hippocampus. Conf Proc IEEE Eng Med Biol Soc 2007:2480-2484.

Morris RG (2001) Episodic-like memory in animals: psychological criteria, neural mechanisms and the value of episodic-like tasks to investigate animal models of neurodegenerative disease. Philos Trans R Soc Lond B Biol Sci 356:1453-1465.

Morris RG, Garrud P, Rawlins JN, O'Keefe J (1982) Place navigation impaired in rats with hippocampal lesions. Nature 297:681-683.

Mountcastle VB (1997) The columnar organization of the neocortex. Brain 120 (Pt 4):701-722.

Navawongse R, Eichenbaum H (2013) Distinct pathways for rule-based retrieval and spatial mapping of memory representations in hippocampal neurons. J Neurosci 33:1002-1013.

Niethard N, Ngo HV, Ehrlich I, Born J (2018) Cortical circuit activity underlying sleep slow oscillations and spindles. Proc Natl Acad Sci U S A 115:E9220-E9229.

Nir Y, Staba RJ, Andrillon T, Vyazovskiy VV, Cirelli C, Fried I, Tononi G (2011) Regional slow waves and spindles in human sleep. Neuron 70:153-169.

O'Keefe J, Dostrovsky J (1971) The hippocampus as a spatial map. Preliminary evidence from unit activity in the freely-moving rat. Brain Res 34:171-175.

O'Keefe J, Nadel L (1978) The hippocampus as a cognitive map. London: Oxford.

Ongur D, Price JL (2000) The organization of networks within the orbital and medial prefrontal cortex of rats, monkeys and humans. Cereb Cortex 10:206-219.

Oyanedel CN, Duran E, Niethard N, Inostroza M, Born J (2020) Temporal associations between sleep slow oscillations, spindles and ripples. Eur J Neurosci 52:4762-4778.

Pagliardini S, Gosgnach S, Dickson CT (2013a) Spontaneous sleep-like brain state alternations and breathing characteristics in urethane anesthetized mice. PLoS One 8:e70411.

Pagliardini S, Funk GD, Dickson CT (2013b) Breathing and brain state: urethane anesthesia as a model for natural sleep. Respir Physiol Neurobiol 188:324-332.

Pagliardini S, Greer JJ, Funk GD, Dickson CT (2012) State-dependent modulation of breathing in urethane-anesthetized rats. J Neurosci 32:11259-11270.

Palacios-Filardo J, Udakis M, Brown GA, Tehan BG, Congreve MS, Nathan PJ, Brown AJH, Mellor JR (2021) Acetylcholine prioritises direct synaptic inputs from entorhinal cortex to CA1 by differential modulation of feedforward inhibitory circuits. Nat Commun 12:5475.

Pavlides C, Winson J (1989) Influences of hippocampal place cell firing in the awake state on the activity of these cells during subsequent sleep episodes. J Neurosci 9:2907-2918.

Paxinos G, Watson C (1998) The Rat Brain In Stereotaxic Coordinates, 4th Edition. San Diego: Academic Press.

Pereira de Vasconcelos A, Cassel JC (2015) The nonspecific thalamus: A place in a wedding bed for making memories last? Neurosci Biobehav Rev 54:175-196.

Petrides M (1995) Impairments on nonspatial self-ordered and externally ordered working memory tasks after lesions of the mid-dorsal part of the lateral frontal cortex in the monkey. J Neurosci 15:359-375.

Picciotto MR, Higley MJ, Mineur YS (2012) Acetylcholine as a neuromodulator: cholinergic signaling shapes nervous system function and behavior. Neuron 76:116-129.

Pirot S, Jay TM, Glowinski J, Thierry AM (1994) Anatomical and electrophysiological evidence for an excitatory amino acid pathway from the thalamic mediodorsal nucleus to the prefrontal cortex in the rat. Eur J Neurosci 6:1225-1234.

Plankar M, Brezan S, Jerman I (2013) The principle of coherence in multi-level brain information processing. Prog Biophys Mol Biol 111:8-29.

Porter MC, Burk JA, Mair RG (2000) A comparison of the effects of hippocampal or prefrontal cortical lesions on three versions of delayed non-matching-to-sample based on positional or spatial cues. Behav Brain Res 109:69-81.

Prasad JA, Chudasama Y (2013) Viral tracing identifies parallel disynaptic pathways to the hippocampus. J Neurosci 33:8494-8503.

Prasad JA, Macgregor EM, Chudasama Y (2013) Lesions of the thalamic reuniens cause impulsive but not compulsive responses. Brain Struct Funct 218:85-96.

Prasad JA, Abela AR, Chudasama Y (2017) Midline thalamic reuniens lesions improve executive behaviors. Neuroscience 345:77-88.

Preston AR, Eichenbaum H (2013) Interplay of hippocampus and prefrontal cortex in memory. Curr Biol 23:R764-773.

Puentes-Mestril C, Roach J, Niethard N, Zochowski M, Aton SJ (2019) How rhythms of the sleeping brain tune memory and synaptic plasticity. Sleep 42.

Quet E, Majchrzak M, Cosquer B, Morvan T, Wolff M, Cassel JC, Pereira de Vasconcelos A, Stephan A (2020) The reuniens and rhomboid nuclei are necessary for contextual fear memory persistence in rats. Brain Struct Funct 225:955-968.

Quirk GJ, Muller RU, Kubie JL (1990) The firing of hippocampal place cells in the dark depends on the rat's recent experience. J Neurosci 10:2008-2017.

Ragozzino ME, Kim J, Hassert D, Minniti N, Kiang C (2003) The contribution of the rat prelimbic-infralimbic areas to different forms of task switching. Behav Neurosci 117:1054-1065.

Rajasethupathy P, Sankaran S, Marshel JH, Kim CK, Ferenczi E, Lee SY, Berndt A, Ramakrishnan C, Jaffe A, Lo M, Liston C, Deisseroth K (2015) Projections from neocortex mediate top-down control of memory retrieval. Nature 526:653-659.

Rich EL, Shapiro ML (2007) Prelimbic/infralimbic inactivation impairs memory for multiple task switches, but not flexible selection of familiar tasks. J Neurosci 27:4747-4755.

Rioch DM (1929) Studies on the diencephalon of carnivora part I. The nuclear configuration of the thalamus, epithalamus, and hypothalamus of the dog and cat. J Comp Neurol 49:1-119.

Rodriguez R, Haberly LB (1989) Analysis of synaptic events in the opossum piriform cortex with improved current source-density techniques. J Neurophysiol 61:702-718.

Rosene DL, Van Hoesen GW (1977) Hippocampal efferents reach widespread areas of cerebral cortex and amygdala in the rhesus monkey. Science 198:315-317.

Roy A, Svensson FP, Mazeh A, Kocsis B (2017) Prefrontal-hippocampal coupling by theta rhythm and by 2-5 Hz oscillation in the delta band: The role of the nucleus reuniens of the thalamus. Brain Struct Funct 222:2819-2830.

Russo SJ, Nestler EJ (2013) The brain reward circuitry in mood disorders. Nat Rev Neurosci 14:609-625.

Sargolini F, Fyhn M, Hafting T, McNaughton BL, Witter MP, Moser MB, Moser EI (2006) Conjunctive representation of position, direction, and velocity in entorhinal cortex. Science 312:758-762.

Sastre JP, Buda C, Lin JS, Jouvet M (2000) Differential c-fos expression in the rhinencephalon and striatum after enhanced sleep-wake states in the cat. Eur J Neurosci 12:1397-1410.

Sauseng P, Klimesch W (2008) What does phase information of oscillatory brain activity tell us about cognitive processes? Neurosci Biobehav Rev 32:1001-1013.

Sauseng P, Klimesch W, Heise KF, Gruber WR, Holz E, Karim AA, Glennon M, Gerloff C, Birbaumer N, Hummel FC (2009) Brain oscillatory substrates of visual short-term memory capacity. Curr Biol 19:1846-1852.

Save E, Cressant A, Thinus-Blanc C, Poucet B (1998) Spatial firing of hippocampal place cells in blind rats. J Neurosci 18:1818-1826.

Scavuzzo CJ, LeBlancq MJ, Nargang F, Lemieux H, Hamilton TJ, Dickson CT (2019) The amnestic agent anisomycin disrupts intrinsic membrane properties of hippocampal neurons via a loss of cellular energetics. J Neurophysiol 122:1123-1135.

Schall KP, Kerber J, Dickson CT (2008) Rhythmic constraints on hippocampal processing: state and phase-related fluctuations of synaptic excitability during theta and the slow oscillation. J Neurophysiol 99:888-899.

Schultz C, Engelhardt M (2014) Anatomy of the hippocampal formation. Front Neurol Neurosci 34:6-17.

Schwabe MR, Lincoln CM, Ivers MM, Frick KM (2021) Chemogenetic inactivation of the nucleus reuniens impairs object placement memory in female mice. Neurobiol Learn Mem 185:107521.

Sesack SR, Deutch AY, Roth RH, Bunney BS (1989) Topographical organization of the efferent projections of the medial prefrontal cortex in the rat: an anterograde tract-tracing study with Phaseolus vulgaris leucoagglutinin. J Comp Neurol 290:213-242.

Sharma AV, Wolansky T, Dickson CT (2010) A comparison of sleeplike slow oscillations in the hippocampus under ketamine and urethane anesthesia. J Neurophysiol 104:932-939.

Sharma AV, Nargang FE, Dickson CT (2012) Neurosilence: profound suppression of neural activity following intracerebral administration of the protein synthesis inhibitor anisomycin. J Neurosci 32:2377-2387.

Shaw AD, Saxena N, L EJ, Hall JE, Singh KD, Muthukumaraswamy SD (2015) Ketamine amplifies induced gamma frequency oscillations in the human cerebral cortex. Eur Neuropsychopharmacol 25:1136-1146.

Shimamura AP, Jurica PJ, Mangels JA, Gershberg FB, Knight RT (1995) Susceptibility to Memory Interference Effects following Frontal Lobe Damage: Findings from Tests of Paired-Associate Learning. J Cogn Neurosci 7:144-152.

Siapas AG, Wilson MA (1998) Coordinated interactions between hippocampal ripples and cortical spindles during slow-wave sleep. Neuron 21:1123-1128.

Siapas AG, Lubenov EV, Wilson MA (2005) Prefrontal phase locking to hippocampal theta oscillations. Neuron 46:141-151.

Sigurdsson T, Duvarci S (2015) Hippocampal-Prefrontal Interactions in Cognition, Behavior and Psychiatric Disease. Front Syst Neurosci 9:190.

Sigurdsson T, Stark KL, Karayiorgou M, Gogos JA, Gordon JA (2010) Impaired hippocampal-prefrontal synchrony in a genetic mouse model of schizophrenia. Nature 464:763-767.

Silver NRG, Ward-Flanagan R, Dickson CT (2021) Long-term stability of physiological signals within fluctuations of brain state under urethane anesthesia. PLoS One 16:e0258939.

Simons JS, Spiers HJ (2003) Prefrontal and medial temporal lobe interactions in long-term memory. Nat Rev Neurosci 4:637-648.

Sirota A, Csicsvari J, Buhl D, Buzsaki G (2003) Communication between neocortex and hippocampus during sleep in rodents. Proc Natl Acad Sci U S A 100:2065-2069.

Sloviter RS, Lømo T (2012) Updating the lamellar hypothesis of hippocampal organization. Front Neural Circuits 6:102.

Spellman T, Rigotti M, Ahmari SE, Fusi S, Gogos JA, Gordon JA (2015) Hippocampal-prefrontal input supports spatial encoding in working memory. Nature 522:309-314.

Spiers HJ (2008) Keeping the goal in mind: prefrontal contributions to spatial navigation. Neuropsychologia 46:2106-2108.

Srinath R, Ray S (2014) Effect of amplitude correlations on coherence in the local field potential. J Neurophysiol 112:741-751.

Staresina BP, Bergmann TO, Bonnefond M, van der Meij R, Jensen O, Deuker L, Elger CE, Axmacher N, Fell J (2015) Hierarchical nesting of slow oscillations, spindles and ripples in the human hippocampus during sleep. Nat Neurosci 18:1679-1686.

Steriade M (2001) Impact of network activities on neuronal properties in corticothalamic systems. J Neurophysiol 86:1-39.

Steriade M (2006) Grouping of brain rhythms in corticothalamic systems. Neuroscience 137:1087-1106.

Steriade M, Llinas RR (1988) The functional states of the thalamus and the associated neuronal interplay. Physiol Rev 68:649-742.

Steriade M, Timofeev I (2003) Neuronal plasticity in thalamocortical networks during sleep and waking oscillations. Neuron 37:563-576.

Steriade M, Nunez A, Amzica F (1993a) A novel slow (< 1 Hz) oscillation of neocortical neurons in vivo: depolarizing and hyperpolarizing components. J Neurosci 13:3252-3265.

Steriade M, Nunez A, Amzica F (1993b) Intracellular analysis of relations between the slow (< 1 Hz) neocortical oscillation and other sleep rhythms of the electroencephalogram. J Neurosci 13:3266-3283.

Steward O, Scoville SA (1976) Cells of origin of entorhinal cortical afferents to the hippocampus and fascia dentata of the rat. J Comp Neurol 169:347-370.

Stickgold R (2005) Sleep-dependent memory consolidation. Nature 437:1272-1278.

Sullivan D, Csicsvari J, Mizuseki K, Montgomery S, Diba K, Buzsaki G (2011) Relationships between hippocampal sharp waves, ripples, and fast gamma oscillation: influence of dentate and entorhinal cortical activity. J Neurosci 31:8605-8616.

Taxidis J, Mizuseki K, Mason R, Owen MR (2013) Influence of slow oscillation on hippocampal activity and ripples through cortico-hippocampal synaptic interactions, analyzed by a cortical-CA3-CA1 network model. Front Comput Neurosci 7:3.

Thierry AM, Gioanni Y, Degenetais E, Glowinski J (2000) Hippocampo-prefrontal cortex pathway: anatomical and electrophysiological characteristics. Hippocampus 10:411-419.

Tierney PL, Degenetais E, Thierry AM, Glowinski J, Gioanni Y (2004) Influence of the hippocampus on interneurons of the rat prefrontal cortex. Eur J Neurosci 20:514-524.

Timofeev I, Steriade M (1997) Fast (mainly 30-100 Hz) oscillations in the cat cerebellothalamic pathway and their synchronization with cortical potentials. J Physiol 504 (Pt 1):153-168.

Tononi G, Cirelli C (2003) Sleep and synaptic homeostasis: a hypothesis. Brain Res Bull 62:143-150.

Tononi G, Cirelli C (2014) Sleep and the price of plasticity: from synaptic and cellular homeostasis to memory consolidation and integration. Neuron 81:12-34.

Troyner F, Bicca MA, Bertoglio LJ (2018) Nucleus reuniens of the thalamus controls fear memory intensity, specificity and long-term maintenance during consolidation. Hippocampus.

Vann SD, Brown MW, Aggleton JP (2000) Fos expression in the rostral thalamic nuclei and associated cortical regions in response to different spatial memory tests. Neuroscience 101:983-991.

Varela C, Kumar S, Yang JY, Wilson MA (2014) Anatomical substrates for direct interactions between hippocampus, medial prefrontal cortex, and the thalamic nucleus reuniens. Brain Struct Funct 219:911-929.

Vertes RP (2002) Analysis of projections from the medial prefrontal cortex to the thalamus in the rat, with emphasis on nucleus reuniens. J Comp Neurol 442:163-187.

Vertes RP (2004) Differential projections of the infralimbic and prelimbic cortex in the rat. Synapse 51:32-58.

Vertes RP (2015) Major diencephalic inputs to the hippocampus: supramammillary nucleus and nucleus reuniens. Circuitry and function. Prog Brain Res 219:121-144.

Vertes RP, Hoover WB, Szigeti-Buck K, Leranth C (2007) Nucleus reuniens of the midline thalamus: link between the medial prefrontal cortex and the hippocampus. Brain Res Bull 71:601-609.

Vertes RP, Hoover WB, Do Valle AC, Sherman A, Rodriguez JJ (2006) Efferent projections of reuniens and rhomboid nuclei of the thalamus in the rat. J Comp Neurol 499:768-796.

Vetere G, Kenney JW, Tran LM, Xia F, Steadman PE, Parkinson J, Josselyn SA, Frankland PW (2017) Chemogenetic Interrogation of a Brain-wide Fear Memory Network in Mice. Neuron 94:363-374 e364.

Viena TD, Linley SB, Vertes RP (2018) Inactivation of nucleus reuniens impairs spatial working memory and behavioral flexibility in the rat. Hippocampus 28:297-311.

Viena TD, Vertes RP, Linley SB (2021) Discharge characteristics of neurons of nucleus reuniens across sleep-wake states in the behaving rat. Behav Brain Res 410:113325.

Vogt BA, Paxinos G (2014) Cytoarchitecture of mouse and rat cingulate cortex with human homologies. Brain Struct Funct 219:185-192.

Voloh B, Womelsdorf T (2016) A Role of Phase-Resetting in Coordinating Large Scale Neural Networks During Attention and Goal-Directed Behavior. Front Syst Neurosci 10:18.

Voytek B, Knight RT (2015) Dynamic network communication as a unifying neural basis for cognition, development, aging, and disease. Biol Psychiatry 77:1089-1097.

Vu T, Gugustea R, Leung LS (2020) Long-term potentiation of the nucleus reuniens and entorhinal cortex to CA1 distal dendritic synapses in mice. Brain Struct Funct 225:1817-1838.

Vyazovskiy VV, Delogu A (2014) NREM and REM Sleep: Complementary Roles in Recovery after Wakefulness. Neuroscientist 20:203-219.

Walsh DA, Brown JT, Randall AD (2017) In vitro characterization of cell-level neurophysiological diversity in the rostral nucleus reuniens of adult mice. J Physiol 595:3549-3572.

Wang XJ (2010) Neurophysiological and computational principles of cortical rhythms in cognition. Physiol Rev 90:1195-1268.

Wang Y, Ye M, Kuang X, Li Y, Hu S (2018) A simplified morphological classification scheme for pyramidal cells in six layers of primary somatosensory cortex of juvenile rats. IBRO Rep 5:74-90.

Ward-Flanagan R, Dickson CT (2019) Neurobiological Parallels, Overlaps, and Divergences of Sleep and Anesthesia. In: Handbook of Sleep Research (Dringenberg HC, ed), pp 223-236: Elsevier.

Warren CP, Hu S, Stead M, Brinkmann BH, Bower MR, Worrell GA (2010) Synchrony in normal and focal epileptic brain: the seizure onset zone is functionally disconnected. J Neurophysiol 104:3530-3539.

Wheeler AL, Teixeira CM, Wang AH, Xiong X, Kovacevic N, Lerch JP, McIntosh AR, Parkinson J, Frankland PW (2013) Identification of a functional connectome for long-term fear memory in mice. PLoS Comput Biol 9:e1002853.

Whishaw IQ, Vanderwolf CH (1973) Hippocampal EEG and behavior: changes in amplitude and frequency of RSA (theta rhythm) associated with spontaneous and learned movement patterns in rats and cats. Behav Biol 8:461-484.

Whissell PD, Tohyama S, Martin LJ (2016) The Use of DREADDs to Deconstruct Behavior. Front Genet 7:70.

Whitten TA, Martz LJ, Guico A, Gervais N, Dickson CT (2009) Heat synch: inter- and independence of body-temperature fluctuations and brain-state alternations in urethane-anesthetized rats. J Neurophysiol 102:1647-1656.

Wierzynski CM, Lubenov EV, Gu M, Siapas AG (2009) State-dependent spike-timing relationships between hippocampal and prefrontal circuits during sleep. Neuron 61:587-596.

Williams JM, Givens B (2003) Stimulation-induced reset of hippocampal theta in the freely performing rat. Hippocampus 13:109-116.

Winkler C, Potter A (1914) An anatomical guide to experimental researches on the cat's brain : a series of 35 frontal sections. Amsterdam: Versluys.

Winterer G, Coppola R, Goldberg TE, Egan MF, Jones DW, Sanchez CE, Weinberger DR (2004) Prefrontal broadband noise, working memory, and genetic risk for schizophrenia. Am J Psychiatry 161:490-500.

Witter MP, Griffioen AW, Jorritsma-Byham B, Krijnen JL (1988) Entorhinal projections to the hippocampal CA1 region in the rat: an underestimated pathway. Neurosci Lett 85:193-198.

Witter MP, Groenewegen HJ, Lopes da Silva FH, Lohman AH (1989) Functional organization of the extrinsic and intrinsic circuitry of the parahippocampal region. Prog Neurobiol 33:161-253.

Witter MP, Doan TP, Jacobsen B, Nilssen ES, Ohara S (2017) Architecture of the Entorhinal Cortex A Review of Entorhinal Anatomy in Rodents with Some Comparative Notes. Front Syst Neurosci 11:46.

Wolansky T, Clement EA, Peters SR, Palczak MA, Dickson CT (2006) Hippocampal slow oscillation: a novel EEG state and its coordination with ongoing neocortical activity. J Neurosci 26:6213-6229.

Wolff M, Alcaraz F, Marchand AR, Coutureau E (2015) Functional heterogeneity of the limbic thalamus: From hippocampal to cortical functions. Neurosci Biobehav Rev 54:120-130.

Wouterlood FG (1991) Innervation of Entorhinal Principal Cells by Neurons of the Nucleus Reuniens Thalami. Anterograde PHA-L Tracing Combined with Retrograde Fluorescent Tracing and Intracellular Injection with Lucifer Yellow in the Rat. Eur J Neurosci 3:641-647.

Wouterlood FG, Saldana E, Witter MP (1990) Projection from the nucleus reuniens thalami to the hippocampal region: light and electron microscopic tracing study in the rat with the anterograde tracer Phaseolus vulgaris-leucoagglutinin. J Comp Neurol 296:179-203.

Wyble BP, Linster C, Hasselmo ME (2000) Size of CA1-evoked synaptic potentials is related to theta rhythm phase in rat hippocampus. J Neurophysiol 83:2138-2144.

Xu W, Sudhof TC (2013) A neural circuit for memory specificity and generalization. Science 339:1290-1295.

Xu W, Morishita W, Buckmaster PS, Pang ZP, Malenka RC, Sudhof TC (2012) Distinct neuronal coding schemes in memory revealed by selective erasure of fast synchronous synaptic transmission. Neuron 73:990-1001.

Yanagihara M, Niimi K, Ono K (1987) Thalamic projections to the hippocampal and entorhinal areas in the cat. J Comp Neurol 266:122-141.

Yun SH, Mook-Jung I, Jung MW (2002) Variation in effective stimulus patterns for induction of long-term potentiation across different layers of rat entorhinal cortex. J Neurosci 22:RC214.

Zar JH (1999) Biostatistical Analysis, 4 Edition. Upper Saddle River, New Jersey: Prentice Hall.

Zhang DX, Bertram EH (2002) Midline thalamic region: widespread excitatory input to the entorhinal cortex and amygdala. J Neurosci 22:3277-3284.

Zimmerman EC, Grace AA (2018) Prefrontal cortex modulates firing pattern in the nucleus reuniens of the midline thalamus via distinct corticothalamic pathways. Eur J Neurosci 48:3255-3272.